Multiplexed affinity peptidomic assays: multiplexing and applications for testing protein biomarkers

Julian Bailes

j.r.bailes@rhul.ac.uk

Thesis

Department of Biological Sciences

Royal Holloway, University of London

Supervisor: Mikhail Soloviev

External Advisor:

Phil Teale (HFL Sport Science)

Declaration

I have signed this declaration to declare that:

1. this thesis comprises only of my original work towards the PhD except where indicated otherwise, where due acknowledgement has been made in the text and,

2. this thesis is less than 100,000 words in length, exclusive of tables, figures and bibliography.

Julian Bailes

Signature:

Date: 24 November, 2020

Acknowledgements

I would like to thank Mikhail Soloviev, Dewi Davies and Phil Teale for their continued guidance, support, patience and understanding throughout my studies. I am also grateful to BBSRC and HFL for their financial support and training as well as Fan Zhang and Anna Dulneva for their help in the lab. And to Meriel, Adrian, Jason and Nick for their faith in me to finish. **Thank you**.

Abstract

Biomarkers are increasingly used in a wide range of areas such as sports and clinical diagnostics, biometric applications, forensic analysis and population screening. Testing for such biomarkers requires substantial resources and has traditionally involved centralised laboratory testing. From cancer diagnosis to COVID testing, there is an increasing demand for protein based assays that are portable, easy to use and ideally multiplexed, so that more than one biomarker can be tested at the same time, thus increasing the throughput and reducing time of the analysis and potentially the costs. Events in recent years, not least the ongoing investigations into claims of widespread state-sponsored doping schemes in sport and the COVID-19 pandemic of 2020 highlight the ever-growing requirement and importance of such tests across multiple frontiers.

The project evaluated the feasibility of new antipeptide affinity reagents and suitable technologies for application to multiplexed affinity assays geared towards quantitatively analysing a range of analytes.

In the first part of this project, key protein biomarkers available from blood serum and covering a range of conditions including cancer, inflammation, and various behavioural traits were chosen from the literature. Peptide antigens for the development of anti-peptide polyclonal antibodies for each protein were selected following in silico proteolysis and ranking of the peptides using an algorithm devised as part of this research. A microarray format was used to achieve spatial multiplexing and increase throughput of the assays. The arrays were evaluated experimentally and were tested for their usability for studying up/down regulation of the target biomarkers in human sera samples.

Another protein assay format tested for compatibility with affinity peptidomics approach was a gold nanoparticle based lateral flow test. An affinity-based lateral flow test device was built and used for the detection of the benzodiazepine Valium. Here spectral multiplexing of detection was considered. The principle was tested using quantum dot nanoparticles instead of traditionally used gold nanoparticles. The spectral deconvolution was achieved for mixtures containing up to six differently sized quantum dots.

In the final part of this project, a search for novel peptide affinity reagents against insulin growth-like factor 1 (IGF-1) was conducted using phage display. Four peptides were identified after screening a phage display library, and the binding of these peptides to IGF-1 was compared to that of traditional antibody.

Contents

List of Figures

List of Tables

Abbreviations

Ab	Antibody
And	Adiponectin
AI	Artificial intelligence
ALS	Acid-labile subunit
AP	Alkaline phosphatase
BALCO	The Bay Area Laboratory Co-operative
BCA	Bicinchoninic acid
βE	Beta-enolase
BLI	Biolayer interferometry
BMI	Body mass index
BSA	Bovine serum albumin
CAD	Coronary artery disease
cDNA	Complementary DNA
CdSe	Cadmium selenide
CdTe	Cadmium telluride
CE-MS	Capillary electrophoresis mass spectrometry
CFs	Conversion factors
CFU	Colony forming unit
CK-MB	Creatine kinase-MB
C-terminus	Carboxyl-terminus
-COOH	Carboxyl group
COVID-19	Corona Virus Disease 2019
CRP	C-reactive protein
cTn1	Cardiac troponin 1
Cy3	Cyanine 3 (dye)
DARPins	Designed ankyrin repeat proteins
dH_2O	Distilled water
DNA	Deoxyribonucleic acid
DSR	Dynamic signal range
E. coli	Escherichia coli
ECM	Extra cellular matrix
ELISA	Enzyme-linked immunosorbent assay
EMA	European Medicines Agency
ES	E-selectin
Fab’	Antibody fragment
FDA	Food and Drug Administration

Fb DD	Fibrinogen D-Dimer
FN	Fibronectin
FPLC	Fast protein liquid chromatography
FT-ICR	Fourier transform ion cyclotron resonance
G6PDH	Glucose-6-phosphate dehydrogenase
GC	Gas chromatography
GH	Growth Hormone
GHR	Growth hormone receptor
GNPs	Gold nanoparticles
H_2O_2	Hydrogen peroxide
$HAuCl_4$	Tetrachloroauric acid
hCG	Human chorionic gonadotropin
HG	Haptoglobin
HIV	Human immunodeficiency virus
HPLC	High performance liquid chromatography
HRP	Horseradish peroxidase
HSP	Heat shock protein
IEDP	The Immune Epitope Database
IFN	Interferon
IGF-1	Insulin-like growth factor-1
IGF-1R	Insulin-like growth factor-1 receptor
IGF-2	Insulin-like growth factor-2
IGF-2R	Insulin-like growth factor-2 receptor
IGFBP	Insulin-like growth factor binding protein
IGFBP-rP	Insulin-like growth factor binding protein-related proteins
IGFD	Insulin-like growth factor deficiency
IgG	Immunoglobulin G
IgM	Immunoglobulin M
IL	Interleukin
In	Insulin
IOC	International Olympic Committee
IRMA	Immunoradiometric assay
IRR	International reference reagent
I-R	Insulin receptor
IT	Ion traps
LB	Lysogeny broth
LC-MS	Liquid chromatography mass spectrometry
Lp	Leptin

LSPR	Localised surface plasmon resonance
MALDI	Matrix-assisted laser desorption ionization
MCR	Measurable range of concentration
MDMA	3,4-methylenedioxy-N-methylamphetamine
MGF	Mechano-growth factor
MIT	Massachusetts Institute of Technology
MLB	Major League Baseball
MMP	Matrix metalloproteinases
MS	Mass Spectrometry
mRNA	Messenger Ribonucleic Acid
N-terminus	Amino-terminus
NAD	Nicotinamide adenine dinucleotide
NAFLD	Non-alcoholic fatty liver disease
NaN_3	Sodium azide
NaCl	Sodium chloride
NDNAD	National DNA Database
$-NH_2$	Amine group
NSILA	Non-suppressible insulin-like activity
OR	Odds ratio
PI3K	Phosphoinositide 3-kinase
P-III-P	Type III procollagen N-terminal peptide
PBS	Phosphate buffered saline
PBSt	Phosphate buffered saline with tween
PCP	Phencyclidine
PED	Performance enhancing drug
PMSF	Phenylmethylsulfonyl fluoride
PNPP	p-Nitrophenyl phosphate
POC	Point-of-care
Prl	Prolactin
PSA	Prostate specific antigen
Px	Peroxidase
QCM	Quartz crystal microbalance
QDs	Quantum dots
QY	Quantum yield
RAMP™	Rapid Analyte Measurement Platform
RCAT	Rolling Circle Amplification Technology
REVS	Rupture event scanning
rhGH	Recombinant growth hormone

rhIGF-1	Recombinant human insulin-like growth factor-1
RITC	Rhodamine B isothiocyanate
RNA	Ribonucleic acid
RSV	Respiratory syncytial virus
RT-PCR	Real-time polymer chain reaction
SA	Streptavidin
SAA	Serum amyloid-A
SARS-Cov-2	Severe acute respiratory syndrome coronavirus 2
scFv	Single-chain variable fragment
SDT	Signal detection threshold
SEC	Size exclusion chromatography
SELDI	Surface-enhanced laser desorption ionization
SELEX	Systematic evolution of ligands by exponential enrichment
SEM	Standard error of the mean
-SH	Mercapto group
SHBG	Sex hormone-binding globulin
SH-SAW	Shear-horizontal surface acoustic wave
SP-A	Surfactant-associated protein A
SPR	Surface plasmon resonance
STDEVP	Standard deviation based on an entire population
Strep A	Group A streptococcus
T1DM	Type 1 diabetes mellitus
T2DM	Type 2 diabetes mellitus
TBS	Tris buffered saline
TBST	Tris buffered saline with tween
TEM	Transmission electron microscopy
TEMED	Tetramethylethylenediamine
TGF-β	Transforming growth factor-beta
TMB	3,3',5,5'-Tetramethylbenzine
TNF- α	Tumour necrosis factor alpha
TNT	Trinitrotoluene
TOF-MS	Time of flight mass spectrometry
UV	Ultraviolet
WADA	World Anti-Doping Agency
WHO	World Health Organization
Y2H	Yeast two-hybrid
ZnS	Zinc sulphide

Chapter 1: Introduction

1.1 Aims & Objectives

The need for fast, accurate, and cost-effective detection of biomolecules has never been greater. From testing for performance enhancing drugs in sport, and biometric forensic analysis at crime scenes, to the screening of dietary supplements, and biomarker profiling in medicine, reliable and rapid test kits that can be run easily and at scale are in-demand more than ever.

1.1.2 Aims

The aim of this project was to develop a test platform capable of quantitatively analysing a range of analytes, from “traditional” small molecule drugs, to peptide and protein markers the presence of which above or below certain thresholds, in isolation or combination, can provide crucial information to the user who might be a regulatory official or medical practitioner. The ability to test for multiple targets simultaneously has obvious advantages in terms of throughput and ways by which this can be achieved will also be explored.

Whilst the priority was to design a system for the analysis of blood (plasma), there is scope to incorporate other body fluids due to the wide range of potential applications. For example, it is likely that blood samples might be recovered from a crime scene, medical patient or animal such as a racehorse, whilst urine samples are more likely to be preferred by home users of a commercial kit, or by human athletes being subjected to a drugs test. Such flexibility should enable screening for a wide range of therapeutic abuses outlawed by the World Anti-Doping Agency (WADA) regulations to evolve from the blood-based system developed here.

Given that sample preservation cannot be guaranteed in the intended settings, it would be advantageous for such an assay to overcome challenges posed by sample degradation. Therefore, the assays were designed against low molecular weight proteolytic fragments of protein targets, i.e. products of controlled protein degradation. Assaying such fragments does not necessitate structural preservation of the protein antigens and even their partial proteolysis should not affect the assay system devised. Traditional affinity assays typically rely upon relatively fragile antibodies that are themselves prone to degradation and so identifying alternative affinity reagents that can improve the stability of such assays was another key aim of this project.

1.1.3 Objectives

1. Conduct a thorough review of existing protein assay formats and methods of detection in order to determine what assays are already available, their capabilities and their limitations.

2. Select suitable targets. An integral part of developing any diagnostic system is deciding what to actually test for, and so an in-depth literature review will be carried out to identify analytes that are of interest to a number of fields, e.g. key biomarkers. Selection of peptide antigens for the chosen targets, and the generation of antibody reagents.

3. Set up multiplex affinity assays using antibodies generated. Evaluate multiplexing opportunities so that multiple analytes can be tested for simultaneously.

4. Set up lateral flow assays to determine the suitability of this format for multiplexing with quantum dot reagents.

5. Explore novel antibody-mimics that are more stable, cost-effective, and easier to produce than traditional monoclonal and polyclonal protein antibodies.

1.2 Biomolecule detection

The following sections provide a comprehensive overview of the principles and formats of immunoassays, methods of detection, and platforms for quantification, including a review of assays that are already available and their capabilities, limitations, and applications in the field of biomolecule detection.

1.2.1 Immunoassay principles and formats

Direct, competitive, and sandwich immunoassay formats

In direct binding assays, signal strength is directly proportional to the amount of antigen being assayed (**Figure 1.1 Panel A**). There remains the need to label samples and that may interfere with recognition epitopes and affect binding.

Competitive assays involve displacement of labelled analyte with unlabelled sample analyte (**Figure 1.1 Panel B**). In such a setup, the signal strength is inversely proportional to the amount of unlabelled analyte present in the sample. The major advantage here is that minimal sample preparation is required as unlabelled sample can simply be mixed with a labelled stock of known concentration prior to incubation with immobilised capture reagents. Here a decrease in signal compared with negative control signifies presence of the target in the sample.

Sandwich assays do not require direct labelling of samples, using instead a second antibody possessing specificity to a second epitope on the captured protein, which is distinct from the capture antibody (**Figure 1.1 Panels E and F**). The second antibody is conjugated to a detection molecule, i.e. either a fluorophore for primary detection, or an enzyme (e.g. horseradish peroxidase) or ligand (e.g. biotin) for secondary detection through a chemiluminescent molecule or a fluorophore. Advantages here include the freedom for molecules to bind in their unmodified native form, and the increased sensitivity achieved through amplification of the signal thus allowing lower abundance proteins to be identified. These are common techniques, widely used for half a century (Cox *et al.*, 2004; Darwish, 2006).

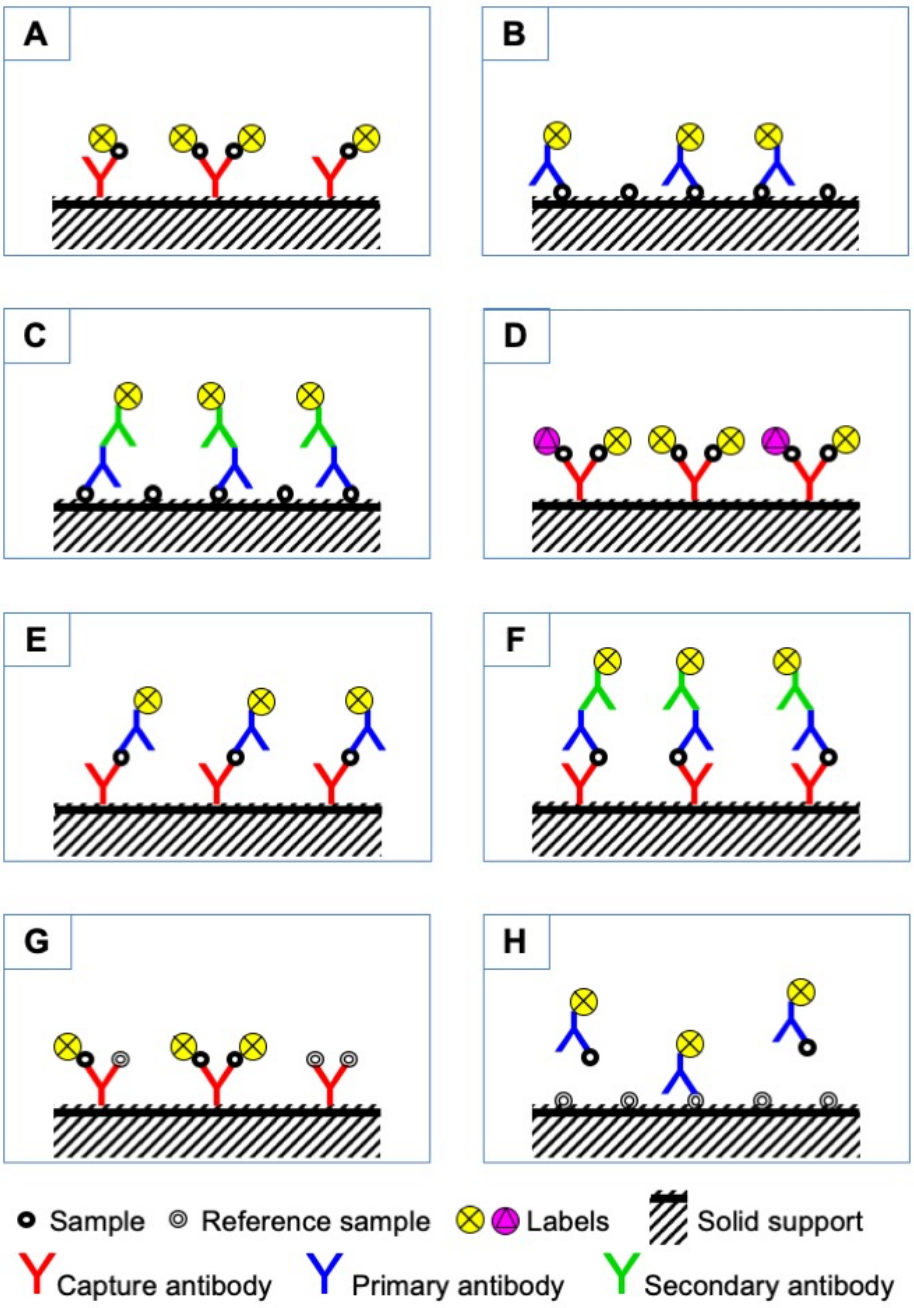

Figure 1.1 Direct, indirect, two-colour, sandwich and competitive immunoassay formats.

[A] Direct binding where fluorescently labelled sample antigen binds immobilised antibody, and **[B]** where fluorescently labelled antibody binds immobilised antigen. **[C]** Indirect binding where labelled secondary antibody is used to detect primary antibody bound to immobilised antigen. **[D]** Two-colour direct binding assay where uniquely labelled sample antigen and reference sample antigen compete for immobilised capture antibodies and ratio of the two colours infers up/down regulation of sample antigen. **[E]** Sandwich assays where antigen bound to capture antibody is detected directly by labelled antibody, and **[F]** indirectly with labelled secondary antibody that binds to primary antibody. **[G]** Competitive binding assays where sample antigen and labelled reference antigen compete for immobilised capture antibodies, and **[H]** where sample antigen and immobilised reference antigen compete for labelled primary antibody. Original figure first appeared in Soloviev *et al.* (Soloviev *et al.*, 2007).

Antigen-Antibody Binding

Immunoassays have both signal detection and signal saturation thresholds (**Figure 1.2 Panel A**). At low antigen concentrations, a signal may be undetectable due to sensitivity limits inherent to the device being used, while high antigen concentrations may saturate binding sites and prevent accurate measurements. Within these thresholds lies the measurable range of concentration (MCR) where the antigen can be both detected and quantified. The rate of reaction is directly proportional to the number of available antigen binding sites and thus the binding isotherm is not linear, meaning the whole range must be calibrated in order to accurately determine antigen concentration (**Figure 1.2 Panel A**) (Barry *et al.*, 2003).

These binding isotherms may also vary greatly between different binders of different antigens (**Figure 1.2 Panel B**), making direct binding assays unsuitable for high-throughput, multiplexed assays where multiple analytes are assayed simultaneously. Competitive assays however are not limited by antigen binding capacity in the same way that direct assays are, making them far more suited to for multiplexed assays such as microarrays where multiple antigens can be quantified simultaneously (**Figure 1.2 Panel C**) (Barry *et al.*, 2003).

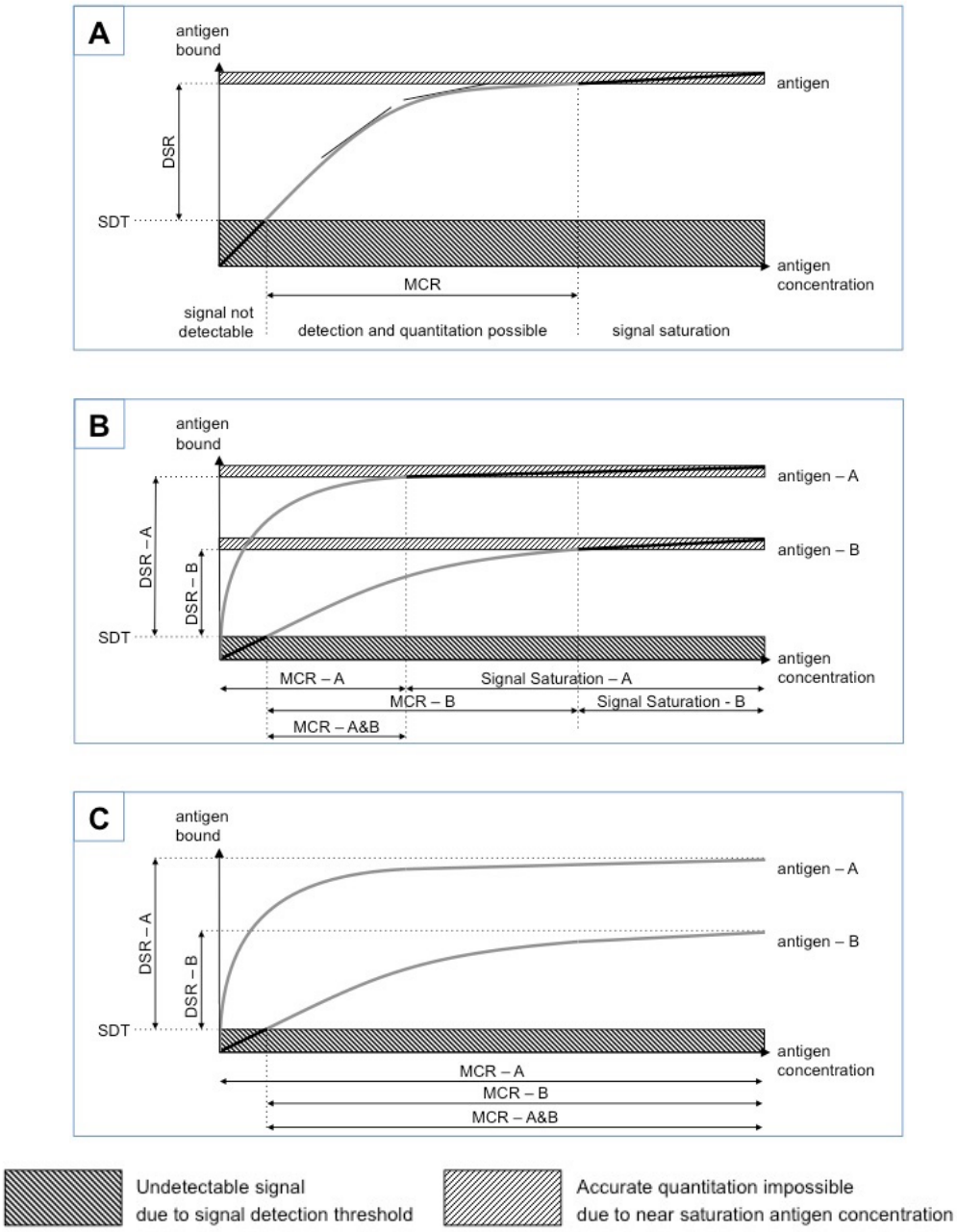

Figure 1.2 Direct and competitive antibody-antigen binding strategies.

[A] Direct binding approach – low concentrations of antigen cannot be detected below signal detection threshold (SDT) determined by the sensitivity limits of the system, and accurate quantitation of high antigen concentrations are impossible due to signal saturation, resulting in a limited measurable range of concentration (MCR). Absolute concentration can only be determined if the entire range is calibrated due to the non-linear binding isotherm. **[B]** The limitations of direct binding strategies are compounded in multiplexed systems where MCRs for multiple antigens only partially overlap, further restricting the individual MCR of each antigen in the test. **[C]** A competitive binding approach typically sees unlabelled sample antigen compete for antibody binding sites with labelled reference antigen meaning there is no signal saturation extending both the MCR and dynamic signal range (DSR). This greatly extends the ranges at which MCRs for different antigens overlap, making the competitive binding approach superior to direct binding for multiplexed affinity assays. (Adapted from figure in Barry *et al*. (Barry *et al.*, 2003).

1.2.2 Means of protein detection

Radiometric, chemiluminescence, colorimetric, fluorescence

A wide range of staining/labelling techniques are used by existing assay types to detect proteins of interest, including colorimetric (Javad Khosravi *et al.*, 1995; Garden & Strachan, 2001; Moorthy *et al.*, 2004), radiometric (Ahlstedt *et al.*, 1976; Yalow & Yalow, 1980; Raja *et al.*, 1988), fluorescence chemiluminescence-based (Rongen *et al.*, 1994a) and label-free detection methods (Jonsson *et al.*, 1991; Ylera *et al.*, 2013; Nguyen *et al.*, 2015; Yu *et al.*, 2016), each incorporating their own form of labels such as radioisotopes for radiometric tests, or organic dyes for fluorescence based assays.

There is a large selection of organic stains available with variable degrees of sensitivity of protein detection. "Stains-all" dye (1-ethyl-2-[3-(ethylnaphtho[1,2-d]thiazolin-2-ylidene)-2-methylpropenyl]naphtho[1,2-d]thiazolium bromide) is capable of detecting 5 ug if protein and can be used for the simultaneous detection of proteins (stained red), DNA (blue) RNA (purple) and polysaccharides (hue) (Green *et al.*, 1973). Coomassie series dyes bring the limit of detection down to 1 - 0.1 ug level (Wilson, 1979). Further increase in the sensitivity of detection can be achieved by using metallic stains (e.g. copper stains detect low "ng" amounts of protein in gels (Lee *et al.*, 1987), or ca 0.1-0.15 ng of protein on a membrane (Root & Reisler, 1989), whilst silver stains are capable of detecting as little as 0.1 ng protein in gels (Ochs *et al.*, 1981). In the last few decades fluorescent dyes have emerged that are quickly taking over other labelling and detection techniques (including radioisotopic labelling), largely due to the fact they are equally sensitive but safer to use and often allow for a more straightforward analysis.

The use of enhancement techniques, such as chemiluminescence based detection (Gillespie & Hudspeth, 1991; Rongen *et al.*, 1994b) and of proximity-dependent DNA ligation assays (Fredriksson *et al.*, 2002; Gullberg *et al.*, 2004), bring the detection limit down to femtomole and zeptomole level respectively (though much remains dependent on the affinity of the primary antibody-antigen recognition pair, the non-specific background staining and on the signal-to-noise ratio).

Fluorescence based detection is, at least in principle, capable of single molecule level detection (van Craenenbroeck & Engelborghs, 2000; Lebofsky & Bensimon, 2003; Willets *et al.*, 2005; Bayley, 2006; Földes-Papp, 2007; Kaji *et al.*, 2007) but typically the sensitivities are lower: e.g. fluorescamine has a 6 ng protein detection limit (Ragland *et al.*, 1974), dansyl chloride 2 ng (Talbot & Yphantis, 1971), Nile Red 1 ng (Daban *et al.*,

1991) and SYPRO orange 0.1 ng (Steinberg *et al.*, 1996). Most recently, further advances have come in the form of the highly fluorescent Alexa Fluor series (Berlier *et al.*, 2003), and fluorophores tailored to specific applications including eFluor dyes (Lekishvili & Campbell, 2018) and Super Bright polymer dyes for multi-colour flow cytometry and immunofluorescence microscopy (Belkina *et al.*, 2017), and BODIPY dyes for high performance liquid chromatography HPLC and capillary electrophoresis (Keithley *et al.*, 2013).

Gold nanoparticles

Over the last few decades gold nanoparticles (GNPs) have become popular in many areas of science and provide an attractive option for visual detection in various forms of immunoassays. Among the many reasons for their popularity in the field of medical diagnostics and biological imaging is the fact that they are non-toxic, possess extinction coefficients far greater than that of organic dyes , and can be produced simply and inexpensively in almost any lab. The simplest and most widely used method of synthesising monodisperse, spherical GNPs involves chemical reduction of tetrachloroauric acid ($HAuCl_4$) solution with sodium citrate (Bailes *et al.*, 2012b). Controlling the amount of reducing solution determines the size of the particles, which in turn determines their colour. Although the citrate method is the most commonly used, other methods of synthesis have been reported over the years (Ferrari & Soloviev, 2020). Particles with a diameter in the range of 10-50 nm appear dark red to the naked eye when monodisperse, due to localised surface plasmon resonance (LSPR), and deep purple when aggregated due to a shift in absorption wavelengths from blue to red and corresponding shift in reflected light from red to blue. To prevent aggregation and maintain dispersion in solution, particles can be coated with ligands such as DNA, antibodies or aptamers that readily adhere to the nanoparticle surface. The optical and physical properties of GNPs mean that they can be detected using a variety of methods, such as colorimetric, scanometric, fluorescence, surface-enhanced Raman scattering, and electrochemically. The simplicity and versatility of GNPs as a labelling option has facilitated the development of new assays with improved sensitivity and specificity, and widespread application for detection of a diverse range of targets including bacterial infections (Niu *et al.*, 2014), explosives such as TNT (Girotti *et al.*, 2010), markers of myocardial injury (Choi *et al.*, 2010), food toxins (Tang *et al.*, 2009), or plant viruses (Drygin *et al.*, 2009). Their biocompatibility and low toxicity has seen them widely utilised in the fields of biosensors and bioimaging, for medical diagnosis, and even the treatment of cancer (Fan *et al.*, 2020).

Quantum Dots

Quantum dots (QDs), sometimes referred to as 'artificial atoms', are highly fluorescent inorganic semiconductor nanocrystals that possess a number of unique and exciting characteristics that have seen them incorporated into a wide spectrum of biological applications and non-biological technologies (Afzaal & O'Brien, 2006; Cai *et al.*, 2006).

QDs typically range between 2 and 10 nm in diameter, corresponding to just 10-50 atoms, with a total of 100-100,000 atoms in their overall volume. It is this nanoscale size that results in the exciting properties of this special subclass of semiconductors, causing them to behave differently when compared to their larger bulk counterparts. Conventional bulk semiconductor materials possess electrons with a range of energies, and these electrons are arranged into different levels accordingly, with only two electrons able to occupy a single energy level. Because of their proximity, the energy levels in bulk semiconductors are continuous. There also exists a region of energy levels known as the bandgap that is not accessible to electrons and is unique to each bulk material. Energy levels below and above the bandgap are known as the valence and conduction bands respectively and the distance between energy levels within these bands is practically zero when compared to the size of the bandgap. The vast majority of electrons occupy the valence band in bulk semiconductors at room temperature, but the application of an external stimulus equal to or above the energy of the bandgap itself can provide some electrons with sufficient energy to cross the divide and reside temporarily in the conduction band before returning to the valence band. Whilst momentarily in the conduction band, the vacated valence band position is described as a hole. This positively charged hole and the elevated electron together are known as an exciton and the average physical separation between the electron and hole is termed the exciton Bohr radius. In bulk semiconductor material the bandgap is fixed, and the exciton Bohr radius is much smaller than the semiconductor crystal within which it is contained. However, as the size of the semiconductor crystal decreases and begins to approach that of the exciton Bohr radius, its energy levels are no longer continuous but discrete, a phenomenon referred to as quantum confinement (Brus, 1991; Takagahara & Takeda, 1992). Semiconductor crystals on the nanoscale therefore differ to bulk semiconductor material because their bandgap is not fixed, but can be tuned simply by changing the size of the nanocrystal, e.g. the bandgap energy of CdSe QDs decreases gradually from 2.6 eV to 1.75 eV as their size increases from 1.2 nm to 12 nm (Hu *et al.*, 1999). This has great importance when one considers its effects on emission wavelength. As mentioned previously, if an external stimulus provides sufficient energy it may cause an electron to jump the band gap from valence to conduction band, remaining there momentarily before returning to

the valence band and emitting electromagnetic radiation of wavelength corresponding to the energy loss during its return. Electrons tend to jump from, and to, regions of the valence and conduction bands close to the bandgap and so the ability to control the bandgap size effectively allows one to fine-tune the emission wavelength of the nanocrystal.

QDs have numerous qualities that make them ideal for superseding existing fluorescent tools in many biological imaging applications. Shortcomings of organic dyes include their pre-set emission wavelength and narrow absorption pattern that can create many difficulties in excitation of certain dyes, and their relatively broad emission spectra also limits the ability to multiplex. Limited stability due to photobleaching over extended periods of time is also a concern when using organic dyes. QDs provide a highly promising alternative to conventional dyes and exhibit a range of unique and superior fluorescent properties that allow them to overcome the aforementioned shortcomings of organic fluorophores. Because the peak emission of a QD is dependent on its composition and size, QDs can be tuned to emit at any given wavelength and have narrow Gaussian shaped emission peaks (dependent on the size distribution of the QDs). The excitation spectra of QDs are strikingly different from the excitation spectra of traditional organic dyes, with any wavelength shorter than that of the emission wavelength capable of excitation, meaning that it is possible to excite different QDs using the same excitation wavelength, creating obvious opportunities for spectrally multiplexing assays (Han *et al.*, 2001). QDs are also brighter and more stable than traditional organic dyes (Chan & Nie, 1998) with excellent resistance to chemical and photo-degradation (Wu *et al.*, 2003).

Of the various materials that can be using to produce QDs, those from periodic groups II and IV such as CdSe and CdTe with their ability to emit narrow bands across the entire optical spectrum, are best understood and most commonly used for biological applications. Furthermore, the addition of an inorganic shell consisting of material with wider bandgap to that of the core semiconductor material reduces crystal defects and imperfections on the QD surface and increases the likelihood that conduction band electrons will return directly to the valence band, thus reducing nonradiative recombination and increasing the quantum yield (QY) (Hines & Guyot-Sionnest, 1996).

The surface chemistry of QDs is crucial for making them compatible with biological applications and without which their unique optical properties would have little use in life sciences. Methods of synthesising QDs from organic solvents results in one particularly undesirable outcome: the formation of hydrophobic ligands on the shell surface, which

prevents solubilisation in aqueous environments. The solution is to either exchange these ligands for amphiphilic ones or shield them so that they are no longer a hindrance. A range of modification techniques and surface coatings are now available, enabling a wide spectrum of medical, biological and biotechnology applications. These surface chemistries must not only be robust, but versatile too in order to make them soluble in biological buffers whilst maintaining their optical properties. Surface modification also involves provision of functional groups such as amine ($-NH_2$), carboxyl (-COOH) and mercapto (-SH) groups suitable for linking proteins, peptides, nucleic acids, metabolites and other targets. The coating must also seek to maintain a small overall size for the QD particularly for live cell and *in vivo* applications where size is critical (Howarth *et al.*, 2005).

Following the advances in surface modification and the advent of water soluble QDs, their application in life sciences has been widespread both in terms of the assay formats and targets for which they have been applied to. Typical examples include the use of QDs as fluorescent biological labels instead of organic molecules (Feng & Qian, 2018), for *in vivo* imaging (Yukawa & Baba, 2017) and (Pohanka, 2017). immunochemistry applications (Vu *et al.*, 2015), in fluorescence energy transfer (FRET) applications (Geißler & Hildebrandt, 2016), for the labelling and detection of DNA (Page *et al.*, 2016), nucleic acids and protein arrays (Gibriel, 2012; Jain *et al.*, 2016) , and for multiplexed fluorescence coding and detection of molecules (Akinfieva *et al.*, 2013). At the early stages of this project few QDs were commercially available but the repertoire has expanded greatly recently and now includes a wide range of naked and modified QDs such as the Qdot range from Invitrogen that include streptavidin, protein A, biotin and a wide range of primary and secondary antibody conjugates, a wheat germ agglutinin (WGA) conjugate, and a Qtracker® range of non-targeted QDs designed to be injected into the tail vein of mice for the study of vascular structure.

1.2.3 Platforms for quantification of proteins

Affinity immunoassays in various shapes and formats have been used widely for achieving specific and sensitive detection and quantification of specific analytes.

Western Blotting

Western blotting is an immunoblotting technique which relies on electrophoretic separation of proteins with subsequent transfer of proteins to membranes (Kurien & Hal Scofield, 2015). As with other blotting techniques, western blots typically involve four stages: electrophoretic separation of sample material, transfer to membrane support, probing with affinity reagents, and visualisation of successfully bound probes. Western blotting is typically used to separate complex mixtures of proteins and to visualise specific protein on the blot. The separation step does not require prior knowledge of the protein (size-separation on the gel) but staining and detection relies on the use of specific antibodies). Whilst western blotting shows both protein size as well as protein presence, the method is generally limited to lab-based settings, requires days for completion, and the information obtained is not quantitative. Therefore, such a method is unsuitable for conducting point-of-care (POC) quantitative analyses which are typically based on affinity assays (Urusov *et al.*, 2019).

Enzyme-Linked Immunosorbent Assay (ELISA)

First used almost 40 years ago, the enzyme-linked immunosorbent assay (ELISA) has become a routine technique for the analysis and quantification of protein and peptides along with non-affinity-based chromatography and electrophoresis. ELISA tests involve the immobilisation of capture reagents or antigen on solid surface (typically the wells of a microtiter plate), followed later by detection with a capture reagent that is also bound to an enzyme capable of inducing colour change upon addition of a suitable substrate. Blocking and washing steps are critical to the method to prevent non-specific binding and to remove unbound reagents respectively. The enzymes typically used in ELISA experiments are horse radish peroxidase (HRP) and alkaline phosphatase (AP) that produce a distinct colour upon addition of suitable substrate such as 3,3',5,5'-tetramethylbenzine (TMB) or p-Nitrophenyl Phosphate (PNPP) for HRP and AP respectively. ELISAs have found numerous applications especially in healthcare and medical diagnostics, life sciences, the food industry and to a smaller degree in forensics (de Soyza, 1991). In medicine, ELISA tests may be used to diagnose a multitude of conditions including HIV (Alexander, 2016), Lyme disease (Tammemagi *et al.*, 1995), Rotavirus (Verma *et al.*, 2019), syphilis (Ji *et al.*, 2019), and Zika virus (Ehmen *et al.*, 2020; Portilho *et al.*, 2020).

Real time binding analyses - SPR (BIAcore), interferometry (BLItz), QCM and other label-free detection methods

Real time assays offer an alternative approach in which the amount of bound protein is monitored during the binding process. A number of real-time assay formats exist and are briefly reviewed below.

SPR (BIAcore)

A very popular label-free approach to assaying an analyte of interest in a sample relies on surface plasmon resonance (SPR), and the first platform to use this was a BIAcore system (Jonsson *et al.*, 1991). SPR is an optical phenomenon occurring when polarised light is reflected off a thin metal film under conditions of total internal reflection (Nguyen *et al.*, 2015). In the BIAcore system, this thin metal film composed of gold forms the floor of a small flow cell and can be modified so that antibodies are immobilised on its surface. Running buffer is passed continuously through the flow cell and a sample containing the analyte of interest can be injected into this mobile phase. Any interactions that occur between sample antigen and immobilised antibody results in a change in the local refractive index that subsequently changes the SPR angle (Leonard *et al.*, 2003). The change in intensity of reflected light is plotted against time, producing a sensorgram. The underlying principles of this technology are presented in **Figure 1.3 (Panel A)**.

Interferometry (BLItz)

Bio-layer interferometry (BLI) is another label-free technology for measuring biomolecular interactions. It analyses the interference pattern of white light reflected from two surfaces, the first being layer of immobilized protein on a biosensor tip, and an internal reference layer. The biosensor tips come in the form of disposable fiber-optic-based sensors that are coated with capture molecules and lowered into sample wells. Light is then directed down sensor and reflected back along the fiber to a spectrometer (see **Figure 1.3 Panel B**). Changes in the number of molecules bound to the biosensor tip results in a change of thickness and consequently a shift in the pattern of light interference. Importantly, the reflected interference pattern is not affected by unbound molecules, changes in flow rate or even the refractive index of the medium, permitting the use of crude samples and the ability to determine the kinetics of binding interactions (Abdiche *et al.*, 2008). This reflective interferometry technique has been commercialised by ForteBio in a range of microfluidic-free instruments. The BLItz instrument permits analysis of a single 4 uL sample, while the Octet range utilises the same technology combined with multi-well plates for significantly increased throughput (Ylera *et al.*, 2013; Yu *et al.*, 2016).

Quartz crystal microbalance (QCM)

The quartz crystal microbalance (QCM) detects very small changes of mass of the sensor in real time. It is a form of acoustic wave technology, so called because an acoustic wave is the mechanism of detection. The velocity or amplitude of the wave changes as it passes through the surface material, and such changes can be detected by measuring the frequency or phase characteristics of the sensor. Any changes can be correlated to physical interactions occurring on the surface of the sensor, such as binding of sample analyte to surface immobilised antibody, which would result in a frequency decrease due to a mass increase from the biological interactions (Thompson *et al.*, 1986; Sakai *et al.*, 1995). Such devices are classified by the mode of wave that propagates through or on the substrate, and of the many wave modes available, shear-horizontal surface acoustic wave (SH-SAW) sensors are best as biosensors due to their superior ability to operate with liquids (Drafts, 2001). A special class of these is the Love wave sensor that consists of a series of coatings on the surface of the device including a final coating with biorecognition capability. The Love wave sensor has demonstrated excellent sensitivity (Gizeli *et al.*, 1992, 1993; Kovacs & Venema, 1992; Du *et al.*, 1996) and the ability to detect anti-goat IgG in solution in the concentration range of 3 x 10-8–10-6 M (Gizeli *et al.*, 1997). QCM technology has been applied to a number of other fields such as detection of a class A drug (Attili & Suleiman, 1996) and mutations in DNA (Su *et al.*, 2004) and is commercially available from a number of providers.

QCM technology was used in another form of biosensor known as rupture event scanning (REVS). However, rather than being used to measure mass increase as is the case with other QCM based detection systems like the Love wave sensor, a piezoelectric substrate is used to detect the binding and estimate the affinity of analyte binding to antibodies covalently attached to the surface by detecting acoustic noise produced from the rupturing of bonds between antigens and antibodies. By applying an alternating voltage to gold electrodes on the upper and lower surfaces of a disk of crystalline quartz, and monotonously increasing the voltage, and thus the amplitude of the transverse oscillation of the QCM, Cooper *et al*. (Cooper *et al.*, 2001) demonstrated a novel way of directly, sensitively and quantitatively detecting virus particles bound to specific antibodies immobilised on the QCM surface. **Figure 1.3 (Panel D)** depicts the general principles involved in REVS. Both the Love wave sensor and REVS have the advantage of providing label-free detection of molecules, allowing interactions to be monitored between unmodified reactants.

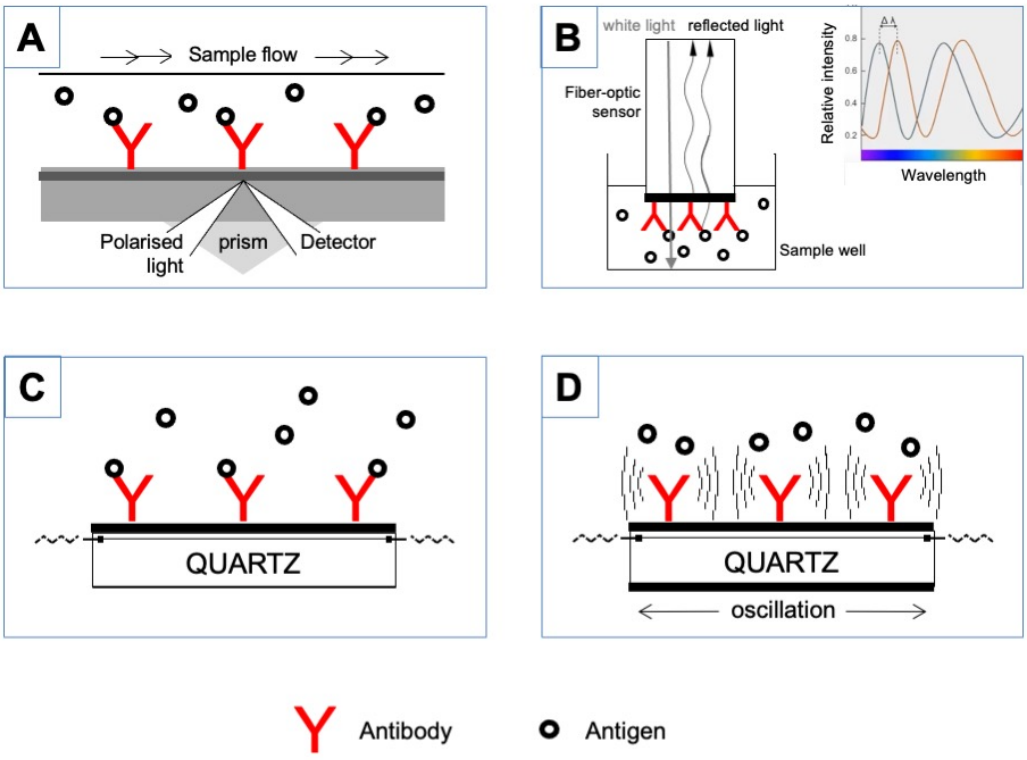

Figure 1.3 Real-time, label-free binding immunoassays.

[A] The BIAcore system detects antigen binding by way of changes to the surface plasmon resonance (SPR) of polarised light brought about by physical interactions on the surface of the sensor. **[B]** BLItz and Octet instruments are based on biolayer interferometry (BLI) where a fiber-optic biosensor tip coated with capture molecules is pushed into the sample allowing binding of analyte to the tip. Light emitted from the BLItz instrument is directed through the biosensor and reflected back. As molecules bind to the tip of the biosensor, it causes shifts in the interference pattern from the reflected light that are detected by a spectrophotometer. **[C]** The Quartz Crystal Microbalance (QCM) is a form of acoustic wave technology that detects binding interactions by monitoring changes to the frequency of and acoustic wave passed through the sensor surface, e.g. a drop in frequency corresponds a mass increase from a binding interaction on the surface. **[D]** Rupture Event Scanning (REVS) devices utilise QCM technology to detect binding reactions on a piezoelectric substrate and estimate binding affinities by analysing the noise generated from the rupturing of these bonds. Original figure first appeared in Soloviev *et al.* (Soloviev *et al.*, 2007).

Microarrays

An array is an ordered arrangement of samples immobilised on a solid substrate. Microarrays (typically hundreds or thousands of <200 um spots) have satisfied an ever-increasing market for new, miniaturised, more accurate, and cost-effective diagnostics capable of multiplexed detection, and in doing so, revolutionised the fields of nucleic acid analysis and proteomics. In the simplest of protein microarrays, a fluorescent or otherwise labelled sample is incubated with antibodies immobilised on a solid support (Haab *et al.*, 2001). High-throughput parallel protein profile studies capable of assaying thousands of proteins simultaneously on a single chip are possible by robotically arraying selected probes to bind potential targets within an experimental sample. Microarrayers fall into two classes: contact printers that utilise free-floating or spring-loaded pins that are dipped in samples (e.g. in a 96 or 384 well plate) and print by way of physically touching the target substrate; and non-contact printers that that are syringe-based or piezoelectric. Contact printers typically feature a print head with gridded pin placements for flexible configuration. Pins hang in place such that they rise up upon contact with the substrate, reducing the risk of damaging delicate surfaces and helping to increase the uniformity of prints, but are prevented from rotating due to the square profile of the pin-head (see **Figure 1.4 Panels A & B**).

There is a wide range of substrates available for proteomics microarrays including porous nylon or nitrocellulose membranes (see **Figure 1.4 Panels E-H)** gels (see **Figure 1.4 Panel C**), and metal films (see **Figure 1.4 panel D**). Desirable properties for a microarray substrate include not only its ability to immobilise the proteins of interest, but also to do so with correct orientation such that its binding sites are available for reaction. The surface substrate should also exhibit minimal non-specific binding in order that the signal:noise ratio is as high as possible.

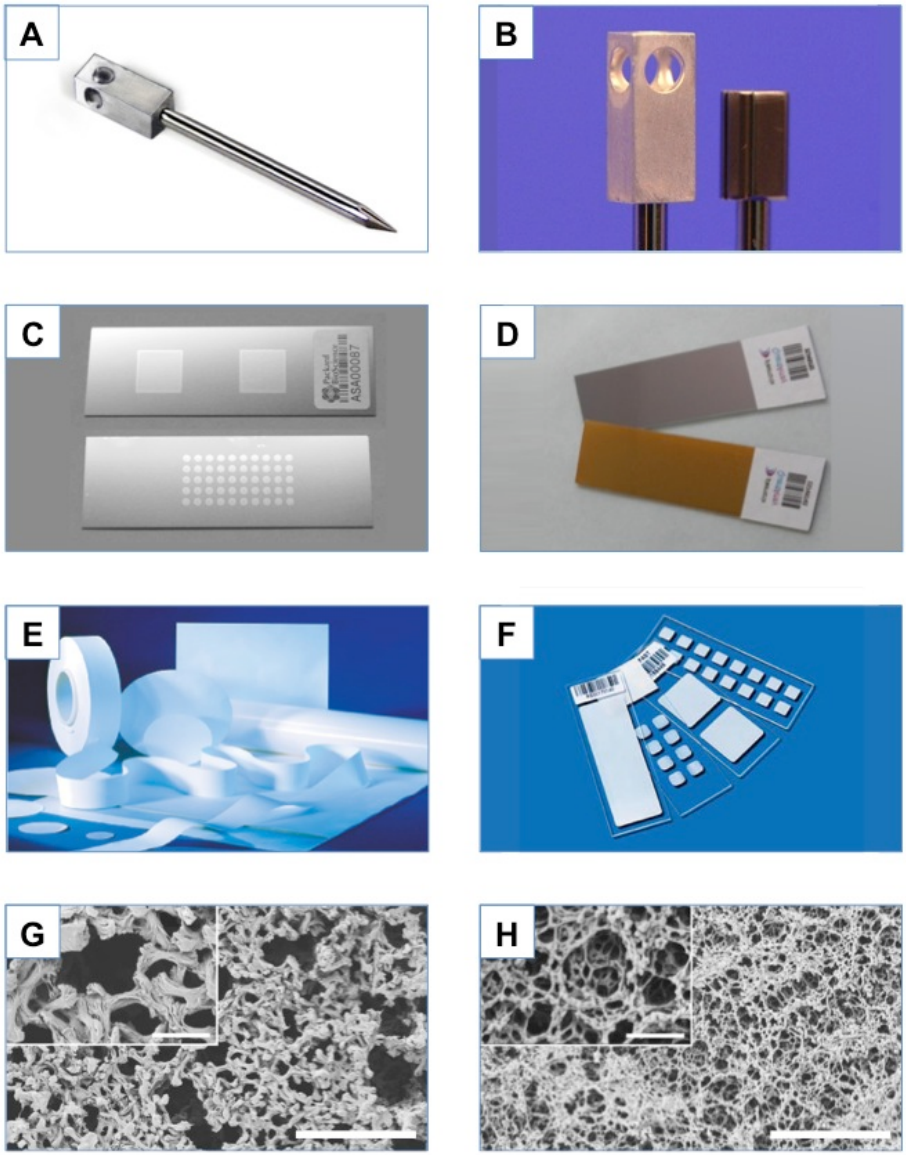

Figure 1.4 Microarray tools and substrates.

[A] Microarrayer pin used for contact printing of ligands to solid support surfaces. **[B]** Close-up of most common pin-head designs – the square head prevents rotation of the pin when assembled as a multi-pin print head, and the hole on the left pin provides an easy means of pin removal. **[C]** Polyacrylamide-based hydrogels on silicon slides suitable for both fluorescence based assays and mass-spectrometry detection were available in various formats such as 1 cm^2 (top) and 10x5 2 mm^2 (bottom) diameter spots, but are no longer commercially available – however, in-house production is feasible with straightforward methods (Fodor *et al.*, 1993; Pease *et al.*, 1994). **[D]** Slides coated with thin films of metal nanoparticles (e.g. gold or silver) enhance fluorescence signal and increase assay sensitivity via plasmonic interaction between the fluorophore and nanoparticle surface coating. **[E]** Membrane substrates such as nylon, PVDF, and nitrocellulose provide a range of surface chemistries for immobilisation of biomolecules and are available in a wide range of shapes and sizes, either backed or unbacked, or even pre-mounted on glass slides **[F]**. Scanning electron microscope images (Hirtz *et al.*, 2013) of nylon **[G]**, and nitrocellulose **[H]** membrane substrates – scale bars represent 10 um in the main images and 2 um in the insets.

Porous membranes provide a convenient support material which is strong and easy to work with but can suffer from higher non-specific binding and thus lower signal:noise results when compared with other substrates. A comparison of various membrane materials is shown in **Figure 1.5** together with evidence demonstrating the importance of cross-linking proteins using an agent such as formaldehyde prior to assaying to ensure they are not removed from the substrate during incubation and wash cycles.

Hydrogels cannot compete with membranes in terms of strength and durability, but they provide the best 3D support for the immobilisation of test molecules (whether proteins or peptides) in their native functional state in highly porous hydrogel substrate suitable for both functional assays and immunoassays (Soloviev *et al.*, 2005). When hydrated, the hydrogels swell, allowing easy access for the molecules and short diffusion times, but when dried, the gel thickness is reduced significantly, resulting in focussing of the trapped fluorescence in a thinner layer. This increases fluorescent readouts (especially on confocal scanners), whilst the background fluorescence remains extremely low (no autofluorescence and no non-specific protein sorption) (Scrivener *et al.*, 2003).

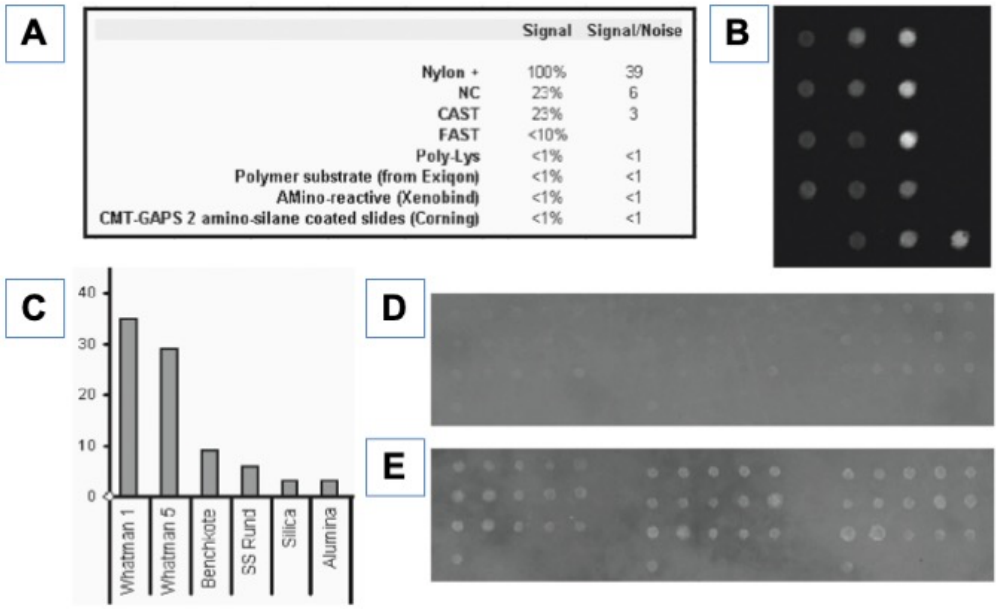

Figure 1.5 Evaluation of anti-peptide affinity array production parameters

[A] Choice of substrate: data obtained by spotting fluorescently labelled albumin onto untreated substrates. The values reflect not only the protein binding capacity of the substrate but also the fluorescence quenching by the substrate. **[B]** An example of the best substrate: Nylon membrane, immobilized onto a glass slide. **[C]** Fluorescence quenching by other (non-traditional) substrates. **[D]** The effect on signal stability when membranes are not pre-treated with a crosslinking reagent (following blocking and washing). **[E]** Membranes incubated in sealed beakers filled with undiluted formaldehyde (10 ml per 100-ml beaker volume) overnight prior to blocking and washing. (Reproduced from figure in Soloviev *et al.* (Soloviev *et al.*, 2007)).

Multiplexity is typically achieved through spatially separating antibodies on a solid support, potentially allowing thousands of proteins to be screened simultaneously on a single array. Alternative approaches for achieving multiplexity include the use of multiple fluorescent labels, each with a distinct emission wavelength, as in (Voura *et al.*, 2004). Such arrays are compatible with a direct immunoassay format where fluorescently labelled sample/antibody binds to antibody/sample immobilised on solid support and fluorescence intensity is directly proportional to the amount of sample antigen concentration, as well as competitive formats where a fluorescently labelled reference competes with sample antigen for immobilised antibodies, or where fluorescently labelled antibody is added to the sample and then the mixture is incubated with immobilised reference antigen. Both competitive formats result in fluorescence intensity being inversely proportional to sample antigen concentration.

Nucleic acid-based microarrays have proved to be powerful and convenient tools, and the potential for array-based proteomics to offer numerous advantages over 2D gels and chromatography by way of higher throughput analysis, better reproducibility and more quantitative protein expression analysis seems like a logical fit. However, protein arrays have not seen quite the same success, nor had quite such a dramatic impact, as that of DNA-based array technology. The problem here is likely due to nucleic acids and proteins actually sharing little in common and so the unsuccessful application of nearly identical techniques to both is perhaps ultimately unsurprising. Working with proteins presents a number of complications that makes designing and optimising an array system arduous when highly multiplexed assays capable of quantitatively detecting proteins are sought (Romanov *et al.*, 2014). Unlike nucleic acids, proteins possess a wider range of physical and chemical properties. For example, protein sizes span over 3 orders of magnitude - from proteins that are small and soluble (e.g. peptide hormones, cytokines of 1-20 kDa molecular weight) to extremely large ones (e.g. Titin, having molecular weight of 3 mega Da). The solubility of proteins ranges widely too - some proteins might be soluble (e.g. cytokines) or contain multiple domains of varying hydrophilicity (e.g. transmembrane receptors) or might become hydrophobic through post-translational modification such as covalent lipid attachment (Chen *et al.*, 2018).

The situation is dramatically different in the nucleic acid array field where all cDNAs are highly soluble, can be made of similar lengths and have nearly identical chemical composition. Attempting to simultaneously optimise conditions for an assay incorporating proteins with a range of physical and chemical properties is a huge undertaking and in many cases may prove too difficult. The situation with proteins is not helped by problems associated with their extraction from biological samples. Many require the presence of

detergents and are highly susceptible to denaturation and degradation (a situation quite different from the extraction and purification requirements for nucleic acids). Additional difficulties specific for protein assay fields include labelling - typically through chemical modification of reactive (usually surface exposed and immunogenic) groups, which can result in significant changes to antigen epitopes and alter reaction affinities further. This is not an issue with nucleic acids, which can be labelled at sites having little or no influence on the base pairs' recognition. The availability of capture reagents presents another bottleneck in protein affinity assays, something that does not apply to the DNA field, where all "capture" reagents can be synthesised chemically and even *in situ* in an array format (Fodor *et al.*, 1993; Pease *et al.*, 1994) at a fraction of the cost of a single monoclonal antibody development. Significant heterogeneity in affinities and the need to characterise protein capture agents also poses problems for achieving reproducible results, especially when trying to implement traditional array techniques where binding of analytes from a sample is crucial. Proteins are also susceptible to a number of external factors such as pH and temperature, which can degrade or even denature them leading to changes in protein structure. This can cause a change in antibody affinity, affecting capture and quantification of the target protein. Sample collection and preservation are two further variables that are often difficult to control. Protein extraction conditions would also vary for proteins, not least because it is highly unlikely that all cellular proteins can be solubilised and extracted in a reproducible manner each time from different samples.

Antibodies also have different and unpredictable affinities compared with DNA where affinity depends mostly on the nucleic acid length and composition, is easily predictable and also easy to engineer. Antibodies are also often cross-reactive and will recognise similar proteins that may be irrelevant to the intended purpose, and antigenic epitopes are often limited, whereas DNA often permits greater choice and so regions with little or no cross-reactivity can be selected. Finally, substantial effort may be required to experimentally identify monoclonal antibodies against different epitopes for even a single protein target, whereas DNA involves simply selecting suitable sequence fragments.

The need for portability and simplicity

There is an ever-increasing demand for smaller, more portable technologies that these established lab-based platforms are unable to meet. Lengthy turnaround times, limited throughput and the need for highly trained practitioners are all barriers to them being adopted by emerging mass markets. End-point users increasingly seek solutions that allow them to test for multiple analytes on-site, whether at a sporting event or in a hospital,

with rapid results that allow them to make decisions or a diagnosis with the confidence that such platforms are no less reliable than conventional lab-based methods. One format that appears well positioned to meet such demands is immunochromatographic assays.

Immunochromatographic assays

When designing assay formats, a trade-off often exists between increased multiplexity versus speed and simplicity. Immunochromatographic assays, otherwise known as lateral flow or strip tests, are one such example embodying speed and simplicity over high multiplexity (Andryukov, 2020). These tests are typically more user friendly and unlike SPR- and QCM-based technologies, and provide rapid results making them well suited to mass market and point-of-care kit tests. Such kits are also stable for long durations across a wide range of environments and conditions and are compatible with all major sample matrices including urine, saliva, serum, plasma and whole blood (Magambo *et al.*, 2014; Carrio *et al.*, 2015; Schramm *et al.*, 2015; Ang *et al.*, 2016; Moreno *et al.*, 2017).

Lateral flow assays are compatible with competitive and direct immunoassay formats, although in practice competitive formats are preferred because they do not require labelling or spotting of the sample prior to use, which is not at all practical in most situations where the tests are to be used. In their simplest form, lateral flow tests consist of a band of capture antibodies immobilised at a particular section along a porous membrane strip, typically nitrocellulose (although nylon, polyethersulfone, polyethylene, and fused silica are sometimes used) (Posthuma-Trumpie *et al.*, 2009). Sample is applied to one end of the membrane and diffuses along the length of the strip by way of capillary forces. A control line can be added after the capture line where a separate binding step can be designed to indicate the completion of the test [See **Figure 1.6 Panel A]**. For direct assay strips the visual presence of a capture band upon completion of the assay indicates a positive sample, whereas in the competitive format reduced colour intensity or disappearance of the capture line entirely is indicative of a target analyte's presence in the sample (Koczula & Gallotta, 2016). Reproducibility between tests is assured by using qualified, semi-automated, equipment that can quantitatively disperse reagents onto membranes in bulk and perform precise cutting of batch preparations into individual strips.

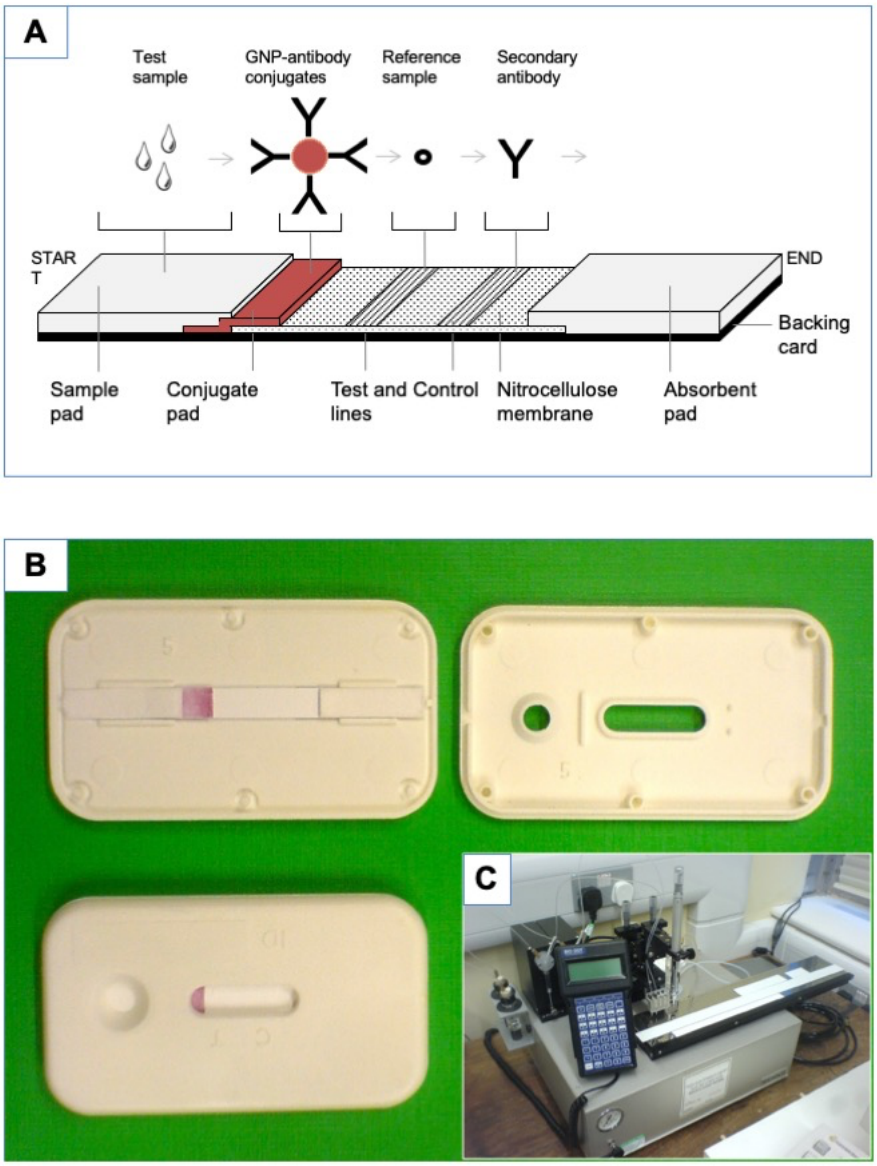

Figure 1.6 Schematic diagram of assembled lateral flow components.

[A] The sample pad is where the test sample is first deposited and regulates flow rate into the subsequent conjugate pad where it mixes with a labelled reference reagent (represented here as a GNP–antibody conjugate) that has been temporarily dried in place. Sample and labelled reference reagent diffuse along a porous membrane coming into contact with test and control lines (represented here as unlabelled reference and secondary antibodies, respectively). In this scenario an absorbent pad completes the lateral flow strip and serves to maximise the sample volume entering the membrane test strip, thus flushing through unbound detection particles, reducing background and increasing sensitivity. All components are batch assembled on an adhesive backing card before being cut into individual strips and inserted into plastic test cassettes with defined sample application and test result windows. **[B]** Photograph of fully assembled test strip inserted into plastic test case with top off (above) and on (below). **[C]** A BioDot XYZ3000 platform used to quantitatively dispense control and test line reagents onto the nitrocellulose membrane prior to assembly.

Lateral flow assays are used widely in clinical settings and for at-home testing where their ease-of-use is important. Pregnancy tests are perhaps the best known of all lateral flow assays, providing accurate results typically for just a single analyte, human chorionic gonadotropin (hCG), in urine (Cole, 2011). The Clearblue Rapid Detection Pregnancy Test delivers results as fast as one minute with over 99% accuracy (**see Figure 1.7 Panel A**). Clearblue's Advanced Digital Ovulation Test identifies the most fertile days of a female's ovulation cycle by measuring levels of luteinising hormone (LH) and estrogen in urine, helping to maximise the user's chances of getting pregnant (Clearblue - clearblue.com).

The continued development and innovation of lateral flow technology has seen a wide array of labelling and visualisation techniques be employed including liposomes that contain reporter agents such as coloured, fluorescent or bioluminescent dyes (Gussenhoven *et al.*, 1997; Ho & Wauchope, 2002; Ho & Huang, 2005), upconverting phosphors (Corstjens *et al.*, 2001; Niedbala *et al.*, 2001; Zuiderwijk *et al.*, 2003), paramagnetic particles (Ronald T. LaBorde, 2000), colloidal carbon particles (van Amerongen *et al.*, 1993; Lönnberg & Carlsson, 2001), silica particles (Xia *et al.*, 2009), electrochemiluminescent particles (Yoon *et al.*, 2003), gold nanoparticles, and even quantum dots (Goldman *et al.*, 2004). Such labels offer increased flexibility on design but often require the use of simple readers or scanners that serve to quantify endpoint measurements. In keeping with the underlying premise of lateral flow tests, such readers are usually built-in, handheld or at least portable devices that may either be necessary or optional components. Examples of such readers include those supplied by Qiagen whose portable ESEQuant Lateral Flow Immunoassay Reader is capable of colorimetric or fluorescence detection (Qiagen), as well as Detekt Biomedical and who offer a range of devices from desktop instruments to portable handheld readers and those that integrate with smartphones (Detekt Biomedical – idetekt.com) (**see Figure 1.7 Panels B, C & D**). Whilst such additional capability is not always required, it can serve to provide more quantitative results where necessary. There are many commercial examples of lateral flow test kits available embodying these advancements in rapid and convenient analyte detection, and the use of lateral flow tests is now widespread in medical establishments such as hospitals where their combination of speed and simplicity can often not only be less invasive and traumatic for patients, but also offer serious health benefits too (Andryukov, 2020).

One commercial example is the Rapid Analyte Measurement Platform (RAMP^{TM}) system by Response Biomedical Corporation that is capable of diagnosing cardiac injury by quantitatively measuring the cardiac markers creatine kinase-MB (CK-MB) and cardiac

troponin 1 (cTn1) in whole blood, as well as biodefense screening for anthrax, ricin, Botulinum toxin and pox, and infectious diseases such as the West Nile virus (Wu *et al.*, 2004). RAMP assays feature two near-identical sets of particles – test particles and internal standard particles. Both sets of particles are polystyrene, the same size, and taken from the same batch to minimise differences between the two, but house distinct fluorescent dyes. Test particles are coated with an analyte-specific monoclonal antibody, while internal standard particles are coated with a non-analyte-specific antibody and serve as an internal standard to overcome inter-strip variability. A dual wavelength fluorescent scanner is used to determine the intensity of each dye at both a test and internal standard capture lines, from which the ratio of the two is calculated and compared against calibration curves to provide an accurate measurement of analyte concentration (Kesavaraju *et al.*, 2012; Burkhalter *et al.*, 2014).

The Triage Cardiac Panel from Quidel is also capable of detecting acute myocardial infarction, providing rapid quantitative measurement of CK-MB and cTn1 as well as myoglobin in under 15 minutes with the use of a portable reader (Quidel Triage Cardiac Panel | Quidel). The Triage range from Quidel also includes a popular qualitative drugs-of-abuse panel test that is used regularly in hospitals (**see Figure 1.7 Panel E**). The Triage system uses micro capillaries to systematically control the flow of reagents through the device. W.H.P.M. offer a number of qualitative rapid one-step immunochromatographic test kits for a range of applications such as screening for drugs of abuse including amphetamines, barbiturates, benzodiazepines, cocaine, ketamine, marijuana, MDMA, methamphetamine, methadone, morphine, oxycodone, and PCP, as well as an ovulation predictor test, and a pregnancy test (W.H.P.M. Inc. - whpm.com).

Magnasense manufactures quantitative lateral flow tests based on superparamagnetic nanospheres that are comprised of a polystyrene matrix containing uniformly distributed iron oxide crystals. These nanospheres act as labels and require no optics for measurement, though a portable reader is required (Mäkiranta & Lekkala, 2005; Mäkiranta *et al.*, 2006).

DiaMondial offer a number of test kits that utilise either monoclonal antibodies conjugated to either dye or colloidal gold for the detection of Rotavirus and Adenovirus antigens, RSV antigens, Strep A antigens, and Clostridium difficile antigens. While the tests are purely qualitative, some devices offer a degree of multiplexing in that they house dual strips that can be run in parallel to test for different targets (DiaMondial - diamondial.com).

Vircell have developed a range of rapid diagnostic kits for the qualitative detection of infectious diseases including tularaemia, Epstein-Barr virus, Legionnaire's disease, and hydatidosis. These VIRapid® tests provide results within 20 minutes that can be read visually by eye or objectively with the help of a simple scanner (Vircell - vircell.com). Hydrosense also offer a rapid lateral flow test kit for the detection of *Legionella pneumophila* serogroup 1 in water with a sensitivity of 100,000 CFU/litre (Hydrosense - hydrosense-legionella.com).

Infectious disease testing comprises nearly one third of the clinical and point-of-care lateral flow diagnostics market with tests including, but not limited to, mosquito-borne diseases, influenza, hepatitis, tuberculosis, and sexually transmitted infections. BioSURE's HIV Self-Test provides simultaneous detection of HIV 1 and HIV 2 from just 2.5 ul of blood (BioSure UK - biosure.co.uk). Results are displayed on the test device for the user within minutes, are 99.7% sensitive and 99.9% specific. AAZ Labs' Autotest VIH® home testing kit offers 100% specificity (Autotest VIH - autotest-vih.eu/en/). Both tests use synthetic gp36, gp41, and gp120 as antigens, and protein A as a control line. The same barrel device that BioSURE use for their HIV test was also used for their recently COVID-19 Self-Test kit that provides qualitative detection of SARS-CoV-2 IgG antibodies from a finger prick blood sample. A binary result of one line (negative) or two lines (positive) in is obtained within 10 minutes with reported 98.3% sensitivity (CI: 90.9-100%) and 98.8% specificity (CI: 96.6-99.8%).

Lateral flow assays are also routinely used in the veterinary sector for the diagnosis of Heartworm (Dirofilaria immitis) (Mäkiranta *et al.*, 2006), feline leukaemia virus (FeLV) and feline immunodeficiency virus (FIV) (Westman *et al.*, 2016; Palerme *et al.*, 2019), rabies (Servat *et al.*, 2019), swine influenza (Le *et al.*, 2017), Salmonella (Yahaya *et al.*, 2020), Newcastle disease (Wu *et al.*, 2019), and equine infectious anaemia (Costa *et al.*, 2016), amongst others.

In the food safety sector, lateral flow assays are used to test for foodborne pathogens, toxins, and contaminants (Liao & Li, 2010), and environmental testing of air, soil and water is also commonplace.

In response to the SARS-Cov-2 coronavirus COVID-19 global pandemic there is urgent demand for testing kits that could provide rapid diagnosis and identify individuals who either needed to self-isolate in order to limit the spread of the disease or, particularly in the case of health workers, had already contracted the virus and acquired immunity and

were able to return to work. Lateral flow test kits quickly emerged as a suitable solution, providing results far faster than RT-PCR based testing that was initially adopted.

The COVID-19 Rapid Test Cassette by UK-based SureScreen Diagnostics detects the presence of IgM and IgG in a blood, plasma, or serum sample (**see Figure 1.7 Panel G**) (SureScreen Diagnostics - surescreen.com). The IgG that the test detects is specific to COVID-19, and while the IgM is a more general antibody, its presence, combined with IgG and/or the common symptoms of COVID-19, also indicate infection with the novel SARS-CoV-2 virus. There are separate test lines for IgM and IgG and visual detection of either in combination with the additional control line indicates a positive sample. A clinical study conducted in Wuhan, China compared the test cassette to conventional laboratory tests for COVID-19 diagnosis for the detection of IgG/IgM in 902 blood samples found the lateral flow test to be effective, with sensitivity > 91%, specificity > 99%, and accuracy > 97%.

Another IgM/IgG lateral flow test was developed by Li *et al*. (Li *et al.*, 2020). The test uses a nitrocellulose membrane and 40 nM colloidal gold nanoparticles as visual marker. The clinical detection sensitivity and specificity of this test were measured using blood samples collected from 397 PCR confirmed COVID-19 patients and 128 negative patients at 8 different clinical sites. Overall test sensitivity was 88.66% and specificity was 90.63%. The test is now being marketed as the COVID-19 IgM IgG Rapid Test from Canada's BioMedomics (**see Figure 1.7 Panel F**) (BioMedomics Inc. - biomedomics.com).

A start-up company created by MIT called E25Bio developed an antigen lateral flow test in conjunction with MIT's Institute for Medical Engineering and Science. When a sample is added to the strip device it mixes with a solution of SARS-Cov-2 specific antibodies conjugated to gold nanoparticles. If viral antigen is present it binds the gold conjugate antibodies and antibodies bound at the test line on the paper strip, resulting in two coloured lines for a positive test. The test takes around 15 minutes to complete. (**see Figure 1.7 Panel H**) (E25Bio - e25bio.com).

Figure 1.7 Examples of commercial lateral flow test kits and platforms.

[A] The Clearblue Rapid Detection Pregnancy Test. **[B]** The ESEQuant Lateral Flow System by QIAGEN. **[C]** The iPhone Rapid Diagnostic Lateral Flow Reader by Detekt Digital Diagnostic Solutions. **[D]** Portable lateral flow reader by Skannex. **[E]** The Triage MeterPro reader by Quidel, and Triage Cardiac Panel cassette (inset). Three of the first SARS-Cov-2 coronavirus COVID-19 rapid testing kits: **[F]** the COVID-19 IgM IgG Rapid Test from Canada's BioMedomics, **[G]** the COVID-19 Rapid Test Cassette by UK-based SureScreen Diagnostics. and **[H]** the SARS-Cov-2 Spike Direct Antigen Rapid Test (DART) by E25Bio, developed in conjunction with MIT's Institute for Medical Engineering and Science.
.

1.3 Peptide based assays

Polypeptides are short chains of between 2 to 50 amino acids and occupy a strategic position between proteins and amino acids, playing many fundamental roles by regulating the vast majority of biological processes in the animal kingdom. The range of biological activities displayed by naturally occurring peptides is truly remarkable; it ranges from toxins that can paralyse or kill, to peptides that have the ability to heal (Pennington *et al.*, 2018). The suitability of peptides as biomarkers stems from the fact that they can be produced as a result of natural, or intentional, degradation from all body fluids, cells and tissues (Schulte *et al.*, 2005; Bhalla *et al.*, 2017).

1.3.1 Peptidomics approach to proteomics

Similarly to "proteomics", the term "peptidomics" has been defined as the systematic analysis of the peptide content within an organism, tissue, or cell in order to determine peptides' identity, quantity, structure and function (Saha *et al.*, 2005). This traditional definition includes the analysis of protein degradomes, of which urine peptidomics may be a good example. The same type of analyses could be applied to artificially generated peptidomes, such as proteolytically digested proteins, protein mixtures or proteomes. In the latter case the application of alternative detection methods may be justified, such as the use of affinity regents. Such applications have been reported and by similarity to naturally occurring peptidomes were dubbed affinity peptidomics rather independently to traditional “omics” analyses of naturally occurring peptides (EP1320754B1 - Detection of peptides - Google Patents; US20020055186A1 - Detection of peptides - Google Patents; WO2002025287A3 - Detection of peptides - Google Patents; Scrivener *et al.*, 2003). Since biologically occurring peptides (whether biologically active or not) are strictly speaking also the products of proteolysis (e.g. insulin which is generated through partial proteolytic digestion of pre-pro-insulin (El-Manzalawy *et al.*, 2008) or biologically active peptides obtained through "non-specific" proteolysis of e.g. haemoglobin (Lian *et al.*, 2014), both meanings of "peptidomics" are therefore very similar in that they refer to the analysis of partially or fully proteolytically digested proteins, i.e. peptides.

Affinity peptidomics

The peptidomics approach to affinity assays requires that sample proteins be digested (e.g. enzymatically) to create a large pool of peptides prior to any affinity assays and the affinity assay is carried out using anti-peptide affinity reagents (e.g. anti-peptide

antibodies). Problems regarding the heterogeneity of anti-protein antibodies affinities and of protein antigens' physical properties, as well as the fact that proteins are prone to denaturing can therefore be addressed if proteins are first proteolytically digested in a predictable way, as in affinity peptidomics. Such digestion can be done with one or a few of the many available proteases or by using chemical digestion, but is usually and most conveniently done with trypsin, which would often yield ca 100 tryptic peptides for a 100kDa protein. This potentially allows for truly high-throughput proteomic analysis by means of a parallel affinity assay in microarray format that does not suffer from the same complications as protein arrays do because peptides are far more similar in their physical and chemical properties than intact proteins, simplifying the optimisation of assay conditions. Critically, the ability to analyse peptide pools (denatured and digested proteins) rather than proteins themselves, overcomes another major drawback of protein-based assays in that degradation and denaturation are no longer a concern because peptides are far more stable and robust than proteins. This makes the peptidomics approach far better suited to applications such as forensic analysis where one could hardly imagine that a sample always be provided in a well preserved state (let alone be "taken" and handled in a reproducible and appropriate manner). It would not be impossible to apply traditional protein separation technique or a combination thereof, followed by mass spectrometry (MS) or liquid chromatography mass spectrometry (LC-MS) approaches to analyse any particular forensic biological sample, but the methods would need to be adjusted each time, depending on the sample origin, preservation quality, etc., and would require major facilities and significant manpower. On the other hand, pre-treating samples with trypsin (or another proteolytic reagent) would lead to a much simplified extraction and assaying procedures and would yield a number of hydrophilic peptides even for hydrophobic proteins (**see Figure 1.8**), making it easier to select suitable candidates and to generate anti-peptide affinity reagents. Since each protein would yield on average 50 tryptic peptides these would provide plenty of opportunities for choosing the most suitable peptide (physical properties, synthesis, modifications, cost, etc) or even multiple peptide antigens for each protein target.

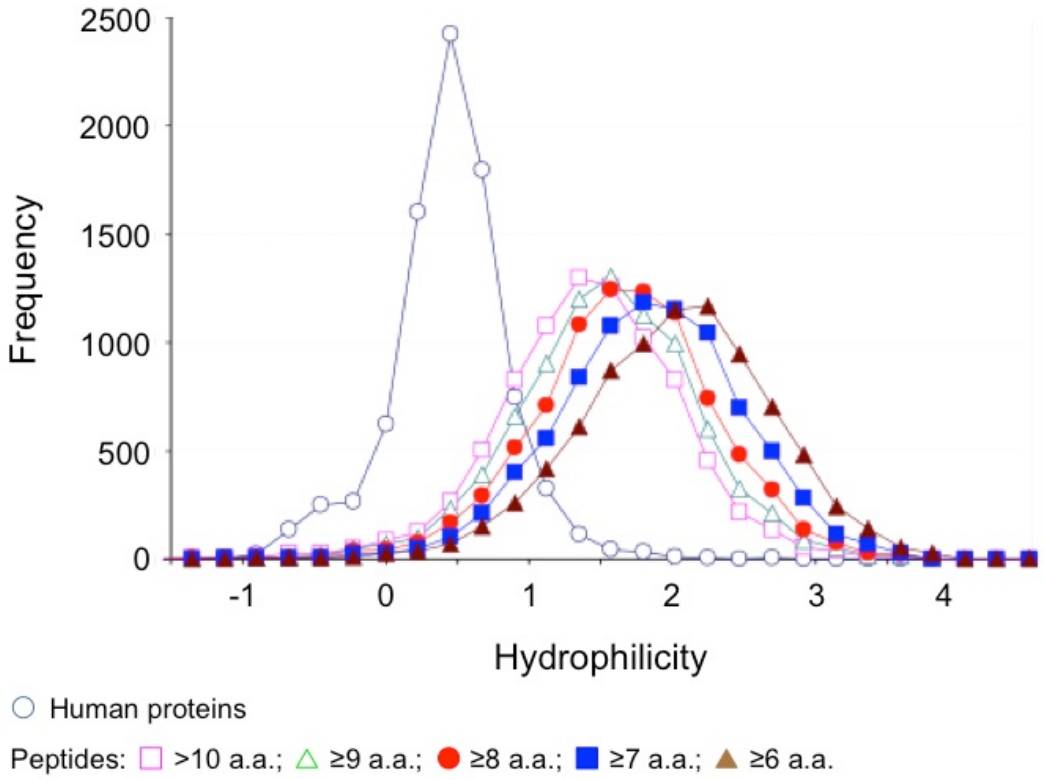

Figure 1.8 Protein vs peptide hydrophilicities.

Frequency distribution of hydrophilicities for human proteins (based on entire SwissProt database and calculated using Kyte and Doolittle weights as described in the Methods & Materials chapter of this thesis (open circles). Similarly calculated hydrophilicities for the entire SwissProt tryptic digest are shown for the best (i.e. most hydrophilic) peptides longer than 10 amino acids (open squares), 9 amino acids or longer (open triangles), over 8 amino acid long (filled circles), over 7 amino acid long (filled squares) and over 6 amino acid long (filled triangles), from each individual SwissProt human protein. The figure is based partially on Soloviev & Finch (Soloviev & Finch, 2005).

Generation of affinity reagents against proteins is a time and resource consuming process, requiring significant amounts of properly folded, often intact protein antigen itself, and such antibodies are typically against only a few strong surface epitopes with very different affinities and require extensive characterisation. Anti-peptide antibodies, whether in the form of traditional IgGs, IgG fragments, other proteinaceous affinity reagents, aptamers, molecularly imprinted polymers or other, can be produced more easily since no intact folded protein antigen is required. Contrary to these, the peptide antigens may be produced cheaply and quickly by chemical synthesis and be based on the sequence information alone. Such antigens are perfectly suitable for traditional immunisation approaches and for any other affinity selection procedures such as phage display (de La Cruzs *et al.*, 1988), ribosome display (Hanes & Plückthun, 1997), mRNA display (Wilson *et al.*, 2001) or other molecular display technologies (Fletcher *et al.*, 2003). Whilst anti-peptide antibodies are often incapable of binding to the original intact protein targets in their conformational states, these anti-peptide antibodies are perfectly suitable for anti-peptide assays. The heterogeneity of these antibody affinities is also less of a problem for peptide-based arrays, where competitive affinity assays may be used to further compensate for differences (Barry *et al.*, 2003). Displacement assay formats are perfectly compatible with such an assay and can be performed by mixing the sample digest with pre-labelled reference peptides prior to incubation with the anti-peptide antibodies (**Figure 1.9**).

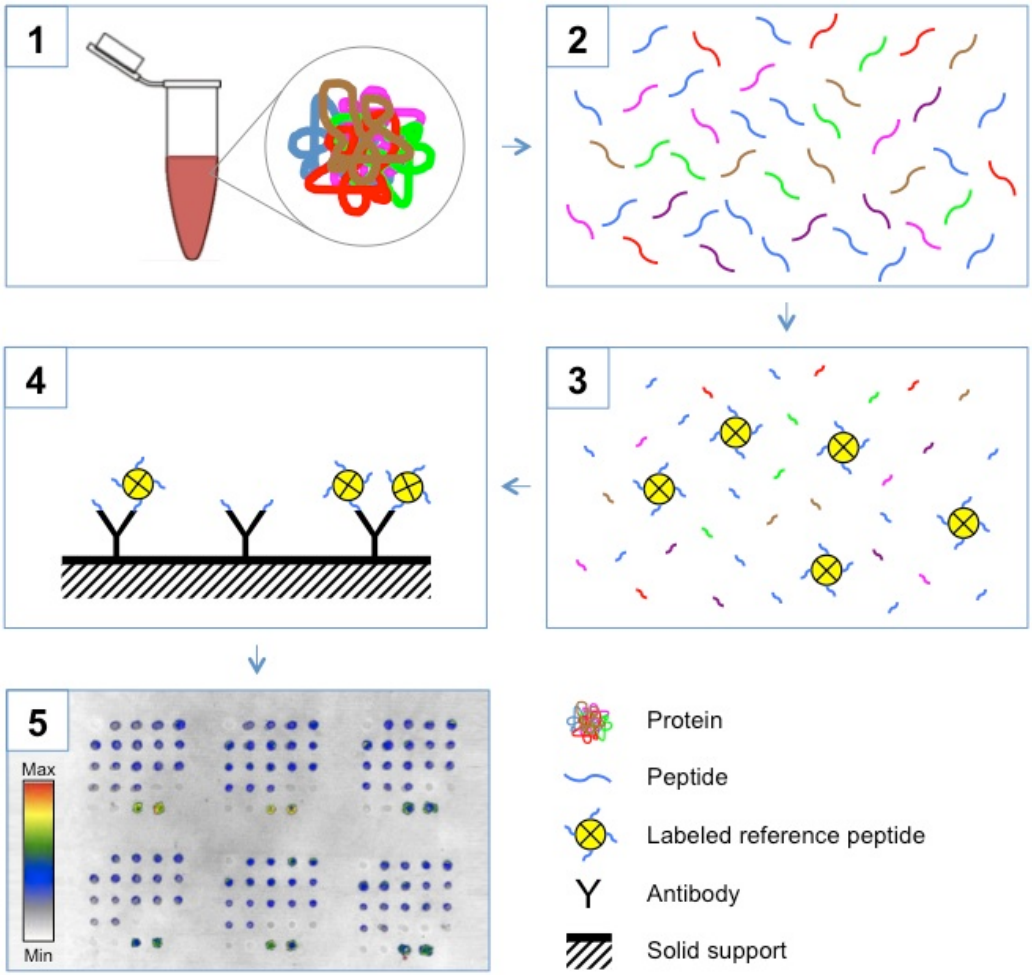

Figure 1.9 Peptidomics approach to competitive displacement affinity assays.

Sample proteins are enzymatically digested (e.g. with trypsin) to generate short linear peptides. These are then mixed with fluorescently labelled reference peptides and incubated with anti-peptide antibodies immobilised on a solid support (e.g. nylon membrane). After a washing stage the membranes are dried and scanned using a fluorescence detector. As sample and labelled reference peptides compete for binding sites, a decrease in fluorescence corresponds to higher sample antigen concentration. Original figure first appeared in Bailes & Soloviev (Bailes & Soloviev, 2007).

1.3.2 Peptide detection in diagnostics and biomarker discovery

One of the main focuses in the field of peptidomics has been the analysis of body fluids (Schrader & Schulz-Knappe, 2001) with the emphasis on diagnostics and biomarker discovery. The ability to identify biomarkers indicative of specific undesirable physiological states has generated a huge amount of interest. Biomarkers that are present at the onset of a condition and are predictive of more long-term effects are increasingly sought as they permit early diagnosis and treatment should it be necessary. Whilst many biomarker-based clinical tests already exist, they typically rely upon a single analyte (often a protein) and are conducted under conditions favourable to that protein, making high throughput multiplexing virtually impossible. Modern peptidomics approaches seek to adopt a more parallel, as opposed to serial, methodology to biomarker discovery whereby numerous biomarkers are elucidated at once without prior consideration of their potential for recognition and monitoring of a particular state.

The peptide content of biological fluids, such as urine for example, can be used to produce a complete peptidomic fingerprint of an individual's health (Metzger *et al.*, 2009). Urinary polypeptide profiles have already shown promise contributing to the existing biomarkers for coronary artery disease (CAD) (Zimmerli *et al.*, 2008), diagnosis and progression of renal and urogenital conditions (Fliser *et al.*, 2005; Julian *et al.*, 2007b,a; Zürbig & Mischak, 2008), and cancer diagnostics (Theodorescu *et al.*, 2005, 2006).

Serum is a rich source of biological material and represents one of the most attractive type of samples. Widely available in clinics, it contains a plethora of disease related biomarkers including proteins and peptides and therefore represents one of the most interesting models for peptidomic analysis. Of the tens of thousands of proteins and peptides present in human sera, only ~20 are highly abundant, representing a staggering 99 % of its proteinaceous content. The remaining 1 % consists of a wide range of molecules, including hugely important ones such as hormones and growth factors, many of which weigh in well under 10 kDa in size. Despite their small size and relatively low abundance, such molecules could represent ideal biomarker candidates of major biological significance even if such polypeptides only result from partial degradation of larger proteins by various proteases. Protein fractionation using size exclusion chromatography or ultrafiltration have been used to isolate the low molecular weight proteinaceous content of serum prior to analysis (Tirumalai *et al.*, 2003; Zheng *et al.*, 2006). Undoubtedly, future work will need to focus on firmly identifying which peptides represent disease-specific proteolysis in order to establish useful biomarkers.

In forensics, traditional techniques for analysing crime scenes are centred on retrieval of DNA with the hope of identifying an individual by matching the data with that in a database, but given that the United Kingdom National DNA Database (NDNAD) covers less than 10% of the population (5.86 million people as of 2016) the chances of obtaining such a match are optimistic at best. Peptidomics aims at building protein and metabolite profiles from forensic samples to establish biometric and behavioural profiles to gain a better understanding of the victim and events and to narrow down lists of potential suspects. Forensic samples are unlikely to be provided in a highly preserved state, with collection and handling may also not have been carried out reproducibly. However, unlike DNA which may help in the identification, proteins and metabolites could provide much needed insight into biochemical, nutritional, behavioural and lifestyle patterns. Not only are proteins representative of the health, disease and lifestyle states of an organism, they constitute the largest type of biopolymers in the human body by mass (~20%) and therefore represent the most attractive, albeit difficult, markers to work with. The affinity peptidomics approach addresses the major remaining problems of proteins (Scrivener *et al.*, 2003), needing no major changes to traditional affinity assays and simply requiring samples to be treated with a proteolytic reagent such as trypsin prior to antibody array-based detection. One additional advantage is that such pre-treated samples are also compatible with well-developed MS-based approaches. Affinity peptidomics is a robust approach that is one of the most favourable options in cases where sample preservation is likely to be difficult, such as forensic samples or aged specimens. Another advantage of peptide-based affinity assays is that a larger choice of potential antigens becomes available for virtually any protein, even if such a protein belongs to a family of structurally related and similarly folded proteins which may not be easily distinguishable by antibodies in their folded state. In contrast, even a single amino acid difference may result in substantial discrimination between otherwise identical peptide sequences.

The ability to analyse peptide pools and determine differential expression of both naturally occurring peptides and those predictably produced from deliberate enzymatic digestion promises much by way of identifying and detecting biomarkers indicative of a range of conditions. These biomarkers must be unambiguous in their indication, able to convey the severity or stage of the condition they represent, simple to detect and consistent across populations, i.e. not resigned to just a single subject. Peptide biomarkers are unlikely to be indicative of a condition individually, but rather changes in the expression or secretion profile of multiple peptides is a more realistic objective to aim for. While there appear to be many examples of peptidomic analysis contributing to multiple fields (Agyei *et al.*, 2018; Conlon *et al.*, 2019; Lee *et al.*, 2019; Sirolli *et al.*, 2020), the vast majority of these studies rely on sophisticated technologies such as LC-MS or

CE-MS (Latosinska *et al.*, 2019; Ziganshin *et al.*, 2019), requiring expensive equipment and highly trained staff in centralised laboratories. The development of an assay incorporating the power and flexibility of the affinity peptidomics approach but utilising a more portable assay system that is simpler to operate and generates more rapid results could prove extremely useful.

1.4 Affinity reagents

Ideally a series of affinity reagents would be available for each and every protein in any given proteome including their various post-translationally modified variations and cleavage products, would exhibit minimal cross-reactivity, be stable across a range of conditions, and be cheap to produce with zero batch-to-batch variability. Whilst this ideal scenario may not be on the immediate horizon, novel methods of identifying and generating affinity reagents that meet many of these desirable features are expanding the available toolset. Types of affinity reagents as well as their respective pros, cons, and suitability to the aims of this project will now be examined.

1.4.1 Traditional affinity reagents

Anti-peptide antibodies for peptidomics affinity assays

Generating antibody affinity reagents for use in peptidomic affinity assays is overall advantageous compared to raising anti-protein antibodies. Peptide antigens can be designed based on the sequence information alone and generated by reproducible chemical synthesis. The purity will often exceed that of native or recombinantly generated full-length protein antigens and unlike larger proteins, peptides will be less susceptible to inadvertent and often irreversible unfolding and denaturing. Target peptide selection involves selecting an appropriate protein target and then choosing a suitable proteolytic peptide to be used as an antigen for generating affinity reagents. In the past, many tools for predicting the antigenicity of proteins and antigenic epitopes were reported, e.g. SYFPEITHI (Rammensee *et al.*, 1999), MHCBN (Bhasin *et al.*, 2003), Bcipep (Saha *et al.*, 2005), The Immune Epitope Database (IEDB) (Vita *et al.*, 2009), ABCpred (El-Manzalawy *et al.*, 2008), EPMLR (Lian *et al.*, 2014), and Lbtope (Saha & Raghava, 2007). Such tools were developed to facilitate the prediction of peptide antigens for generating antibodies capable of detecting the original natively folded antigens, not just the peptides used for immunisation. None of the tools though appear to be suitable for predicting, selecting and ranking proteolytic peptides for the development of anti-peptide antibodies. Many of the tools reported so far rely heavily on protein structural information or aim to identify solvent-exposed linear epitopes based on protein structure and may not select sequences that are "antigenic" but are not fully solvent exposed. Such tools have only limited usability in the analysis of proteolytic peptides for their antigenicity. However, some limited yet clear correlation exists between tryptic peptides' amino acid composition and their ability to generate strong polyclonal

serum, as will be discussed in Chapters 3 and 4. However, parent protein structure, folding and fragment solvent exposure play no role in determining tryptic peptides' antigenicities.

While antibodies have undoubtedly contributed much to biomolecule analysis they are not without their shortcomings. Cross-reactivity, while an evolutionary advantageous in-vivo for combatting related pathogens, is not so desirable for assaying specific antigens where specificity is key. Antibodies themselves are also susceptible to the same degradation factors as other proteins with excessive freeze/thawing or improper storage conditions causing structural conformation changes that can have devastating implications in terms of their ability to bind target antigen molecules effectively (le Basle *et al.*, 2020). There are a number of drawbacks inherent to the production of antibodies in animals, not least the potential for contamination with animal proteins, and the inability to generate antibodies against antigens that are toxic and may result in the death of the host before the antibodies can be produced. The reliance on animal subjects to produce these reagents is also coming under increasing criticism from an animal welfare perspective now that non-animal-derived alternatives are becoming more readily available (Gray *et al.*, 2020).

1.4.2 Recombinant affinity reagents

As the understanding of human and other species' proteomes increases so does the demand for more renewable affinity reagents that match an increasingly expansive list of target antigens, and overcome the aforementioned issues associated with traditional antibody-based affinity reagents. There are a variety of recombinant affinity reagents that can be produced *in vitro.*

Recombinant antibodies

Antibody fragments retain antigen binding capability, these include: Fab' (with thiol groups), Fab (lacking thiol groups), and Fv fragments (**Figure 1.10 Panels B to E**). Fab fragments can be obtained via either recombinant synthesis (Choe *et al.*, 1994) or by proteolytic cleavage of a whole antibody (Ryan *et al.*, 2008), while Fv fragments can only reliably be synthesised via recombinant methods (Ward, 1992). Fv fragment consist only of the variable domains of a heavy and light chain and as such are held together by relatively weak interactions. More stable modifications of these fragments have been produced including disulphide stabilised Fv (dsFv) and single chain Fv (scFv) molecules, the latter of which include a linker peptide between the heavy and light chains and have seen the widest adoption (Reiter *et al.*, 1994; Tsumoto *et al.*, 1998). Many antibody fragments are currently available from a range of companies for diagnostics and therapeutics applications including Adalimumab (Humira) from Abbvie primarily for the treatment of arthritis, Nivolumab from Bristol-Myers Squibb, Pembrolizumab from Merck & Co and Trastuzumab from Roche for the treatment of various cancers, and Infliximab from Johnson & Johnson primarily for Crohn's Disease (Lu *et al.*, 2020).

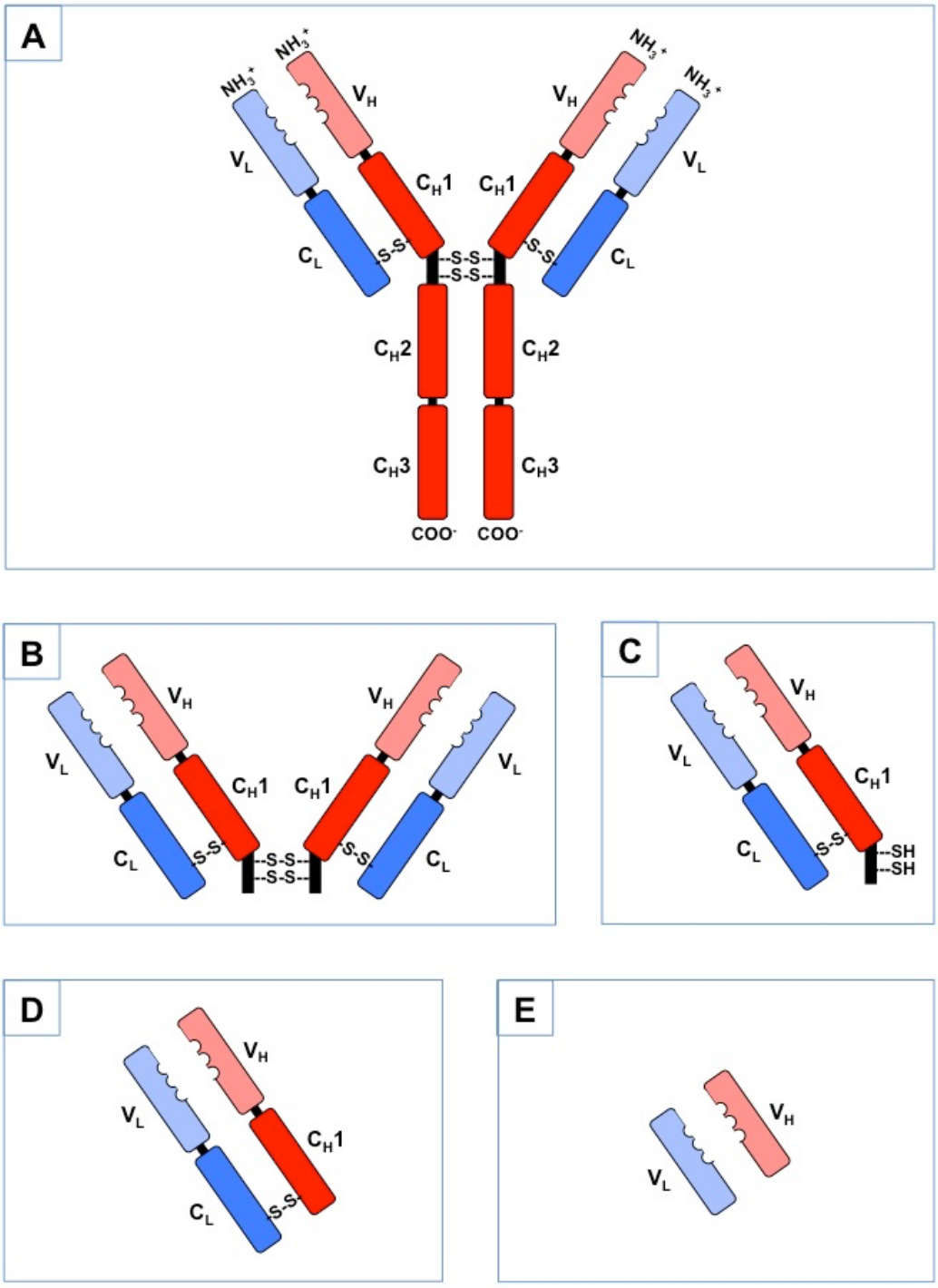

Figure 1.10 Structure of immunoglobulin G (IgG).

[A] Whole antibody with two heavy (H) and two light (L) chains, each with constant (C) and variable (V) domains; disulphide bridges in the hinge region between the two heavy chains, and between the constant domains of the heavy and light chains **[B]** F(ab')$_2$ fragment following proteolytic cleavage of heavy chain domains **[C]** Fab' fragment (with thiol groups) and **[D]** Fab fragment (without thiol groups) following proteolytic cleavage with papain **[E]** Fv fragment consisting only of variable domains of the heavy and light chains.

There exists a range of molecular display technologies used to identify and generate these novel recombinant affinity reagent molecules, including bacterial systems such as E. coli, phage display (de La Cruzs *et al.*, 1988), ribosome display (Hanes & Plückthun, 1997), mRNA display (Wilson *et al.*, 2001) and yeast (Gera *et al.*, 2013) amongst others (Fletcher *et al.*, 2003).

Phage display is a molecular display system suitable for generating scFv reagents and involves libraries consisting of billions of clones, e.g. the human single chain antibody libraries from Creative Biolabs that range from $1.42x10^9$ to $2.36x10^{10}$ clones. Clones are modified so that surface proteins of interest on the phage coat and can be screened against an antigen of interest. Screening involves incubation of the phage library with antigen immobilised on a solid support, typically the wells of a microtiter plate. A panning stage sees phages displaying non-specific antigen affinity reagents washed away, followed by the elution of specific affinity reagents that are then amplified by infection into a bacterial host. Following multiple panning rounds, the resulting affinity reagent DNA is sequenced, and the encoded protein can be recombinantly expressed (Messmer *et al.*, 2000; Kay *et al.*, 2001; Noren & Noren, 2001). Phage display technology has been used in the past to generate therapeutics including Humira which is prescribed for the treatment of rheumatoid arthritis and is the most successful recombinant therapeutic antibody to date (Krupanidhi; Kempeni, 1999; Winter, 2019).

scFv fragments have been used in QCM sensors where they were used to detect parathion immobilised on gold-coated disks (Horáček *et al.*), and where the scFv fragments have themselves been immobilised and used for the detection of cholera toxin (Larsson *et al.*, 2005) and cowpea mosaic virus (CPMV) (Torrance *et al.*, 2006). They have also been used in SPR-based assays for the detection of avian influenza virus neuraminidase (NC10) (Pearce *et al.*, 1997), and morphine metabolites (Dillon *et al.*, 2003), florescence based immunoassays for the detection of Bacillus anthracis protective antigen (PA) (Wang *et al.*, 2006) and electrochemical sensors for the detection of E.histolytica antigen (EHA) in stool samples (Grewal *et al.*, 2013).

Nucleic acid aptamers

Aptamers are sometimes referred to as chemical antibodies due to the fact that they are synthetically produced single chain RNA, DNA or PNAs that are capable of folding into unique molecular shapes and thus designed to mimic the specificity of antibodies. The affinities (K_D) between aptamers and their antigen epitopes are comparable and may be

better than those of monoclonal antibodies (Jayasena, 1999). The production process of nucleic acid aptamers was coined as the “systematic evolution of ligands by exponential enrichment” (SELEX) by Tuerk & Gold (Tuerk & Gold, 1990). This initial process can be quite costly and time consuming, involving the screening of huge pools of nucleic acid libraries to elucidate those that bind to the antigen of interest, followed by several rounds of amplification and enrichment. However, once the aptamer sequences have been determined, subsequent chemical synthesis is relatively straightforward and fast – this combined with the absence of animal dependent stages in their production make them an attractive alternative to traditional polyclonal and monoclonal antibodies. Like scFv fragments, aptamers have also proven to be versatile in their coupling to a range of surfaces and other reagents, including GNPs (Pavlov *et al.*, 2004) and QDs (Hansen *et al.*, 2006). While such nucleic aptamers have the ability to regain their analyte binding ability after denaturation and can be stored for relatively long period of time (vs their Fab’ or scFv fragment counterparts), aptamers are susceptible to nuclease degradation in serum. This can be overcome with modifications to the oligonucleotide chains, or potentially by treating samples with enzyme inhibitors prior to the introduction of aptamer affinity reagents. An interesting feature of DNA based aptamers is the ability to remove them from their target using DNA nucleases, essentially restoring the target to its label-free condition (Terazono *et al.*, 2010).

Peptide aptamers

Another class of biomolecule might stand to supersede those listed thus far and despite much of the initial focus on them being directed towards their use as protein silencing tools *in vivo*, peptide aptamers have potential application as diagnostic tools for biomolecule identification. Peptide aptamers typically exhibit a smaller binding footprint allowing for more precise interrogation of the target compared to DNA-based probes (Hamdi & Colas, 2012).

Peptide aptamers are made up of short, 5-20 amino acid residues long sequences, that are usually embedded as a loop within a stable protein scaffold, also known as a “loop on a frame” design (Colas *et al.*, 1996). With their short single strands of amino acids that exhibit little to no secondary structure, peptides are not susceptible to the same denaturation risks as proteins or nucleic acids and are also easy to generate once the sequence is known. The scaffold provides important conformational constraint, whereas the peptide loop provides the variable region for selection against a target of interest.

Scaffolds should be soluble, non-toxic and capable of high-level expression in prokaryotic systems. The range of scaffold designs available today is diverse and includes thioredoxins, monobodies, anticalins, Kunitz domains, avimers, knottins, fynomers, and atrimers, whereas scaffold designs containing rigid combinatorial motifs include Designed Ankyrin Repeat Proteins (DARPins), affibodies, affilins, armadillo repeats, and OBodies (Reverdatto *et al.*, 2015).

Selection techniques can be divided into two classes, either *in vitro* methods such as phage display, cell surface display, ribosomal display, mRNA display, DNA display, or *in vitro* compartmentalisation, or in-cell selection methods such as the Yeast two Hybrid (Y2H) screen (Hamdi & Colas, 2012).

Faster, easier and less expensive to discover and manufacture, the flexibility of peptide aptamers has seen them rapidly being applied to biomedical therapeutics and diagnostics and bioanalytical applications that have traditionally been dominated by antibodies and nucleic acids aptamers (Wurch *et al.*, 2012; Banta *et al.*, 2013; Mintz & Crea, 2013; Weidle *et al.*, 2013).

Peptide aptamers have been developed for the treatment of cancers (Boersma & Plückthun, 2011; Emanuel *et al.*, 2011; Tolcher *et al.*, 2011; Weidle *et al.*, 2013; Lorey *et al.*, 2014; Richter *et al.*, 2014) , stimulating T-cell responses (Schönfeld *et al.*, 2009), asthma (Wurch *et al.*, 2012), age-related macular degeneration and diabetic macular edema (Zahnd *et al.*, 2010), Crohn's disease (Silverman *et al.*, 2005), hereditary angioedema and prevention of blood loss in cardiothoracic surgery (Nixon *et al.*, 2014). Whilst poor therapeutic agents due to their tendency to generate immune responses, affibody scaffolds have been applied to bioimaging applications where their small size and fast renal clearance is advantageous and has permitted high contrast cancer imagery (Baum *et al.*, 2010).

1.5 Insulin-like growth factor-1 (IGF-1)

Insulin-like growth factor-1 (IGF-1) plays an important role in cell proliferation, differentiation, and apoptosis, regulating normal growth during childhood and having a strong anabolic effect in adults. Originally reported as "sulphation factor" in 1957 by Salmon & Daughaday (Salmon & Daughaday, 1957), and later as non-suppressible insulin-like activity (NSILA) by Froesch *et al.*in 1963 (Cappa *et al.*, 2009) and

"somatomedin" by Daughaday *et al.* in 1972 (Froesch *et al.*, 1963), the term IGF-1 was eventually coined by Rinderknecht & Humbel in 1976 (Rinderknecht & Humbel, 1976).

Structure, function, and mode of action

IGF-1 is a 70 amino-acid single chain peptide with a molecular weight of 7649 Da (**Figure 1.11**) (Sato *et al.*, 1993). It contains 3 disulphide bridges, between amino acids 6 and 48, 18 and 61, and 47 and 52, that create tertiary structure critical for optimum binding to the IGF-1 receptor (IGF-1R) (Owers-Narhi *et al.*, 1993). As its name suggests, IGF-1 is structurally similar to insulin and is capable of binding the insulin receptor (I-R), albeit at a lower affinity than to its own. IGF-1 in the principal mediator of growth hormone (GH) and plays a crucial role in promoting cell growth and differentiation in childhood and continues to have an anabolic effect in adults. When GH is produced by the anterior pituitary gland, its release into the bloodstream stimulates the production and release of IGF-1, which subsequently binds to the IGF-1 Receptor (IGF-1R) displayed on the surface of nearly every cell in the body. The IGF-1R is comprised of two alpha and two beta subunits linked by disulphide bonds. The transmembrane beta subunits each have intracellular tyrosine kinase domains that are activated upon binding of IGF-1 to the extracellular alpha subunits. Activation of these kinase domains results in phosphorylation (Kato *et al.*, 1994) and activation of multiple signalling pathways including the PI3K/Akt pathway and the Raf/MEK/ERK cascade that ultimately prevent apoptosis and promote cellular growth and survival (Gusscott *et al.*, 2016). Controlling these critical pathways means IGF-1 and its receptor IGF-1R play a pivotal role in healthy tissue homeostasis, but also a far less desirable role in diseases such as cancer where they can be responsible for the survival and proliferation of malignant cells. IGF-1 acts mostly as an endocrine hormone secreted primarily by the liver (Sjögren *et al.*, 1999; Yakar *et al.*, 1999) and transported to target tissues, but is also produced by tissues outside the liver where it acts locally in a paracrine fashion. It is also believed to play an important autocrine role in cancer (Baserga, 1999).

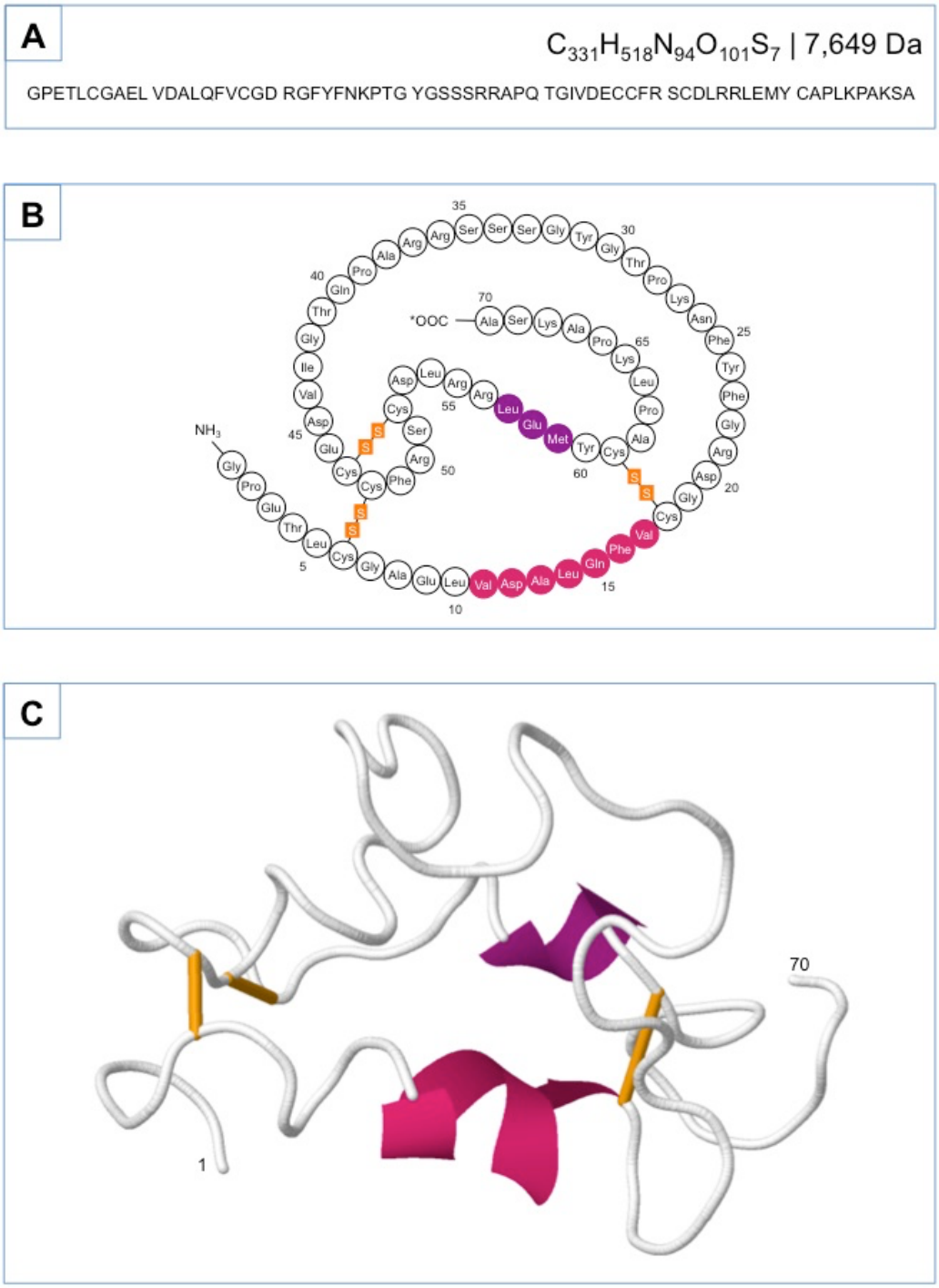

Figure 1.11 Structure of human insulin growth-like factor 1 (IGF-1).

[A] Primary structure, chemical formula, and molecular weight of human IGF-1. **[B]** Secondary structure detailing disulphide bridge between amino acids 6 and 48, 18 and 61, and 47 and 52. **[C]** 3D tertiary structure showing folding of the polypeptide chain and secondary structural elements as ribbons in pink and in purple. Image from the RCSB Protein Data Bank of PDB ID 1BQT (RCSB PDB - 1BQT: Three-dimensional Structure Of Human Insulin-like Growth Factor-I (IGF-I) Determined By 1H-NMR And Distance Geometry, 6 Structures; SATO *et al.*, 1993).

Related growth factors and IGF binding proteins

IGF-1 is part of a wider network of growth factors, receptors, and binding proteins involved in mediating cellular proliferation, differentiation, and survival (**Figure 1.12**).

IGF-2 is a closely related protein to IGF-1 and in addition to being the sole ligand of the IGF-2 receptor (IGF-2R), also has affinity for the IGF-1 receptor (IGF-1R). However, whilst the IGF-1R is capable of signal transduction, IGF-2R is not and binding results in lysosomal degradation of IGF-2. This provides an indirect method of IGF-1 regulation by regulating the level of IGF-2 that is available to bind to the IGF-1R.

Another set of related molecules that play a major role in the bioavailability of the IGFs are insulin-like growth factor binding proteins (IGFBPs). These regulating proteins bind to IGF-1 in circulation with equal or greater affinity than that of the IGF-1R (K_d ~10^{-10}M vs K_d ~10^{-8} - 10^{-9}M, respectively) (Kuemmerle, 2012; Clemmons, 2018). There are six IGFBPs, binding approximately 98% of all circulating IGF-1, and serving as carrier proteins to regulate its transport and lengthen its otherwise comparatively short half-life (Jones & Clemmons, 1995). Of the six known IGF-BPs, IGFBP-3 is by far the most common, accounting for around 80% of all bound IGF-1, typically forming a 150kDa tri-molecule complex with it and the acid-labile subunit (ALS), known as the IGF-IGFBP-ALS complex (Baxter, 1988). By binding IGF-1, IGFBPs play a critical role in regulating its action and consequently cellular homeostasis. The up/down regulation of these important proteins is a complicated aspect of the IGF-signalling pathway and has yet to be comprehensively defined. Their action can be either IGF-dependent or independent and altered by various post-translational modifications. Such variations in IGFBP expression profiles have themselves been suggested as suitable markers for serious clinical conditions and even as potential therapeutics (Durai *et al.*, 2007).

The superfamily of IGF binding proteins extends to a further ten proteins known as IGFBP-related proteins (IGFBP-rPs) that also have affinity for the IGFs, albeit at much lower affinities than the IGFBPs (Hwa *et al.*, 1999; Shibata *et al.*, 2004). The justification for their nomenclature has been questioned on the basis of their low affinity for IGFBPs, questionable ability to significantly influence IGF effects, and the fact they share limited phylogenetic relationship with other members of the family (Rodgers *et al.*, 2008).

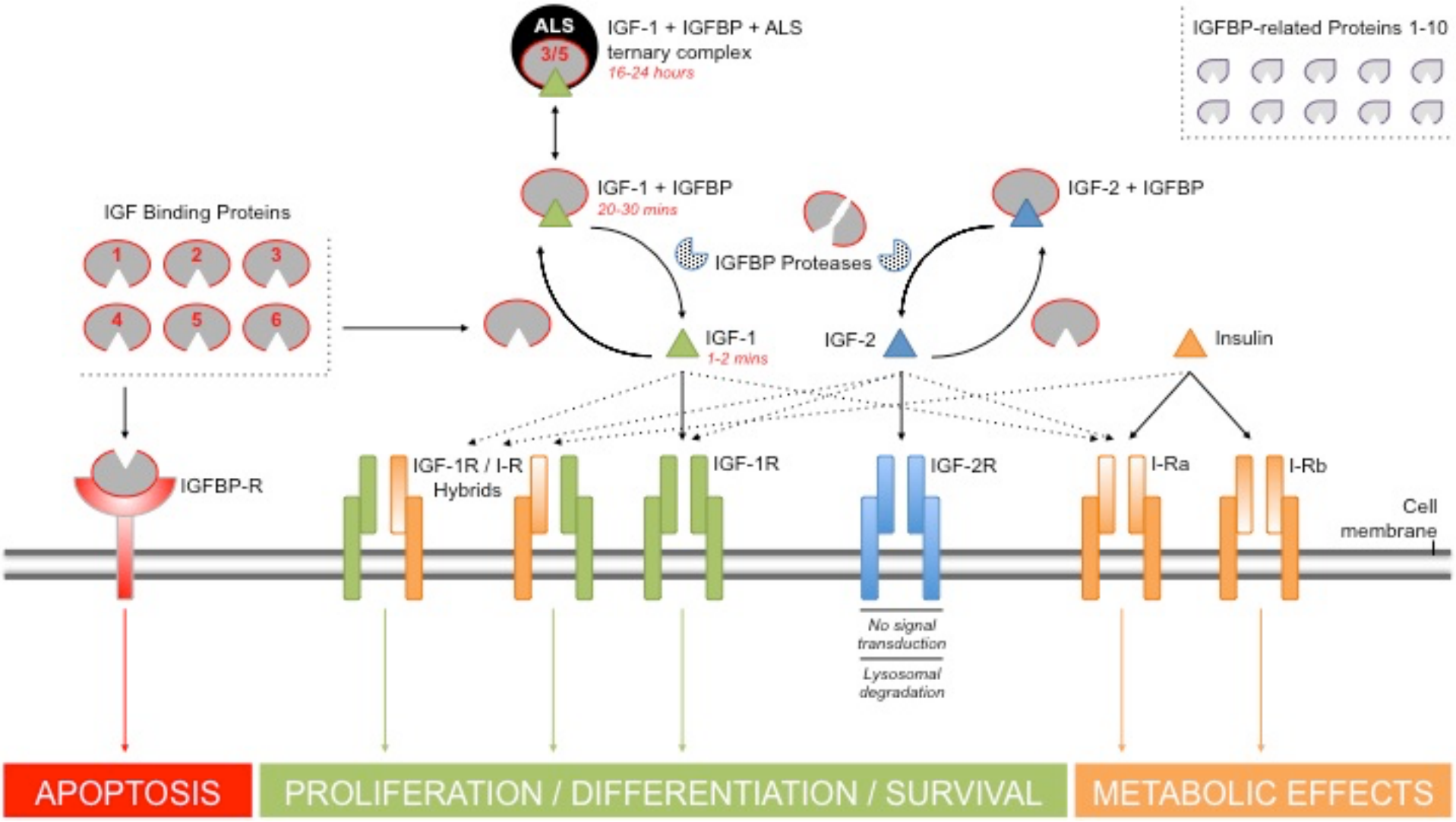
ALS
3/5
IGF-1 + IGFBP + ALS
ternary complex
16-24 hours
IGFBP-related Proteins 1-10
IGF-1 + IGFBP
20-30 mins
IGF-2 + IGFBP
IGF Binding Proteins
1
2
3
4
5
6
IGFBP Proteases
IGF-1
1-2 mins
IGF-2
Insulin
IGFBP-R
IGF-1R / I-R
Hybrids
IGF-1R
IGF-2R
I-Ra
I-Rb
Cell
membrane
No signal
transduction
Lysosomal
degradation
APOPTOSIS
PROLIFERATION / DIFFERENTIATION / SURVIVAL
METABOLIC EFFECTS

Figure 1.12 The Insulin-like Growth Factor Network

IGF-1 is part of a complex network that plays a critical role in regulating cellular growth, differentiation and survival. In addition to IGF-1 two other peptides feature prominently (IGF-2 and insulin), as well as multiple membrane-bound receptors including the type-1 and 2 IGF receptors (IGF-1R and IGF-2R), two insulin receptor isoforms (I-Ra and IRb), and a number of hybrid receptors between the I-R and IGF-1 receptors (IGF-1R / I-R) and the two I-R isoforms themselves (not shown). All three peptides bind their respective receptor with highest affinity (denoted by solid black arrows), but also share some crossover affinity with each other's receptors (dashed arrows). The bioavailability of IGF-1 & 2 is regulated by a group of six binding proteins (IGFBPs 1-6) that chaperone the peptides in circulation. The majority of IGF-1 is bound to IGFBP3 or 5, and the acid-labile subunit (ALS), forming a ternary structure known as the IGF-IGFBP-ALS complex. Half-life times for bound and unbound IGF-1 are shown in red italics. Cell surface interactions or IGFBP proteolysis frees IGF-1 to bind its receptor. IGF-2 further regulates IGF-1 signalling by binding to the IGF-1R. While the IGF-2R does not result in signalling, it does lead to lysosomal degradation of IGF-2, thus reducing competition for the IGF-1R when required. IGFBPs also show an IGF-independent role, binding to a potential IGFBP receptor (IGFBP-R) and promoting apoptosis via signalling pathways and/or intracellular activity having been internalised by the cell. IGFBP-related proteins (IGFBP-rPs – shown top right) are another class of molecules involved in the IGF network with affinity for IGFs, albeit at lower affinities than the IGFBPs.

IGF-1 as a marker in medical conditions and disease

IGF-1 has been reported as being up/down regulated in a number of clinical conditions suggesting it has the potentially to provide crucial information as to the state of an individual's health, either as a standalone marker or as part of a profile. A few typical examples of such conditions where IGF-1 expression varies discussed below.

Laron syndrome and Severe primary IGF deficiency

Much of what is known about the function of IGF-1 has been established through studies of IGF-1 deficiencies (Vasques *et al.*, 2019; Pfäffle & Kiess, 2020). IGF1 deficiency is an autosomal recessive disorder characterised by growth retardation, sensorineural deafness and mental retardation. Humans deficient in IGF-1 (Laron syndrome) are treated with recombinant IGF-1 (Laron & Werner, 2020; Werner *et al.*, 2020). Humans who can produce IGF-1 but are deficient in GH are given recombinant GH to stimulate IGF-1 production. If left untreated in childhood individuals will have a diminished stature. Severe primary IGF deficiency (severe primary IGFD) is the term given to a group of rare diseases resulting from the inability to make or respond to IGF-1 (Cohen *et al.*, 2014). Severe primary IGFD is characterised by distinctive growth failure, with sufferers exhibiting normal to high GH levels, height below -3SDs, and IGF-1 levels below -3SD. These individuals cannot respond to GH treatment due to mutations in GH receptor, post-receptor mutations and/or IGF mutations.

Acromegaly

Acromegaly is a condition resulting from excess GH, typically caused by a benign tumour on the pituitary gland. Symptoms include abnormal enlargement of the hands and feet, and in some cases the forehead, nose and jaw bones. In children the condition can lead to gigantism. Once diagnosed treatment can be provided by removal of the pituitary tumour, and/or medication to reduce the production of GH. Because IGF-1 is the prime mediator of GH in the body, it has been used as a marker for the condition with up-regulation observed in patients of all ages who suffer from the condition (Tanimoto *et al.*, 2008). The use of IGF-1 as a marker becomes even more important if the GH receptor antagonist pegvisomant is used as a treatment as this form of therapy means circulating levels of GH are no longer suitable to monitor the status of the disease (Muller *et al.*, 2004; Giustina *et al.*, 2014).

Cancer

The pivotal role IGF-1 plays in cell growth and proliferation suggests a possible involvement in the of development of cancer and as a result the IGF-1 signalling pathway has become a prime target for new cancer therapeutics (Atzori *et al.*, 2009; López-Calderero *et al.*, 2010; Fettig & Yee, 2020). The positive correlation between IGF-1 expression and cancer has been widely reviewed with one study that included 18 years of follow-up reporting a 1.82 fold risk of cancer mortality among men who had a baseline IGF1 level above 100 ng/ml compared with men with lower levels, a risk that was increased to 2.61 for men who had a baseline IGF-11 level over 200 ng/ml (Major *et al.*, 2010).

Breast cancer risk across quartiles for premenopausal women was found to be weakly associated with serum IGF-1 levels when adjusted for insulin, glucose, and body mass index (Krajcik *et al.*, 2002). The study, which involved 66 women who were premenopausal and 60 who were postmenopausal at the time of being diagnosed with breast cancer, did not find the same association with those in the postmenopausal group. For the postmenopausal group a decrease in serum IGF-1 was actually observed, and those with glucose levels in the diabetic range were at increased risk for developing breast cancer (van Sickle *et al.*, 2009). This decrease in IGF-1 serum levels is likely due to the same mechanism of GH/IGF-1 axis dysregulation observed in sufferers of type-1 diabetes mellitus with poor glucose control. This modest positive correlation between IGF-1 levels and risk of breast cancer in premenopausal women has been confirmed in a nested case-control study among 35,105 middle-age Norwegian women (Vatten *et al.*, 2008). More recently, complementary observational and Mendelian randomisation analyses of ~430,000 women in the UK Biobank further support a probable causal relationship between circulating IGF-1 concentrations and breast cancer, suggesting that interventions targeting the IGF pathway may be beneficial in preventing breast tumorigenesis (Murphy *et al.*, 2020).

Prostate cancer is one of the most prevalent cancers in men, with most cases occurring in men over 50 years old. The suggestion that elevated IGF-1 levels may serve as a marker of risk has been long established (Chan *et al.*, 1998; Stattin *et al.*, 2004), however several studies reported conflicting results, suggesting that IGF-1 was only a tumour marker rather than an etiologic factor in prostate cancer and as such was unsuitable as a long term predictor of the disease (Lacey *et al.*, 2001; Woodson *et al.*, 2003; Chen *et*

al., 2005; Meyer *et al.*, 2005). More recently, the largest systematic review of studies on the association of IGF-1 with the risk of prostate cancer concluded that there is a 21% increase risk of prostate cancer per standard deviation increase in IGF-1, with a stronger association of IGF-1 with more aggressive and advanced cases (Rowlands *et al.*, 2009). After monitoring 200,452 men participating in the UK Biobank, Travia et al. (Travia *et al.*, 2019) found that men with higher concentrations IGF-1 more likely to be diagnosed with prostate cancer. For every increase of 5 nanomoles in the concentration of IGF-1 per litre of blood (5 nmol/L), men were 9% more likely to develop prostate cancer, corresponding to a 25% greater risk in men who have the highest levels of IGF-1, compared to those with the lowest.

Diabetes & Obesity

Diabetes is a group of metabolic diseases characterised primarily by elevated blood sugar levels that persist over a prolonged period of time. There are two types of diabetes: type 1 diabetes mellitus (T1DM), where the body is incapable of producing sufficient levels of insulin to regulate blood sugar levels and is typically brought on via autoimmune destruction of the pancreatic B-cells responsible for production of insulin (Hedman *et al.*, 2004); and type 2 diabetes mellitus (T2DM), where the body fails to respond to insulin adequately and is often occurs in individuals who become obese.

IGF-1 levels have been reported as down-regulated in T1DM (Mastrandrea *et al.*, 2008), yet up-regulated in T2DM. The decrease in IGF-1 levels in T1DM is despite and otherwise normal or elevated level of GH, suggest GH-resistance is a factor. Elevated levels of interleukin-8 (IL-8) and other pro-inflammatory markers have also been observed in T1DM individuals and may contribute to an inflammatory response that has shown to lower IGF-1 levels in chronic inflammatory diseases (van Sickle *et al.*, 2009).

While T2DM can be treated through improved diet and exercise as well as medications including insulin injections, the condition still results in a number of related complications. The most common complication among T2DM sufferers is an increased risk of cardiovascular mortality caused by atherosclerosis and equivalent to over 10 years of ageing. Obesity independent T2DM also increases risk of acute myocardial infarction, and three quarters of all diabetic deaths are a result of coronary artery disease (O'Gara *et al.*, 2013). The evaluated IGF-1 levels as a result of insulin-resistance is thought to be responsible for vascular deterioration and that modulation of its levels may help mitigate these adverse effects (Cubbon *et al.*, 2016).

Non-alcoholic fatty liver disease (NAFLD)

NAFLD is a condition characterised by fat deposits in the liver that are not the result of excessive alcohol consumption. Like T2DM it is closely linked to insulin resistance and obesity and can lead to many of the same cardiovascular complications including advanced carotid atherosclerosis (Brea *et al.*, 2005) and endothelial dysfunction. IGF-1 is known to play a protective role in ischemic heart and cardiovascular disease and atherosclerosis (Janssen *et al.*, 1998; Juul *et al.*, 2002; Laughlin *et al.*, 2004; Page *et al.*, 2008), and a study by Ichikawa *et al*., (Ichikawa *et al.*, 2007) confirmed down regulation in IGF-1 in NAFLD patients due to an inhibition of IGF-1 secretion via interleukin-1β (IL-1β), interleukin-6 (IL-6) and TNF-α.

Sepsis

Sepsis is the systemic response to infection in which apoptosis of Küpffer cells is triggered by TNF-α that results in organ dysfunction. Through its activation of the phosphoinositol-3 kinase (PI3K) pathway and phosphorylation of the apoptosis inhibitor protein XIAP, IGF-1 acts to protect Küpffer cells and counter the potentially lethal effects of sepsis. IGF-1 levels have shown to be decreased in children with Meningococcal sepsis, and more so in those for whom the infection was fatal (de Groof *et al.*, 2002). The potential for IGF-1 replacement as a treatment for both the prevention and management of sepsis has been demonstrated in mice where it improved overall survival rates through enhanced hepatic bacterial clearance (Ashare *et al.*, 2008) and in rats as a cognitive therapeutic when administered within 6 hours of septic encephalopathy (Yang *et al.*, 2019).

IGF-1 as a PED: Doping in sports

IGF-1 has gained a reputation as one of the most popular doping agents in sport, featuring in many of the most high-profile doping cases in recent years including the BALCO, MLB, and Tour de France scandals to name a few. The peptide's stimulatory effect on muscle growth and tissue repair has inevitably attracted the attention of athletes and trainers for whom increased strength and shorter recovery times are advantageous. Synthetic IGF-1 analogues primarily intended for therapeutic treatment of conditions such as growth failure in children with severe primary IGF-1 deficiency (Cappa *et al.*, 2009) have been around since the late 1980s. Mecasermin is the generic name for recombinant human IGF-1 (rhIGF-1) derived from either yeast or E. coli and is primarily intended for use by children exhibiting severe IGF-1 deficiency. Mecasermin has been available since 1986 when it was developed by the Japanese company, Fujisawa, and later launched in 1995 marketed under the name Somazon. However, it was not for yet another decade that it received approval by the FDA for the US market when two companies, Tercica and Insmed, released their respective products Increlex and Iplex in 2005 – Increlex was in fact Somazon, for which Tercica had acquired worldwide licensing rights outside Japan. Insmed's Iplex however was an IGF-1/IGFBP-3 complex called mecasermin rinfabate (iPlex^{TM}) (Kemp, 2009) designed to better mimic IGF-1's natural state and thus reduce side effects whilst also increasing its circulatory half-life (Kemp *et al.*, 2006; Kemp, 2007; Rosenbloom, 2007, 2009). Despite this, Insmed later agreed to withdraw its product from the US market in 2007 after it was found to infringe on patents licensed by Tercica. 2007 also saw the EMA approve mecasermin for use in Europe for the exclusive treatment of children and adolescents who are not GH deficient and therefore cannot be expected to respond to GH therapy, but suffer from severe primary IGFD due to mutations in the GHR, the post-GHR signalling pathway, and IGF-1 gene defects, resulting in height SDS score at or below -3 and basal IGF-1 SDS equal or below -3 (-2.5 for EMA) for age and gender. A year later however in 2008, average 100m and 200m sprint times of elite athletes began to significantly decrease, leading some to draw parallels with the way distance running times began to dramatically fall a few years after erythropoietin (EPO) was introduced to the market. While Ernst & Simon (Ernst & Simon, 2013) are perhaps somewhat hasty in proposing IGF-1's FDA clearance and improving sprint times as cause and effect (IGF-1 had been around for over a decade by this point with anecdotal evidence suggesting its use was already widespread among bodybuilders and elite athletes including the 2000 Olympic Games gold medallist, Maurice Greene), the approval will undoubtedly have made the peptide more easily obtainable. Such abuse as a performance-enhancing drug (PED) has led to exogenous IGF-1 being listed as a

Prohibited Substance and officially outlawed by WADA, yet there is still no internationally recognised test for detecting rhIGF-1 abuse in sport.

While Increlex and Iplex are likely to have been the traditional sources of rhIGF-1 abused by athletes, in recent years a number of new IGF-1 compounds, analogues and products have become available, some even to the general public. The increase in availability of rhIGF-1 has come at a time when tests for GH have also become more sophisticated, a development that only further increased adoption of IGF-1 as a doping agent for which most of the same desired effects from administering exogenous GH could be achieved. WADA currently employs two types of assay when testing for GH abuse: the so called Differential Isoforms Immunoassay that determines the ratio between the 22 kDa rhGH isoform and endogenous isoforms; and the hGH Biomarkers Test that is based on the measurement of IGF-1 and the N-terminal pro-peptide of type 3 collagen (P-III-P) as two markers shown to increase in a dose-dependent manner following GH administration (Wallace *et al.*, 1999, 2000).

The biomarker approach was developed by the GH-2000 group, a multi-centre team led by Peter Sonksen at the appointment of the International Olympic Committee (IOC) (Sönksen, 2009). The initial IGF-1 measurements were conducted using a commercial radioimmunoassay (RIA) kit produced by Nichols Institute Diagnostics (see Table 1.1) (Dall *et al.*, 2000). However, the kit was discontinued in 2005 and while it was advised WADA pursue the development an in-house assay to prevent such occurrences, the subsequent GH-2004 team chose to implement alternative commercial assays such as the DSL-5600 and Immunotech A15729 immunoradiometric assays (Table 1.1) and apply conversion factors to align results and make use of the reference range data that had been built using the prior assay (Holt *et al.*, 2009). The biomarker approach involving IGF-1 and P-III-P is capable of positive identification of doping up to 2 weeks post administration of GH (vs just 12-24 hours post-final dose with the isoforms method). Gender specific reference ranges of the two markers immediately following competition were established from studies carried out on over 800 elite athletes. The test was capable of detecting 100% of men using GH as a doping agent, with a false-positive rate better than 1:10,000 (Powrie *et al.*, 2007). Whilst still successful, detection was less sensitive in females as they tend to exhibit greater resistance to the effects of GH. Further validation for factors such as sex, ethnicity and the effect of injury (Powrie *et al.*, 2007; Erotokritou-Mulligan *et al.*, 2008, 2009, 2012; Holt *et al.*, 2009, 2010) increased sensitivity and saw the test introduced for the London 2012 Olympics leading to the disqualification of two Russian powerlifters.

Recently, the same group examined the applicability of these two markers for detection of exogenous rhIGF-1/IGFBP-3 in a randomised, double-blind, placebo-controlled study involving fifty-six recreational athletes (Guha *et al.*, 2014). While a relatively small rise in maximum marker levels was detectable (4x increase in males and females for IGF-1; 40-50% increase in women, 35%-50% increase in men for P-III-P), the GH-2000 formulae applied for GH testing resulted in just 61% of women and 80% of men being correctly identified as having taken rhIGF-1. The study concluded that a greater sensitivity could be achieved (94% in both men and women) using a test based solely on IGF-1 concentrations.

Challenges of monitoring IGF-1 levels: Complications and shortfalls of existing assays

The crucial role IGF-1 plays in human growth and development, the number of different clinical conditions that it is associated with, combined with the potential for its abuse in sports and its status a marker for GH abuse, makes detecting its differential expression extremely important. At first glance, IGF-1 does indeed exhibit a number of characteristics desirable in a biomarker too: it is generally considered to be stable for several days after collection (Evans *et al.*, 2001; Hartog *et al.*, 2008), during long-term storage at -25 C for up to 12 months (Elmlinger *et al.*, 2005), and has even shown to be insensitive to repetitive freeze-thaw cycles (Baxter & Martin, 1986; Yu *et al.*, 1999) and displays only minor circadian fluctuations negating the need for repetitive standardised sampling procedures as is required with GH due to the pulsatile nature of its release and diurnal variation. A number of commercially available IGF-1 assay kits have long been available to researchers and physicians around the world – notable players are listed in Table 1.1. Despite this, interpreting IGF-1 results is still far from straightforward.

The first major hurdle that became apparent shortly after the first IGF-1 assay was the discovery of IGFBPs, the presence of which significantly reduced the levels of immunoreactive IGF-1 in samples leading to misleadingly low results. The identification of IGFBPs was a major step forward in IGF-1 immunoassays as separating them prior to assay helped eliminate a significant source of error. Eliminating interference from IGFBPs can be achieved by removing them through effective yet laborious size exclusion chromatography at low pH (e.g. FPLC) but is more commonly done so by acid-ethanol extraction and centrifugation. The latter involves dissociation of IGFBPs from IGF-1 by low pH, followed by ethanol precipitation and removal via centrifugation. However, this method is still not perfect as centrifugation can result in either the undesired loss of IGF-

1 from the sample, or retention of residual IGFBPs in the supernatant (Clemmons, 2007). As such, the technique is often combined with, or centrifugation forgone in favour of, the addition of an "IGFBP blocking agent". IGF-2 has proved useful in this regard, being added in excess to samples to reduce interference from residual IGFBPs, but as Table 1.1 shows, methods are not consistent across different assays. The fact that established assays use different antibodies with differing epitope specificity has further contributed to the issue of contrasting results between assays (Bidlingmaier & Freda, 2010; Frystyk *et al.*, 2010). Furthermore, it wasn't until 2008 that the World Health Organization (WHO) introduced the first International Standard for IGF-1 (02/254) (Burns *et al.*, 2009) replacing the former International Reference Reagent (IRR 87/518) that had been widely used to calibrate the majority of IGF-1 assays up until this point despite the reagent's protein content having been shown to be incorrectly assigned nearly a decade earlier (Quarmby & Quan, 1999). The implications of this are that total IGF-1 concentrations reported by those assays were approximately 2-fold higher than actual values, calling into question the accuracy of a vast amount of IGF-1 data over a considerable time span.

The interpretation of IGF-1 assay results is yet further complicated by the lack of a comprehensive set of reference ranges that define normal circulating levels across multiple populations. The Nichols Advantage immunochemiluminescent assay is widely referred to in the literature as having been the "gold standard" of IGF-1 testing and benefitted from a relative wealth of reference data across populations. However, its removal from the market when Nichols ceased trading in 2005 highlighted the importance of such reference ranges as researchers grappled with replacement kits that lacked the same level of normative data. While so-called conversion factors (CFs) have been reported, their reliability for comparing data between kits is questionable as demonstrated by Krebs *et al*. (Krebs *et al.*, 2008) who compared identical blood samples from 173 patients with GH deficiency using five different assays, as well as Brabant & Wallaschofski (Brabant & Wallaschofski, 2007), who deemed their use as infeasible. Furthermore, Khosravi *et al*. (Khosravi *et al.*, 2005) reported that IGF-1 may well be more susceptible to post-sampling proteolysis than previously thought, and that this could be one source of variability observed between results from multi-assay comparison tests that are otherwise highly correlated for fresh or well-preserved samples. As crucial as such reference value data sets are, their creation is no trivial task. While IGF-1 levels may exhibit minimal diurnal fluctuation, they are influenced by a number of other biological factors including age and pubertal stage, BMI extremes, pregnancy, and to a lesser but still significant degree, sex and ethnicity. In summarising the recommendations of an expert workshop between members of The Growth Hormone Research Society, the IFF, the International Society for IGF Research, and the Pituitary Society, Clemmons

(Clemmons, 2011) suggests that such a set or normative data should be based on the central 95% interval of a randomly selected set of individuals across all age groups from the background population, excluding those whose medical conditions, or medication, are likely to affect their IGF-1 levels (e.g. those suffering from cirrhosis, diabetes, renal failure). The group also concluded that reference values should be presented at narrower intervals, and in Tanner stages, for children and adolescents to reflect the greater change in IGF-1 levels at these ages, as well as sex-specific values between 6 and 18 years of age where gender-related variation is also greatest.

The heterogeneity of assay characteristics and lack of a comprehensive reference values, combined with previously inadequate calibration standards, and cumbersome CFs required to compare values between studies obtained with different assay kits, have all contributed to the current situation. While the introduction of the IS 02/254 in 2009 (Burns *et al.*, 2009) is a step in the right direction, there clearly still exists quite some way to go if testing for IGF-1 is to produce results that can be interpreted and compared with confidence. The standardisation of sampling procedures and affinity reagents, as well as novel ways to eradicate the interference from IGFBPs will mark significant progress towards achieving this goal and provide greater rigour in assays for a molecule that is intrinsically linked to so many important clinical conditions.

Table 1.1 Human IGF-1 Assays

Manufacturer	Model	Format	Sensitivity (ng/mL)	Intra-assay CV (%)	Inter-assay CV (%)	Sample pre-treatment	References
Nichols Institute Diagnostics	**Nichols Advantage***	Automated two-site immunochemiluminescent assay using a biotinylated antibody prepared against the IGF-1 C-terminal 62–70 amino acid sequence for capture. The second antibody is directed against the amino acid sequences of 1–23 and 42–61 and is labelled with acridinium ester for detection.	6	3.5-5.2 [a] 4.8 [b]	≤10 6.7 [b]	Sample is acidified to separate IGF-1 from IGFBPs. Then excess IGF-2 is added in the assay to block the IGFBP binding sites. The acidified sample is incubated simultaneously with the biotinylated capture antibody, excess IGF-2, and the acridinium ester labelled tag antibody.	Prostate Cancer [c] Acromegaly [a] Mortality [b] GH-deficient adults [d] Comparison [e] Retarded growth, children [l] Doping [s]
Nichols Institute Diagnostics	**RIA**	Competitive RIA based on the formation of a complex between anti-IGF-1 polyclonal rabbit antibodies and the IGF-1 protein, present in the sample and in competition with ^{125}I-labeled IGF-1.	0.06	4	≤10	Acid-ethanol extraction to separate IGF-1 from IGFBPs.	Prostate Cancer [f] [c] Doping [g]
DSL/ Beckman Coulter	**DSL-10-5600**	One-step ELISA.	1.2	4.5-7.1	4.8-8.8	Modified three-step acid-ethanol extraction step including precipitation, centrifugation and neutralization, in which IGF-1 is separated from its binding protein.	Cancer [m] Cognitive decline [q] Comparison [e]

Table 1.1 (cont.) Human IGF-1 Assays

Manufacturer	Model	Format	Sensitivity (ng/mL)	Intra-assay CV (%)	Inter-assay CV (%)	Sample pre-treatment	References
DSL/ Beckman Coulter	**DSL-10-2800**	Two-step non-extraction ELISA.	1	4.5-8.6	3.3-6.8	Dissociation buffer to avoid IGFBP interference.	
DSL/ Beckman Coulter	**DSL-5600**	Two-site non-competitive immunoradiometric assay (IRMA) in which sample IGF-1 is sandwiched between 2 antibodies. The first antibody is immobilized to the inside wall of the tubes, and the second antibody is radiolabeled with ^{125}I for detection.		3.3-4.6 [h] 3.0-3.8 [n] <4 [q]	9.3-15.8 [h] 6.6-12.3 [n] <14 [q]	Sample is pre-treated with acid-ethanol to release IGF-1 from its binding proteins.	Sports injury [h] Doping [t] Prostate cancer [n] Cognitive decline [q] Lung cancer [p]
Immunotech (Beckman Coulter)	**A1 5729**	Sandwich IRMA using two monoclonal antibodies prepared against two different antigenic sites of IGF-1. The first is coated on a solid phase (coated tube) and the second is radiolabeled with ^{125}I.	2	1.4-6.3 [a] 6.3 [o]	3.8-8.8 [a] 6.8 [o]	Acid ethanol extraction to separate IGF-1 from IGFBPs.	Acromegaly [a] Colorectal cancer [k] Osteoporosis [o]
Diagnostic Research Group (DRG)	**IGF-1 ELISA 600 (EIA-4140)**	Manual competitive ELISA. Incubation with biotinylated IGF-1 leads to a signal reverse proportional to the concentration in the sample.	1.3	4.7-6.6	7.2-7.8	Acid + neutral + blocking	Comparison [e]

Table 1.1 (cont.) Human IGF-1 Assays

Manufacturer	Model	Format	Sensitivity (ng/mL)	Intra-assay CV (%)	Inter-assay CV (%)	Sample pre-treatment	References
R&D Systems	**Quantikine - DG 100**	Quantitative sandwich ELISA immunoassay based on the formation of a complex between well-coated anti-IGF-1 monoclonal antibodies, IGF-1 in the sample and enzyme-linked anti-IGF-1 polyclonal antibodies.	2.6	3.5-4.3	7.5-8.3	Dissociation of IGF-1 from IGFBPs was achieved by acidification with supplied buffer solution.	Doping [g]
Mediagnost, DiaSorin	**RIA-CT /R22**	Competitive RIA based on the formation of a complex between tube-coated streptavidin, anti-rabbit-IgG conjugated with biotin, anti-IGF-1 polyclonal rabbit antibodies and the IGF-1 protein present in the sample and in competition with ^{125}I-labeled IGF-1.	0.107	2.5-3.5 2.6-6.4 [a]	4.5-6.2 5.5-8.2 [a]	Acidification following neutralization in excess of IGF-2.	Acromegaly [a] Doping [g]
Mediagnost, DiaSorin	**E20**	Manual sandwich ELISA in which IGFBPs are not removed, but function and interference is neutralised.	1.9	5.1-6.7	2.3-6.8	Samples diluted with acidic buffer to dissociate IGFBPs then pipetted directly to wells. Anti-IGF-1 diluted in buffer with IGF-2 and added to wells, neutralising samples. IGF-1 binds antibody, and IGF-2 binds IGFBPs.	Comparison [e]

Table 1.1 (cont.) Human IGF-1 Assays

Manufacturer	Model	Format	Sensitivity (ng/mL)	Intra-assay CV (%)	Inter-assay CV (%)	Sample pre-treatment	References
Siemens	**Immulite 2500**	Solid-phase enzyme-labeled chemiluminescent immunometric assay on the Immulite 2500 analyzer with no need for manual sample preparation.	20	1.7-2.2 [e]	1.9-3.6 [e]	Non extraction acidification and neutralisation	Comparison [e]
Octoeia IDS	**AC-27F1**	Two-site ELISA. The capture antibody is a polyclonal sheep anti-IGF-1, the second antibody is a peroxidase-labeled monoclonal anti- IGF-1.	3.1	4.6-7.2	4.3-6.5	Samples are incubated briefly with a reagent to inactivate binding proteins, and then diluted for assay.	Comparison [e] *Equine* [r]
Schering CisBio	**RIACT**	Sandwich IRMA using two monoclonal antibodies prepared against two different antigenic sites of IGF-1 molecule. The first is coated on a solid phase (coated tube) and the second is radiolabeled with 125I	1	3.2-6.7 [a] <5 [j]	3.5-6.7 [a] <8 [j]	Acid step + IGF-2	Acromegaly [a] Fetal Growth Restriction [i] Noonan syndrome (growth, children) [j] Retarded growth, children [l]

*discontinued
[a] (Massart & Poirier, 2006)
[b] (Friedrich *et al.*, 2009)
[c] (Kurek *et al.*, 2000)
[d] (Moock *et al.*, 2009)
[e] (Krebs *et al.*, 2008)
[f] (Mantzoros *et al.*, 1997)
[g] (Abellan *et al.*, 2005)
[h] (Erotokritou-Mulligan *et al.*, 2008)
[i] (Beltrand *et al.*, 2008)
[j] (Bertelloni *et al.*, 2013)
[k] (Palmqvist *et al.*, 2002)
[l] (Edouard *et al.*, 2009)
[m] (Morris *et al.*, 2006)
[n] (Chen *et al.*, 2005)
[o] (Paccou *et al.*, 2012)
[p] (Ünsal *et al.*, 2005)
[q] (Dik *et al.*, 2003)
[r] (Lygren *et al.*, 2013)
[s] (Holt, 2009)
[t] (Holt *et al.*, 2010)

1.6 Benzodiazepines

Small molecules drugs represent another class of molecule for which multiplexed diagnostic testing is crucial. Many drugs are classed as small molecules including those that are more commonly abused such as opiates, benzodiazepines, barbiturates, cannabinoids, amphetamines, and cocaine (Feng *et al.*, 2007; Favretto *et al.*, 2018).

Given their relatively similar size (vs peptides to proteins), it is possible to envisage an assay that can simultaneously test not only peptide targets, either naturally occurring or as products of degradation, but for small molecule drugs also. Benzodiazepines represent a widely used, and abused, class of drugs for which testing is important but not without its limitations.

Benzodiazepines represent a large family of man-made small molecule drugs designed to cause mild to severe depression of the nerves within the central nervous system and sedation by enhancing the effects of gamma-aminobutyric acid (GABA) in the brain. They are prescribed for the treatment of anxiety, insomnia, agitation, seizures, muscle spasms, and alcohol withdrawal, but also sought after by heroin and cocaine users looking to minimise withdrawal symptoms, as well as those looking to combat social or work-related anxiety (Jones *et al.*, 2012). While they are well-tolerated, safe, and effective for short-term use, due to their effects on the brain, benzodiazepines can be highly addictive and may result in strong dependence for the user if prescription and withdrawal is not controlled. More alarmingly, they are also used as "date-rape" drugs as their strong hypnotic effects render a victim incapable of resisting an attack.

Many benzodiazepines are widely available under well-known brand names, including the 1,4-benzodiazepines such as diazepam (Valium), temazepam (Restoril) and oxazepam (Serax), and the often more potent diazolo- and triazolo-groups such as alprazolam (Xanax), midazolam (Versed), triazolam (Halcion) and others.

The strong physiological and psychological responses elicited by these drugs mean that they can have potentially fatal effects on day-to-day activities such as driving. Their effect is also potent in other species and can be administered for a host of unintended uses, e.g. in horse-racing to illegally calm an animal prior to competition.

Due to their widespread use and availability, benzodiazepine testing is extremely important. Notable commercial tests available include the CEDIA™ Benzodiazepine Assay, capable of semi-quantitative determination of benzodiazepines in human urine at a cut-off concentration of 200 ng/mL, and the DRI™Serum Toxicology Benzodiazepine Assay used for testing serum samples in emergency room situations where urine samples are not conveniently available. The complexity of the metabolic pathways of these agents, particularly diazepam, and the potential for limited cross-reactivity of the IA resulting in false negatives (lorazepam and clonazepam). The CEDIA™ Benzodiazepine assay is based on the bacterial enzyme β-galactosidase, which has been genetically engineered into two inactive fragments that spontaneously reassociate to form the fully active enzyme that will generate a colour measurable change in the assay if it cleaves a substrate. Any drug in the test sample competes with drug conjugated to one inactive fragment of β-galactosidase for antibody binding sites. If drug is present in the sample, it binds to antibody, leaving the inactive enzyme fragments free to form active enzyme. If drug is not present in the sample, antibody binds to drug conjugated on the inactive fragment, inhibiting the reassociation of inactive β-galactosidase fragments, and no active enzyme is formed. The amount of active enzyme formed, and resultant absorbance change are proportional to the amount of drug present in the sample. The DRI™ Serum Toxicology Benzodiazepine Assay is also a competitive assay, where drug labelled with the glucose-6-phosphate dehydrogenase (G6PDH) enzyme competes with the drug from the sample for a fixed amount of specific antibody binding sites that detect most benzodiazepines and their metabolites in human serum or plasma with a 50 ng/mL cut-off. Absence of the drug from the sample results in the drug labelled with G6PDH binding and inhibition of enzyme activity. However, presence of drug in the sample leaves the G6PDH-drug conjugate free and active. Enzyme activity is determined spectrophotometrically at 340 nm by measuring its ability to convert nicotinamide adenine dinucleotide (NAD) to NADH.

One common limitation of current benzodiazepine testing is that the immunoassays are typically designed to detect nordiazepam, oxazepam, and temazepam, all of which are metabolites of diazepam (Craven *et al.*, 2014). Other benzodiazepine drugs that are structurally similar can also be detected based on their ability to cross-react. However, certain drugs such as lorazepam and clonazepam have low cross-reactivity leading to false negatives. It is therefore important that current benzodiazepine assays such as the CEDIA™ and DRI™ test are used only to provide preliminary analytical test results only, and a more specific chemical method such as GC/MS or LC-MS/MS be used to confirm the results.

1.7 Summary & Hypotheses

There exists a demand for immunoassays capable of specific and sensitive detection that are not restricted to central laboratories but can instead be used quickly and easily by untrained individuals anywhere. The progress in the field of high-throughput parallel proteomic analysis has so far been hindered, justifying attempts to explore complementary approaches with the aim to develop a multiplexed system capable of rapid results. This system should ideally be compatible with a novel class of affinity reagents that are more stable and homogenous in their chemo-physical properties and can be more easily identified and produced for a plethora of target molecules.

To achieve this, the following hypotheses and methods to test them were proposed:

(i) A peptidomics approach where samples are enzymatically digested prior to analysis could provide a solution to the pitfalls associated with assaying proteins in their affinity-active conformational states. An affinity peptidomic approach was therefore chosen as a means to overcome these challenges and quantitatively assay samples with minimal sample preservation or preparation. In particular, an attempt was made to generate antibodies against tryptic peptides selected *in silico* based on the list of prioritised targets (Chapter 3).

(ii) One way to achieve multiplexed analysis is through spatial separation of targets. Microarray assays were therefore used to try and achieve such spatial multiplexing for a peptidomics assay with large numbers of samples printed on a single slide (Chapter 4). Alternatively, spectral multiplexing could be used. The intention was therefore to also evaluate the feasibility of such a spectral based approach (Chapter 5).

(iii) Direct binding assays where signal strength is directly proportional to the amount of antigen being assayed are appealing in their apparent simplicity. However, competitive displacement formats appear to offer several advantages over direct binding for multiplexed assays, eliminating the threat of signal saturation while extending measurable concentration ranges and permitting simultaneous detection of antigens whose binding isotherms may vary significantly. Therefore, a competitive displacement assay format was tested to see if the anti-peptide antibodies could be used for assaying tryptic digests of serum samples (Chapter 4).

(iv) Lateral flow tests provide a fast and relatively simple assay format suitable for us by untrained end-users. Whilst lateral flow tests may not be able to match the spatial

multiplexing capability of microarrays, their aforementioned benefits and suitability towards the end-goals of this project warranted an investigation into the possibility of achieving lateral flow multiplexing spectrally and/or spatially, e.g. one or more test lines, each with one or more targets (Chapter 5.

(v) To address the problem of antibody stability and to alleviate the dependence on laboratory animals, an attempt was made to explore a phage display *in vitro* screening and selection approach to generate a recombinant affinity reagent (Chapter 6) against one of the targets selected (Chapter 3). The important challenges here include the suitability of phage display derived polypeptides for the peptidomics approach where antigens are relatively small peptides themselves. IGF-1 was chosen as the starting point and as a challenging model small protein. The interest in and prioritisation of IGF-1 was partially due to its functional roles and potential new applications of anti-IGF-1 affinity reagents beyond and in addition to the affinity detection *per se*. There are many different IGF-1 immunoassays, but the studies and results are often impossible to compare and there is a need for more reliable testing from which results can be more easily compared between individuals, conditions and studies.

It is hoped that this research will contribute to the development of a quantitative and multiplexed immunoassay system, based on novel affinity reagents and with the potential to be incorporated into a small, portable kit format for simple, fast, and accurate use in the field of sports testing, medicine and health diagnostics.

Chapter 2: Materials & Methods

2.1 Materials

2.1.1 General

Phosphate buffered saline (PBS): 0.01 M phosphate buffer, 0.0027 M potassium chloride, 143 and 0.137 M sodium chloride, pH 7.4, at 25 °C.

2.1.2 Anti-peptide affinity reagents and their applications

Uniprot protein database (UniProtKB).
Expasy *in silico* digestion online tool (Expasy PeptideMass - web.expasy.org/peptide_mass/).
Synthetic peptide generation (Sigma)
Anti-peptide antibodies raised in rabbits (Sigma)
Waters 600E pump and system controller (Waters)
Sephadex® G-100 size exclusion chromatography (SEC) resin, 10 mL bed volume: 75% suspension swelled in 10 m*M* K_2HPO_4 (Pharmacia Fine Chemicals)
Sephadex® G-25 size exclusion chromatography (SEC) resin, 5 mL bed volume: 75% suspension swelled in 10 m*M* K_2HPO_4 (Pharmacia Fine Chemicals)
SEC running buffer: 0.8% Tween-20 in 10 m*M* K_2HPO_4 (pH 7.1)
Spectroflow 757 absorbance detector (Applied Biosystems)
Positively charged nylon membrane: 0.45 um (Biodyne)
BioChip microarray scanner: channel 1 – 550 nm, channel 2 - 650 nm (Packard Bioscience)
Goat anti-rabbit IgG-Cy3 (Sigma)
Fluorescently labelled Albumin (BSA-646)
Tween-20

Flexys microarray gridding robot (Genomic Solutions Inc.)
384-microwell plates
BSA-646: in-house fluorescently labelled BSA
Total rabbit IgG (Sigma)
Coomassie Brilliant Blue G-250
Formaldehyde: 37%
Microarray blocking buffer (PBS, 9 % BSA, 0.1 % Tween-20)
Microarray washing buffer (PBS, 0.1 % BSA, 0.02 % Twee-20)

Serum samples x16: before and after samples for two treatments from four unique individuals (supplied by Victor R, Preedy, King's College London)
Trypsin: sequencing grade (Promega)
Trypsin inhibitor: 10 mM phenylmethylsulfonyl fluoride (PMSF) in isopropanol (Thermo Scientific)
Tris: 1 M, pH 8
Petri dishes (54 mm)

2.1.3 Lateral flow and spectral multiplexing using QDs

Synthesis and characterisation of GNPs and GNP-protein conjugates

Tetrachloroauric acid hydrate ($HAuCl_4$) (Alfa Aesar 36400)
Sodium citrate (Sigma)
Sodium azide (NaN_3)
Sodium chloride (NaCl)
Bovine Serum Albumin (BSA)
LKB Biochrom Novaspec 4049 Spectrophotometer
Helios Beta UV-Vis spectrophotometer

Potassium carbonate buffering reagent (K_2CO_3)
GNPs: 40 nm - British Biocell International (BBI)
pH paper test strips: pH range 0-14
Hydrogen peroxide (H_2O_2): 30% solution in water
Mouse anti-benzodiazepine monoclonal antibody: unconjugated, clone BEN1 (Biogenesis, now part of AbD Serotec), protein-A purified in PBS buffer (pH 7.2) with 0.05 % sodium azide
Benchtop refrigerated centrifuge capable of 14,000 g at 4 °C with 2 mL microcentrifuge tubes
Resuspension solution: 1 % Sucrose, 0.1 % sodium azide, in dH_20
Release agent: 0.5% % Tween-20, 0.5% human serum albumin (HAS), in dH_20
Dispensing solution: 20 mM PBS, 5 % methanol, 0.1 % lactose
Blocking solution: 1% Marvel, 0.1 % sodium azide in dH_20
Capture reagent: 2.5 mg/mL oxazepam—3-hemisuccinate/BSA conjugate (OX-3HS-BSA) in dispensing solution

Control reagent: 1 mg/mL Goat anti-mouse IgG, whole molecule (Sigma) in 0.135 M sodium chloride
Glass fibre pads: 10 x 300 x 0.41 mm (G041 from Millipore)
Nitrocellulose membrane: Hi-Flow Plus 240 SN-HF, mylar-backed nitrocellulose, capillary flow rate 240 s per 4 cm (Millipore UK Ltd.)
Dispensing robot for dispensing control and capture line onto membrane: BioDot XYZ3000 Platform with BioJetQuanti 3000 (BioDot Ltd.)
Cutting module for cutting batch product into individual test strips: BioDot CM4000 Guillotine Cutting Module (BioDot Ltd.)
SureWick Cellulose fibber sample pads: 17 x 300 mm and 20 x 300 mm, plastic backed (Millipore)
Adhesive backing card: 60 x 300 mm (Millipore)
Plastic test cassettes (HFL custom order)
Diazepam: 1 mg/mL solution in methanol
Pooled blank equine plasma (HFL)

Quantum dots:

QDs 1-6: Colloidal dispersions of CdSe/ZnS Core/Shell "EviDots" in toluene (Evident Technologies: DK-C11-TOL-Kit6): Properties detailed in **Table 2.1.**
SA-QDs: Colloidal dispersion of streptavidin conjugated Core/Shell “EviFluors” in diH_2O (Evident Technologies): Em. Max listed as 620 nm
Adobe Photoshop
Toluene
Perkin Elmer LS-50B spectrofluorimeter
Quartz cuvette
Positively charged nylon membrane: 0.45 um (Biodyne)
Standard glass microscope slides (Menzel-Glaser, Braunschweig, Germany)
Double-sided adhesive tape
BioChip microarray scanner: channel 1 – 550 nm, channel 2 - 650 nm (Packard Bioscience)
Rhodamine B isothiocyanate (RITC)
Standard aluminium foil
UVP CL-1000 UV Crosslinker

Table 2.1 Properties of CdSe/ZnS Core/Shell "EviDots" quantum dots (QDs1-6)

QD#	QD emission[a] (nm)	Emission FWHM[a,b] (nm)	Estimated crystal diameter[a] (nm)	Estimated mol. Weight[c] (g/mol)	Approx. quantum yield[a] (%)
QD1	515	< 35	2.1	10,000	30-50
QD2	546	< 30	2.4	15,000	30-50
QD3	561	< 30	2.6	23,000	30-50
QD4	575	< 30	3.2	44,000	30-50
QD5	596	< 30	4.0	86,000	30-50
QD6	616	< 30	5.2	200,000	30-50

[a] as specified by the manufacturer (Evident Technologies)
[b] full width at half maximum
[c] for core material, excludes shell

2.1.4 IGF-1 affinity reagents

Phage display

Phage display library: Ph.D.-C7C™ Phage Display Peptide Library Kit (New England BioLabs), 2 x 10^{10} pfu/µL, 1.2 x 10^9 transformants.
Sequencing Primer: "-96 gIII primer" 5'– CCC TCA TAG TTA GCG TAA CG – 3'
E. coli ER2738 strain: F´ *lacI*^{q} *Δ(lacZ)M15 proA*$^+$*B*$^+$ *zzf::Tn10(Tet*^{r}*)/fhuA2 supE thi Δ(lac-proAB) Δ(hsdMS-mcrB)5* (r_k^- m_k^- McrBC$^-$). (Supplied in the New England BioLabs, In. Phage Display Peptide Library Kits).
IGF-1: 1 mg/mL – LONG R3 recombinant analog of human IGF-1 (Sigma)
Corning® Universal-BIND™ multi-well plates (Corning Life Sciences)
Stratalinker(R) for UV crosslinking (Stratagen)
Lysogeny broth (LB) medium: 1% (w/v) tryptone, 0.5% (w/v) yeast extract, 0.5% (w/v) NaCl in dH_2O. Autoclaved, and stored at +4 ˚C.
IPTG/X-gal: 50 mg/mL IPTG, 40 mg/mL X-gal in dimethylformamide. Stored at -20˚C in the dark.
LB/IPTG/X-gal plates: 1% (w/v) tryptone, 0.5% (w/v) yeast extract, 0.5% (w/v) NaCl, 1.5% (w/v) agar in dH_2O. Autoclaved and allowed to cool to below 70˚C. 0.1% (v/v) IPTG/X-gal added and poured onto plates. Stored at +4 ˚C in the dark.
Agarose: 1% (w/v) tryptone, 0.5% (w/v) yeast extract, 0.5% (w/v) NaCl, 0.1% (w/v) $MgCl_2x6H_2O$, 0.7% (w/v) agarose in dH_2O. Autoclaved and stored at room temperature. Melted in microwave prior to use.
Antibiotics: 0.005% (w/v) tetracycline in ethanol. Stored at -20˚C in the dark.
LB-tetracycline plates: 1% (w/v) tryptone, 0.5% (w/v) yeast extract, 0.5% (w/v) NaCl, 1.5% (w/v) agar in dH_2O. Autoclaved and allowed to cool to below 70˚C. 0.0001% (v/v) tetracycline stock added and poured onto plates. Plates stored at +4˚C in dark.
TBS: 10% (v/v) 0.5 *M* Tris-HCl, 150 m*M* NaCl, pH 7.5.
0.1% TBST: 10% (v/v) 0.5 *M* Tris-HCl, 150 m*M* NaCl, 0.1% (v/v) Tween-20, pH 7.5.
PEG/NaCl: 20% (w/v) polyethylene glycol-8000, 2.5 *M* NaCl.
TE buffer: 1 m*M* EDTA, 10 m*M* Tris-HCl, pH 8.
2% (w/v) BSA in PBS and 0.1 mg/mL BSA in 0.1% TBST.
Elution buffer: Glycine-HCl, 1mg/mL BSA, pH 2.2.
Phenol: 10 mg of phenol in 1 mL dH_2O, add 10 mL ethanol, mix, allow phases to separate. Collect upper phase. Repeat procedure by adding 10 mL ethanol, mix, allow to separate, collect upper phase. Repeat 2-3 times.
Solution of 3 *M* Sodium Acetate (pH 5.5) and 70% cold ethanol.

Peptide assays on hydrogels

Standard glass microscope slides (Menzel-Glaser, Braunschweig, Germany)
Cleaning solution: 10% (w/v) sodium hydroxide.
Solvents: 100% Ethanol
Binding silan: 3 µL f 3-(Trimethoxysilyl)propyl metharylate; 1 mL of 100% ethanol; 250 µL of 10% (v/v) Acetic acid.
Hydrogel frames and incubation chambers: 1.5 cm x 1.6 cm adhesive gaskets (Abgene).
Hydrogel components: 1*M* Acrylamide; 20 m*M* N,N'-Methylenebisacrylamide; 0.1% TEMED; 1mg/ml ammonium persulfate.
Hydrogel activation solution: 25% glutaraldehyde.
Micro Bio-Spin 30 Columns, SSC buffer (BioRad)
Sample dilution and Hydrogel assay buffer: 0.005% (v/v) Tween 20 in PBS.
Hydrogel washing buffer: PBS (pH 7.4)
Negative control protein: 1 mg/ml BSA in 0.005% (v/v) Tween 20 in PBS.
Labelling buffer: 1 *M* K_2HPO_4 pH 9.0.
Fluorescent dye for labelling through sulfhydryl groups: 0.1% (w/v) NIR-664-iodoacetamide in 100% methanol.
Synthetic peptides (Sigma).
Reducing reagent: 200 m*M* Butyltriphenylphosphonium bromide (TBP).
SEC resin: Sephadex® G-25 (Pharmacia Fine Chemicals) 75% suspension swelled in 10 m*M* K_2HPO_4.
Disposable 1mL syringes (BD Plastipak™) and filter paper.
Falcon centrifuge tubes (15 mL).
Centrifuge (Beckman Coulter?)
BioChip microarray scanner: channel 1 – 550 nm, channel 2 - 650 Nm? (Packard Bioscience)

Peroxidase labelling

Synthetic peptides: 10% (w/v) in DMSO (100 mg/mL)
Maleimide activated peroxidise: 4mg/mL in PBS (Sigma)
2-Mercaptoethanol: 0.01M diluted from 1M stock in PBS.
Bio-Spin P-30 Columns, SSC buffer (BioRad)

Binding characterisation of antibody and peptide affinity reagents

The protein of interest 10 µg/mL diluted from the stock solutions in PBS.

IGF-1: 100 ug/mL (HFL, NIBSC 100308 CB)

IGF-1: 1 mg/mL – LONG R3 recombinant analog of human IGF-1 (Sigma)

Negative control protein: 10µg/mL BSA in PBS.

96-well ELISA plates or 8-well strips (greiner bio-one).

Washing buffer: PBS-Tween 0.05% (v/v), PBS-Tween 0.005% (v/v) and PBS.

ELISA assay buffer: 0.01% (w/v) BSA in PBS.

Blocking buffer: 1% (w/v) BSA in PBS.

Detection substrate: 3,3′,5,5′-tetramethylbenzidine (TMB) liquid substrate system for ELISA, Supersensitive (Sigma T4444)

ELISA stop reagent: Sulfuric acid (H_2SO_4): 1 M

ELx 800 Plate reader (Biotek).

2.2 Methods

2.2.1 Anti-peptide affinity reagents and their applications

Peptide antigen selection for antibody generation in rabbits

For *in silico* digestion protein sequences or database accession numbers for a list of 35 proteins of interest (**Table 3.1**) were entered into the PeptieMass online service. The following criteria were selected: "reduced" option for Cysteines; no acrylamide adducts; no Methionine oxidation; $(M+H)^+$ and monoisotopic masses. "Trypsin" was chosen as the proteolytic enzyme with "no missed cleavages" results instructed to display all peptides (i.e. bigger than 0 Dalton). Peptides were then sorted by peptide masses**,** displaying all post-translational modification, database conflicts, all polymorphisms and splice variants**.** The list of predicted tryptic peptides was then copied and pasted into an Excel datasheet, where hydrophilicities for each were calculated using Kyte and Doolittle weights and a subset of peptides suitable for chemical synthesis were selected automatically using a Visual Basic macro with specific selection criteria: Ranking was mainly based on the peptide's amino acid content but parameters that are relevant to protein synthesis and stability such as the presence of prolines, serine series, DG, DP, GNG or QGQ combinations, charge distribution and glycine and proline distribution were also taken into account when ranking the peptides. The analysis yielded a number of suitable peptide antigens from each of the proteins analysed and one peptide was chosen for each protein target as the antigen for polyclonal sera generation. Chosen peptides were chemically synthesised and each peptide injected into a pair of rabbits (70 rabbits total) for polyclonal antibody generation by Sigma using the 77 days standard protocol for polyclonal antibody production (Custom Rabbit Polyclonal Antibody Production Protocols | Thermo Fisher Scientific - thermofisher.com).

Purification of anti-peptide antibodies from rabbit sera

Seventy anti-peptide antibodies were purified from serum samples using a Sephadex® G-100 size exclusion chromatography (SEC) column running at 1 mL/minute (75% swelled in SEC running buffer: bed volume 10mL). An IgG elution profile was first calibrated by running a serum sample spiked with fluorescent IgG-Cy3. Elution absorbance was monitored on a Spectroflow 757 absorbance detector connected in series with the SEC column (**Figure 2.1 Panel A**). Volume of each individual elution samples collected every 10 minutes were confirmed by weighing each collection tube. To estimate IgG concentration 1 uL or each collected sample was hand-spotted onto Biodyne® positively charged nylon membrane in triplicate and fluorescence intensity measured using a BioChip microarray scanner. Absorbance and fluorescence were plotted against elution time to determine when the antibody fraction is eluted from the column. An unspiked (non-fluorescent) serum sample was then purified on the column and serial collections assayed with 1:200 goat anti-rabbit IgG-Cy3 which confirmed the elution times. All 70 rabbit sera samples were purified on the column (typical sample: 1.75 mL serum sample + 1.25 mL SEC running buffer) and 2x 2 mL fractions collected per sample 30 minutes after the sample was added to the column. Purified antibody samples were stored at -20 °C.

Competitive anti-peptide antibody microarrays

Immobilisation of anti-peptide antibodies on nylon membranes

A Flexys microarray gridding robot was setup with 6 pins, each programmed to print a 5x5 grid per membrane (one grid per pin). Positively charged nylon membranes were attached to glass slides using small paper stickers and placed in the robot holder. Samples and controls were pipetted to pre-defined wells in 384-microwell plates and placed in position in the robot. A humidifier was used during spotting to maintain high humidity inside the robot casing and prevent samples from drying out during the printing run. To maintain high reproducibility between membranes, the robot was instructed to print membranes in batches of three, with each sample spot repeated five times. To clean pins and avoid carry-over contaminations and achieve a high reproducibility of spotting the following wash cycle was used between samples: 1 % Tween-20 for 30 seconds; PBS for 10 seconds; 1 % Tween-20 for 30 seconds; PBS for 10 seconds; 0.1 % BSA in PBS with 0.1 % Tween-20 for 30 seconds. The microarray layout is summarised in **Figure 4.3**. After printing, membranes were removed from the robot and transferred into a sealed chamber containing a few millilitres of 37 % formaldehyde and kept for two

hours at room temperature in a fume cupboard in order to facilitate cross-linking of proteins to the membrane. Cross-linked membranes were then individually immersed in 50 mL of microarray blocking buffer (PBS, 9 % BSA, 0.1 % Tween-20) for two hours.

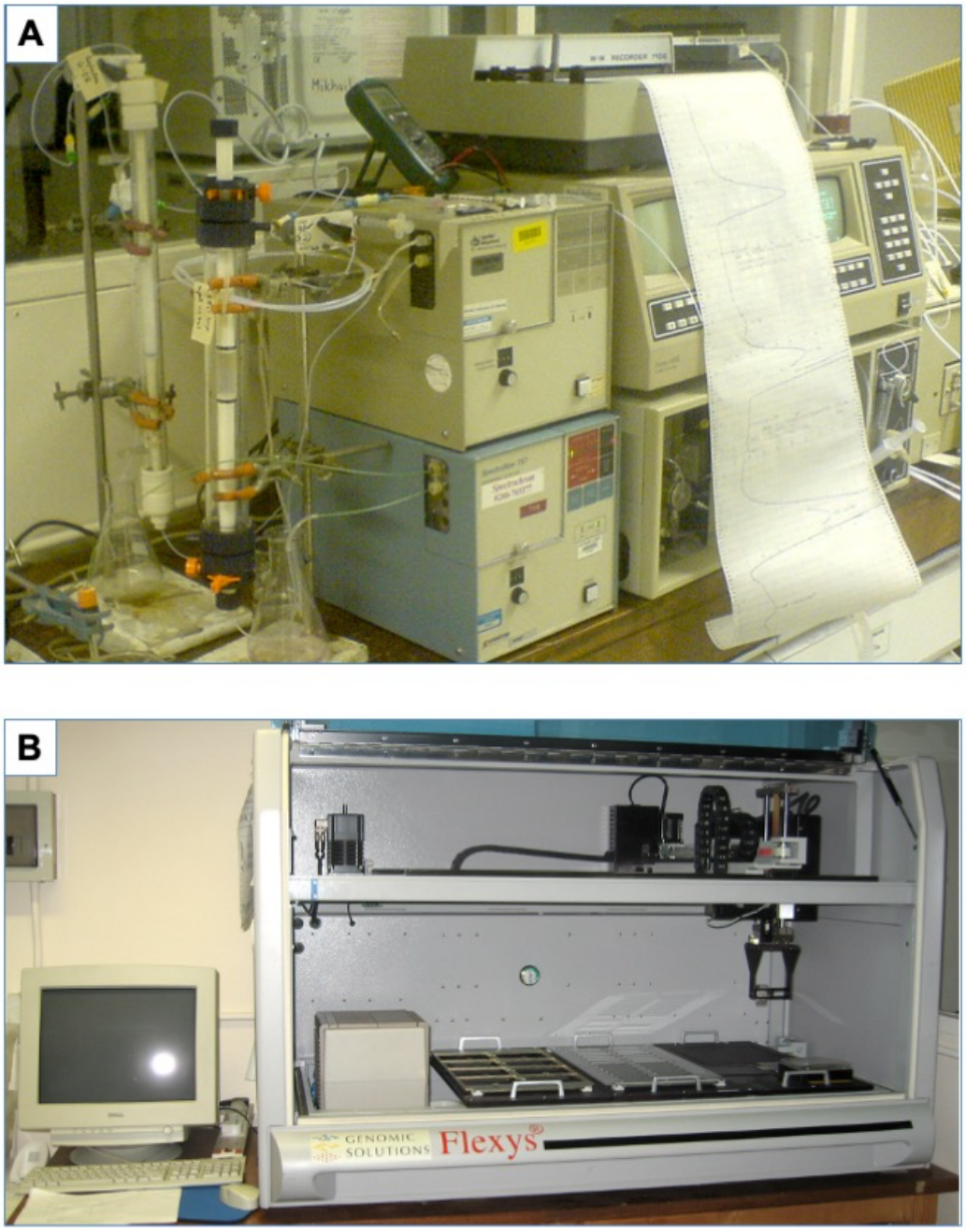

Figure 2.1 Liquid chromatography setup and robotic microarray printer.

[A] LPLC setup consisting of Waters 600E pumps, Sephadex® G-100 and G-25 SEC columns, and Spectroflow 757 absorbance detectors, and used to purify antibodies from 70 rabbit serum samples. **[B]** Flexys microarray gridding robot used to print anti-peptide arrays in humidity controlled chamber prior to cross-linking.

Microarray sample preparation

Typically, 100 uL aliquots of the serum samples were adjusted to pH8 by adding a few microlitres of 1M K_2HPO_4 (pH was checked each time by spotting a fraction of a microliter of the buffered serum onto pH paper). A pooled-sera sample was also made by mixing 50 uL of all serum samples being tested. 20 uL of 2.5% trypsin was added to each 100 uL sample, and 160 uL 2.5 % trypsin added to the 800 uL pooled serum sample. All samples were then incubated at 37 °C overnight. All digestions were stopped by adding 20 uL 10 mM PMSF protease inhibitor to inactivate the trypsin. A 20 uL aliquot of the pooled serum sample was then fluorescently labelled by adding 80 uL PBS and 100 uL of 1 % Rhodamine B isothiocyanate (RITC) before incubating at room temperature for 1 hour. The labelling reaction was stopped by adding 20 uL 1 M Tris pH 8. To separate labelled peptides from trypsin and unincorporated RITC, the pooled labelled serum digest was purified on a Sephadex® G-25 SEC column. The SEC column was calibrated by injecting a trypsin sample spiked with RITC and absorbance of the eluent monitored at 280 nm to identify the elution peaks for trypsin and unincorporated RITC. The gap between these two peaks was used as the collection window when subsequently purifying labelled peptides. After thorough washing of the column with Tween-20 and recalibration with SEC running buffer, 100uL of the labelled pooled digested serum was loaded into the SEC column and four 2 mL collections made corresponding with the previously defined collection window. The sample preparation workflow is summarised in **Figure 2.2**

Displacement assays

To determine the ratio of unlabelled sample required to displace ~50% of labelled pooled serum digest, four membranes were assayed with a range of labelled:unlabelled ratios (mixes shown in **Table 2.2**).

Table 2.2 Typical displacement series sample mixes.

MIX #	1	2	3	4
Assay buffer (uL)	149.8	149	145	140
Labelled (uL)	50	50	50	50
Unlabelled (uL)	0.2	1	5	10
TOTAL (uL)	**200**	**200**	**200**	**200**

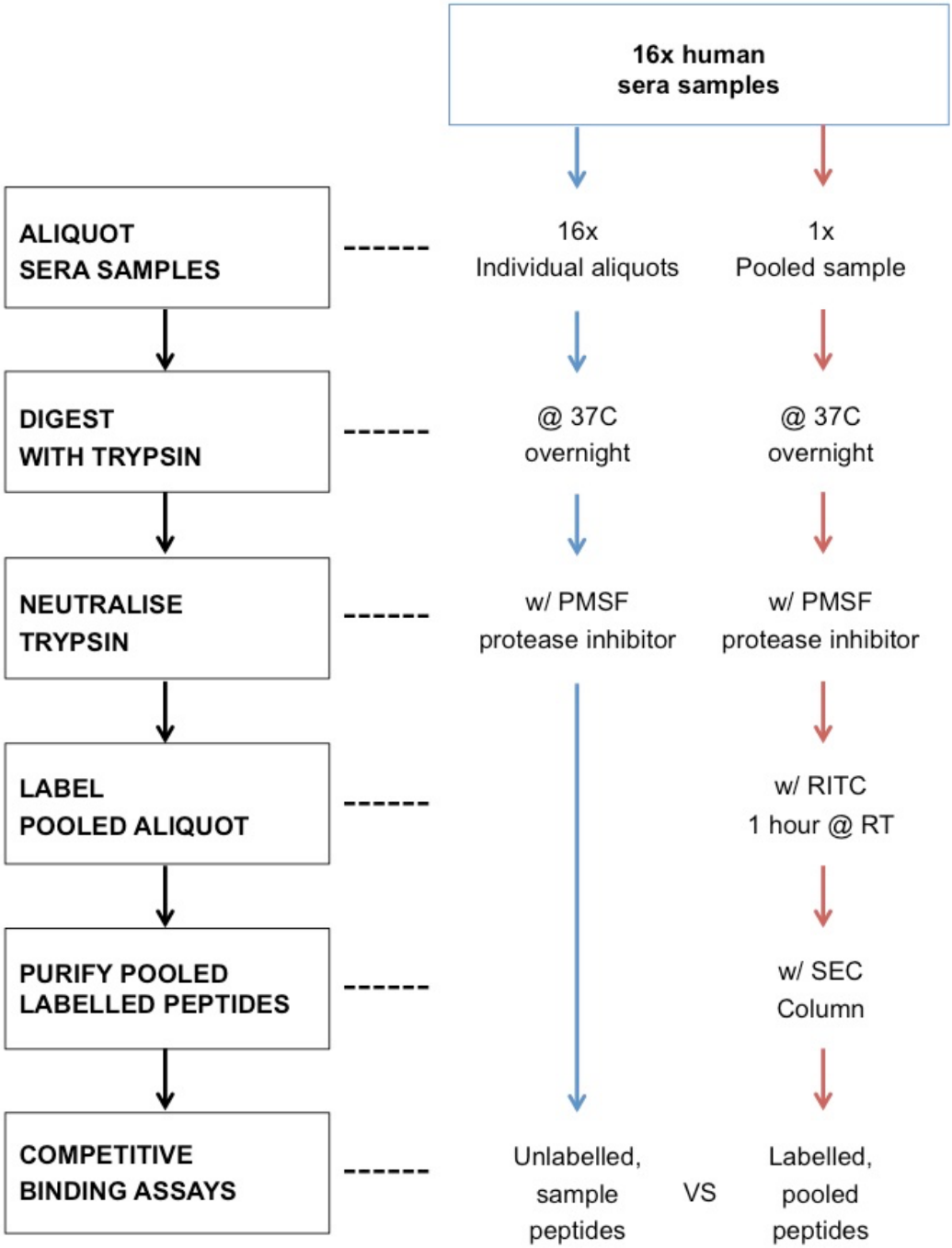

Figure 2.2 A sample preparation workflow for anti-peptide competitive displacement microarrays.

Trypsin is added to all individual serum samples and a pooled sample to facilitate digestion of all proteins into tryptic peptides. The proteolysis is stopped by neutralising trypsin with a protease cocktail, and then the pooled sample is fluorescently labelled with Rhodamine B isothiocyanate (RITC). Labelled peptides are purified from the pooled serum sample by size exclusion chromatography. Unlabelled samples are then each mixed with labelled pooled sample and compete for anti-peptide antibodies in competitive binding assays to identify up/down regulation of target proteins.

Microarray assays

Anonymised rodent sera samples obtained from 16 individuals following 2 different treatments were stored at -20 °C. All individual samples were processed as described in section "**Microarray sample preparation**". A single pooled mixture was also made as described in the section "**Displacement assays**". Individual assay mixtures were prepared for each of the sera samples as described in **Table 2.3.** The displacement assays design was based on Barry *et. al.* (Barry *et al.*, 2003), to accommodate a wider range of antibody affinities and individual sample concentrations. The use of a single labelled master mix created from multiple pooled sera samples ensures that concentrations of all labelled (reference) peptides ("master mix" in **Table 2.3**) are approximately the same as those of the unlabelled samples ("serum sample" in **Table 2.3**) and therefore approximately 50% displacement is achieved in each individual displacement assay in all spots in all arrays. Such conditions correspond to the linear part of a typical sigmoidal displacement curve and would therefore ensure the lowest experimental error and an approximately linear response within a +/- order of magnitude difference of the unlabelled (displacement) peptide concentrations.

Membranes were always trimmed to minimal size (~30 x 20 mm) and 100 mL of assay mix pipetted to individual small Petri dishes. Membranes were placed arrayed-side face down in incubation mix, and the remaining 100 uL of the assay mix added on top of the membrane. Petri dishes were closed and kept at room temperature in the dark for 2 hours. Each membrane was then washed for 10 seconds, 5 minutes and 10 minutes with 50 mL of fresh microarray washing buffer (PBS, 0.1 % BSA, 0.02 % Tween-20) each time. Membranes were then dried on blotting paper (arrayed side up) for 1 hour in darkness. Dried membranes were mounted on glass slides using double-sided adhesive tape and scanned using a BioChip microarray scanner. The scanner's laser intensity and photomultiplier attenuation settings were not changed between slides, but focus was adjusted for each slide using the same x/y reference point.

To determine grid quality and minimize the effect of membrane irregularity and artefacts such as minor scratches or variable background that might otherwise compromise the results, the standard deviation for each 6x6 background grid population was calculated and compared to the mean standard deviation across all background grids. Where a grid's standard deviation based on an entire population (STDEVP) was lower than the average the grid was assigned a quality weighting of 1, but where a background grid's STDEVP exceeded the average, the grid was assigned a reduced weighting to

acknowledge the lower quality data. Also, any background grid values outside the confidence range of their grid were removed.

Net signal values were then determined by subtracting the mean signal of four background grid circles from the signal grid circle that they directly surround.

To normalise values between grids (pin-to-pin), signal values were multiplied by their respective pin factors based on relative pin sizes. Mean pin sizes were each derived from four different pin size calculations – see **Table 4.1**

To normalise values between arrays (membrane-to-membrane), pin-normalised values were multiplied by an array factor determined by comparing the Channel 1 (IgG-Cy3) reference spot signals between membranes. Signal values were then multiplied by the grid quality scores derived from the Background Grid analysis, and then averaged across their triplicate repeats from pins 1, 2, & 3, and 4, 5 & 6, to create weighted means for each sample. Each individual antibody response to each individual sample was calculated, as described above, from 3 replicated spots.

Our experimental approach to multiplexed displacement assays described above in this section allowed some degree of signal normalisation and has compensated for the large difference in the test protein concentrations in the sera. Nevertheless, because of the natural differences in the antibody affinities and the range of peptide marker absolute concentrations, comparing absolute fold difference values generated for different marker peptides would not be correct. Therefore, we sought to use a data analysis method which can compare pairs of individual datasets and yield a degree of data set correlation yet be independent of the signal's measure (i.e. all very strong or all very weak). Pearson pair-wise correlation analysis provides such capability and it was therefore applied using the CORREL function in Microsoft Excel to find the pairwise correlation coefficients of all signal values on one slide vs another and thus determine the relationship (degree of similarity, based on the similarity of marker peptide expression profiles) between samples. Pearson correlation generates normalised covariance values and therefore yields values ranging between -1 and +1 to indicate the linear correlation of data variance. The use of our displacement strategy brought the raw data to be approximately normally distributed, thus allowing the application of Pearson correlation analysis. The equation for the correlation coefficient is:

$$Correl(X,Y) = \frac{\sum (x-\bar{x})(y-\bar{y})}{\sqrt{\sum (x-\bar{x})^2 \sum (y-\bar{y})^2}}$$

where X and Y are the two sets of expressions data from the pair of microarrays being compared, and $\bar{x}$ and $\bar{y}$ are the array sample means and calculated by averaging all signals from each microarray.

These coefficients are show in **Table 4.2** with coefficients closer to +1 or -1 indicating a positive or negative correlation between the samples respectively, and coefficients closer to 0 indicating weak or no correlation.

Table 2.3 Sample mixes for competitive displacement assays

Mix #	Serum sample	Individual	Treatment	Timepoint </> treatment	Serum sample (uL)	Master Mix* (uL)	TOTAL (uL)
1	1.1 A	1	1	Before	10	190	**200**
2	1.2 A	1	2	Before	10	190	**200**
3	1.1 I	1	1	After	10	190	**200**
4	1.2 I	1	2	After	10	190	**200**
5	2.1 A	2	1	Before	10	190	**200**
6	2.2 A	2	2	Before	10	190	**200**
7	2.1 I	2	1	After	10	190	**200**
8	2.2 I	2	2	After	10	190	**200**
9	3.1 A	3	1	Before	10	190	**200**
10	3.2 A	3	2	Before	10	190	**200**
11	3.1 I	3	1	After	10	190	**200**
12	3.2 I	3	2	After	10	190	**200**
13	4.1 A	4	1	Before	10	190	**200**
14	4.2 A	4	2	Before	10	190	**200**
15	4.1 I	4	1	After	10	190	**200**
16	4.2 I	4	2	After	10	190	**200**

*Master mix: 2.94 mL microarray blocking buffer (PBS, 9 % BSA, 0.1 % Tween-20) + 1.05 mL labelled purified pooled serum digest.

Test serum samples

Serum samples of rodent origin were provided courtesy of King's College London for the purpose of methodological development. The 16 samples were supplied labelled as per **Table 2.4**.

Table 2.4 Serum samples for methodological development

Serum sample	Individual	Treatment	Timepoint </> treatment*
1.1 A	1	1	Before
1.2 A	1	2	Before
1.1 I	1	1	After
1.2 I	1	2	After
2.1 A	2	1	Before
2.2 A	2	2	Before
2.1 I	2	1	After
2.2 I	2	2	After
3.1 A	3	1	Before
3.2 A	3	2	Before
3.1 I	3	1	After
3.2 I	3	2	After
4.1 A	4	1	Before
4.2 A	4	2	Before
4.1 I	4	1	After
4.2 I	4	2	After

*Specific treatment details from the prior wet lab stages are irrelevant for the purposes of this study which simply aims to identify up/down regulation of markers for each individual for methodological development.

2.2.2 Lateral flow and spectral multiplexing with QDs

Synthesis and characterisation of GNPs and GNP-protein conjugates

Gold nanoparticles (GNPs) were prepared by reducing tetrachloroauric acid hydrate with sodium citrate. 40 mL of 0.02 % w/w solution of $HAuCl_4$ in dH_2O (equivalent to 0.01 % w/w gold) was prepared and heated to boiling point under constant stirring. 4 mL of 1 % sodium citrate was added under rapid stirring, which continued for another 15 minutes until the solution reached a deep red colour, after which the flask was removed from the hotplate and allowed to cool at room temperature. Sodium azide was added to cooled sols to a final concentration of 0.05 % (w/v). To determine the protein binding capacity of GNPs, a log dilution series of BSA ranging from 1 ng/mL to 10 mg/mL was made. 100 uL of each BSA dilution was added to individual 500 uL aliquots of GNPs and the samples were incubated at 25 °C with constant, gentle agitation. Following a 30-minute incubation, 600 uL aliquots of 20 % NaCl were added to individual GNP-BSA samples. Saturated NaCl causes aggregation of particles in mixes with insufficient protein concentration for total coverage of the GNPs and a change of colour from red to blue. 100 uL of 1 mg/mL BSA (per 500 uL of the GNP preparation) was the lowest concentration that displayed no colour change upon addition of NaCl and was used to make a stock of GNP-BSA conjugate by mixing 1 mL of 0.1 % BSA with 5 mL of GNPs. Absorbance of these GNPs and GNP-BSA conjugates was measured using an LKB Biochrom Novaspec 4049 Spectrophotometer. A further set of GNP-BSA conjugates were subsequently made and absorbance scanned using a Helios Beta UV-Vis spectrophotometer.

Benzodiazepine (diazepam) for lateral flow assays with GNPs

Conjugation of BEN1 anti-benzodiazepine monoclonal antibody to GNPs was achieved as follows. 0.2 M potassium carbonate buffering reagent (K_2CO_3) was prepared by dissolving 0.691 g K_2CO_3 in 25 mL dH_2O. The pH of 33 mL BBI GNPs was adjusted to 9.5 (0.5 units above the isoelectric point of BEN1 monoclonal antibody) using 0.2 M K_2CO_3 and pH paper test strips. 110 uL 30 % H_2O_2 was added to the GNP solution (final 0.1 %). 61.3 uL of 5.3 mg/mL mouse anti-benzodiazepine monoclonal BEN1 antibody was dissolved in 6.5 mL dH_2O (final 50 mg/mL) and then mixed with 32.5 mL of GNPs (1:5 ratio) by slowly adding the GNPs to the antisera solution with brisk mixing - adding the protein solution to the gold can result in a less stable conjugate and can even result in flocculation (aggregation of gold particles). The solution was mixed gently for 10 to 15

minutes at toom temperature. 0.7 g BSA was dissolved in 10 mL dH_2O and 6.5 mL added to the GNP-BEN1 conjugate solution (final 1 % BSA). The solution was mixed gently for 10 minutes and then centrifuged at 4 °C for 1 hour at 10,000 x *g*. The supernatant was carefully removed, and the pellet resuspended in 15 mL of resuspension solution (1% sucrose, 0.1 % sodium azide in dH_2O). Absorbance at 520 nm was determined and the solution stored at 4 °C.

Lateral flow assays

Preparation of lateral flow strips is illustrated using Oxazepam assays as typical example. Glass fibre strips (10 x 300 x 0.41 mm) were soaked in release agent (0.5 % Tween-20, 0.5 % human serum albumin, in dH_20) and dried at 37 °C for 2 hours. Dried, treated glass fibre strips were then soaked in GNP-BEN1 conjugate and dried at 37 °C for 2 hours. Dispensing solution was prepared in pH 4.5, 20 mM phosphate with 5 % methanol and 0.1% lactose. Control reagent was prepared by reconstituting 1 mg anti-mouse IgG (whole molecule) in 1 mL 0.135 M sodium chloride and then diluted 1/10 (100ug/mL final) in dispensing solution (20 mM PBS, 5% methanol, 0.1% lactose). Capture reagent was prepared by dissolving 2.03 mg oxazepam-BSA in 0.812 mL dispensing solution. Control and capture reagents were then dispensed 130 mm and 160 mm respectively from the start of 300 mm lengths of nitrocellulose membrane (SN-HF) at 0.1 uL/mm using a BioDot XYZ3000 Platform. Membranes were dried at 37 °C for 15 minutes, blocked with blocking solution (1 % Marvel, 0.1 % sodium azide, in dH_2O) for 30 minutes at room temperature, before being rinsed with dH_2O and dried at 37 °C for 30 minutes. The prepared materials were then assembled on adhesive backing card as shown in **Figure 2.3**, and a BioDot CM4000 guillotine cutting module used to cut the assembled batch into individual 5 mm wide strips that were then inserted into plastic test cassettes. 1 mg/mL diazepam was prepared in methanol and used to prepare the five serial dilutions in both PBS and pooled equine plasma ranging from 1 to 10,000 ng/mL. 3-4 drops of sample were then deposited onto the test device sample ports and allowed to run for 15-30 minutes.

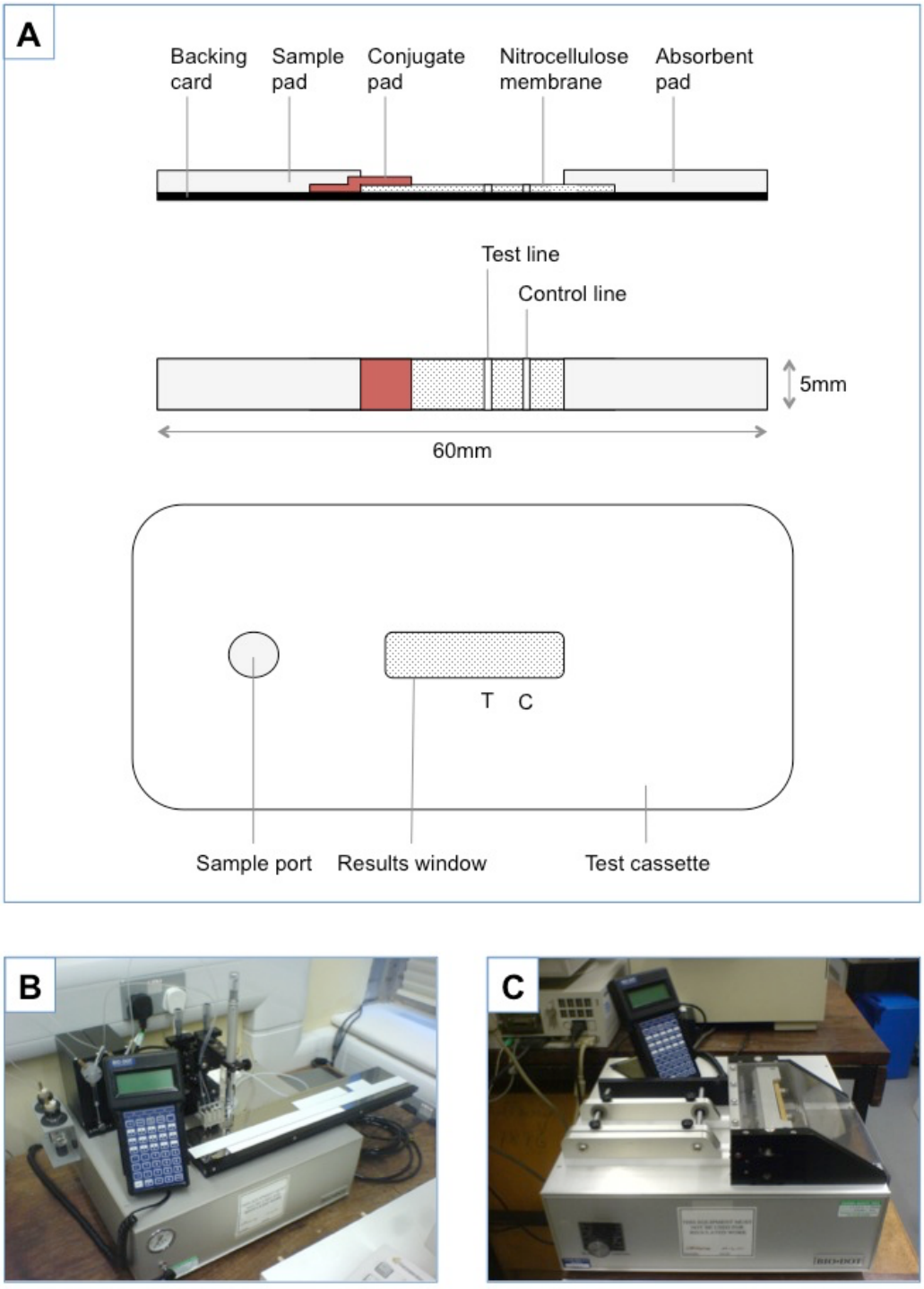

Figure 2.3 Lateral flow assay assembly and equipment.

[A] Cross-sectional diagram of how lateral flow materials were assembled on adhesive backing card (top); top-down views of a single 5 mm wide test strip both standalone (middle) and enclosed within a plastic test cassette (bottom). **[B]** The BioDot XYZ3000 platform used to quantitatively dispense control and test line reagents onto the nitrocellulose membrane prior to assembly. **[C]** The BioDot CM4000 guillotine cutting module used to cut batch assemblies into individual 5 mm individual test strips.

Quantum dots: Size characterisation

TEM micrographs were obtained for QDs 1-6 courtesy of Dr Ivanov of Université de Haute-Alsace, Mulhouse, France (Bailes *et al.*, 2009). Particle diameters were determined for all particles within magnified regions from images of QD3 and QD6 using the measuring tool in Adobe Photoshop.

Quantum dots: Spectral characterisation

QD1 was diluted 1/2000 in toluene, loaded into a quartz cuvette and analysed using a Perkin Elmer LS-50B spectrofluorimeter. Four excitation wavelengths (300nm, 340nm, 380nm and 450nm) were used to generate emission spectra from which the emission maximum was determined. The emission maximum of 518 nm was then used to generate a full excitation spectrum (200 - 518 nm). Slit width was set at 5 nm and the scanning rate was 100 nm/min in all cases. QDs 1-6 were then each diluted 1/1000 in toluene and their emission spectra taken in turn with excitation set at 380 nm.

Quantum dots: Spectral deconvolution

1 uL of each of QDs 1-6 was added to a single 1 mL vial of toluene to recreate a 1/1000 mix of all QD stocks. The emission spectra for the 6 QD mix was measured using a Perkin Elmer LS-50B spectrofluorimeter: slit width was 5 nm and the scanning rate was 100 nm/min, with an excitation wavelength of 380 nm.

Quantum dots: Fluorescence emission detection using BioChip microarray scanner

1 uL each of QDs 1-6 was hand-spotted using a 2 uL Gilson pipette onto positively charged nylon membrane. Once dry, the spotted membrane was mounted on a glass microscope slide using double-sided adhesive tape and scanned using on both channels (550 nm and 650 nm) of a BioChip microarray scanner.

Photostability: QDs vs organic fluorophores

For photostability experiments, 1 uL spots of a QD3 and RITC were hand-spotted on positively charged nylon membrane as five sets of three spots. The membrane was then mounted on a glass microscope slide using double-sided adhesive tape and scanned using a BioChip microarray scanner to determine pre-UV-exposure fluorescence. Aluminium foil was then used to successively wrap each set of three spots, effectively shielding them from light exposure. Foil wraps were done in such a way that removing successive layers exposed an additional set of three QD spots each time (see **Figure 2.4 Panel A**). QD and RITC solutions were both 63 nmol/mL in concentration, therefore 1 uL/spot = 63fmol/spot. Slides were placed inside a UVP CL-1000 UV Crosslinker and exposed to maximum UV exposure (999,900 microjoules/cm^2) for 60 minutes (see **Figure 2.4 Panel C**). At specific timepoints, the crosslinker was paused and a foil layer removed (see **Figure 2.4 Panel E**). Each set of three spots was exposed for either 1, 3, 10, or 30 minutes. Following the final exposure, slides were re-scanned to determine post-UV-exposure fluorescence. A follow up experiment followed the same procedure using QD3, RITC, and atto-565-biotin (Em. Max 565 nm) as samples, and an additional set of spots for each for a 60-minute exposure time point.

Effect of short duration UV exposure on QD fluorescence

Streptavadin-conjugated QDs (SA-QDs) were diluted 1/4 with dH_2O and five 1 uL samples hand-spotted onto a piece of 2 x 1 cm positively charged nylon membrane. The membrane was allowed to dry fully for 15 minutes and then attached to a glass microscope slide using double sided tape. The slide was scanned three times using a BioChip microarray scanner (Channel 2, settings: 45x50), with five-minute intervals between each scan. The slide was then exposed to UV radiation using the CL1000 UV Crosslinker (999,900 microjoules/cm^2) for 30 seconds before repeating the same scan routine. A total of six sets of triplicate scans and five 30 second UV exposures were performed.

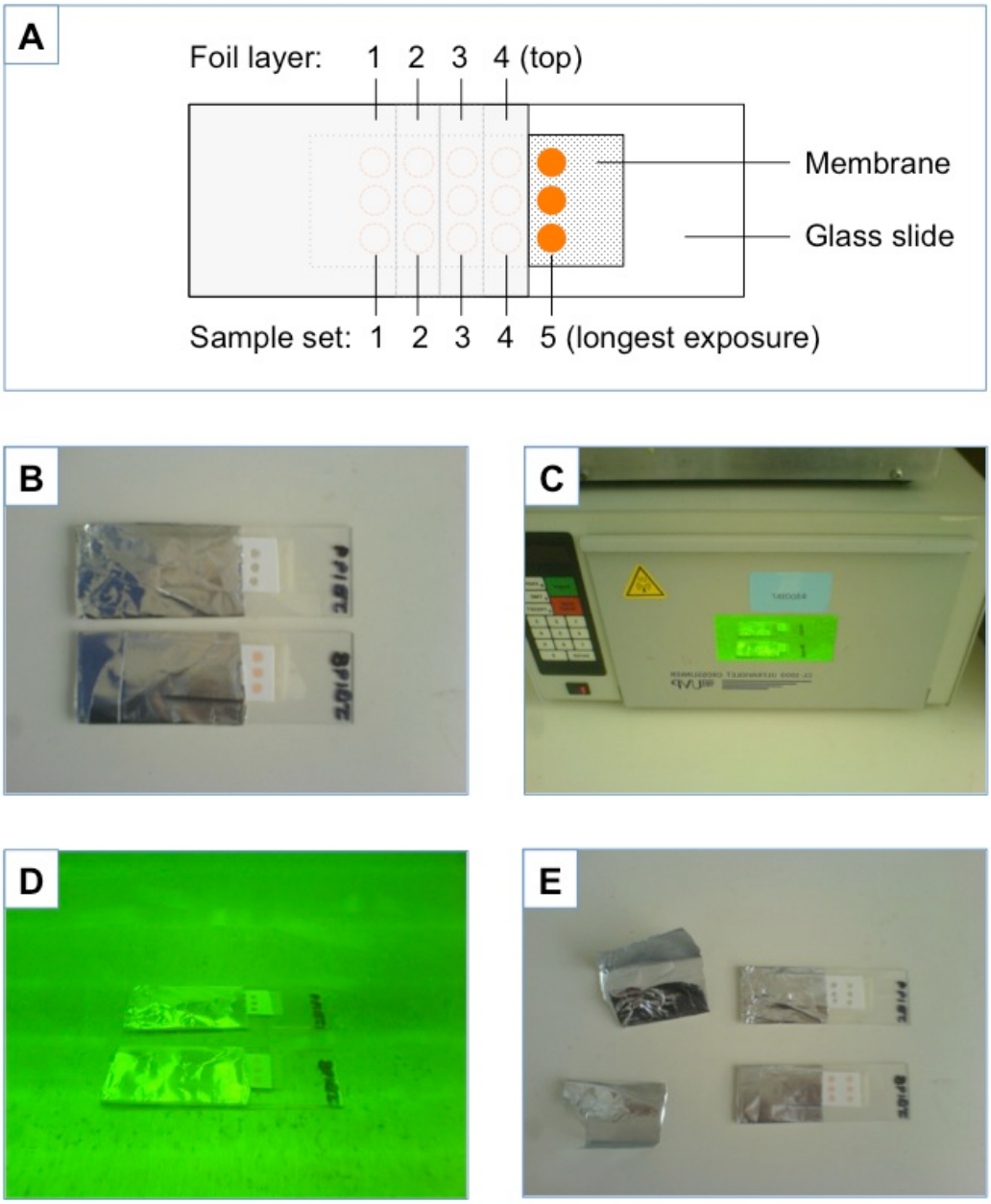

Figure 2.4 Exposure of QDs and RITC to UV radiation

[A] Diagram showing layout of hand-spotted samples on positively charged nylon membrane, secured on a glass slide. Foil was used to sequentially wrap each set of three spots. **[B]** QD slide (top) and RITC slide (bottom) prior to UV exposure. **[C]** Slides inside CL 1000 Crosslinker, and close-up **[D]** being exposed to UV radiation. **[E]** Slides with top layer of foil removed, exposing next set of spots.

2.2.3 Generation of anti-IGF-1 peptides by phage display

Generation of anti-IGF-1 peptides by phage display

Novel anti-IGF-1 peptides were generated via phage display, using one phage display library that expresses a circularised (constrained) 7 amino acid long random peptide. The **library contained** 2.0 x 10^{10}pfu/µl (complexity = 1.2 x 10^{9} transformants) and was used in phage display experiments against IGF-1 as shown in **Figure 2.5**

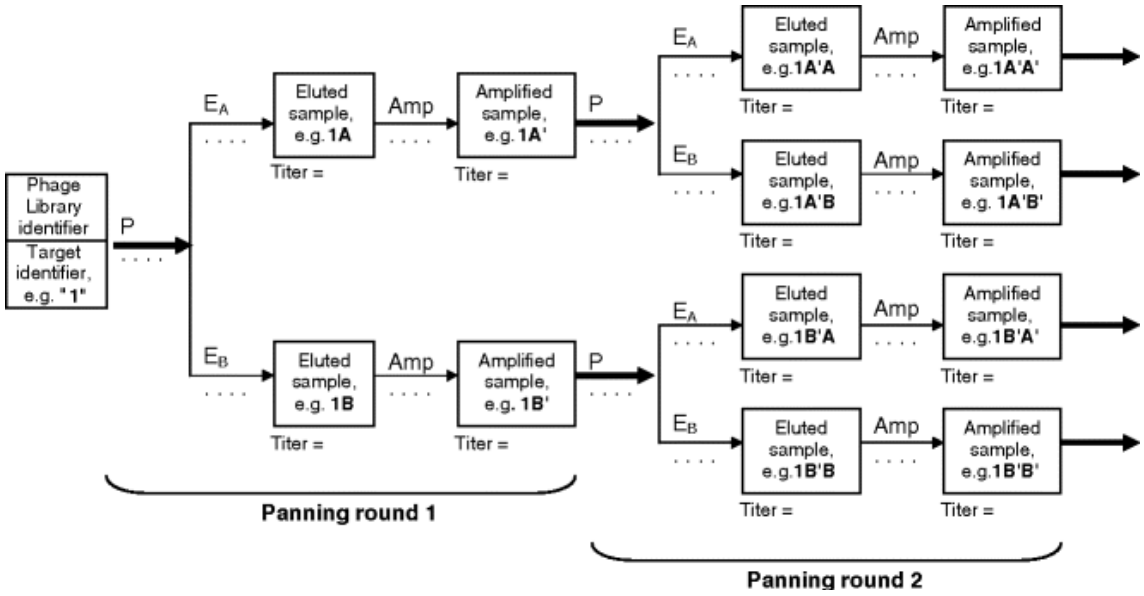

Figure 2.5 Phage panning flowchart.

Phage display work was carried out by group member, Anna Dulneva, following this design (González-Quintela *et al.*, 2000). "P" denotes panning, "EA" and "EB" denote Elutions, whilst the superscript denotes elution conditions, e.g. specific and non-specific elution, or soft and stringent elution. "Amp" denotes amplification.

Panning

IGF-1 was dissolved in 1 mL of 10 mM HCl to a final concentration of 100 µg/mL. 300 µL of the diluted protein was added to each well of a Costar's multi-well plate and incubated for 1 hour at room temperature in the dark. The solution was then decanted, and protein immobilized by exposing the plate to UV using Stratalinker (energy setting 500). The plate was rinsed once with dH_2O, and twice with PBS before being blocked with 2% BSA (in PBS) for 30 min. A Ph.D.-C7C™ Phage Display library was diluted in 300 µL of 0.1 mg/mL BSA (in 0.1% TBST) and added to the IGF-1 coated wells. The plate was then sealed to prevent evaporation and incubated at room temperature overnight. 20 mL LB medium were inoculated with 2-3 colonies of E. coli (streaked one day beforehand on an LB-tetracycline plate and kept at +4°C in the dark) and incubated at 37°C with 120 rpm shaking for 2 hours. The phage solution was removed from the wells and the plate washed ten times with 0.1% TBST to remove all unbound phages. The plate was tap-dried face down on clean paper towel after each wash step to remove as much washing buffer as possible each time. Bound phages were eluted non-specifically by incubating the well with 100 µL of 0.2M Glycine-HCl (pH 2.2) containing 1mg/mL BSA for eight minutes. The eluted phage solution was collected and neutralised with 15 µL of 1 M Tris-HCl (pH 9.1) and then stored at -20 °C. Eluted phage was tittered following the titering method outlined in the next section below.

To amplify phages, an aliquot of the 2-hour E. coli culture described above was transferred to a sterile 50 mL Falcon tube and diluted with fresh LB so that the final OD_{600} = 0.01 and the final volume was 2 mL. The eluted phage sample was then divided in two equal aliquots, with half being stored at -20 ˚C, and the remaining half added to the 2 mL diluted E. coli culture. The phage culture was then incubated in a shaking incubator at +37 °C (250 rpm) for 4.5 hours. The culture was then transferred to 2.0 mL Eppendorf tubes and centrifuged for 10 minutes at 10,000 g at +4 °C. After centrifugation, the supernatant was transferred to a fresh tube and centrifuged again on the same settings. The upper 80% (1.6 mL) of the supernatant was carefully collected and transferred to a fresh tube with 400 µL of PEG/NaCl. The phage was then allowed to precipitate at +4 °C overnight. The following day, phage was precipitated by spinning for 15 minutes at 10,000 g at +4 °C. before carefully removing the supernatant, re-spinning the tubes for 5 sec at room temperature and carefully removing the residual supernatant with a fine pipette. The phage pellet was resuspended in 200 µL TBS + 0.02% NaN3, and the solution kept on ice for 5 minutes before being centrifuged for 1 min at 10,000 g at +4°C to pellet any remaining insoluble matter. The supernatant (amplified phage) was

transferred to a fresh tube. Amplified phages were tittered and the rest of the phage solution stored at -20 °C for use in the next round of panning.

Phage titering

20ml of LB were inoculated with 2-3 colonies of *E.coli* and incubated at +37˚C with 120 rpm shaking until mid-log phase (OD_{600} ~ 0.5). LB/IPTG/X-gal plates were pre-warmed at +37°C approximately one hour before the cells have reached their mid-log phase. Agarose top was melted in the microwave and 3 mL were dispensed into sterile 15ml Falcon tubes (one Falcon per one phage dilution). The Falcons were incubated in a +45 °C water bath until needed. Phage dilutions were prepared in LB and 10 µl of each phage dilution was kept in a separate 1.5 ml tube. Once the culture has reached the mid-log phase, 400 µl culture was put into 1.5 mL tubes with 10 µl phage in it. The mixture was vortexed and left to incubate at room temperature for 5 minutes. The infected cells were transferred to tubes containing +45 °C agarose top, mixed with a pipette tip and immediately poured onto a pre-warmed LB/IPTG/X-gal plate. Agarose was evenly spread by tilting the plate and allowed to cool for ~5 minutes. The plates were then incubated at +37 °C overnight. The following day, the phage titer (in pfu per 10 uL) was calculated for each plate by multiplying the number of blue plaques by the dilution factor.

Single stranded DNA extraction and sequencing

20 mL of LB medium was inoculated with *E. coli* and incubated in a shaking incubator at +37 °C (250 rpm) for 2 hours. Following the initial incubation, the bacterial culture was diluted with fresh LB so that the final OD_{600} measured 0.01, and then 2 mL aliquots transferred into sterile 50 mL Falcon tubes. Single blue plaques from the plates used for titering the phage were added to the 2 mL *E. coli* cultures and incubated in a shaking incubator at +37 °C (250 rpm) for 4.5 hours. The culture was transferred to 2.0 mL microcentrifuge tubes and centrifuge for 10 minutes at 10,000 g at +4 °C after which the supernatant was transferred to a fresh tube and centrifuged again at the same settings. The upper 80% (1.6 mL) of the supernatant was then carefully collected, transferred to a fresh tube with 400 µL of PEG/NaCl and the phage allowed to precipitate at +4 °C overnight. The next day the tubes were spun for 15 minutes at 10,000 g at +4 °C, the supernatant removed, and tubes re-spun for 5 seconds at room temperature before the residual supernatant was carefully removed with a fine pipette. The pellet was resuspended in 100 µL TE Buffer Mix and 100 µL of phenol added followed by a short vortexing to ensure thorough mixing. The mixture was centrifuged at 10,000 g for 5

minutes at room temperature and then 80% of the upper (water) phase pipetted to fresh tubes. 100 µL of phenol:chloroform (1:1) was added and vortexed for 3 minutes at room temperature before being centrifuged again at 10,000 g for 5 minutes at room temperature. The top 80% of the upper water phase was transferred to fresh tubes and 70 µL of chloroform added before vortexing the tubes for a further 3 minutes at room temperature and centrifuging at 10,000 g for 5 minutes at room temperature. The top 80% of the upper water phase was again transferred to fresh tubes and combined with 1/10 volume of 3 M Sodium Acetate pH 5.5 and 2.5 volumes of ethanol. The tubes were vortexed briefly before being incubated at -20 ˚C overnight. The following day, tubes were centrifuged at 14,000 g at +4 ˚C for 20 minutes. The supernatant was removed, and the tubes washed once with 1 mL of cold 70% ethanol and left to dry at room temperature for one hour. 30 µL of deionised H_2O was then used to re-suspend the single-stranded DNA pellets, which were then stored at -20 ˚C prior to sequencing. Samples of phage DNA extraction together with a specific -96 gIII sequencing primer (see materials) were sent to University of Cambridge DNA automated Sequencing Facility.

2.2.4 Peptide assays on hydrogels

Making hydrogels

Microscope glass slides were rinsed in ethanol and soaked in 10% sodium hydroxide overnight. Slides were then rinsed four times in deionised water and twice in ethanol before being treated with binding silan solution for 5 min and then washed with ethanol and died at room temperature. Once fully dry, two adhesive gaskets were assembled onto each glass slide. Fresh polymerisation solution (1*M* acrylamide, 20 m*M* N,N'-Methylenebisacrylamide, 0.1% TEMED) was made and 1 mg/mL ammonium persulfate subsequently added to the mix. 80 µL of the assembled polymerisation mix was pipetted into the gaskets and the frame sealed with plastic cover slips. Once the gel had formed and polymerisation finished, plastic coverslips were removed, and the hydrogels were washed in water overnight to remove any unpolymerized acrylamide. The following day hydrogel slides were dried at room temperature and stored in a dry clean slide box until required.

Target immobilisation on hydrogels

Hydrogels were activated by immersing the slides in 25% glutaraldehyde overnight. Slides were then washed with deionised water twice for 5 min and dried at room temperature. IGF-1 and BSA samples were diluted to 1 mg/mL in hydrogel assay buffer and 3 x 0.5 µL spots of each hand-spotted on to each hydrogel pad. Spots were allowed to dry fully at room temperature before the slides were transferred to a humidified chamber and incubated at +4 °C overnight. The following day, hydrogels were fully rehydrated in the hydrogel assay buffer prior to running affinity assays.

Affinity binding assays on hydrogels

Synthetic peptides were prepared at 10% (w/v) in DMSO and then diluted 1:10 in 10 m*M* K_2HPO_4, pH 7.1 to yield 1% (w/v) peptide stock solutions. To fluorescently label these peptides using their free sulfhydryl groups (cysteines), 10 µL of 1% peptide solution was mixed with 70 µL labelling buffer, 2 µL of 200 m*M* TBP (final concentration 5 mM) and incubated at room temperature for 30 minutes. 30 µL of 0.1% NIR-664-iodoacetamide fluorescent dye was then added to the mixture and incubated at room temperature for 1 hour in darkness. Whilst incubating the labelling reactions, spin columns were prepared for SEC purification of the labelled peptides (one column per labelling reaction): plungers were removed from 1 mL disposable syringes and filter paper cut to just over twice the cross-sectional area of the syringe. The filter paper was then folded and pushed to the bottom of the syringe. 1 ml of 75% Sephadex® G-25 gel was loaded into each syringe column, which were then placed inside 15 mL Falcon tubes. Spin columns were spun at 1,000 g for 5 minutes, after which the Falcon tubes were replaced, and the labelled sample (~ 112 µL) loaded into the centre of the spin column. Columns were then centrifuged at 1,000 g for 5 minutes. Spin columns were then disposed of and the purified peptide samples transferred to fresh microcentrifuge tube and store at -20 °C. Two assay mixtures were prepared for each peptide tested: the first contained only labelled peptides, but no unlabelled peptide; the second assay mixture also contained a 100 fold excess of the unlabelled peptide for a displacement assay. Hydrogel assay buffer was used to make up the volume of all assay mixtures to 65 µL. The assay mixtures were added to the hydrogel pads and incubated at room temperature overnight in the dark. Slides were then washed in hydrogel washing buffer three times for 5 minutes and in deionised water twice for 5 minutes. Air-dried slides were then scanned using the BioChip microarray scanner.

2.2.5 Binding characterisation of antibody affinity reagents

Secondary antibody concentration optimisation

Monoclonal anti-IGF-1 antibody was diluted with PBS to a final concentration of 500 ng/mL (enough to saturate binding capacity of the well) and 100 uL loaded to wells #1-7 of 2 8x1 well ELISA strips. 100 uL PBS was loaded to wells #8 as a negative control. Strips were incubated at +4 °C for 17 hours (wrapped with clingfilm), before being emptied and tap dried. All wells were filled with blocking buffer (~330 uL) and incubated at +25 °C with shaker and clingfilm cover for 3 hours. Blocking buffer was discarded and wells tap dried before being rinsed twice with ELISA washing buffer #1, and twice with ELISA washing buffer #2 (~330 uL per well, per wash). A 3-fold dilution series of anti-mouse IgG-peroxidase was made with ELISA assay buffer ranging from 1/1,000 to 1/243,000 of unknown stock concentration. 100 uL of dilutions were loaded to wells #1-6 and #8 of each strip. 100 uL of assay buffer was loaded to wells #7 as an anti-mouse IgG-peroxidase negative control. All strips were incubated at +25 °C with shaker and clingfilm cover for 3 hours. Once the incubations had completed, all strips were emptied, tap-dried and rinse washed with three well volumes of PBS. 100 uL 3, 3', 5, 5' supersensitive liquid TMB was loaded to all wells. Absorbance was measured at 660 nm on a Biotek ELx 800 plate reader after 5 minutes. 100 uL ELISA stop solution was loaded to each strip 8 minutes after substrate was added and in same way/order/time. Finally, absorbance was then measured at 450 nm on the plate reader.

Secondary antibody association kinetics

Monoclonal anti-IGF-1 antibody was diluted with PBS to a final concentration of 500 ng/mL (enough to saturate binding capacity of the well) and 100 uL loaded to wells #1-7 of 2 8x1 well ELISA strips. 100 uL PBS was loaded to wells #8 as a negative control. Strips were incubated at +4 °C for 5 hours 30 minutes (wrapped with clingfilm), before being emptied and tap dried. All wells were filled with blocking buffer (~330 uL) and incubated at +25 °C with shaker and clingfilm cover for 3 hours. Blocking buffer was discarded and wells tap dried before being rinsed twice with ELISA washing buffer #1, and twice with ELISA washing buffer #2 (~330 uL per well, per wash). A 1/25,000 dilution of anti-mouse IgG-peroxidase was made with ELISA assay buffer and 100 uL loaded to well #1 of each strip. 100 uL of assay buffer was loaded to all other strips. Assay buffer for wells #2-6 and #8 were replaced with 100 uL anti-IGF-1 antibody solution at staggered timepoints. Well #7 was only incubated with assay buffer throughout, serving

as an anti-mouse IgG-peroxidase negative control. All strips were incubated at 25 °C and antibody dilutions kept at +4 °C. Once the incubations had completed, all strips were emptied, tap-dried and rinse washed with three well volumes of PBS. 100 uL 3, 3', 5, 5' supersensitive liquid TMB loaded to all wells. Absorbance was measured at 660 nm on a Biotek ELx 800 plate reader after 5 minutes. 100 uL ELISA stop solution was loaded to each strip 8' after substrate was added and in same way/order/time. Finally, absorbance was then measured at 450 nm on the plate reader.

Primary antibody concentration optimisation

A log dilution series of monoclonal anti-IGF-1 antibody in PBS was made ranging from 0.1 ng/mL to 10 ug/mL and 100 uL loaded to wells #1-7 of 2 8x1 well ELISA strips. 100 uL PBS was loaded to wells #8 as a negative control. Strips were incubated at +25 °C for 2 hours (wrapped with clingfilm), before being emptied and tap dried. All wells were filled with blocking buffer (~330 uL) and incubated at +25 °C with shaker and clingfilm cover for 3 hours. Blocking buffer was discarded and wells tap dried before being rinsed twice with ELISA washing buffer #1, and twice with ELISA washing buffer #2 (~330 uL per well, per wash). A 1/20,000 dilution of anti-mouse IgG-peroxidase was made with ELISA assay buffer and 100 uL loaded to wells #1-6 and #8 of each strip. 100 uL of assay buffer was loaded to wells #7 as an anti-mouse IgG-peroxidase negative control. All strips were incubated at +25 °C with shaker and clingfilm cover for 3 hours. Once the incubations had completed, all strips were emptied, tap-dried and rinse washed with three well volumes of PBS. 100 uL 3, 3', 5, 5' supersensitive liquid TMB loaded to all wells. Absorbance was measured at 660 nm on a Biotek ELx 800 plate reader after 5 minutes. 100 uL ELISA stop solution was loaded to each strip 8 minutes after substrate was added and in same way/order/time. Finally, absorbance was then measured at 450 nm on the plate reader.

Primary antibody association kinetics

IGF-1 was diluted with PBS to a final concentration of 100 ng/mL and 100 uL loaded to all wells of 2 8x1 well ELISA strips. Strips were incubated at +25 °C for 2 hours (wrapped with clingfilm), before being emptied and tap dried. All wells were filled with blocking buffer (~330 uL) and incubated at +25 °C with shaker and clingfilm cover for 2 hours. Blocking buffer was discarded and wells tap dried before being rinsed twice with ELISA washing buffer #1, and twice with ELISA washing buffer #2 (~330 uL per well, per wash).

A 1/1,000 dilution of monoclonal anti-IGF-1 antibody was made in ELISA assay buffer (500 ng/mL final) and 100 uL loaded to well #1 of each strip. 100 uL of assay buffer was loaded to all other strips. Assay buffer for wells #2-6 and #8 were replaced with 100 uL anti-IGF-1 antibody solution at staggered timepoints. Well #7 was only incubated with assay buffer throughout, serving as a primary antibody negative control. All strips were incubated at 25 °C and antibody dilutions kept at +4 °C. Once the primary antibody incubations had completed, all strips were washed twice with each ELISA washing buffer and then 100 uL of 1/5000 dilution of anti-mouse IgG-peroxidase in assay buffer was added to wells #1-7. 100 uL assay buffer only was added to wells #8 as a secondary antibody negative control. Strips were wrapped with clingfilm and kept at +25 °C with shaker for 2 hours. All strips were then washed twice with each washing buffer. 100 uL 3, 3', 5, 5' supersensitive liquid TMB loaded to all wells. Absorbance was measured at 660 nm on a Biotek ELx 800 plate reader after 5 minutes. 100 uL ELISA stop solution was loaded to each strip 8 minutes after substrate was added and in same way/order/time. Finally, absorbance was then measured at 450 nm on the plate reader.

Primary antibody dissociation kinetics

IGF-1 was diluted with PBS to a final concentration of 100 ng/mL and 100 uL loaded to wells 1-7 of 8x1 well ELISA strips. Well #8 of each strip was loaded with 100 uL PBS as an IGF-1 negative control. Strips were incubated at +25 °C for 2 hours (wrapped with clingfilm), before being emptied and tap dried. All wells were filled with blocking buffer (~330 uL) and incubated at +25 °C with shaker and clingfilm cover for 60 minutes. Blocking buffer was discarded and wells tap dried before being rinsed twice with ELISA washing buffer #1, and twice with ELISA washing buffer #2 (~330 uL per well, per wash). A 1/2000 dilution of monoclonal anti-IGF-1 antibody was made in ELISA assay buffer (250 ng/mL final) and 100 uL loaded to wells #1-6 & 8 of each strip. 100 uL of the assay buffer only was loaded to wells #7 of all strips as primary antibody negative control, and all strips then incubated at +25 °C for 8 hours minimum (long enough to reach association equilibrium). The following wash procedure: removal of primary antibody solution, 1 rinse wash with 330 uL ELISA washing buffer #1, 1 rinse wash with ELISA washing buffer #2, and 1 extended wash with ELISA washing buffer #2, was performed at such intervals that the final all wash steps (including incubation with secondary antibody) lasted for the following durations: wells #1 for 9 hours; wells #2 for 6 hours; wells #3 and the control wells (5*, 6, 7, 8) for 3 hours (*glycine HCl (pH 2.2) was used for the final extended wash of wells #5 as a low pH reference); wells #4 for 1 hours. Wash buffer (or glycine HCl for wells #6) was replaced every hour. Once the dissociation

washes had completed, all strips were rinsed once with both wash buffers and then 100 uL of 1/5000 dilution of anti-mouse IgG-peroxidase in assay buffer was added to wells #1-5, 7 and 8. 100 uL assay buffer only was added to wells #6 as a secondary antibody negative control. Strips were wrapped with clingfilm and kept at +25 °C with shaker for 1 hour. All strips were then washed twice with washing buffer #1 and twice with PBS. 100 uL 3, 3', 5, 5' supersensitive liquid TMB loaded to all wells. Absorbance was measured at 660 nm on a Biotek ELx 800 plate reader after 5 minutes. 100 uL ELISA stop solution was loaded to each strip 8' after substrate was added and in same way/order/time. Finally, absorbance was then measured at 450 nm on the plate reader.

Binding characterisation of peptides affinity reagents

To conjugate anti-IGF-1 peptides to peroxidase, 0.4 µL of 100 mg/mL peptide stock was mixed with 25 µL of 4 mg/mL maleimide activated peroxidase solution and incubated for 2 hours at 25 ºC. At the end of the incubation, 0.4 µL of 0.01 M 2-Mercaptoethanol was added to the mix and incubated for a further 15 minutes to block the remaining active sites of activated peroxidase (20 mM in the final concentration). During the incubation, Bio-Spin P-30 columns were prepared by exchanging the column buffer with PBS by allowing 3 column volumes to drain by gravity before spinning the columns at 1000 g for 1 minute to remove the excess buffer. Peptide-peroxidase samples were then pipetted to the centre of the column gel surface and spun at 1000 g for 4 minutes to remove free peptide. The purified peroxidase-labelled peptides were then stored at -20 ºC.

A typical dissociation kinetics experiment was performed as follows:
IGF-1 was diluted with PBS to a final concentration of 10 ug/mL (enough to saturate binding capacity of the well). 100 uL of 10 ug/mL antigen was loaded to wells 1-7 of 8x1 well ELISA strips. Well #8 of each strip was loaded with 100 uL PBS as negative control. Strips were incubated at +4 °C overnight (wrapped with clingfilm), before being emptied and tap dried. All wells were filled with blocking buffer (~330 uL) and incubated at +25 °C with shaker and clingfilm cover for 90 minutes. Blocking buffer was discarded and wells tap dried before being rinsed twice with ELISA washing buffer #1, and twice with ELISA washing buffer #2 (~330 uL per well, per wash). Peroxidase conjugated peptide affinity reagents were diluted 1/1,000 in ELISA assay buffer and 100 uL loaded to wells #1-6 & 8 of each strip (0.1 uL of original peptide conjugate per well). 100 uL of the assay buffer only was loaded to wells #7 of all strips as an Ab negative control, and all strips then incubated at +4 °C overnight (long enough to reach association equilibrium). The following wash procedure: removal of Pep-Px solution, 2 rinse washes with 330 uL

washing buffer #1, 1 rinse washes with PBSt, and 1 extended wash with PBSt, was performed at such intervals that the final PBSt extended wash lasted for the following durations: wells #1 and the control wells (6*, 7, 8) for 4 hours; wells #2 for 2 hours; wells #3 for 1 hour; wells #4 for 30 minutes; and wells #5 for 3 minutes (*PBSt was replaced with glycine HCl (pH 2.2) for the final wash of wells 6 as a low pH reference). Strips were kept at +25 °C with shaker and wrapped with clingfilm. PBSt (or glycine HCl for wells #6) was replaced every hour. Once the dissociation washes had completed, strips were rinsed twice with PBS (~330 uL per well, per wash), and 100 uL 3, 3', 5, 5' supersensitive liquid TMB loaded to all wells. Absorbance was measured at 660 nm on a Biotek ELx 800 plate reader after 5 minutes. 100 uL ELISA stop solution was loaded to each strip 8' after substrate was added and in same way/order/time. Finally, absorbance was then measured at 450 nm on the plate reader.

Chapter 3: Anti-peptide affinity reagents

This section focuses on the design and selection of peptides for novel anti-peptide antibody generation against the 35 protein markers of interest detailed in Table 3.1. An anti-peptide antibody approach would not only expand the range of affinity reagents available against the selected targets, but also reduce stringent sample preservation requirements. This is because the first step in the affinity peptidomics approach relies on complete proteolytic digestions of the samples being analysed prior to testing. Such a step removes the need to protect material from proteases or partial protein unfolding or degradation. Peptides are also far more homogenous in their physical and chemical properties than intact proteins, simplifying the optimisation of assay conditions and potentially permitting truly high-throughput proteomic analysis by means of parallel affinity assays (Barry *et al.*, 2003).

This work seeks to determine whether proteolytically digested material can yield peptides that are predictably suitable for antibody generation, and the production of high-affinity anti-peptide antisera.

3.1 Selection of biomarker targets

The expression patterns of particular proteins often provide a great deal of evidence as to the physiological state of a cell and an organism, providing strong markers and even therapeutic targets for diseases, indication of illegal performance enhancing activity in sports, or in the case of forensics, provide crucial information when profiling individuals from samples found at a crime scene. Quantitative data for expression profiles under different conditions already exists for many such markers.

3.1.1 Protein markers of interest

Myoglobin

Myoglobin is the primary oxygen carrying protein found in muscle tissues. Chen *et al*., (Chen *et al.*, 1980) have identified a number of expression differences to determine important biometric characteristics. The study showed that mean serum myoglobin concentrations were significantly higher in males than females in both white and black individuals (35 vs. 31 microgram/L for whites and 44 vs. 29 microgram/L for blacks). The report further notes that of the two races studied, black men had the highest serum myoglobin values and that myoglobin levels were always higher for the older groups than younger, regardless of race or sex. As mentioned previously, blood or blood stains containing large amounts of D-Dimer and only very small amounts of myoglobin could

be identified as menstrual blood (Miyaishi *et al.*, 1996), whereas myoglobin depletion in neck muscle fibres in tandem with myoglobin accumulation in the intra- and extracellular spaces indicates neck trauma with survival time of just a few minutes (Fieguth *et al.*, 2003b). (Zhu *et al.*, 2001) suggest that high post-mortem urinary myoglobin levels (>1000ng/mL) may be an indicator of ante-mortem massive skeletal muscle damage or hypoxia related events in acute and subacute death cases.

Tumour necrosis factor alpha

Tumour necrosis factor alpha (TNF-α) is one of the body's proinflammatory cytokines and its presence can provide useful information on a number of areas including hair loss resulting from skin inflammation where increased levels of TNF-α have shown to result in increased rate of epidermal and hair bulb keratinocyte apoptosis (Ruckert *et al.*, 2000), and coffee consumption which increases the levels of proinflammatory markers, notably 28 % higher levels of TNF-α in both male and female coffee drinkers compared to coffee non-drinkers ($P<0.05$) (Zampelas *et al.*, 2004). Another area where TNF-α might prove to be a useful marker is with identifying vitality and age of skin wounds where its levels are increased compared to control skin values ($P<0.05$), and especially for stab or incised wounds with very short survival times of less than five minutes ($P<0.001$-0.05) (Grellner *et al.*, 2000). A study into the effect of thermal injury on the levels of TNF-α was carried out on rats and showed elevated tissue TNF-α mRNA levels in major organs 2 hours after thermal injury, peaking at 8 hours and remaining elevated for 24 hours (Zhai *et al.*, 1999).

Fibrinogen

Fibrinogen is a plasma glycoprotein synthesised by the liver that plays an active role in blood clotting where it is converted into fibrin. The products of fibrinogen degradation, namely D-Dimer (DD), have proved to be a potential marker in distinguishing the vitality of incised skin wounds, with its concentration at such sites being far higher on average compared to controls ($P<0.01$) (Hernández-Cueto *et al.*, 1995). It has also been demonstrated to be a useful marker in the identification of menstrual blood if its concentration is determined simultaneously with myoglobin, with menstrual blood containing a ratio of approximately 200:1, DD to myoglobin (Miyaishi *et al.*, 1996). Fibrinogen is also reported as being inversely correlated with leg length, and to a lesser extent trunk length (Davey Smith *et al.*, 2001).

C-reactive protein

C-reactive protein (CRP) is a major acute phase protein synthesised in the liver whose levels are elevated as a result of inflammatory responses and is already used a clinical marker for a number of conditions (Young *et al.*, 1991; Ballou & Kushner, 1992; Baumann & Gauldie, 1994). This response may be brought about by sudden trauma, ill health such as infection (Tsokos *et al.*, 2001; Petrikkos *et al.*, 2005) or even indicate a state of obesity (Khaodhiar *et al.*, 2004) and so CRP acts as a good marker for biometric, lifestyle as well as trauma and death profiling. CRP level in normal blood is below 10mg/l but rises to between 50-300mg/l during acute inflammatory process. Post-mortem elevated CRP levels drop 35 % on average (irrespective of time up to 6 days) when compared to ante-mortem values but still prove to be a strong reflection of ongoing inflammatory states prior to death (Sano *et al.*, 2007). CRP has also shown to be mediator for the associated link between socioeconomic status and cardiovascular disease (Jousilahti *et al.*, 2003) with a significant inverse relationship observed ($p<0.001$) between CRP levels and socioeconomic status (2.32, 1.90, 1.52 mg/l for low, middle and high socioeconomic classes) even after adjustment for other factors such as smoking, waist to hip ratio and long standing diseases. CRP has been evaluated as a forensic marker with respect to cause of death and survival time (Fujita *et al.*, 2002), with CRP levels remaining low for almost all immediate deaths (<0.5mg/dl for 15/16 cases studied) and elevated levels indicating longer survival times and conditions such as severe infection prior to death.

Interferons

Interferons belong to the family of cytokines and are important in the body's immune defence. There are three types of IFNs, α, β, γ, and several studies indicate the potential of IFN-γ as a marker with expression levels linked to a number of conditions. Ruckert *et al.* (Ruckert *et al.*, 2000) investigated the effect of three cytokines on the apoptosis of epidermal and hair bulb keratinocytes (KCs) *in vivo*, by injecting them intradermally into the backs of mice. KC apoptosis may well play a critical role in hair loss following inflammation. Epidermal and hair bulb KCs appeared to be far more prone to cytokine induced apoptosis when IFN- γ was inserted in combination with TNF-α and IL-1β with a significant increase being observed 6hours after injection and further still after 24hours. Despite the Injection of IFN- γ on its own resulting in no significant increase of KC apoptosis in either region, the presence of elevated levels of all three cytokines in combination may well prove to be a useful biometric marker for hair loss profiling. A number of papers also highlight the potential of IFN-γ as a time-related marker due to

seasonal fluctuations in its expression. In 1993 Katila *et al.* (KATILA *et al.*, 1993) reported a decrease during summertime in the IFN producing capacity of 49 healthy individuals from Finland that provided blood samples over the course of one year. This seasonal variation was supported when Shearer *et al.* (Shearer *et al.*, 2002) conducted a study to investigate whether isolation during the Antarctic winter would cytokine balance. Their results showed a significant increase in plasma IFN-γ (P=.039) for those individuals isolated in the Antarctic compared to control individuals, suggesting a shift towards a pro-inflammatory cytokine profile. Lam *et al*. (Lam *et al.*, 2004) also hypothesised in 2002 that individuals suffering from Seasonal Affective Disorder (SAD) would likely show increased levels of pro-inflammatory cytokines including IFN in winter compared to summer. IFN- γ levels have also been shown to decrease in samples collected 18hours after acute alcohol consumption by healthy subjects (Szabo *et al.*, 2001). Differential expression of IFN- γ has also been reported between suicidal and non-suicidal depressed patients (94±36 vs. 42±30, P=0.038) (Mendlovic *et al.*, 1999).

Interleukins

Interleukins (IL) are a group of cytokines that play a major role in the body's immune system. Several of these are ranked among our top 20 protein markers:

IL-1

Thomas *et al*. (Thomas *et al.*, 2005) report the significantly higher levels (170 %) of IL-1β in adults over the age of 60 suffering from depression compared to healthy individuals and that these levels were strongly correlated to the current severity of the individual's depression. IL-1β is also capable of being an effective marker to help determine wound vitality and age, especially in stab and incised wounds, where its concentration rising significantly (P=0.001) in cases of shortly survived trauma. IL-1β levels also have a tendency to rise with wound age in non-fatal cases compared to control skin (P=0.05) (Grellner *et al.*, 2000).

IL-2

IL-2 is a type-1 cytokine and has been reported as being upregulated in the T-cell mediated autoimmune disease Alopecia areata (AA), that is characterised by partial or total loss of scalp and body hair (Price, 2003). In a study of 60 patients suffering from

burn trauma, IL-2 was shown to be upregulated in proportion to the severity of the burn wound size, with significant elevation of IL-2 levels being recorded in those patients with 20 to 40 percent burns when compared to patients with greater than 40 percent and a control group ($P<0.0001$) (Kowal-Vern *et al.*, 1994).

IL-4

IL-4 is a Th2 cytokine that serves to down-regulate inflammatory responses. Its expression levels are reported to be down-regulated as a result of ethanol exposure and burn trauma, as seen in mice subjected to such treatments and compared to a control group ($p < 0.05$) (Messingham *et al.*, 2002). In a fascinating report Mendlovic *et al*. report that T-cell profiles differ between suicidal and non-suicidal depressed patients, with Th1 and Th2 expression characteristics being observed respectively (Mendlovic *et al.*, 1999). IL-4 is down-regulated in suicidal depressed patients therefore but upregulated in the non-suicidal depressed (3.4+4.8 vs. 10.7+2.6, $P=0.054$), making it a potentially useful marker along with IL-5 and IFN- γ which both showed similar differential expression for the condition.

IL-6

IL-6 is a proinflammatory cytokine, playing an important role in response to injury and trauma, wound healing and various other inflammatory responses. For this reason, it is a suitable candidate marker for estimating vitality and wound age as reported by Grellner (Grellner *et al.*, 2000; Grellner, 2002).

Baseline levels of IL-6 are also known to be significantly higher ($P=0.0005$) than those in healthy individuals (González-Quintela *et al.*, 2000) but that these levels significantly reduce ($P=0.0001$) after a few days if alcohol abusers abstain from consuming alcohol. IL-6 levels are positively correlated with BMI across a broad range of obesity, including morbid states (Khaodhiar *et al.*, 2004) findings that support the idea that obesity itself is in fact an inflammatory state. Another health risk linked to inflammation is that of coronary heart disease. A study in Greece found that individuals who exercised regularly had a 32 % reduction in IL-6 blood levels compared to a control group devoted to a sedentary life ($P<0.05$). Such findings suggest that IL-6 may be a possible marker for lifestyle factors such as regular physical activity.

In a study of 10 burn patients, Yeh *et al*. (Yeh *et al.*, 2000) report that IL-6 levels were significantly higher ($P<0.05$) upon admission (5-13 hours post burn) among the patients that later expired compared to those that recovered, and that there was also significantly higher levels amongst those with more than 50 % total body surface area affected by the injury. Such results confirm other data that IL-6 is a useful marker of the severity of injury following trauma, something noted by Mimasaka *et al*. (Mimasaka *et al.*, 2001) who identified significant differences between mean IL-6 levels amongst individuals that had suffered traumatic death (8606.97 pg/mL) compared to those that had suffered non-traumatic death or disease (2205.65 and 3266.64 pg/mL, respectively).

IL-8

In addition to IL-6 and IL-10, IL-8 levels are also known to be higher among alcoholics but decline a few days post alcohol abstinence (although IL-8 did not decline significantly (González-Quintela *et al.*, 2000)). The same study reports significantly ($P=0.043$) elevated levels of IL-8 in healthy subjects with no history of alcohol abuse, 36 hours after acute intake of alcohol, suggesting IL-8s possible use as a marker of alcohol consumption in the short term or for alcohol abuse.

IL-10

In the same study into effects of alcohol on circulating levels of interleukins, IL-10 was reported to be significantly ($P=0.0007$) higher in alcohol abusers compared with control individuals, but that these levels decreased ($P=0.004$) following alcohol abstinence (González-Quintela *et al.*, 2000), and that acute alcohol intake results in increased IL-10 levels, also reported elsewhere (Girouard *et al.*, 1998). IL-10 levels are also thought to decrease during winter months compared to summer for suffers of SAD (Lam *et al.*, 2004).

Beta-enolase

Enolase exists in mammalian tissues as a dimmer of 3 subunits (α, β, or γ) (Rider & Taylor, 1974; Fletcher *et al.*, 1976). The β forms are muscle-specific, with the ββ type predominantly found in skeletal muscle (Kanefusa *et al.*, 1983). Because of this localisation, β-enolase serves as a marker for origin or blood and also as an indicator or injury to skeletal muscle, with its ratio to total protein being increased 10-30-fold in

trauma blood compared to non-trauma blood. Matsuda *et al*. (Matsuda *et al.*, 1999) demonstrated this, as well as the ability to distinguish crime weapons that had passed through skeletal muscle by way of a sensitive sandwich enzyme immunoassay to detect the elevated ratio, this time some 40 times higher compared to none skeletal muscle stab simulations.

E-selectin

Selectins are a family of cell surface adhesion molecules of which E-selectins are present on endothelial cells. Enhanced levels of E-selectin characterise cardiovascular disease and have shown to represent a number of lifestyle factors such as smoking, hypertension, hypercholesterolemia, and diabetes mellitus (Brown & Hu, 2001) making it an excellent protein marker capable of distinguishing between dietary patterns. This was supported in a study conducted by Lopez-Garcia *et al*. (Lopez-Garcia *et al.*, 2004) where Western dietary patterns characterised by increased consumption of red and processed meats, sweets, desserts, French fries and refined grains, were shown to have a positive correlation with E-selectin plasma concentrations ($P<0.001$) even after adjustment for compounding factors such as age, BMI, physical activity, smoking status and alcohol consumption. Further to this, E-selectin has also shown to be important in establishing at what time a trauma or wound may have occurred (Dressler *et al.*, 2000) with detection levels decreasing significantly ($P<0.05$) 12 hours after the time of injury, and also significant differences between injured and uninjured skin ($P<0.01$).

Fibronectin

Fibronectin is a glycoprotein that circulates in the blood and is a vital component of basement membranes and interstitial connective tissue. It plays an important role during many wound healing processes including cell migration (Postlethwaite *et al.*, 1981), phagocytosis promotion (Molnar *et al.*, 1978; Grinnell, 1980), angiogenesis (Clark *et al.*, 1982), and wound contraction (Niewiarowski *et al.*, 1972). Fibronectin has shown to be a useful marker for age estimation in early stages of wound healing (Fieguth *et al.*, 2003a) confirming previous work by Betz *et al*. (Betz *et al.*, 1992). Fiegurth and colleagues used a polyclonal antibody and stain to immunohistochemically detect fibronectin in a range of wound tissues. Skin samples were taken during autopsies of thirteen individuals that have suffered immediate fatal trauma, and also from forty-six wounds of patients that required surgical treatment following non-fatal trauma. Autopsy collected samples had a post-mortem interval of 1-3 days whilst surgically treated wound samples ranged in age

from 10 minutes to 30 days, with patients aged between 16 and 93 years old. It was not possible to visualise strongly stained fibronectin complexes in any of the wounds incurred as a result of fatal trauma. Strongly stained fibronectin could be regularly visualised in non-fatal wounds older than 20 minutes however, and massive fibronectin networks were detected in some samples over 40 minutes, indicating their potential for establishing vitality in fresh wounds shortly after trauma.

Haptoglobin

Haptoglobin is another glycoprotein found in the blood plasma and has high affinity for free haemoglobin. Clinically it is used as a marker for haemolytic anaemia but it has proven to be a good marker for age and body mass index (BMI) in humans (Chiellini *et al.*, 2004), with serum haptoglobin levels being positively associated with body fat for both males and females ($P<0.05$, $P<0.01$ respectively), the significance of which increases when haptoglobin is plotted against fat mass adjusted for lean mass (muscle, vessels, organs) ($P<0.001$ for males, $P<0.005$ for females). These findings suggest haptoglobin should join a growing list of proteins that are upregulated in human obesity, including TNF-α (tumour necrosis factor alpha), IL-6 (interleukin-6), CRP (C-reactive protein) and leptin, all of which are included in this list of top markers and all of which contribute in some way to inflammatory and or immune responses.

Heat shock proteins

Heat shock proteins (HSPs) are common to every cell in the human body and play important roles in the repair of degenerated proteins as well as having a critical role in the regulation of the cell cycle, cell proliferation, differentiation and apoptosis. Upregulation of HSPs can be induced by a number of stresses including temperatures, alcohol, heavy metals, oxidants, UV, and tobacco smoke and is usually followed by temporary increased resistance to the particular stress involved (Trautinger, 2001). French *et al*. (French *et al.*, 2001) provide a highly plausible link between mobile phone radiation and HSP induced cancer. Their hypothesis suggests that non-thermal radiofrequency radiation exposure from using a mobile phone handset at close proximity to the head could result in chronic over-expression of HSPs that can induce and promote the onset of cancer and/or increase resistance to anti-cancer drugs. Hashiguchi *et al*. (Hashiguchi *et al.*, 2001) report the significantly enhanced expression levels of HSP27, HSP60, HSP70 and HSP90 in polymorphonuclear leukocytes (PMNLs) of patients at various time intervals following trauma, compared to those of healthy volunteers.

Bachelet *et al.* (Bachelet *et al.*, 2002) observed over-expression of HSP70 in human monocytes exposed to either cadmium or tobacco smoke. For a comprehensive review of the HSP70 family see (Kiang & Tsokos, 1998). The response of HSPs to a wide array of stress factors make them ideal markers for a number of profiling uses.

Leptin

Leptin is a peptide hormone produced mainly by fat cells that helps to regulate appetite and metabolism by decreasing the content of neuropeptide Y (NPY) in the hypothalamus (thus reducing desire for food intake) and increasing the body's resting metabolic rate (Zhang *et al.*, 1994). Upregulated in obesity, it has shown to be an important signal between the condition and its related complications such as infertility (Chehab *et al.*, 1996), diabetes (Taylor *et al.*, 1996) and autoimmune diseases (Kuchroo & Nicholson, 2003). Al-Harithy (Al-Harithy, 2004) reported its suitability as a marker for a number of profiling uses including gender (females had higher leptin concentration (6.04 ± 4.71 ng/mL versus 1.72 ± 0.95 ng/mL, $p<0.0001$) than males) and BMI (positive correlation between BMI and leptin was highly significant in female ($r=0.64$; $p=0.0001$) and male ($r=0.49$; $p=0.0001$)). Further studies support the use of leptin as a marker for these biometric conditions (Sinha *et al.*, 1996; Ruhl *et al.*, 2004) and others such as dietary habits (Fung *et al.*, 2001; Yannakoulia *et al.*, 2003). It has also been suggested as an indicator of alcohol misuse (Santolaria *et al.*, 2003) because alcohol abusers are often malnutritioned and show reduced low serum leptin levels as a result.

Prolactin

Prolactin is a peptide hormone secreted by the anterior pituitary gland. In a stimulating study, Exton *et al*. (Exton *et al.*, 2001) report that levels of prolactin are elevated significantly above baseline levels ($P<0.001$ for both males and females) as a result of coitus-induced orgasm and remain so for one hour, making it an ideal marker for indicating an individual's sexual behaviour. It has also shown to be a good indicator of ante-mortem stress levels indicating possible causes of death (Jones & Hallworth, 1999), where mean prolactin levels are significantly elevated above the normal range (up to 500mU/l) in cases of postoperative death or chronic disease (1027 uM/l) and suicide (1398 uM/l). It should be noted that some of the rise in prolactin levels observed in suicide cases is likely attributable to the effects of drug use.

Transforming growth factor-beta

Transforming growth factor-beta (TGF-β) is a cytokine with many functions in the development of cells as well as immune and inflammatory processes. Levels of TGF-β have been shown to significantly rise as a result of *in vitro* treatment of adherent monocytes with ethanol ($P < 0.045$ for 50mM and $P < 0.001$ for 150mM) (Szabo *et al.*, 1992). It was suggested therefore that alcohol consumption might contribute to reduced T-cell proliferation, leading to a depressed immune system, a mechanism that has been documented before (Zhou *et al.*, 1991). TGF-β-1 also appears to have an important role in regulating septic inflammatory responses after burn injuries (Yeh *et al.*, 2002). In a study examining 15 burn patients, of which 8 recovered without sepsis and 7 expired following sepsis, peak serum TGF-β-1 levels were detected within one day of post-burn, followed by a second peak later. Whereas there was no significant difference between the first TGF-β-1 peak levels of the surviving group and those that expired, there was a significant difference ($P<0.01$) between the two groups for mean TGF-β-1 levels of the second peak (51,256 ± 14,264 pg/mL and 24,079 ± 10,399 pg/mL respectively). Such results suggest that a low secondary TGF-β-1 response following burn trauma may contribute to the onset of sepsis and death in burn patients.

Adiponectin

Adiponectin is a hormone synthesised in the adipose tissues that is involved in regulating a number of metabolic processes such as the regulation of insulin resistance and glucose metabolism, as well as lipid homeostasis, with adiponectin enhancing the ability of insulin to suppress glucose production (Berg *et al.*, 2001). It may be possible to use adiponectin as a biometric marker, with circulating adiponectin levels shown to be much higher in females than in males, and also that serum adiponectin levels are positively correlated with fat mass ($P<0.05$) but negatively associated with waist-to-hip ratio ($r=-0.48$, $P<0.01$) (Yannakoulia *et al.*, 2003). Low plasma adiponectin concentration levels have shown to be associated with obesity and type-2 diabetes (Weyer *et al.*, 2001).

Insulin

Insulin is a polypeptide hormone synthesised in the pancreas and secreted in response to rises in blood sugar levels. Upon binding to insulin receptors of cells, glucose is absorbed from the blood into these cells. Marked differences between dietary patterns

and insulin levels have been observed, with Western diets showing significant positive correlation with higher levels of insulin (0.32, P<0.01) compared with prudent diets that were inversely correlated with insulin concentrations (-0.25, P<0.05) (Fung *et al.*, 2001). Western diets are characterised by higher consumption of red and processed meat, high-fat dairy products, sugar containing beverages, sweets and desserts, which is in stark contrast to prudent diets that consist mainly of fruit, vegetables, fish, whole grains and legumes.

Matrix metalloproteinases (MMPs 1, 2, 3, 9, 11)

Matrix metalloproteinases are a group of zinc dependant enzymes capable of degrading a wide range of extracellular matrix proteins. A number of MMP proteins have shown to have high expression levels in menstrual blood only (Bauer & Patzelt, 2002) indicating that their detection may well serve as a highly useful forensic marker when attempting to determine blood origin, possibly to confirm results from simultaneous DD and myoglobin analysis as mentioned previously.

Prostate specific antigen

Prostate-specific antigen (PSA or kallikrein III, seminin, semenogelase, γ-seminoprotein and P-30 antigen as it is also sometimes referred to) is a glycoprotein produced by the prostate gland and secreted into seminal plasma. Low amounts of PSA (0-4ng/mL) (Myrtle & Ivor, 1989) are found in the blood of healthy males, increasing naturally due to a number of reasons such as, age as the prostate itself enlarges, as a result of prostatitis, prostate cancer, and also due to sexual activity. Many methods have demonstrated PSA to be a good marker for the presence of semen, with ELISA methods capable of detecting as low as 4ng/mL. Whilst these methods are restricted to laboratory tests, techniques applicable to clinical environments are available with sensitivity to match ELISA methods. These immunochromatographic tests have been successfully used to detect semen samples from a wide range of sample origins (Hochmeister *et al.*, 1999).

Serum amyloid-A

SAA (serum amyloid-A) proteins are a family of apolipoproteins predominantly produced by the liver and associated with acute phase response to inflammatory stimuli and the development of chronic inflammatory diseases. SAA has four isoforms, of which two

(SAA1 and SAA2) are suitable marker candidates. The expression of these two isoforms is regulated by the proinflammatory cytokines IL-1, IL-6 and TNF-α, and their expression has been seen to increase 1000-fold in mice following acute inflammatory conditions (Zhang *et al.*, 2005). Inflammation plays an important role in the development of cardiovascular disease (CVD), the likelihood of which can be predicted by socioeconomic status alone independent of established risk factors such as smoking and cholesterol levels. As a result, SAA joins the previously identified CRP and fibrinogen as potential markers capable of identifying an individual's socioeconomic status. Jousilahti *et al*. (Jousilahti *et al.*, 2003) identified an inverse relationship between these inflammatory markers and socioeconomic status, particularly among men below the age of 60. The study reports a substantial decrease in SAA concentration with increasing socioeconomic status ($p = 0.018$ for the trend), which remained, although non-significant ($p = 0.118$), after smoking, waist to hip ratio and prevalent longstanding diseases had been accounted for.

Another study supports the use of SAA as a marker for dietary profiling, linking rising inflammatory markers to increased coffee consumption (Zampelas *et al.*, 2004). Coffee is one of several dietary factors considered to have a significant effect on inflammation, although its role in development of CVD such as ischemic heart disease is conflicting. Zampelas *et al.* (Zampelas *et al.*, 2004) identified a significant relationship between coffee consumption and increase in all inflammatory markers observed, but only when comparing participants who drank >200mL coffee with those that did not drink coffee. This observation remained significant even when taking confounding factors into account such as age, sex, BMI, smoking, physical activity status etc. The group also noted a positive association for males and females between coffee consumption and hypercholesterolemia. The study also suggests that the positive association between coffee consumption and IL-6 production may account for increases in SAA, in keeping with the understanding that IL-6 regulates SAA expression. Mean percentage increases in all markers observed in the study for those drinking >200mL of coffee compared to those that drank none are as followed: Men had 50 % higher interleukin 6 (IL-6), 30 % higher C-reactive protein (CRP), 12 % higher serum amyloid-A (SAA), and 28 % higher tumour necrosis factor alpha (TNF-alpha) concentrations and 3 % higher white blood cell (WBC) counts (all: $P < 0.05$); Women had 54 % higher IL-6, 38 % higher CRP, 28 % higher SAA, and 28 l% higher TNF-alpha concentrations and 4 % higher WBC counts (all: $P < 0.05$).

Sex hormone-binding globulin

SHBG is a glycoprotein that binds specifically to the sex hormones testosterone and estradiol. In doing so it inhibits their function, preventing their mode of action. As a result, only a small percentage of the sex hormones circulating in the blood are biologically active and free to enter cells. Because it can have such a dramatic effect on the bioavailability of testosterone, levels of SHBG can be used to identify a number of testosterone dependent characteristics. The production of SHBG is inhibited by growth hormone and insulin-like growth factor-1, and so reduced levels of these can in turn result in decreased testosterone levels which occur in older men (Vermeulen *et al.*, 1996). Body mass index (BMI) is negatively correlated with serum testosterone levels but the level of bioavailable testosterone remains about the same because SHBG levels show a similar negative correlation with BMI, although extreme obesity (BMI>40kg/m2) sees testosterone levels fall more than SHBG. For a more comprehensive review of the behavioural and physical effects of testosterone in healthy men, see the review by Zitzmann & Nieschlag (Zitzmann & Nieschlag, 2001). Many of the SHBG and testosterone findings of this paper are confirmed by Allen *et al*. (Allen *et al.*, 2002) who conducted a questionnaire and measured serum sex hormone levels among 696 men. The results showed that men aged 70 or above had 12 % lower testosterone and 40 % lower bioavailable testosterone compared to men aged 20-29 years old. This correlated with 90 % higher SHBG levels in men of the oldest age group compared to those in the youngest. Dietary factors were also examined with men possessing BMIs in excess of 30 kg/m2 having lower testosterone and SHBG levels (30 % and 45 % respectively) compared to men with BMIs under 20 kg/m2. Even after BMI consideration, a high waist circumference proved to result in 12 % lower testosterone and SHBG levels. Higher testosterone and SHBG levels (15 % and 22 % respectively) were also seen in individuals that smoke 10+ cigarettes a day compared to subjects that had never smoked, and higher levels again (11 % and 16 %) for those that undertook vigorous exercise for more than 3hours a week. Although diet appeared not to have a strong influence on the levels of sex hormones, saturated fat did prove to be negatively associated with SHBG ($r = 0.10$; $p = 0.01$) and a previous study has suggested that men over 70 with a low protein diet may possess elevated SHBG levels (Longcope *et al.*, 2000).

Surfactant-associated protein A

The lungs' alveolar surface is covered by a substance called pulmonary surfactant (Haagsman & van Golde, 1991), the major protein component of which is surfactant-

associated protein A (SP-A). The attraction of this molecule as a marker is its specificity to lung tissue and so detection in serum samples can potentially reveal a great deal of information regarding the state of an individual's lungs which might otherwise be less easily identified. Tests designed to identify development of the foetal lung by determining SP-A levels in amniotic fluid already exist (Kuroki *et al.*, 1985; Tekesin *et al.*, 2004). In the case of forensics, serum SP-A content is essential in providing information on cause and mode of death, because presence of SP-A in the blood indicates damage to the alveolar-capillary membrane. Such damage may result from a number of scenarios such as stab or gunshot wounds to the chest, or from drowning. A group in Japan investigated the link between serum SP-A levels and cause of death (Ishida *et al.*, 2000), identifying markedly increased levels in hyaline membrane diseases, as well as elevated levels for fatal drowning, fire victims and chest trauma (dependent on size or wound). With drowning, damage to the alveolar capillary membrane occurs through aspiration of the water, with salt-water deaths showing a larger rise in serum SP-A levels. The group investigated further in 2002 (Zhu *et al.*, 2002), this time focusing on SP-A levels in cases of fatal drowning. Whilst there was no significant difference found between serum SP-A levels freshwater and saltwater cases, cardiac blood readings confirmed results of previous work that there was a significant ($P<0.05$) increase compared to acute myocardial infarction, confirming its status as a suitable marker for investigating death from drowning.

Table 3.1 Protein markers of interest

#	Protein	Length
1	Myoglobin	154
2	Tumour necrosis factor alpha	233
3	C-reactive protein	224
4	Fibrinogen (D Dimer)	89
5	Fibrinogen (D Dimer)	491
6	Fibrinogen (D Dimer)	437
7	Interferon gamma	166
8	Interleukin 1a	271
9	Interleukin 1b	269
10	Interleukin 2	153
11	Interleukin 4	153
12	Interleukin 6	212
13	Interleukin 8	99
14	Interleukin 10	178
15	Beta-enolase	434
16	E-selectin	610
17	Fibronectin	2386
18	Haptoglobin	406
19	Heat shock protein(s)	247
20	Insulin-like growth factor I	153
21	Leptin	167
22	Prolactin	227
23	Transforming growth factor-beta 1	390
24	Transforming growth factor-beta 4	366
25	Adiponectin	244
26	Insulin	110
27	Matrix metalloproteinase 1	469
28	Matrix metalloproteinase 2	660
29	Matrix metalloproteinase 3	477
30	Matrix metalloproteinase 9	707
31	Matrix metalloproteinase 11	488
32	Prostate specific antigen	261
33	Serum amyloid-A	122
34	Sex hormone-binding globulin	402
35	Pulmonary surfactant-associated protein A	248

35 protein markers of interest to forensic, biometric, and health analysis, selected from surveying over 200 publications spanning more that 15 years' worth of relevant forensic and biomedical research.

3.2 Selection of peptide antigens

Selecting peptide antigens in favour of parent protein antigens aims to address fundamental issues associated with the heterogeneity of proteins' physical properties, as well as problems associated with denaturation and degradation. Digestion with trypsin is predictable and on average produces 50 tryptic peptides for each protein in the human proteome. These peptide antigens are not expected to maintain their original secondary structure and are therefore considered denatured. The scope for further degradation is much reduced compared to that of the original fully folded intact protein. And unlike fully folded native proteins, peptide antigens could be generated synthetically and therefore offer consistent availability and purity unlike traditional native fully folded protein antigens required for antibody production. The peptidomics approach requires the peptide sequence alone for the generation of synthetic peptide antigens. Further still, the many tryptic peptides typically generated following a proteolysis, offer the option of selecting peptides with desired physical properties, e.g. hydrophobicity and solubility. In the past peptide hydrophobicity was correlated to peptide immunogenicity, because surface exposed linear epitopes allowed generating antibodies which could recognise the fully folded proteins (Young *et al.*, 1994). More recently, hydrophilicity of peptide antigens was shown to correlate with their detection in affinity assays (Soloviev & Finch, 2005). That is unlikely to be related to surface exposure of the peptide antigens, but more likely is due to better solubility and hence availability of the antigens in an affinity assay (Hopp, 1993).

The ability to predict or select antigenic peptide sequences would provide a crucial advantage to any antibody generation programme. However, no such information was available for selecting peptide antigens for peptidomic applications. Therefore, following an *in silico* proteolysis of each of the 35 proteins, the peptides generated were ranked in order of their hydrophilicity, calculated using published hydrophobicity scores and our own EXCEL based calculator. For *in silico* digestion, database accession numbers from Uniprot were retrieved for all 35 proteins of interest (**Table 3.1**) and entered into the PeptideMass online service. The following criteria were selected: "reduced" option for Cysteines; no acrylamide adducts; no Methionine oxidation; $(M+H)^+$ and monoisotopic masses. "Trypsin" was chosen as the proteolytic enzyme with "no missed cleavages" results instructed to display all peptides (i.e. bigger than 0 Dalton). Peptides were then sorted by chronological order**,** displaying all post-translational modification, database conflicts, all polymorphisms and splice variants**.** Hydrophilicity value for each of the tryptic peptide generated were calculated by averaging individual using Kyte and Doolittle hydrophobicity amino acid scores over the length of each peptide. Peptides

lengths were limited to between 9 and 16 amino acids, as recommended by the peptide manufacturer. The analysis yielded a number of suitable peptide antigens from each of the proteins analysed, many of which were more hydrophilic than their parent protein (**Figure 3.1)**. One peptide was chosen for each protein target as the antigen for polyclonal sera generation. Peptides selected for each of the 35 proteins are shown in **Table 3.2**.

In most cases the top ranked (most hydrophilic) peptide was selected from the tryptic digested, e.g. as for Myoglobin (**Figure 3.2**), but in some instances (Fibrinogen D-Dimer Fb(b), Beta-enolase, Heat shock protein, Transforming growth factor-beta 1, Adiponectin, Matrix metalloproteinases 9 and 11, Prostate specific antigen, Serum amyloid-A, and Sex hormone-binding globulin) a less hydrophilic peptide was selected on the basis of other parameters relevant to protein synthesis and stability such as the avoidance of prolines, serine series, DG, DP, GNG or QGQ combinations, charge distribution, and glycine and proline distribution. For Fibrinogen (D-Dimer) Fb(a), Interferon gamma, and Interleukin 1a, the top ranked peptide in each case was only selected after the minimum peptide length was relaxed from 9 amino acids to 7 to increase the choice of available peptides. Peptides selected for Tumour necrosis factor alpha and Insulin were selected by manually cleaving long tryptic peptides to produce a better ranked peptide in each case.

For synthesis, CG was added to all (C as linker with SH group, G as a flexible linker) unless G was already in the sequence near the N termini, in which case the peptides were truncated there and just C added, e.g. in the case of Myoglobin (HP**G**DFGADAQGAMNK to **CG**DFGADAQGAMNK), beta-enolase (**G**NPTVEVDLHTAK to **CG**NPTVEVDLHTAK), IGF-1 (**G**FYFNKPTGYGSSSR to **CG**FYFNKPTGYGSSSR), and adiponectin (**G**EPGEGAYVYR to **CG**EPGEGAYVYR). In some cases, just C was added in the absence of G, e.g. Heat shock protein (TTPSYVAFTDTER to **C**TTPSYVAFTDTER), leptin (INDISHTQSVSSK to **C**INDISHTQSVSSK), TGFb1 (LSEPAELTDAVK to **C**SEPAELTDAVK with the cleavage of L too). For insulin, the manually cleaved peptide of choice was further modified at the C-terminus with the substitution of the second C for A (CSLYQLENY**C**N to CSLYQLENY**A**N).

Each of the 35 peptides listed in **Table 3.2** were synthesised with a biotin moiety at the N-terminus and used to generate anti-peptide antibodies in pairs of rabbits (70 antisera total). **Table 3.3** also shows ELISA titers obtained for each of the anti-peptide antisera.

Out of 70 antisera generated only 3 failed to yield any response and the majority of sera resulted in high affinity/titre antisera.

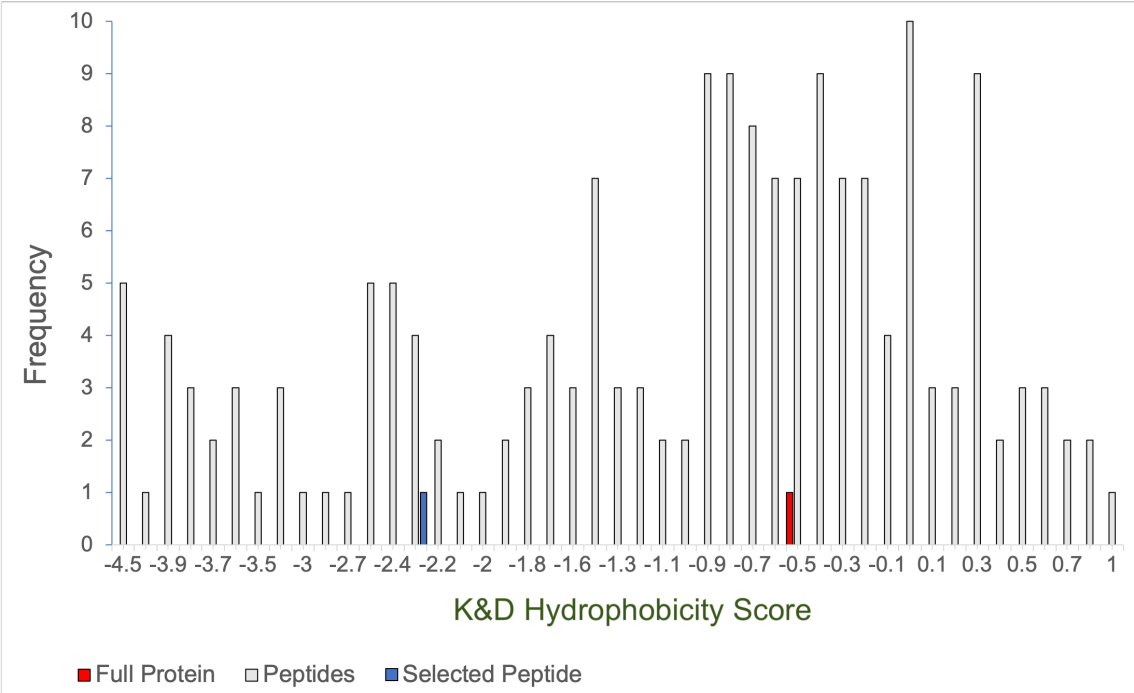

Figure 3.1 Kyte & Doolittle hydrophobicity scores for Fibronectin tryptic peptides vs parent protein

Bar diagram shows the frequency of K&D hydrophobicity scores for tryptic peptides of Fibronectin. Tryptic digestion generates many peptides more hydrophilic than the fibronectin parent protein (red bar). Peptide selected as peptide antigen shown as blue bar.

A

MYOGLOBIN
154 a.a.
UniProtKB ID: **P02144**

MGLSDGEWQL VLNVWGKVEA DIPGHGQEVL
IRLFKGHPET LEKFDKFKHL KSEDEMKASE
DLKKHGATVL TALGGILKKK GHHEAEIKPL
AQSHATKHKI PVKYLEFISE CIIQVLQSKH
PGDFGADAQG AMNKALELFR KDMASNYKEL
GFQG

Kyte & Doolittle Score: -0.48

B

Mass	Position	Sequence
1800.93	2–17	GLSDGEWQLVLNVWGK
1632.87	18–32	VEADIPGHGQEVLIR
407.27	33–35	LFK
910.46	36–43	GHPETLEK
409.21	44–46	FDK
294.18	47–48	FK
397.26	49–51	HLK
738.30	52–57	SEDEMK
662.34	58–63	ASEDLK
147.11	64–64	K
1350.81	65–78	HGATVLTALGGILK
147.11	79–79	K
147.11	80–80	K
1853.96	81–97	GHHEAEIKPLAQSHATK
284.17	98–99	HK
456.32	100–103	IPVK
1913.01	104–119	YLEFISECIIQVLQSK
1515.66	**120–134**	**HPGDFGADAQGAMNK**
748.44	135–140	ALELFR
147.11	141–141	K
828.36	142–148	DMASNYK
650.31	149–154	ELGFQG

D

PEPTIDE ANTIGEN

Tryptic peptide:
HPGDFGADAQGAMNK

Synthetic peptide:
Biotin-CGDFGADAQGAMNK

Hydrophilicity change:
-0.012

C

	A	C	D	E	F	G	H	I	J	K	L	M	N	O	P	Q	R	S	T	U	V
	seq into the cells below	RANK	SET RANGE	9	16	Read K&D	RANK	Amino acid positions with individual K&D scores shown below. do not hcnage the table o													
	to 1000 rows with gaps	all peptides	PEP LENGTH	Suitable				1	2	3	4	5	6	7	8	9	10	11	12	13	1
3	GLSDGEWQLVLNVWGK	16	16	YES	-0.12	2		-0.40	3.80	-0.80	-3.50	-0.40	-3.50	-0.90	-3.50	3.80	4.20	3.80	-3.50	4.20	-0.9
4	VEADIPGHGQEVLIR	17	15	YES	-0.07	3		4.20	-3.50	1.80	-3.50	4.50	-1.60	-0.40	-3.20	-0.40	-3.50	-3.50	4.20	3.80	4.5
5	LFK	21	3	NO				3.80	2.80	-3.90											
6	GHPETLEK	7	8	NO				-0.40	-3.20	-1.60	-3.50	-0.70	3.80	-3.50	-3.90						
7	FDK	8	3	NO				2.80	-3.50	-3.90											
8	FK	14	2	NO				2.80	-3.90												
9	HLK	10	3	NO				-3.20	3.80	-3.90											
10	SEDEMK	6	6	NO				-0.80	-3.50	-3.50	-3.50	1.90	-3.90								
11	ASEDLK	12	6	NO				1.80	-0.80	-3.50	-3.50	3.80	-3.90								
12	K	1	1	NO				-3.90													
13	HGATVLTALGGILK	22	14	YES	1.00	5		-3.20	-0.40	1.80	-0.70	4.20	3.80	-0.70	1.80	3.80	-0.40	-0.40	4.50	3.80	-3.9
14	K	1	1	NO				-3.90													
15	K	1	1	NO				-3.90													
16	GHHEAEIKPLAQSHATK	11	17	NO				-0.40	-3.20	-3.20	-3.50	1.80	-3.50	4.50	-3.90	-1.60	3.80	1.80	-3.50	-0.80	-3.2
17	HK	5	2	NO				-3.20	-3.90												
18	IPVK	20	4	NO				4.50	-1.60	4.20	-3.90										
19	YLEFISECIIQVLQSK	18	16	YES	0.61	4		-1.30	3.80	-3.50	2.80	4.50	-0.80	-3.50	2.50	4.50	4.50	-3.50	4.20	3.80	-3.5
20	HPGDFGADAQGAMNK	13	15	YES	-0.92	1		-3.20	-1.60	-0.40	-3.50	2.80	-0.40	1.80	-3.50	1.80	-3.50	-0.40	1.80	1.90	-3.5
21	ALELFR	19	6	NO				1.80	3.80	-3.50	3.80	2.80	-4.50								
22	K	1	1	NO				-3.90													
23	DMASNYK	9	7	NO				-3.50	1.90	1.80	-0.80	-3.50	-1.30	-3.90							
24	ELGFQG	15	6	NO				-3.50	3.80	-0.40	2.80	-3.50	-0.40								
25																					

Figure 3.2 Selection of peptide antigen for Myoglobin

[A] Protein length, database accession number, amino acid sequence and protein hydrophilicity score for Myoglobin. **[B]** Tryptic digestion of myoglobin protein, with final choice peptide antigen highlighted for reference. **[C]** Results and ranking of peptide suitability for antigen generation based primarily on hydrophilicity scores for peptide sequences. **[D]** Chosen tryptic peptide alongside final peptide sequence submitted for synthesis and hydrophilicity change of final peptide (excluding biotin moiety) compared to parent protein. Equivalent figures for the remaining 34 protein targets are included in the appendix.

Table 3.2 Peptides chosen as antigens for generation of anti-peptide antibodies

Antibody #	Target	Protein length	Peptide sequence	Peptide length	Hydrophilicity change[a]
1	Myoglobin	154	**Biotin-CGDFGADAQGAMNK**	14	-0.012
2	Tumour necrosis factor alpha	233	**Biotin-CGQAEGQLQWLNR**	13	0.860
3	C-reactive protein	224	**Biotin-CGESDTSYVSLK**	12	0.401
4	Fibrinogen (D Dimer)	866	**Biotin-CGDYEDQQK**	9	1.467
5	Fibrinogen (D Dimer)	491	**Biotin-CGDNDGWLTSDPR**	13	1.530
6	Fibrinogen (D Dimer)	437	**Biotin-CGYLQEIYNSNNQK**	14	1.747
7	Interferon gamma	166	**Biotin-CGDDQSIQK**	9	0.767
8	Interleukin 1a	271	**Biotin-CGEMPEIPK**	9	0.285
9	Interleukin 1b	269	**Biotin-CGDDKPTLQLESVDPK**	16	0.586
10	Interleukin 2	153	**Biotin-CGNFHLRPR**	9	0.948
11	Interleukin 4	153	**Biotin-CGQFYSHHEK**	10	1.155
12	Interleukin 6	212	**Biotin-CGFESSEEQAR**	11	0.947
13	Interleukin 8	99	**Biotin-CGTYSKPFHPK**	11	1.081
14	Interleukin 10	178	**Biotin-CGAHVNSLGENLK**	13	-0.115
15	Beta-enolase	434	**Biotin-CGNPTVEVDLHTAK**	14	0.128
16	E-selectin	610	**Biotin-CGNWAPGEPNNR**	12	1.294
17	Fibronectin	2477	**Biotin-CGHYQINQQWER**	12	1.219
18	Haptoglobin	406	**Biotin-CGHYEGSTVPEK**	12	0.629
19	Heat shock protein(s)	641	**Biotin-CTTPSYVAFTDTER**	14	0.095
20	Insulin-like growth factor I	153	**Biotin-CGFYFNKPTGYGSSSR**	16	0.498
21	Leptin	167	**Biotin-CINDISHTQSVSSK**	14	0.545

Table 3.2 (cont.) Peptides chosen as antigens for generation of anti-peptide antibodies

Antibody #	Target	Protein length	Peptide sequence	Peptide length	Hydrophilicity change[a]
22	Prolactin	227	**Biotin-CGEQAQQMNQK**	11	1.508
23	Transforming growth factor-beta 1	390	**Biotin-CGEQLSNMIVR**	11	-0.375
24	Transforming growth factor-beta 4	366	**Biotin-CGQEMYIDLQGMK**	13	0.188
25	Adiponectin	244	**Biotin-CGEPGEGAYVYR**	12	0.290
26	Insulin	110	**Biotin-CSLYQLENYAN**	11	0.693
27	Matrix metalloproteinase 1	469	**Biotin-CGWEQTHLTYR**	11	0.560
28	Matrix metalloproteinase 2	660	**Biotin-CGWEHGDGYPFDGK**	14	0.818
29	Matrix metalloproteinase 3	477	**Biotin-CGNSMEPGFPK**	11	0.387
30	Matrix metalloproteinase 9	707	**Biotin-CGFTEGPPLHK**	11	0.169
31	Matrix metalloproteinase 11	488	**Biotin-CGFPWQLVQEQVR**	13	-0.032
32	Prostate specific antigen	261	**Biotin-CSEPAELTDAVK**	12	0.296
33	Serum amyloid-A	122	**Biotin-CGEANYIGSDK**	11	0.268
34	Sex hormone-binding globulin	402	**Biotin-CGQVSGPLTSK**	11	-0.021
35	Pulmonary surfactant-associated	248	**Biotin-CVEMYTDGQWNDR**	13	0.823

35 chosen protein targets and the corresponding tryptic peptides selected for generation of anti-peptide polyclonal antibodies in rabbits. All peptides were synthesised with a biotin moiety at the C-terminus.

[a] Hydrophilicity was calculated for original protein and chosen peptide using the Kyte-Doolittle algorithm. Values shown represent the difference between those of the original protein and chosen peptide – positive values indicate peptides are more hydrophilic than their parent protein.

Table 3.3 ELISA data for anti-peptide sera

Antibody #	Target	ELISA (mean)[a]
1	Myoglobin	**22,500**
2	Tumour necrosis factor alpha	**37,500**
3	C-reactive protein	**100,000**
4	Fibrinogen (D Dimer)	**2,000**
5	Fibrinogen (D Dimer)	**75,000**
6	Fibrinogen (D Dimer)	**12,000**
7	Interferon gamma	**212,500**
8	Interleukin 1a	**60,000**
9	Interleukin 1b	**300,000**
10	Interleukin 2	**225,000**
11	Interleukin 4	**2,000**
12	Interleukin 6	**0**
13	Interleukin 8	**400,000**
14	Interleukin 10	**500,000**
15	Beta-enolase	**500,000**
16	E-selectin	**50,000**
17	Fibronectin	**500,000**
18	Haptoglobin	**25,000**
19	Heat shock protein(s)	**15,000**
20	Insulin-like growth factor I	**100,000**
21	Leptin	**35,000**
22	Prolactin	**15,000**
23	Transforming growth factor-beta 1	**162,500**
24	Transforming growth factor-beta 4	**300,000**
25	Adiponectin	**60,000**
26	Insulin	**22,500**
27	Matrix metalloproteinase 1	**62,500**
28	Matrix metalloproteinase 2	**15,000**
29	Matrix metalloproteinase 3	**60,000**
30	Matrix metalloproteinase 9	**15,000**
31	Matrix metalloproteinase 11	**22,500**
32	Prostate specific antigen	**20,000**
33	Serum amyloid-A	**87,500**
34	Sex hormone-binding globulin	**400,000**
35	Pulmonary surfactant-associated	**150,000**

35 chosen protein targets and the corresponding tryptic peptides selected for generation of anti-peptide polyclonal antibodies in rabbits. All peptides were synthesised with a biotin moiety at the C-terminus.

[a] ELISA data refers to the mean of two independently raised anti-peptide sera. These indicate the affinity and the titre of the antibody in sera samples obtained.

3.3 Conclusions

1. 35 protein targets were chosen based on their expression patterns across multiple conditions.

2. Proteolytically digested material yields peptides often more suitable for antibody generation than their original proteins. A single peptide antigen was selected for each of the 35 protein targets chosen.

3. 30 of the 35 peptides chosen for synthesis were more hydrophilic than their parent protein, and the majority of the 70 antisera generated resulted in high titre antibodies with only 3 failing to yield any response.

Chapter 4: Multiplexed affinity assays: spatial signal multiplexing using microarrays

This section focuses on the design and development of multiplex affinity assays using microarrays. Microarrays provide a convenient platform, which suits both the multiplex goal of the assays and also provides a sufficiently flexible platform to develop and optimise the assays. Microarrays achieve multiplexing through spatial separation of individual anti-peptide antibodies. A competitive assay format was chosen over traditional direct binding assays to avoid repetitive labelling of the experimental samples and compensate for any heterogeneity of the antibody affinities. The end-to-end workflow for the chapter is summarised in **Figure 4.1**.

The work seeks to determine whether high-throughput proteomic analysis can be achieved using microarrays and the novel anti-peptide antibodies generated in **Chapter 3**.

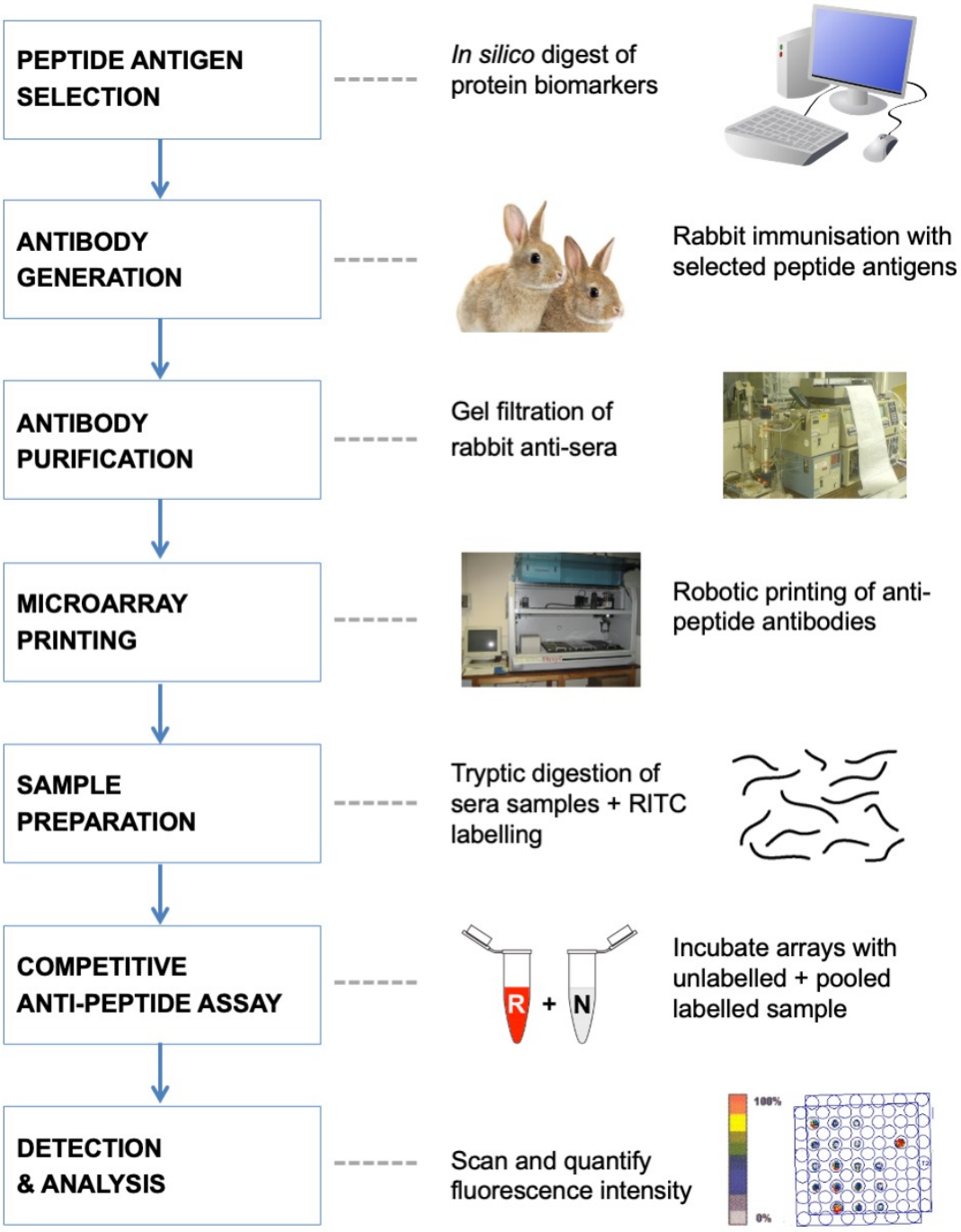

Figure 4.1 An end-to-end peptidomics workflow for anti-peptide microarrays.

Target protein biomarkers are digested *in silico* to generate pool of candidate tryptic peptide sequences. Selected peptides are synthesised and used to raise polyclonal anti-peptide antibodies. Rabbit anti-sera are then purified via SEC and anti-peptide antibodies spotted on microscope slides with immobilised porous membrane. Sera samples are tryptically digested and purified unlabelled samples are used for quantitative competitive displacement assays. The same fluorescently labelled reference sample is used for all assays. Washed and dried membranes are then scanned, and fluorescence intensity quantified to determine up/down protein expression in each sample.

4.1 Purification of anti-peptide antibodies from rabbit serum

Antisera from all 70 rabbits immunised with the 35 peptides generated in **Chapter 3** were purified via gel filtration to isolate the IgG component of the sera. Absorbance began to increase rapidly after 3 minutes signifying the front of the serum's protein elution peak. Fluorescence intensity began to increase shortly after at 4 minutes signifying the elution of the IgG-Cy3 component. To confirm the IgG elution profile an anti-peptide antibody serum sample from one rabbit was then run and serial collections assayed with anti-Rabbit IgG-Cy3 (overlayed in blue on **Figure 4.2**). Two IgG collection intervals were then determined (shaded areas on **Figure 4.2**) corresponding to the 3rd & 4th and 5th & 6th mL of eluent post sample loading to the column. All 70 rabbit sera samples were purified in this way.

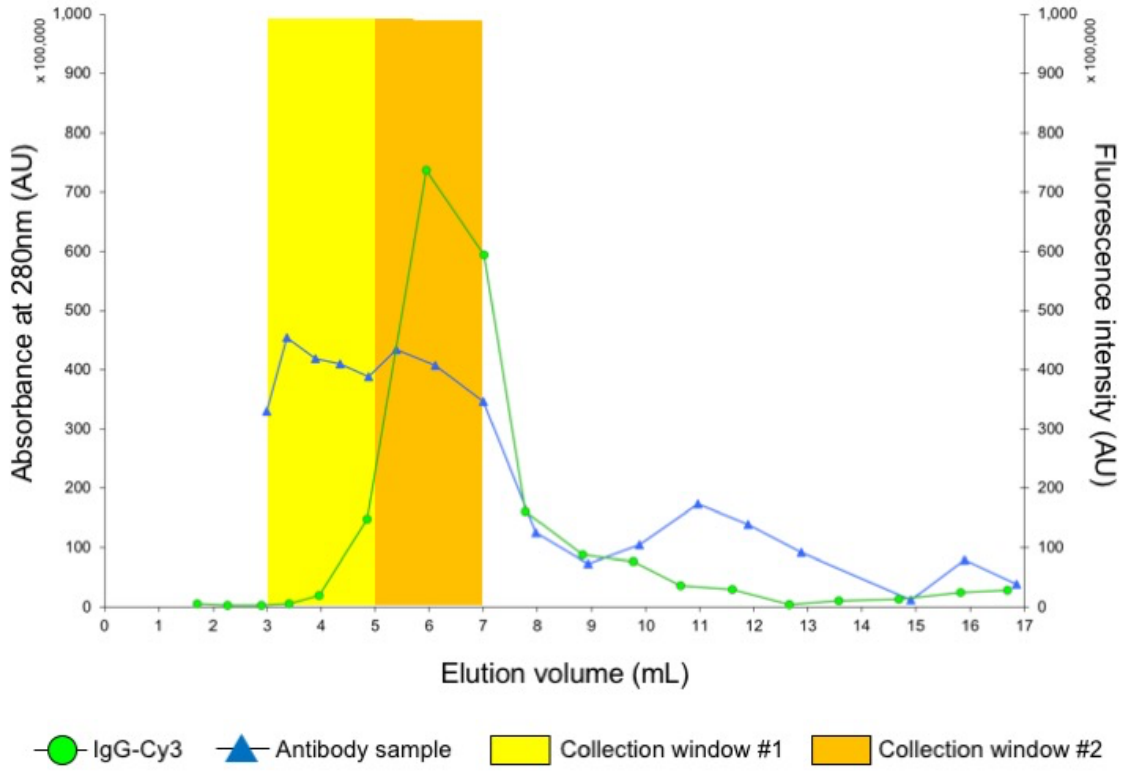

Figure 4.2 Purification of polyclonal anti-peptide IgGs

A serum sample spiked with fluorescent IgG-Cy3 was used to calibrate the IgG elution profile of a Sephadex G100 SEC column prior to the purification of anti-peptide antibodies from rabbit anti-sera. Antibody elution commenced approximately 30 minutes after sample loading, and fluorescence (green) indicates IgG elution follows soon after. This was confirmed by assaying serial collection of eluent from a second serum sample with anti-Rabbit IgG-Cy3 and overlaying the fluorescence plot (blue line). Shaded areas represent the two collection windows used for all subsequent sera samples purified on the column.

4.2 Competitive anti-peptide antibody microarrays

4.2.1 Immobilisation of anti-peptide antibodies on nylon membranes

Thirty-three anti-peptide antibodies were printed in triplicate on positively charged nylon membranes as shown in **Figure 4.3** (antibodies #4 and #12 were excluded due to unsuccessful purification). Additionally, printed samples included visual markers to aid orientation while handling the membranes, and fluorescent reference samples for post-assay pin-to-pin and membrane-to-membrane normalisation.

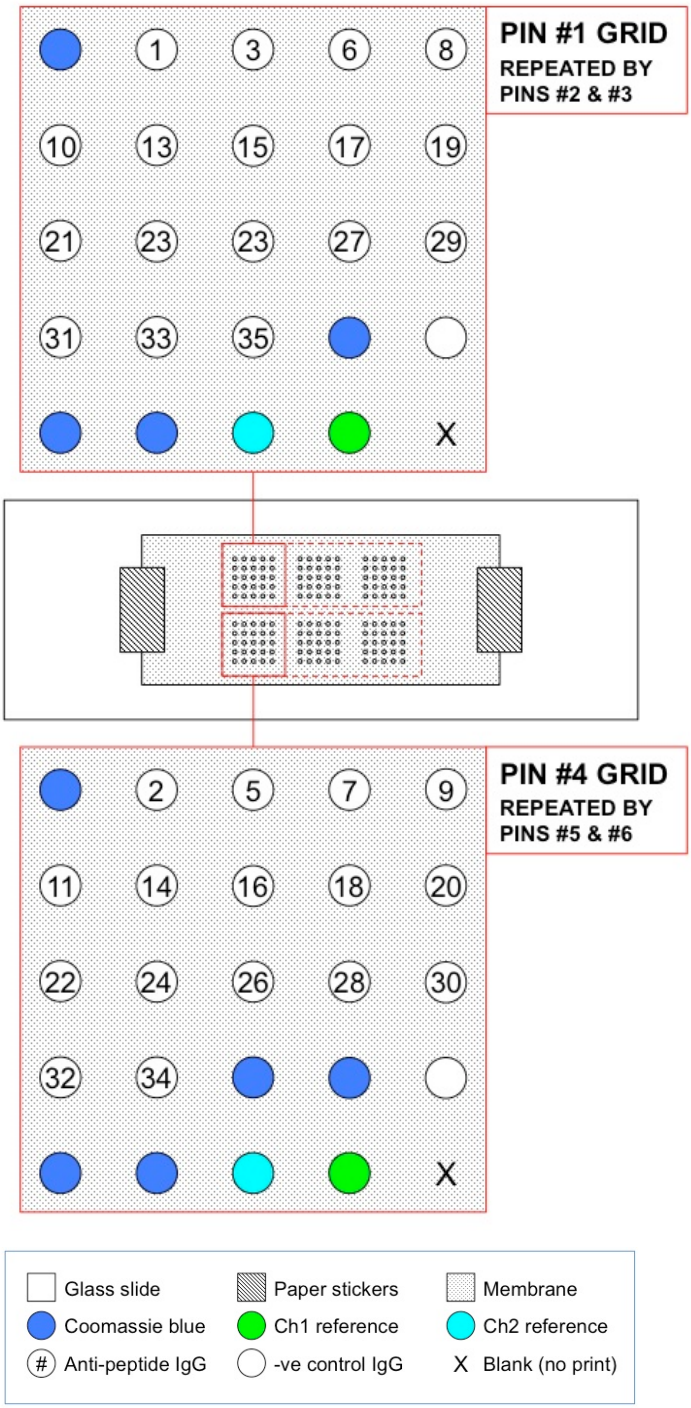

Figure 4.3 A typical printing layout for anti-peptide antibody microarrays.

Membranes were temporarily attached to glass slides using paper stickers during printing. A Flexys microarray gridding robot was loaded with 6 pins for contact printing of samples, with each pin printing a 5x5 grid. Two unique grids were printed in triplicate by pins #1-3 and #4-6 respectively. Coomassie blue was used as a visual marker to aid orientation while handling the membranes. For pin-to-pin and inter-membrane normalisation on a dual-channel Biochip scanner, goat anti-rabbit IgG-Cy3 (emission at 570 nm) and fluorescently labelled Albumin (BSA-646, emission at 646 nm) were used as fluorescent reference samples for Channel 1 and Channel 2 respectively. Anti-peptide antibody sample locations are indicated by numbers – note: antibody #4 and #12 are absent due to unsuccessful purification of these sera samples. Total rabbit IgG was used as a negative control. The final spot in each grid was left unprinted (blank).

The unlabelled:labelled incubation ratio was determined in a preliminary experiment where a range of displacement ratios were tested (**Figure 4.4)**.

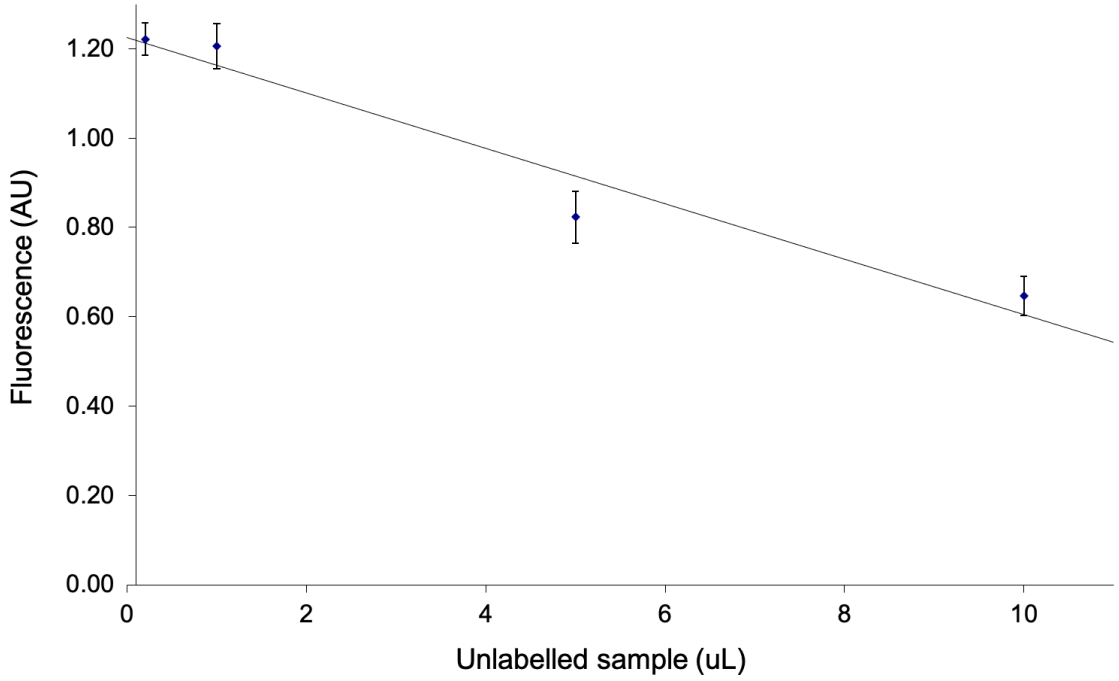

Figure 4.4 Displacement of labelled tryptic peptides.

Fluorescent intensity for microarrays incubated with a range of unlabelled:labelled ratio samples (50 uL of labelled pooled serum used in all samples). Values are averages of all samples on the array. Error bars represent average standard deviation of samples 1, 2, 34 and 35. 10 uL of unlabelled peptide resulted in ~50% displacement of fluorescence when mixed with 50 uL of labelled peptide (1:5).

4.2.2 Case Study: Serum sample assay

Serum samples of rodent origin were provided courtesy of King's College London for the purpose of methodological development. The samples were taken during a study investigating the effect of alcohol consumption on protein expression, and all animals received humane care in compliance with KCL institutional guidelines for the care and use of laboratory animals (Niemelä *et al.*, 2002). Alcohol consumption is known to have wide ranging effects on protein expression (Miles, 1995; Marballi *et al.*, 2016; Zhou *et al.*, 2017) and so it is hypothesised that up/down regulation of all of the 33 protein markers will be observed when comparing samples pre- and post-treatment.

Tryptic serum sample digests were each mixed with a pooled tryptic digest labelled with RITC (5:1) and incubated with the anti-peptide arrayed membranes in a competitive binding assay.

Scanned membranes are shown in **Figure 4.5**. To analyse fluorescence intensities, imaging software was used to overlay two 6x6 grids over each 5x5 pin-printed grid as shown in **Figure 4.5 Panel D**. A total of 6 signal/background grid pairs were used for each membrane.

Readouts were normalised pin-to-pin (using data from pin normalisation scans – see **Table 4.1**) and array-to-array (using fluorescent reference spots – see **Figure 4.5**).

Table 4.1 Pin sizing for pin-to-pin normalisation.

Pin #	Pin size				Mean	FINAL PIN
	a	*b*	*c*	*d*	pin size	FACTORS
Pin 1	1.03	0.94	0.84	0.90	**0.93**	**1.08**
Pin 2	0.82	0.75	0.65	0.68	**0.73**	**1.38**
Pin 3	1.31	1.34	1.27	1.37	**1.32**	**0.76**
Pin 4	0.80	0.84	1.25	1.17	**1.01**	**0.98**
Pin 5	0.78	0.80	0.87	0.85	**0.82**	**1.21**
Pin 6	1.26	1.34	1.12	1.03	**1.19**	**0.84**
CheckSum:	6.00	6.00	6.00	6.00	6.00	

Pin sizes calculated:
a. by normalised means of Channel 1 reference signals
b. by minimising SUMSQ of STDEVPs of Channel 1 reference signals
c. by minimising SUMSQ of STDEVPs of SIGNAL means
d. by minimising SUMSQ of weighted deviations of weighted SIGNAL means

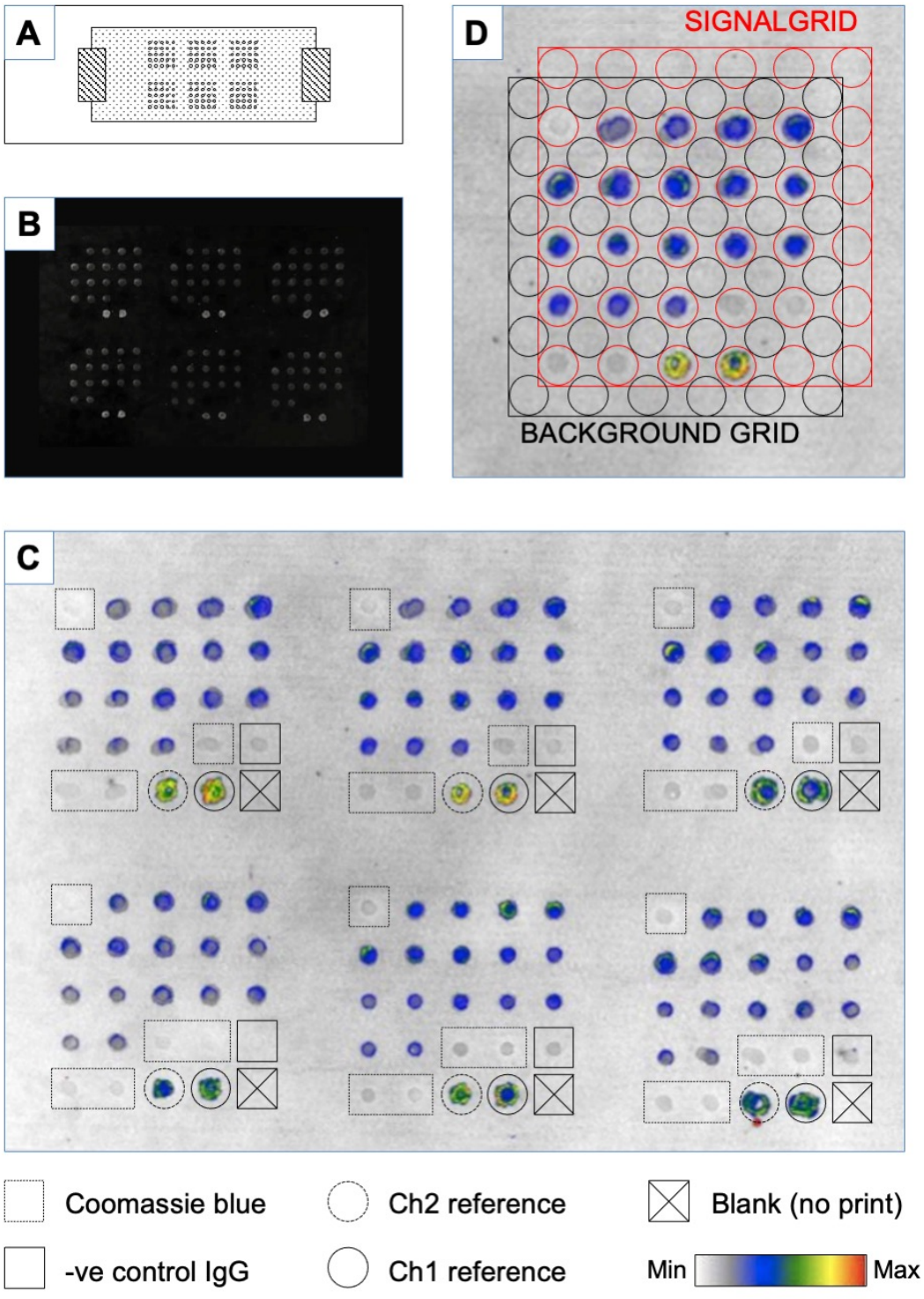

Figure 4.5 Microarrays for fluorescent detection and quantification of peptides

[A] Schematic diagram of printed microarray immobilised on glass slide ready for scanning. **[B]** Fluorescent readout at 550 nm of a microarray containing six grids with 33 anti-peptide antibodies, spotted in triplicate on positively charged nylon membrane and incubated with the proteolytic serum peptides in a competitive binding assay. **[C]** False colours represent signal intensities. **[D]** Imaging software is used to overlay two 6x6 grids to analyse signal strength for each spot. The mean of four background spots surrounding each sample spot are subtracted to provide true signal intensities.

Table 4.2 shows the relationship between samples using pair-wise correlation analysis. Correlation values are shaded red (strongest correlation) to blue (weakest correlation). With the exception of *Individual 2* whose before and after samples correlate strongly with *Individual 1's* after sample and *Individual 3's* before samples respectively, the analysis shows strong intra-individual correlations for *Individual 1*, *3*, and *4*.

The data was then examined to determine which proteins had been up or down regulated as a result of the two treatments. For this, pre- and post-treatment fluorescence was compared, with an increase in fluorescence post-treatment corresponding to a down regulation in sample protein and vice-versa due to the competitive nature of the assay. Up/down regulation of each protein in each of the four individuals is shown in **Figure 4.6**.

While up/down expression of all protein markers was not consistently observed between before and after samples, it was for some of the markers. **Table 4.3** summarises the up/down regulation of each protein after both treatments. 100% scores indicate proteins were either all up or all down regulated in all four individuals; 75% when in three out of four individuals; and 50% when a protein was up regulated in two individuals, but down regulated in the other two. These scores are grouped in **Figure 4.7**. For Treatment 1, matrix metalloproteinase 1 & 2 and pulmonary surfactant-associated protein A were up-regulated in all individuals, and myoglobin, E-selectin, and transforming growth factor-beta 4 were down-regulated in all individuals. For Treatment 2, beta-enolase was up-regulated in all individuals, and interleukin 1b down-regulated in all individuals.

The aim was not to measure individual differences in the expression level of marker peptides, but to identify which of the sera showed similar expression patters of the selected marker peptide and which showed changes, and to quantify a degree of such cumulative changes. The strong intra-individual correlations observed for 3 of the 4 individuals and clear differences between pre- and post-treatment samples validates the method for detecting differential protein expression using multiplexed microarrays with anti-peptide antibodies.

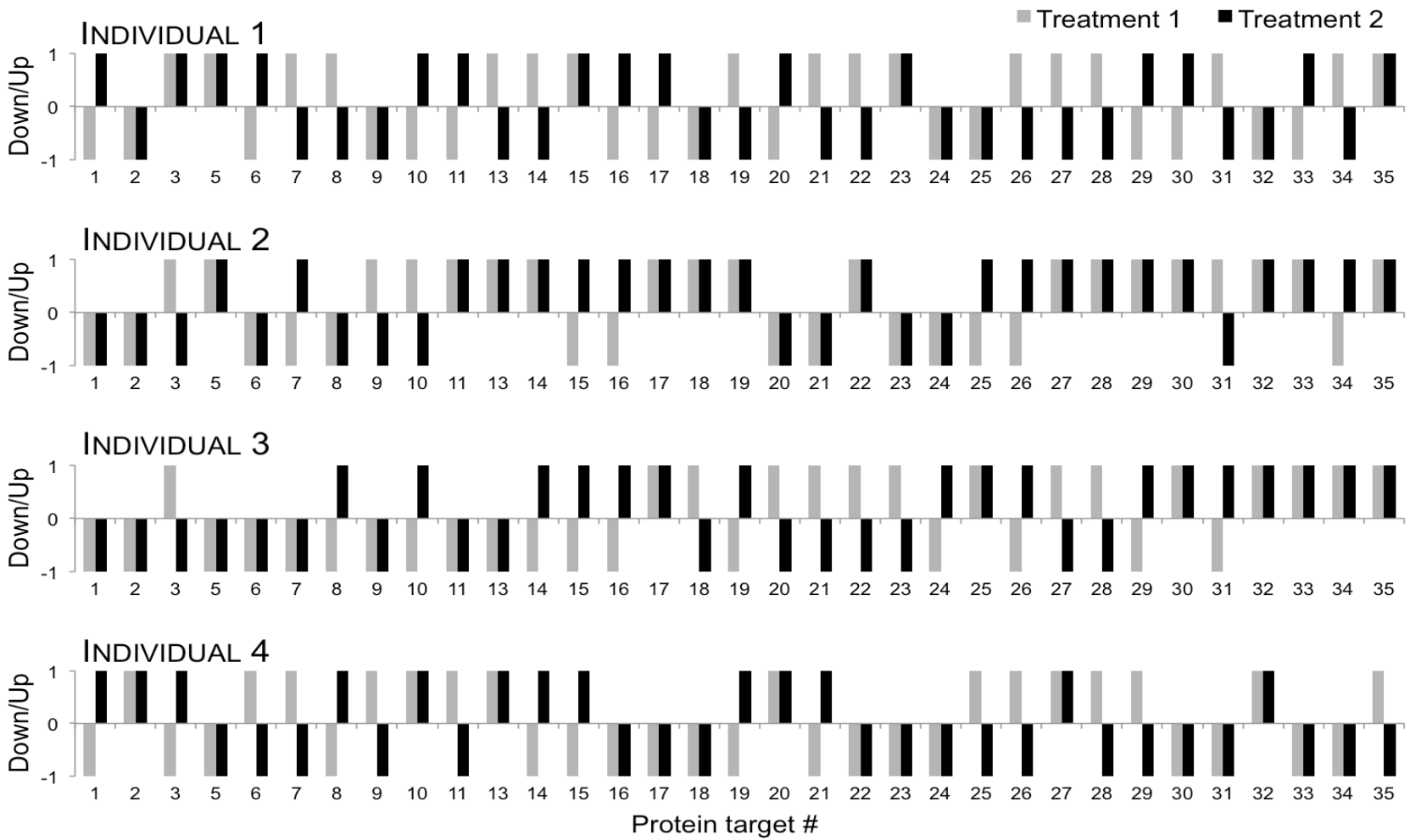

Figure 4.6 Up/down regulation of 33 proteolytic serum peptide markers in four individuals.

Bars represent up (+1) and down (-1) regulation of the 33 peptide markers assayed in samples from four individuals subjected to two treatments. Grey bars show results for treatments 1; black bars show results for treatment 2. For confirmation on target names refer to **Table 3.1**.

Table 4.2 Pair wise correlations indicating the relationship between samples

			SLIDE # :	*JB081*	*JB082*	*JB083*	*JB084*	*JB085*	*JB086*	*JB087*	*JB088*	*JB089*	*JB090*	*JB091*	*JB092*	*JB093*	*JB094*	*JB095*	*JB096*
				INDIVIDUAL 1				**INDIVIDUAL 2**				**INDIVIDUAL 3**				**INDIVIDUAL 4**			
				BEFORE		**AFTER**		**BEFORE**		**AFTER**		**BEFORE**		**AFTER**		**BEFORE**		**AFTER**	
				TR1	**TR 2**	**TR1**	**TR 2**	**TR1**	**TR 2**	**TR1**	**TR 2**	**TR1**	**TR 2**	**TR1**	**TR 2**	**TR1**	**TR 2**	**TR1**	**TR 2**
			Array #	**1**	**2**	**3**	**4**	**5**	**6**	**7**	**8**	**9**	**10**	**11**	**12**	**13**	**14**	**15**	**16**
IND. 1	**BEFORE**	**TR1**	**1**		0.35	0.53	0.54	0.38	0.36	-0.09	-0.25	-0.21	-0.04	-0.09	0.05	-0.43	-0.23	-0.30	-0.42
		TR2	**2**			0.57	0.43	0.43	0.32	-0.06	-0.10	-0.17	0.13	0.12	0.06	-0.49	-0.33	-0.47	-0.46
	AFTER	**TR1**	**3**				0.53	0.55	0.50	0.04	0.01	-0.13	0.14	0.20	0.16	-0.59	-0.38	-0.61	-0.53
		TR2	**4**	**0.49**				0.37	0.56	-0.36	-0.16	-0.35	-0.16	-0.25	-0.13	-0.47	-0.46	-0.53	-0.58
IND. 2	**BEFORE**	**TR1**	**5**						0.42	0.22	0.19	0.13	0.21	0.13	0.06	-0.50	-0.36	-0.69	-0.47
		TR2	**6**							-0.42	-0.14	-0.27	-0.01	-0.36	-0.31	-0.37	-0.45	-0.44	-0.18
	AFTER	**TR1**	**7**								0.54	0.53	0.43	0.71	0.69	-0.16	-0.16	-0.18	-0.27
		TR2	**8**	**0.16**				**0.13**				0.50	0.43	0.51	0.35	-0.03	-0.27	-0.12	-0.05
IND. 3	**BEFORE**	**TR1**	**9**										0.33	0.62	0.46	-0.20	-0.07	-0.09	-0.10
		TR2	**10**											0.60	0.38	-0.23	-0.20	-0.15	-0.22
	AFTER	**TR1**	**11**												0.72	-0.20	-0.19	-0.18	-0.29
		TR2	**12**	**-0.04**				**0.23**				**0.52**				-0.29	-0.07	-0.21	-0.24
IND. 4	**BEFORE**	**TR1**	**13**														0.53	0.41	0.62
		TR2	**14**															0.40	0.50
	AFTER	**TR1**	**15**																0.47
		TR2	**16**	**-0.46**				**-0.29**				**-0.18**				**0.49**			

Correlation values highlighted in grades of red (strongest correlation) through to blue (weakest correlation). Lower left values represent means of upper-right scores. Samples originating from the same individual show highest correlation values to one another – mean values: 0.49 for Individual 1; 0.52 for Individual 3; 0.49 for Individual 4. Individual 2 is an exception to this, with samples showing higher correlation with those from Individuals 1 and 3 (0.16 and 0.23 respectively) than its own (0.13).

Table 4.3 Up/down regulation of 33 proteolytic peptide markers.

Proteolytic peptide marker		Treatment 1		Treatment 2	
#	**Parent protein**	**Up/Down***	**% of cases****	**Up/Down***	**% of cases****
1	Myoglobin	DOWN	100%	up/down	50%
2	Tumour necrosis factor alpha	DOWN	75%	DOWN	75%
3	C-reactive protein	UP	75%	up/down	50%
5	Fibrinogen (D Dimer)	up/down	50%	up/down	50%
6	Fibrinogen (D Dimer)	DOWN	75%	DOWN	75%
7	Interferon gamma	up/down	50%	DOWN	75%
8	Interleukin 1a	DOWN	75%	up/down	50%
9	Interleukin 1b	up/down	50%	DOWN	100%
10	Interleukin 2	up/down	50%	UP	75%
11	Interleukin 4	up/down	50%	up/down	50%
13	Interleukin 8	UP	75%	up/down	50%
14	Interleukin 10	up/down	50%	UP	75%
15	Beta-enolase	DOWN	75%	UP	100%
16	E-selectin	DOWN	100%	UP	75%
17	Fibronectin	up/down	50%	UP	75%
18	Haptoglobin	up/down	50%	DOWN	75%
19	Heat shock protein(s)	up/down	50%	UP	75%
20	Insulin-like growth factor I	up/down	50%	up/down	50%
21	Leptin	up/down	50%	DOWN	75%
22	Prolactin	UP	75%	DOWN	75%
23	Transforming growth factor-beta 1	up/down	50%	DOWN	75%
24	Transforming growth factor-beta 4	DOWN	100%	DOWN	75%
25	Adiponectin	up/down	50%	up/down	50%
26	Insulin	up/down	50%	up/down	50%
27	Matrix metalloproteinase 1	UP	100%	up/down	50%
28	Matrix metalloproteinase 2	UP	100%	DOWN	75%
29	Matrix metalloproteinase 3	up/down	50%	UP	75%
30	Matrix metalloproteinase 9	up/down	50%	UP	75%
31	Matrix metalloproteinase 11	up/down	50%	DOWN	75%
32	Prostate specific antigen	UP	75%	UP	75%
33	Serum amyloid-A	up/down	50%	UP	75%
34	Sex hormone-binding globulin	up/down	50%	up/down	50%
35	Pulmonary surfactant-associated protein A	UP	100%	UP	75%

*UP/DOWN = 100%; Up/Down = 75%; up/down = 50%.
** 100% = 4/4 individuals; 75% = 3/4 individuals; 50% = 2/4 individuals.

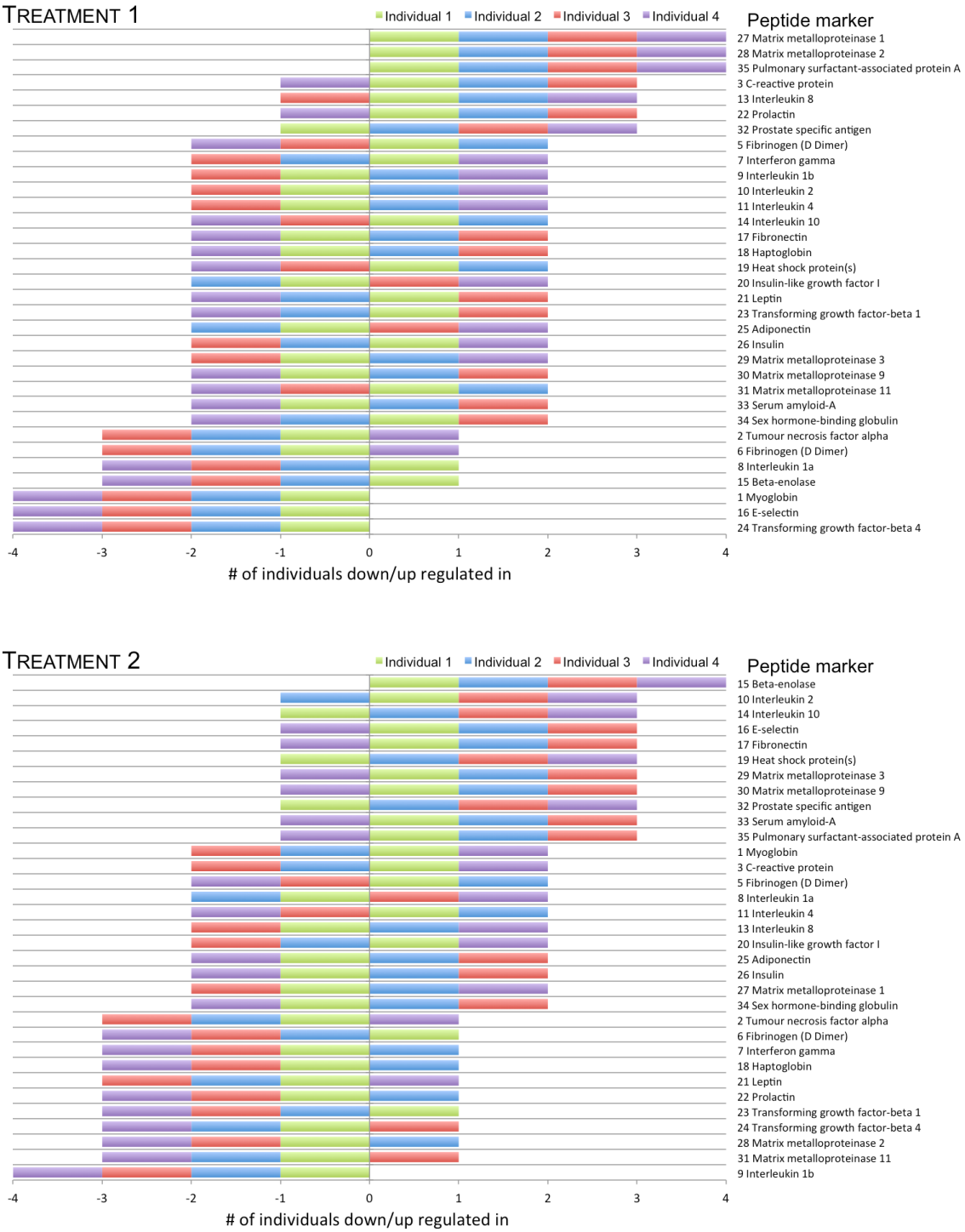

Figure 4.7 Grouping of differentially expressed peptide markers

Stacked bars grouping peptides found to be most commonly up-regulated (top of chart) to most commonly down-regulated (bottom of chart) after Treatment 1 (top chart) and Treatment 2 (lower chart). For Treatment 1, three peptides were found to be up-regulated (matrix metalloproteinase 1 & 2 and pulmonary surfactant-associated protein A), and three down-regulated (myoglobin, E-selectin, and transforming growth factor-beta 4), in all individuals. For Treatment 2, beta-enolase was up-regulated, and interleukin 1b down-regulated, in all individuals.

4.3 Conclusions

1. 68 of the 70 rabbit serum samples were purified with a Sephadex G-100 SEC column to isolate their IgG fraction. These were suitable for printing onto the membrane support and were spotted successfully on positively charged nylon membrane.

2. The intensity of binding can be measured quantitatively in competitive displacement assays using tryptically digested and purified unlabelled samples vs a fluorescently labelled reference sample.

3. Normalisation of grids and spots is crucial and was achieved here through pin-head size factors (for pin-to-pin normalisation), and fluorescent marker reference spots printed within each grid (for grid-to-grid normalisation).

4. Microarrays are suitable assay format for spatial multiplexing. 33 anti-peptide antibody samples were used in a single assay, printed in triplicate on each membrane.

5. Positively charged nylon membrane is suitable for immobilisation of anti-peptide antibodies but is prone to irregularity and artefacts that can increase background intensity on scans and thus decrease the signal:noise ratio.

6. Raw data must be refined through removal of mean background signal, normalisation of values between grids on a single membrane and between individual membranes, and by weighting of values based on relative grid quality. This data refinement is a time intensive process.

7. Strong intra-individual correlations were observed for 3 of the 4 individual sera samples (0.49 for Individual 1; 0.52 for Individual 3; 0.49 for Individual 4). After Treatment 1, three peptides were found to be up-regulated (matrix metalloproteinase 1 & 2 and pulmonary surfactant-associated protein A), and three down-regulated (myoglobin, E-selectin, and transforming growth factor-beta 4), in all individuals. After Treatment 2, beta-enolase was up-regulated, and interleukin 1b down-regulated, in all individuals.

8. The strong intra-individual correlations observed for 3 of the 4 individuals and clear differences between pre- and post-treatment samples validates the method for detecting differential protein expression using multiplexed microarrays with anti-peptide antibodies.

Chapter 5: Multiplexing approaches to membrane and solution-based assays

This chapter explores multiplexing approaches to membrane and solution-based assays with QDs as a means to increase the number of analytes that can be assayed simultaneously.

The work seeks to determine if lateral flow devices could be a simpler and faster alternative to microarrays, as well as explore their compatibility with QDs to provide superior detection capabilities over traditional labelling reagents and achieve multiplexed testing.

5.1 Immobilised and lateral flow single-plex assays

5.1.1 Synthesis and characterisation of GNPs and GNP-protein conjugates

Gold nanoparticles were synthesised by reducing tetrachloroauric acid hydrate with sodium citrate, using the workflow summarised in **Figure 5.1**. Protein molecules readily adhere to GNP surfaces due to electrostatic and hydrophobic interactions, but insufficient protein concentration will cause GNPs to aggregate when mixed with high concentration salt solution, therefore it was important to determine the protein concentration required to produce stable GNP-protein conjugates.

To do this, a salt titration was performed with aliquots of GNPs mixed with a range of BSA concentrations. Solutions with insufficient protein concentration turned blue and aggregated when treated with a high concentration of NaCl as can be seen in **Figure 5.2**. The lowest BSA concentration that provided sufficient blocking of the GNP surface in 30 minutes, was 0.1 mg BSA per 1 mL of GNPs. Protected GNPs display no colour change when exposed to high concentrations of NaCl. The absorbance spectra of unprotected GNPs and GNP-BSA conjugates were then compared using a spectrophotometer. Protein conjugated GNPs exhibited a clear red-shift of 7 nm at absorbance maximum compared with unconjugated GNPs (see **Figure 5.3**).

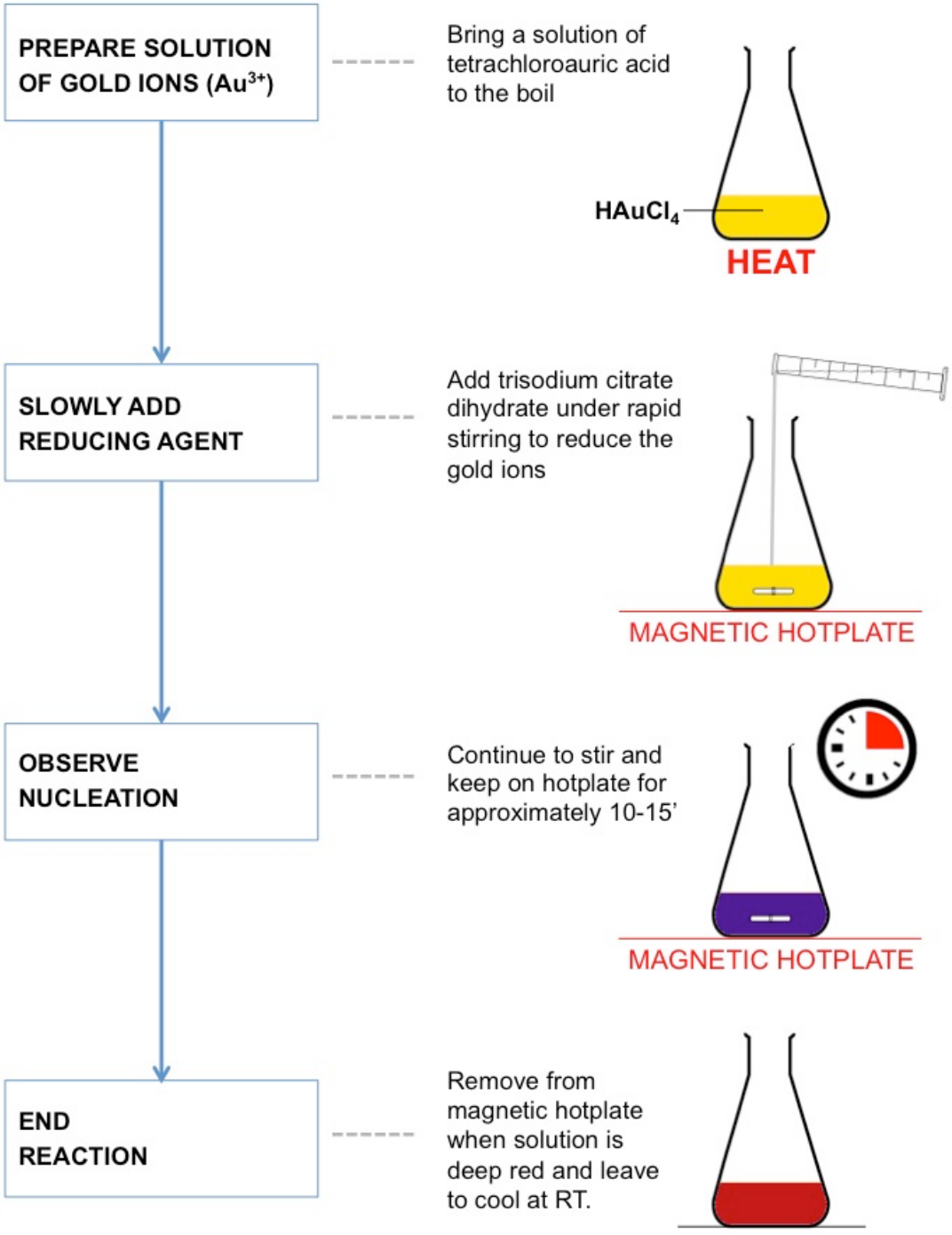

Figure 5.1 Workflow for synthesis of gold nanoparticles.

A solution of tetrachloroauric acid ($HAuCl_4$) was heated to boiling point and then reduced by slowly adding sodium citrate dehydrate under rapid stirring. As the gold ions begin to aggregate and form gold nanoparticles the solution changes colour from yellow to dark blue. The solution eventually turns deep red, signalling the endpoint of the reaction.

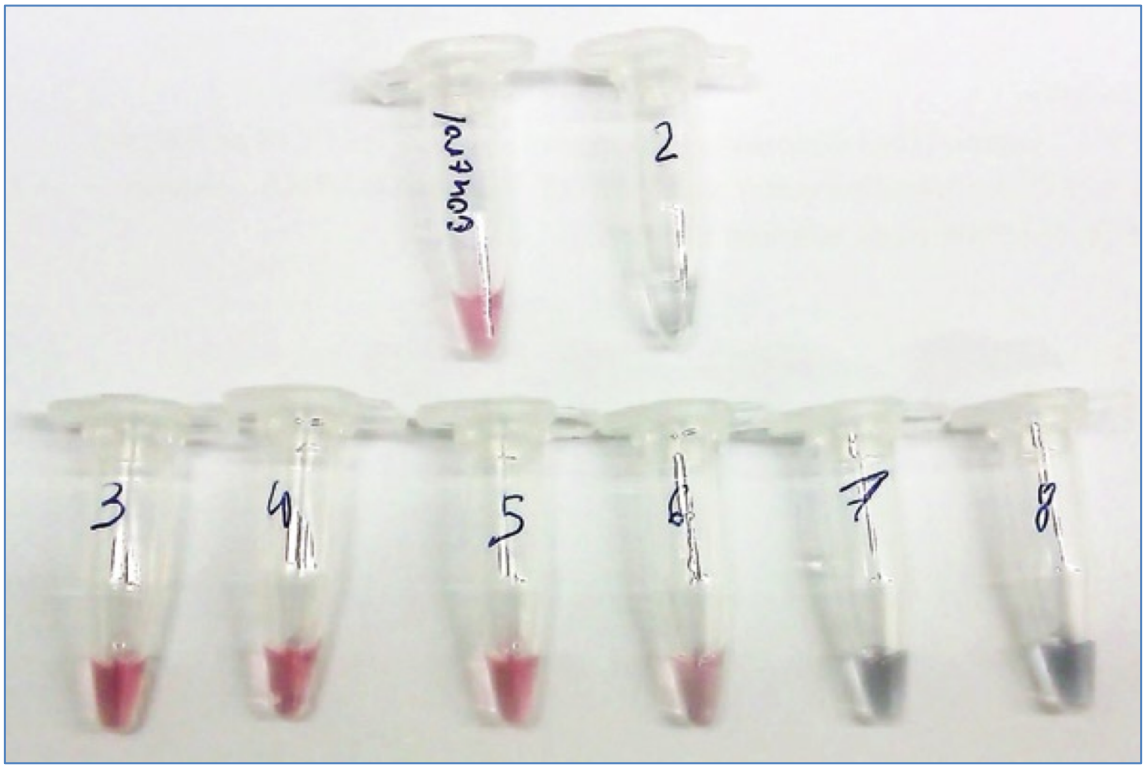

Figure 5.2 Results of GNP-BSA conjugate dilution series following same salt-titration series.

Tube 1 (“Control”) contains no salt (no protein, no salt control). Tube 2 is negative control (no protein, 4 % NaCl). Each sample had 20 mL of GNPs preincubated with variable amounts of protein prior to the addition of salt (5, 2.5, 2, 1, 0.5, and 0.25 mg in tubes 3–8 respectively; final 4 % NaCl in each tube). The binding 2 mg per 20 mL of GNP (0.1 mg BSA per 1 mL GNPs) results in blocking the surface and prevents aggregation of nanoparticles. [Photo of set that followed the same protocol detailed in 2.2.2 (Bailes *et al.*, 2012a).

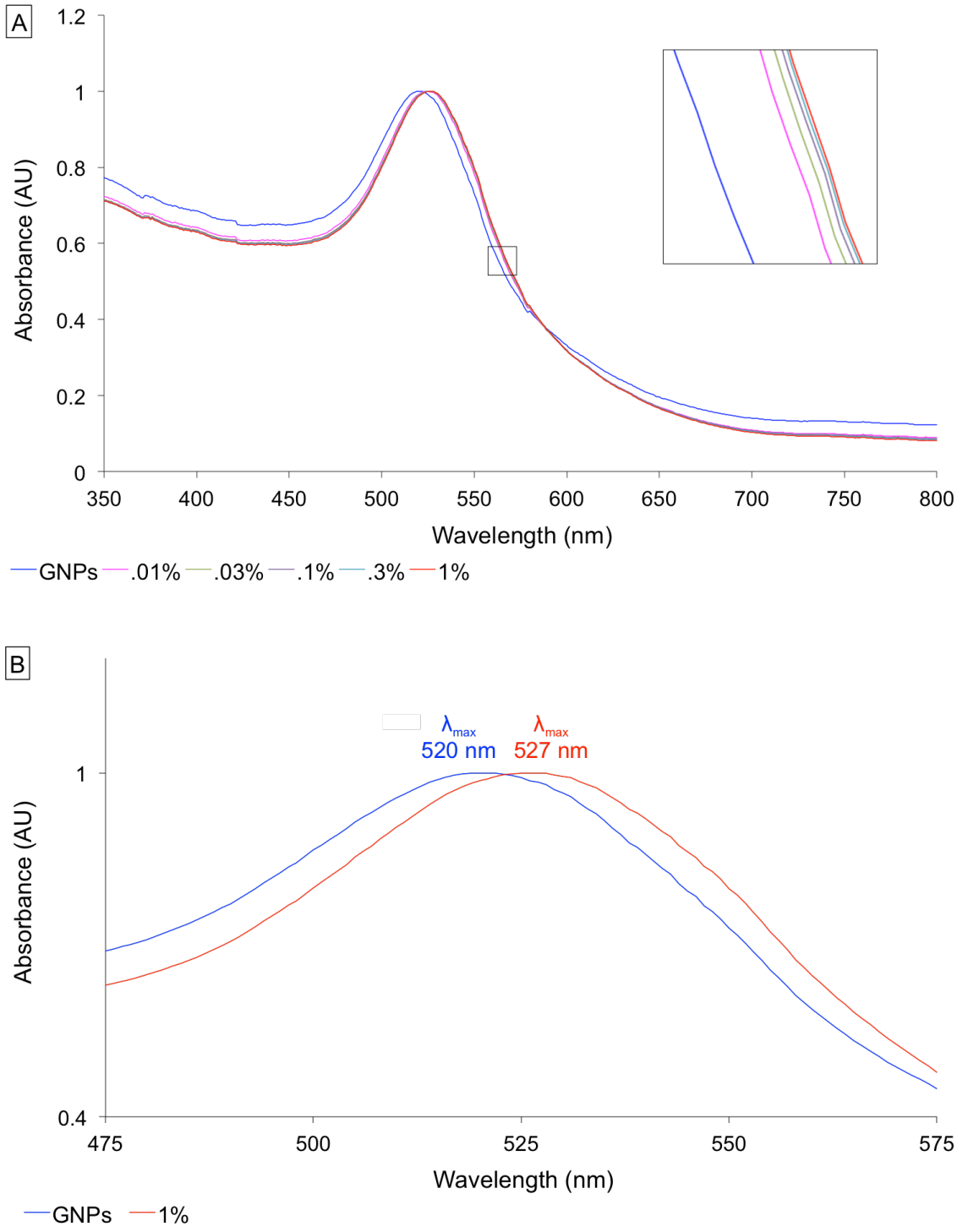

Figure 5.3 Absorption spectra for GNPs and GNP-BSA conjugates

[A] Normalised absorption spectra for non-derivatised GNPs and GNP-protein conjugates with range of BSA concentrations (0.01% – 1%). Insert (top right corner) shows blown-up section of the absorption spectra to highlight the cluster of GNP-BSA spectra clearly distinct from the unconjugated GNP spectrum and increasing red shift with increasing protein concentration. **[B]** Absorption maxima for GNPs and GNP-BSA showing red shift of 7 nm for λ_{max} of GNP conjugates.

5.1.2 Benzodiazepine lateral flow assays

Lateral flow tests against the benzodiazepine, diazepam were prepared and assembled.

The lateral flow tests were competitive immunoassays where sample is applied directly to the device and mixes with GNP-conjugated capture antibody as it diffuses along the test strip. The GNP-antibody conjugate was prepared by conjugating a BEN1 anti-benzodiazepine monoclonal antibody to GNPs. The GNP-BEN1 conjugates were dried in place on glass fibre strips that were then assembled on backing card with sample and absorbent pads, and nitrocellulose membrane as shown in **Figure 2.3**. The membrane was striped with a test line at 13 mm, and a control line at 16 mm from its leading edge. The test line consisted of a BSA-oxazepam conjugate (BSA is required to ensure reliable binding to the membrane and provide optimum orientation of the oxazepam molecule for recognition by the antibody), and the control line was anti-mouse IgG. Batch assembled materials were cut into individual strips using a BioDot CM4000 guillotine cutting module and inserted into plastic cases as shown in **Figure 5.4 (Panel A)**. Buffer and equine plasma samples were spiked with a serial dilution of the benzodiazepine, diazepam. In negative samples, no sample analyte binds to the GNP-antibody conjugate which in turn binds freely to the oxazepam immobilised at the test line and to the anti-mouse antibody at the control line, resulting in two clearly visible red lines. Positive samples display a fading, or complete disappearance depending on concentration of the sample analyte, of the test line as sample analyte binds GNP-antibody conjugates and prevents their binding to oxazepam at the test line. Both scenarios are shown in **Figure 5.4 (Panel B)**, where a buffer sample spiked with 10 ug/mL of diazepam results in a weaker control line (left test case), and a negative plasma sample displays two strong lines (right test case). All assays took less than 10 minutes to complete following application of the sample, with appearance of the control lines signifying the end of the test.

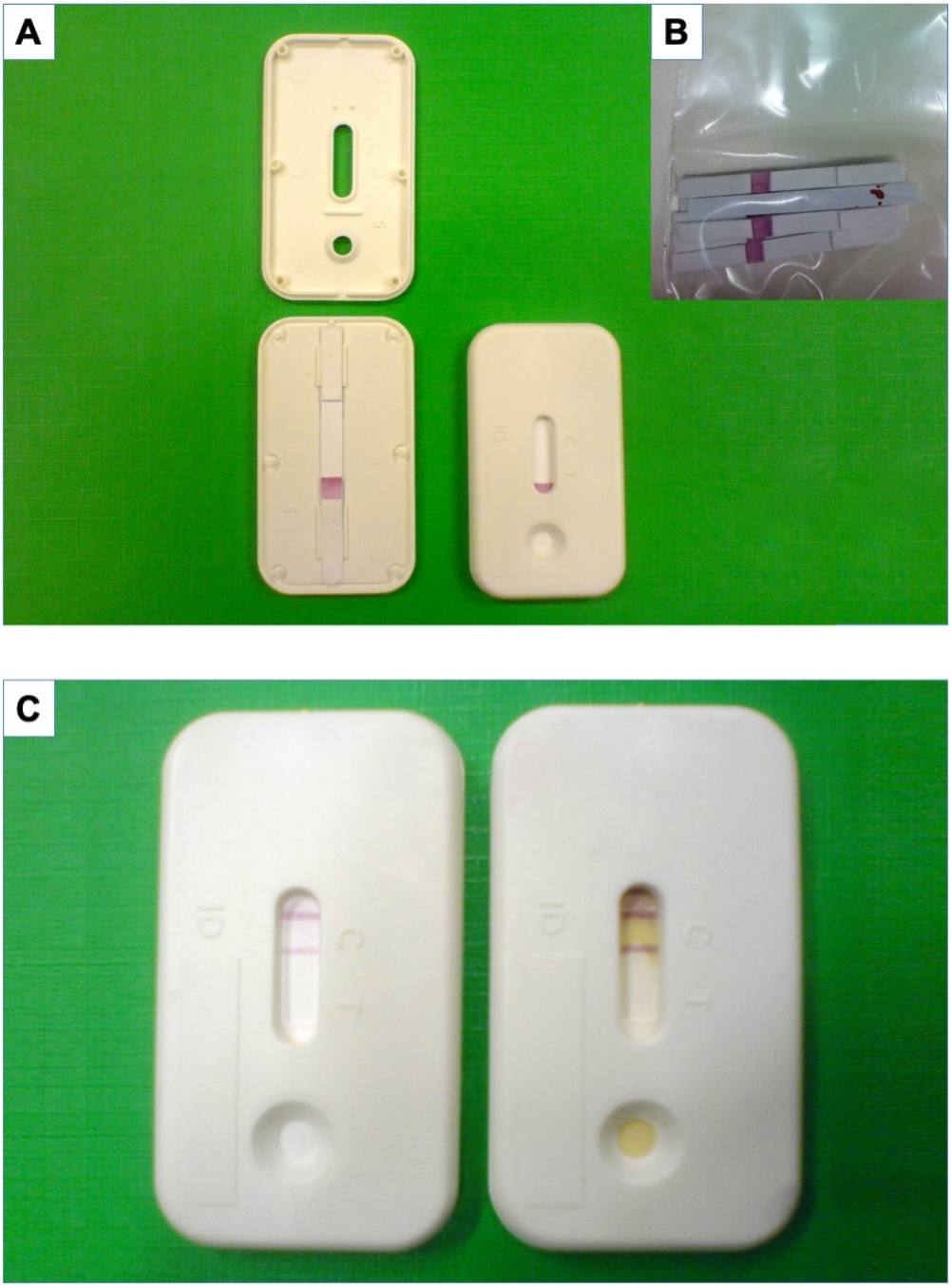

Figure 5.4 Benzodiazepine lateral flow test devices

[A] Photograph of unused benzodiazepine lateral flow test devices with top casing removed (left) and fully assembled (right) complete with designated sample well and results window. **[B]** Assembled lateral flow strips stored in dry conditions – can be kept for 12 months before use. **[C]** Benzodiazepine lateral flow test devices following application of sample in buffer (left) and in equine plasma (right). The buffer applied to the left test was spiked with 10 ug/mL of diazepam resulting in a weaker capture line (deposited at 13 mm from origin of membrane) compared to the control line (at 16 mm), whereas the negative plasma sample applied to the right test device results in two equally strong lines.

5.2 Spectral multiplexing

5.2.1 Characterisation of unmodified toluene-based quantum dots

Emission spectra properties of CdSe/ZnS Core/Shell "EviDots" (QDs 1-6) are determined mainly by their size. Size dispersion of ODs in each individual preparation will determine the range of emitted wavelengths and will ultimately determine the degree of spectral multiplexing achievable. Therefore, determining accurate emission spectra for all available stocks was required. Furthermore, accurate deconvolution of complex multiplexed spectra depends on the accurate calibration and precise knowledge of the individual QD emission spectra.

Size characterisation

Transmission electron microscopy (TEM) was used to determine nanoparticle diameter, an important characteristic because the emission wavelength of a QD is size dependent. **Figure 5.5** shows TEM micrographs obtained for samples of QDs 1-6 deposited on the surface of carbon-coated copper grids (emission maxima are as quoted by the manufacturer). Adobe Photoshop's measuring tool was used to measure the diameter of particles from QD3 and QD6 populations in two different ways: firstly, by measuring the edge-to-edge of individual particles; and secondly by measuring centre-to-centre distances between neighbouring particles on the basis that two particles cannot be closer than a particle's diameter. Hundreds of measurements were taken to determine the average particle diameter for both populations (see **Figure 5.6**). A TRIMMEAN average of diameter measurements excluding 10% outliers provided values closest to those supplied by the manufacturer, with populations QD3 and QD6 averaging 2.79 nm +/- 0.41 nm and 5.52 nm +/- 0.70 nm, vs 2.6 nm and 5.2 nm respectively (see **Table 5.1**). While centre-to-centre measurements should in theory provide the most accurate determination of particle diameter, these averages greatly differed from those specified by the manufacturer. This is likely due to low density of particles distributed on the copper grids. Other "EviDots" preparations were not analysed.

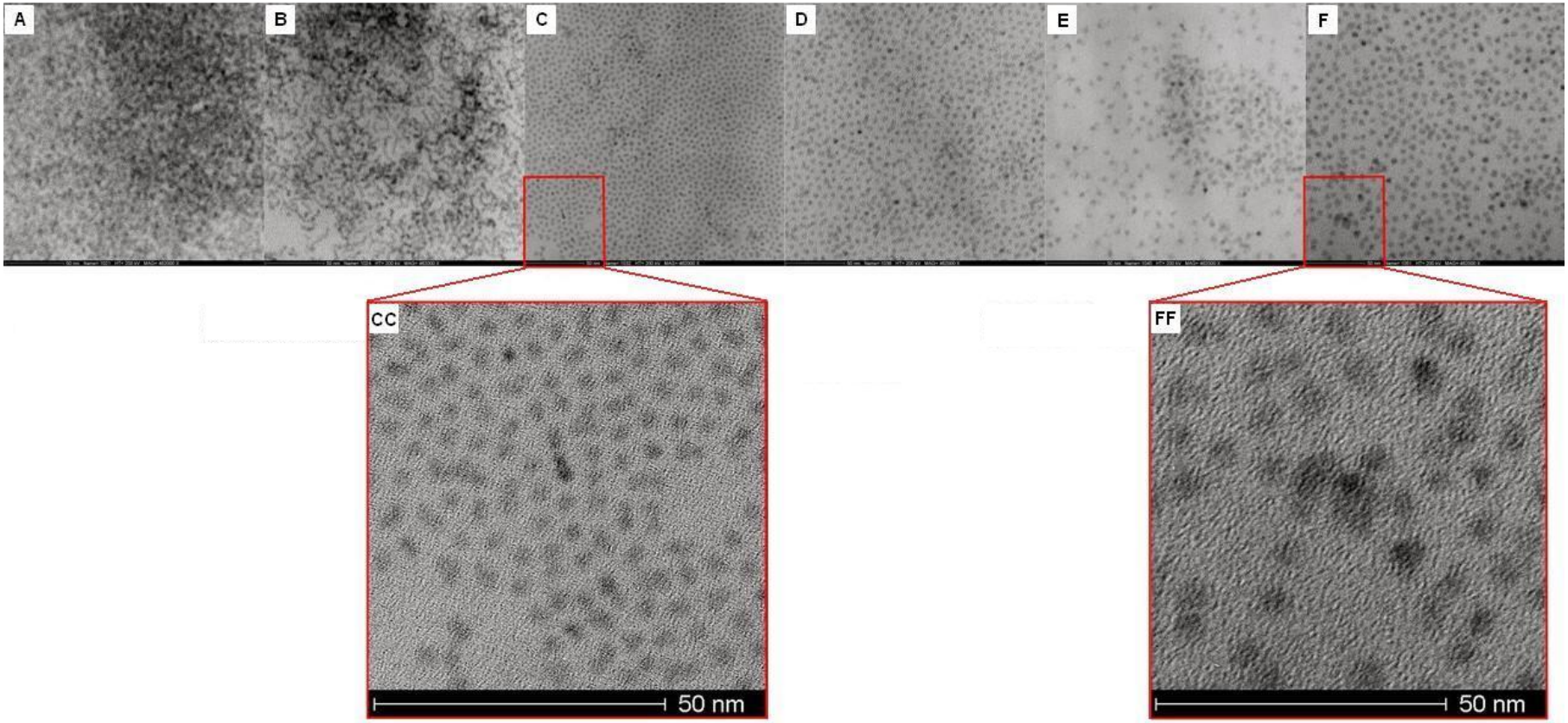

Figure 5.5 Size characterisation of CdSe/ZnS QDs deposited on the surface of carbon-coated copper grids.

[A-F] TEM micrographs of QDs 1-6. **[A]** QD1 Em. Max 517nm; **[B]** QD2 Em. Max 544nm; **[C]** QD3 Em. Max 566nm; **[D]** QD4 Em. Max 579nm; **[E]** QD5 Em. Max 598nm; **[F]** QD6 Em. Max 612nm. Emission maxima are as quoted by the manufacturer. [CC & FF] 500% magnified segments of **[C]** and **[F]** respectively and used to estimate mean particle size for each population using Adobe Photoshop's measuring tool. QDs 3 and 6 were found to have a mean particle size of 2.79 nm +/- 0.41 nm and 5.52 nm +/- 0.70 nm respectively. Size information supplied by the manufacturer is 2.6 nm and 5.2 nm respectively. Images kindly provided by Dr Ivanov of Université de Haute-Alsace, Mulhouse, France (Bailes *et al.*, 2009).

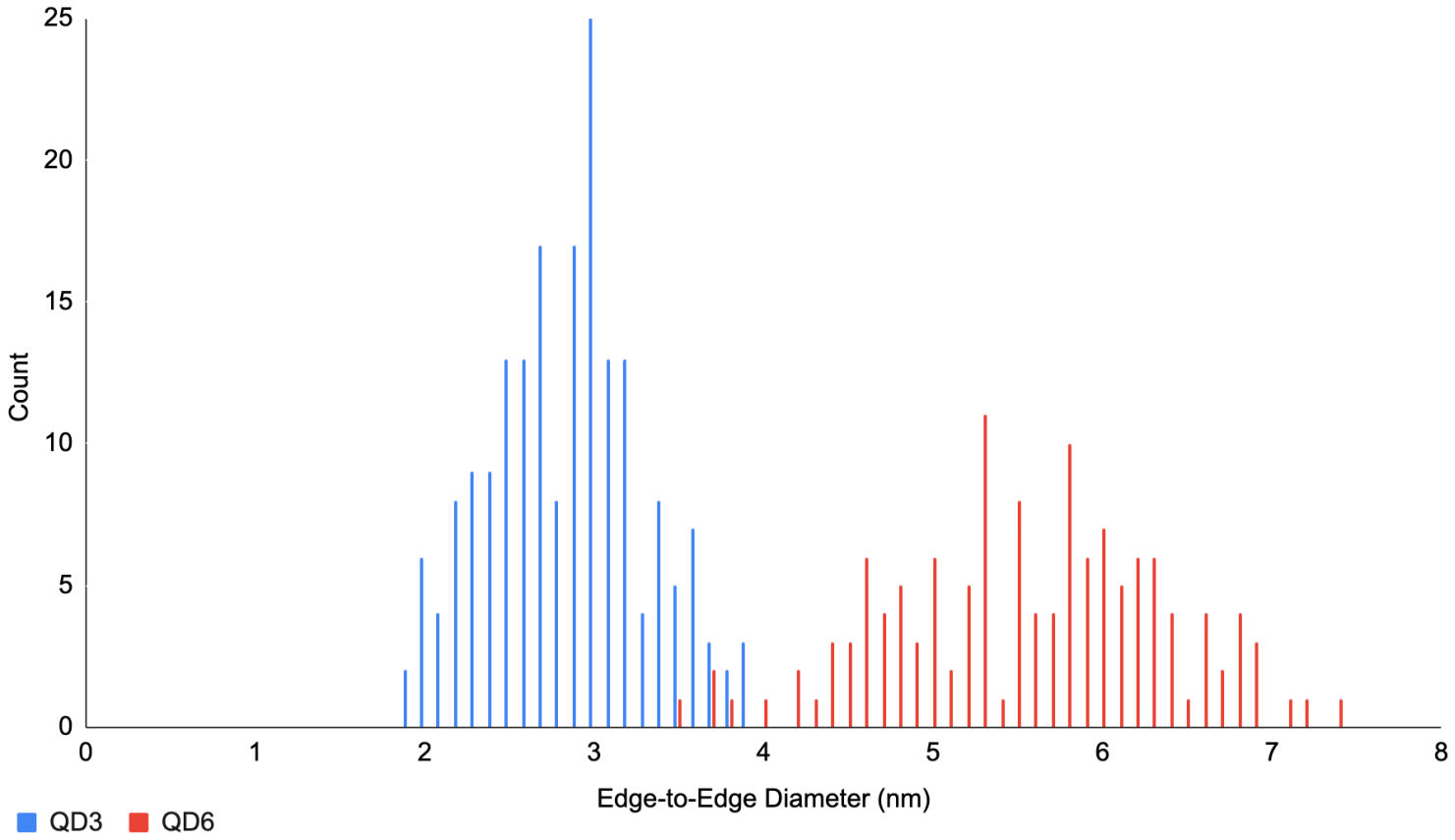

Figure 5.6 Particle size distribution for QD3 & QD6 populations

Edge-to-edge diameter measurements for QD3 and QD6 populations. TRIMMEAN diameter for QD3 was 2.79 nm +/- 0.41 nm, and 5.52 nm +/- 0.70 nm for QD6.

Table 5.1 Size of CdSe/ZnS Core/Shell "EviDots" quantum dots (QDs 3 & 6)

	Manufacturer	**Centre-to-Centre** (between two dots)			**Edge-to-Edge** (of single dots)		
QD#	**Diameter (nm)**	**MEAN diameter (nm)**	**MODE diameter (nm)**	**TRIMMEAN diameter (nm)**	**MEAN diameter (nm)**	**MODE diameter (nm)**	**TRIMMEAN diameter (nm)**
QD3	**2.6**	5.08 (1.24)	4.9	5.02 (0.67)	2.80 (0.45)	3.0	**2.79 (0.41)**
QD6	**5.2**	6.76 (1.55)	5.3	6.73 (1.38)	5.51 (0.81)	5.3	**5.52 (0.70)**

Bracketed values represent standard deviation. TRIMMEAN values of edge-to-edge measurements most closely match those values provided by the manufacturer (Evident Technologies) suggesting that the populations were not densely packed when imaged.

Spectral characterisation

Excitation and emission spectra of QDs 1-6 were characterised using a Perkin Elmer LS50B spectrofluorimeter.

The excitation spectrum obtained for QD1 using an experimentally determined emission maximum (518 nm) shows excitation intensity increases towards the UV end of the spectrum **Figure 5.7 (Panel A)**.

Four individual emission spectra obtained for the same population of QDs using four separate excitation wavelengths (300 nm, 340 nm, 380 nm and 450 nm) show emission intensity increases with decreasing excitation wavelength **Figure 5.7 (Panel B)**. Whilst the use of lower excitation wavelengths provides stronger emission spectra, excitations at 300 nm, 340 nm, 380 nm and 450 nm generate second order peaks at 600 nm, 680 nm, 760 nm and 900 nm respectively (not shown) which could potentially interfere with emission spectra of some QDs. In this instance, an excitation wavelength of 380 nm provides a good compromise between relative emission intensity and avoidance of second order peak interference at 760 nm as none of the QDs being investigated have an emission profiles that would overlap in this range.

Emission spectra for all toluene-based QDs 1-6 with a single excitation wavelength of 380 nm show QD emission intensity varies between samples and QD2 emission is extremely weak **Figure 5.8 (Panel A)**. Many of the emission spectra overlap and would require filtering from one another (deconvolution) if used together in an assay mixture. Normalised spectra are shown in **Figure 5.8 (Panel B)** with emission maxima for each QD population. These emission maxima are ±5 nm of the values quoted by the manufacturer.

The physical properties for QDs 1-6 are summarised in **Table 5.2**.

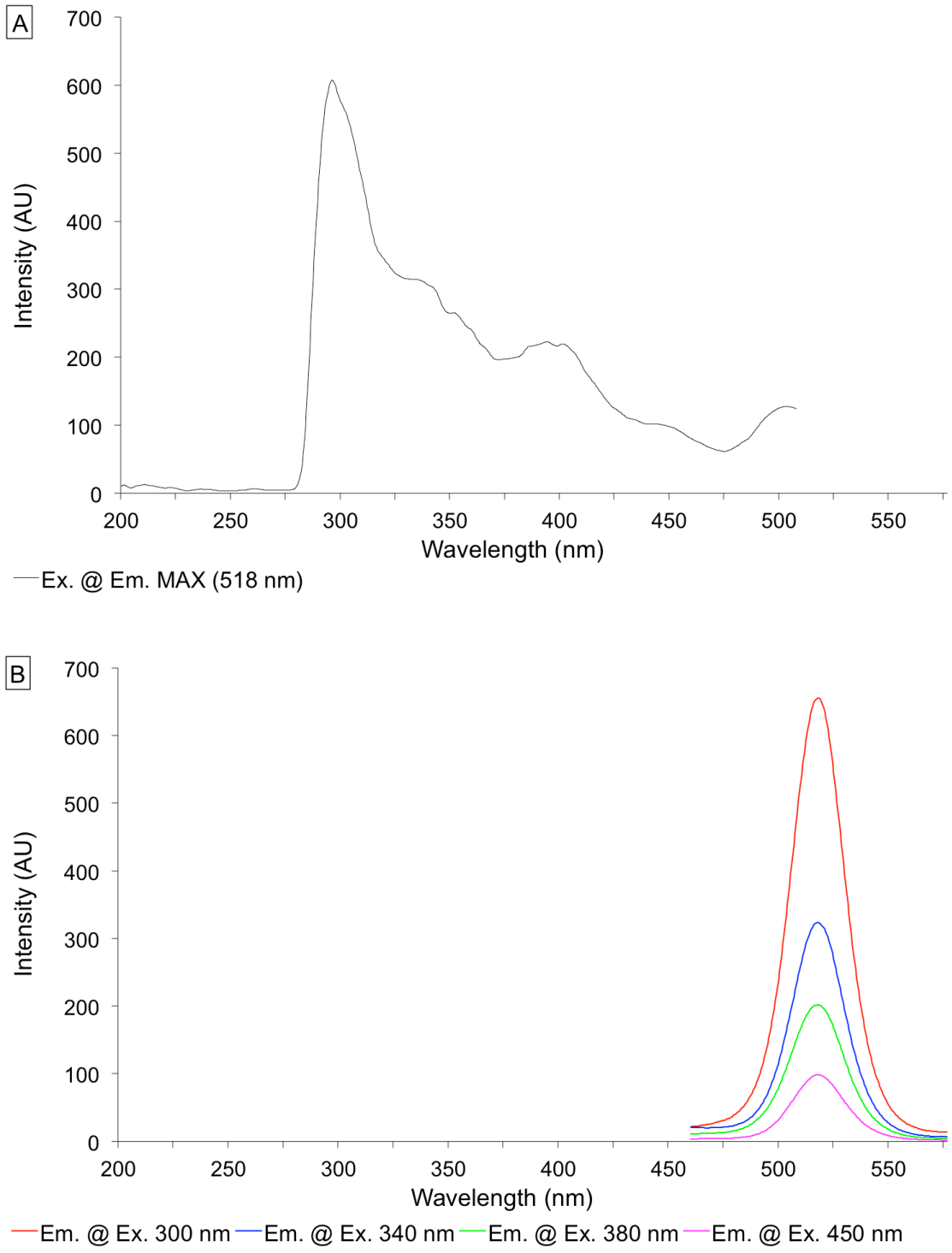

Figure 5.7 Excitation and emission spectra for single population of CdSe/ZnS QDs.

[A] Full excitation spectrum for a single population of QD1 diluted 1/2000 in toluene, at emission maximum of 518nm. Excitation intensity is seen to increase into the UV. **[B]** Emission spectra for sample of QD1, using multiple excitation wavelengths (300 nm, 340 nm, 380 nm, and 450 nm). Emission intensity is seen to increase with decreasing excitation wavelength.

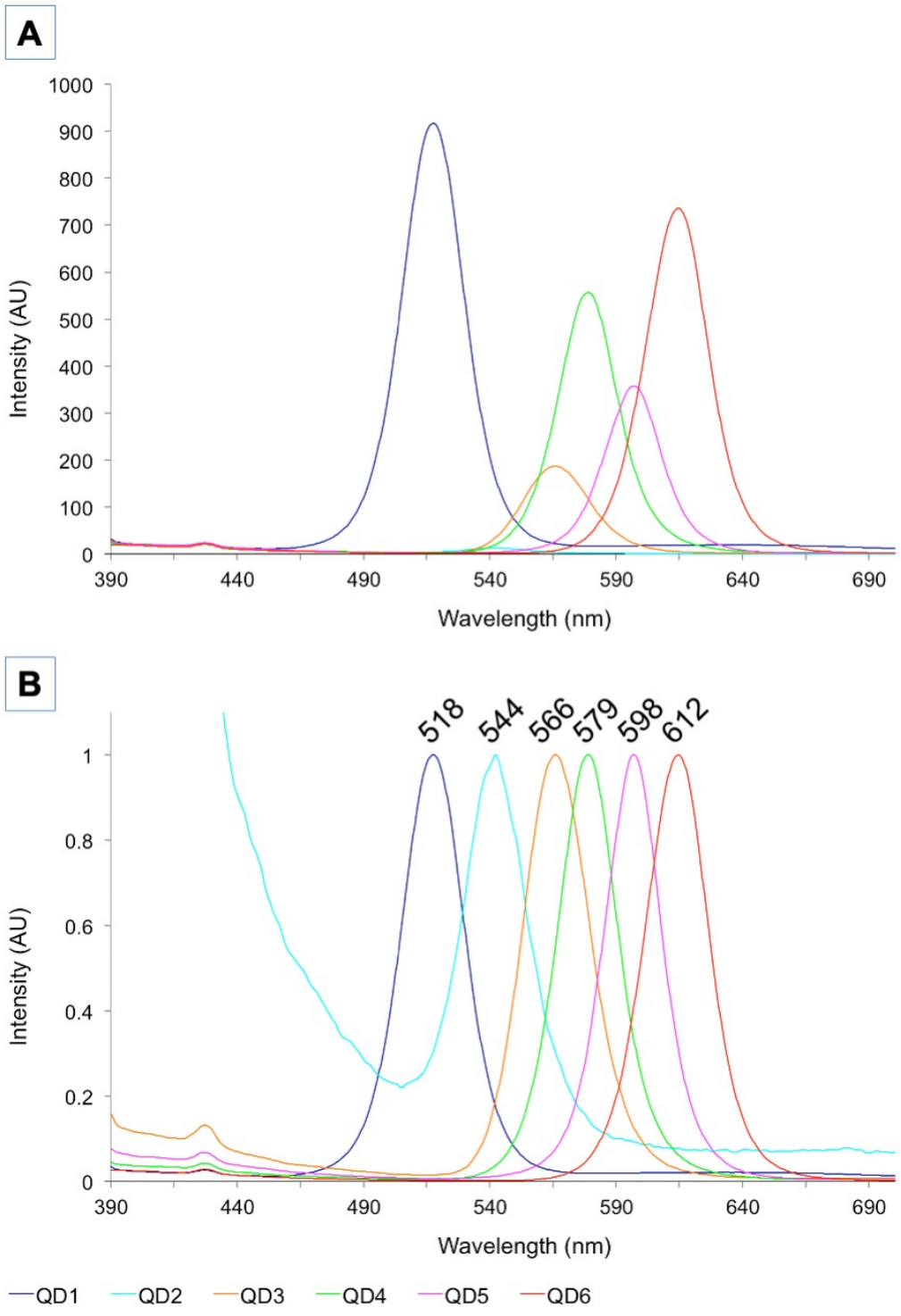

Figure 5.8 Emission spectra for all CdSe/ZnS QDs 1-6.

[A] Individual emission spectra for CdSe/ZnS QD populations 1-6, each diluted 1/1000 in toluene, and using an excitation wavelength of 380nm. Emission intensity varies between populations and QD2 emission is extremely weak. **[B]** Normalised spectra allowing clearer comparison of emission spectra, including QD2. Emission maxima for each QD population are shown above each peak.

Table 5.2 Properties of CdSe/ZnS Core/Shell "EviDots" quantum dots (QDs1-6)

QD#	QD emission[a] (nm)	QD emission[b] (nm)	Emission FWHM[a,c] (nm)	Estimated crystal diameter[a] (nm)	Estimated mol. weight[d] (g/mol)	Approx. quantum yield[a] (%)
QD1	515	518	< 35	2.1	10,000	30-50
QD2	546	544	< 30	2.4	15,000	30-50
QD3	561	566	< 30	2.6 (2.8[e])	23,000	30-50
QD4	575	579	< 30	3.2	44,000	30-50
QD5	596	598	< 30	4.0	86,000	30-50
QD6	616	612	< 30	5.2 (5.5[e])	200,000	30-50

[a] as specified by the manufacturer (Evident Technologies)
[b] measured experimentally, see **Figure 5.8**
[c] full width at half maximum
[d] for core material, excludes shell
[e] estimated, based on TEM data, see **Figure 5.5**

5.2.2 Spectral deconvolution of QD mixtures

Individual emission spectra were used to help deconvolute those from mixtures of QDs with overlapping emission spectra. This is necessary if QDs are to provide spectral multiplexing in future assays. **Figure 5.9 (Panel A)** shows the emission spectra for a mixture of QD stocks (QDs 1-6). The individual emission peaks (overlaid for reference in Panel B) are indistinguishable from one another and would require deconvoluting in order to be able to identify which QDs are present in an unknown mixture.

An Excel tool was developed that uses emission spectra of individual QD populations to calibrate fitting and deconvolute emission spectra from multi-QD mixtures (**Figure 5.10)**. The tool's results panel (**Figure 5.10 Panel C)** provides a number of settings and options that can be adjusted for fitting sample spectra and refining results. **Table 5.3** shows spectra of samples containing one, two, three, and all six QDs matched against reference samples using the Excel deconvolution tool. Above average values are automatically highlighted in green, identifying the correct QD constituents of each sample. QD2 values were manually removed from mixes where it is was known to be absent to avoid false positives that would otherwise occur due to the extremely low intensity of its reference spectrum relative to the other QD populations (see **Figure 5.8**). Percentages reflect the signal correctly attributed to QD populations known to be in the samples and decrease slightly as mixtures get more complex: 100% for single QD samples; 97% for 2 QD samples; 95% for 3QD samples. These results are shown in **Figure 5.11** using 3D bar charts where bar heights represent the percentage share of signal for each QD identified in a sample.

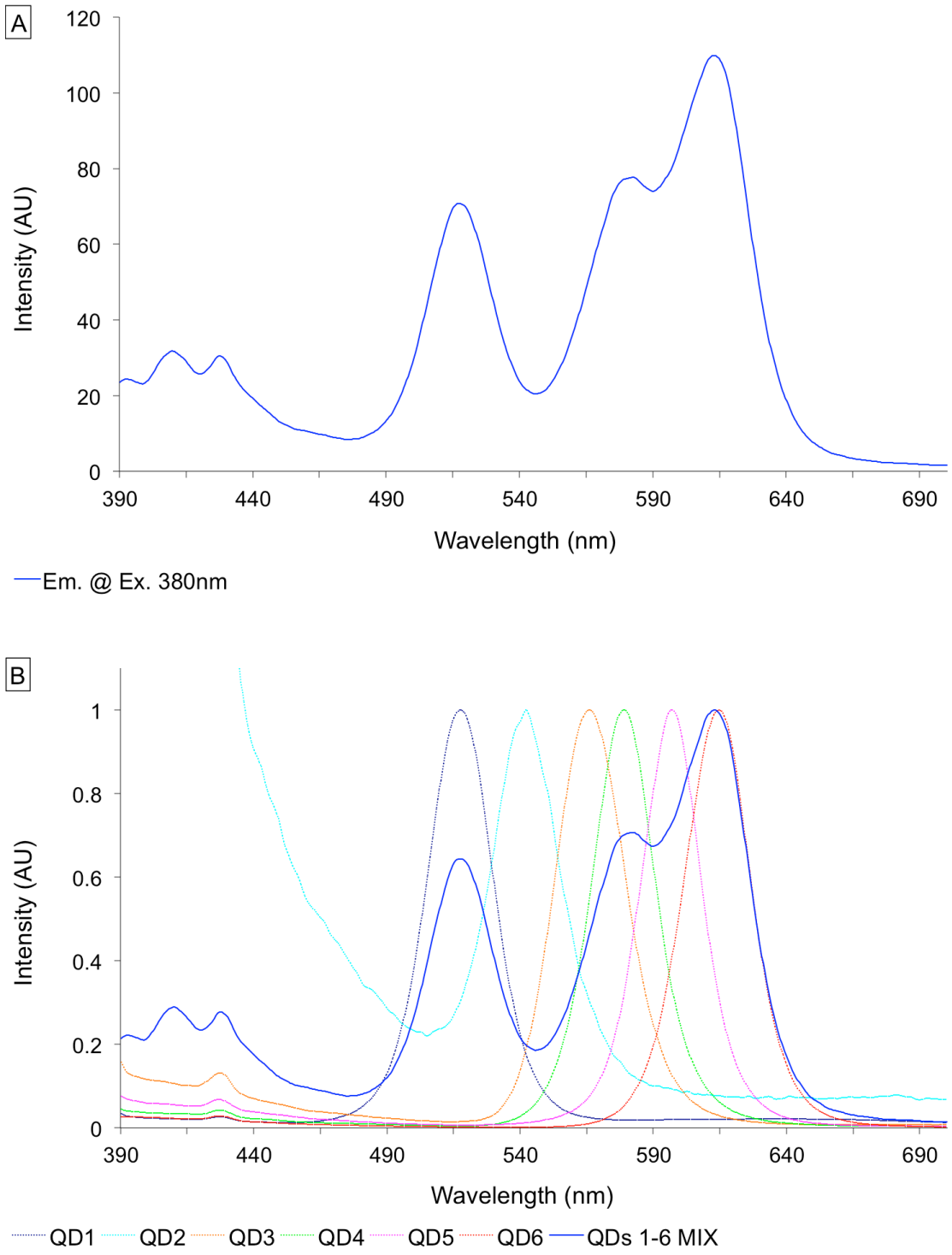

Figure 5.9 Emission spectrum for a mixture of QDs 1-6

[A] Emission spectra for a single sample mixture of CdSe/ZnS QD populations 1-6, using an excitation wavelength of 380nm. All QDs populations were a 1/1000 final dilution in toluene. Individual emission peaks are not all easily identified because emission spectra overlap. QD1 is less affected by this masking only because of the weak emission intensity of QD2 (See Figure 4ABDa). **[B]** Mixture emission spectrum overlaid for comparison with normalised emission spectra for each individual QD population.

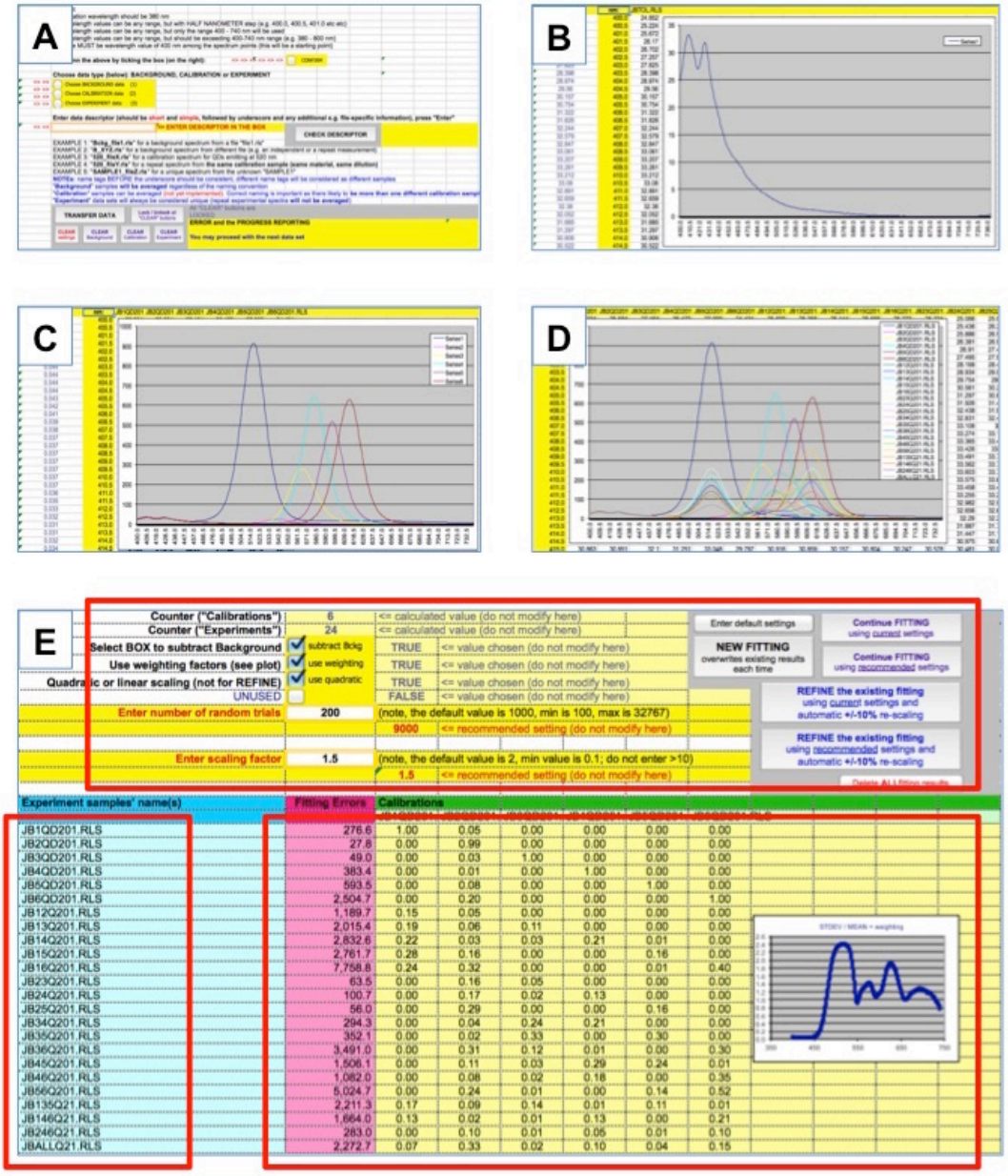

Figure 5.10 Multiplexed emission deconvolution tool.

Screen shots of the Excel tool that was developed to use emission spectra of individual QD stock populations to calibrate fitting and deconvolute emission spectra from samples containing QD mixtures. The tool includes a control panel for configuring data input **[A]**; screens for background and signal calibration **[B]** and **[C]**, and experimental sample plot generation **[D]**; and a results output and fitting panel **[E]**. The results panel contains settings and options (red box, top) that can be adjusted for fitting sample spectra (listed in red box, left) and refining the results (red box, right).

Table 5.3 Results for emission spectra deconvolution from equimolar QD mixtures.

Sample #	QDs in Sample	QDs detected from emission spectra of sample						Correctly attributed	
		QD1	QD2	QD3	QD4	QD5	QD6		
Sample 1	1	100%	0%	0%	0%	0%	0%	100%	100%
Sample 2	2	0%	100%	0%	0%	0%	0%	100%	
Sample 3	3	0%	0%	100%	0%	0%	0%	100%	
Sample 4	4	0%	0%	0%	99%	0%	0%	99%	
Sample 5	5	0%	0%	0%	0%	100%	0%	100%	
Sample 6	6	0%	0%	0%	0%	0%	100%	100%	
Sample 7	1 + 2	74%	24%	2%	0%	0%	1%	98%	97%
Sample 8	1 + 3	63%	0%	36%	0%	0%	1%	99%	
Sample 9	1 + 4	47%	0%	7%	45%	1%	0%	92%	
Sample 10	1 + 5	62%	0%	1%	0%	36%	1%	98%	
Sample 11	1 + 6	36%	0%	0%	0%	2%	61%	97%	
Sample 12	2 + 3	0%	78%	22%	0%	0%	0%	99%	
Sample 13	2 + 4	0%	52%	6%	41%	0%	0%	93%	
Sample 14	2 + 5	0%	64%	0%	0%	35%	0%	99%	
Sample 15	3 + 4	0%	0%	54%	46%	0%	0%	100%	
Sample 16	3 + 5	0%	0%	52%	1%	47%	1%	99%	
Sample 17	3 + 6	0%	0%	27%	3%	0%	70%	97%	
Sample 18	4 + 5	0%	0%	6%	51%	42%	1%	93%	
Sample 19	4 + 6	0%	0%	4%	33%	0%	63%	96%	
Sample 20	5 + 6	0%	0%	2%	0%	21%	77%	98%	
Sample 21	1 + 3 + 5	39%	0%	33%	2%	25%	2%	97%	95%
Sample 22	1 + 4 + 6	27%	0%	2%	27%	1%	43%	97%	
Sample 23	2 + 4 + 6	0%	36%	4%	18%	4%	38%	92%	
Sample 24	1 + 2 + 3 + 4 + 5 + 6	10%	47%	3%	14%	5%	22%	100%	100%

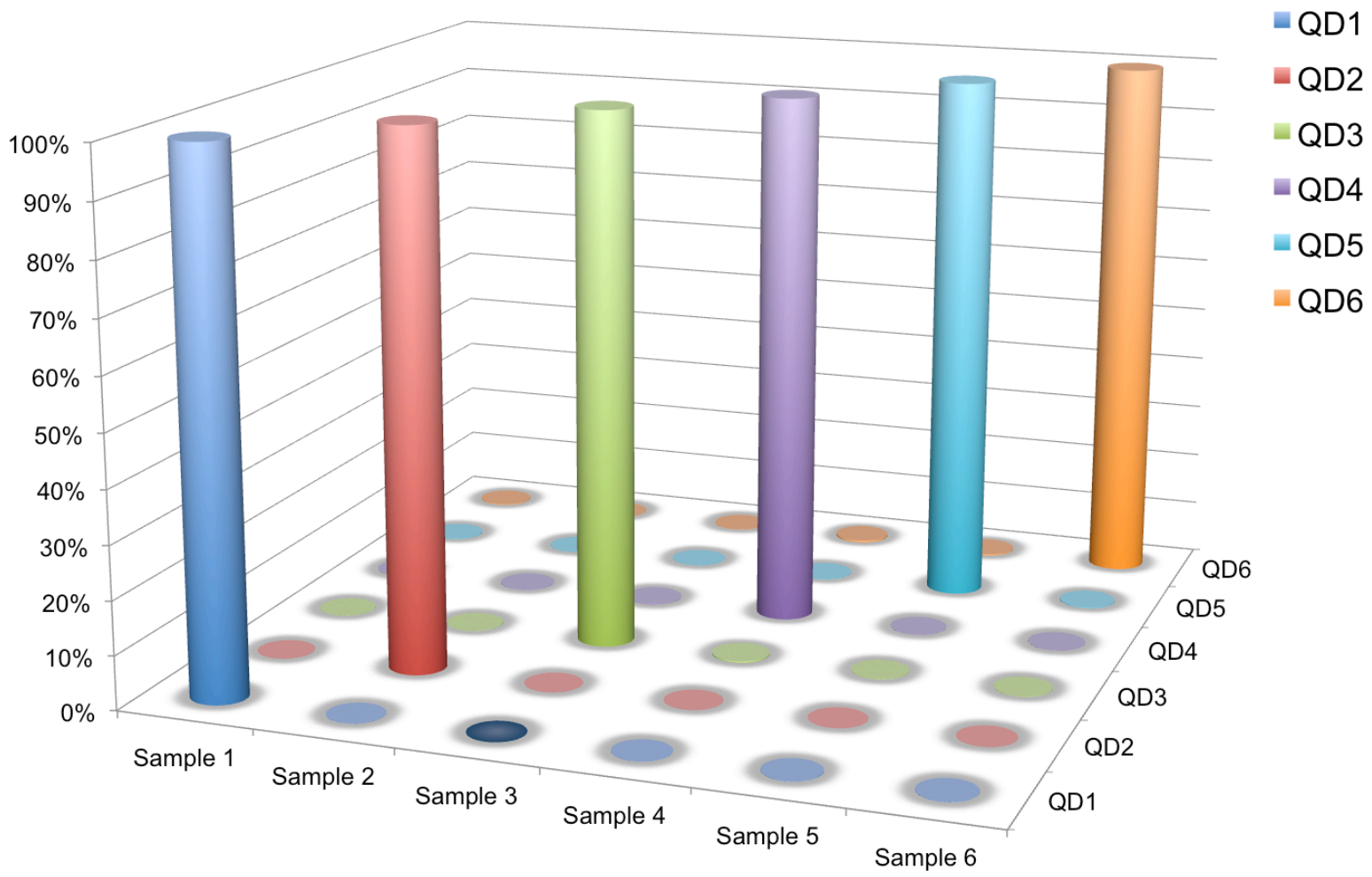
QD1
QD2
QD3
QD4
QD5
QD6
100%
90%
80%
70%
60%
50%
40%
30%
20%
10%
0%
Sample 1
Sample 2
Sample 3
Sample 4
Sample 5
Sample 6
QD6
QD5
QD4
QD3
QD2
QD1

Figure 5.11(i)

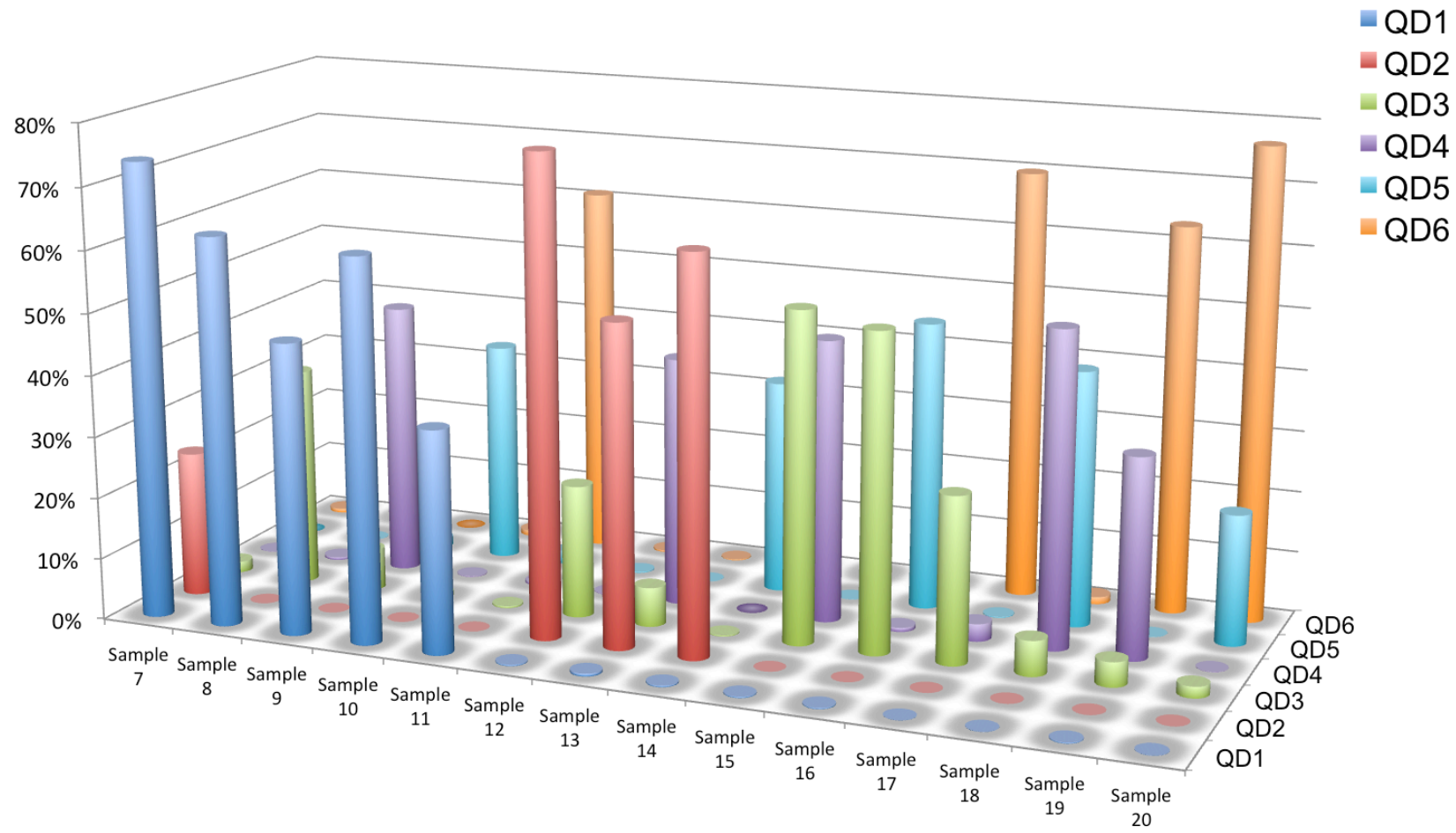

Figure 5.11(ii)

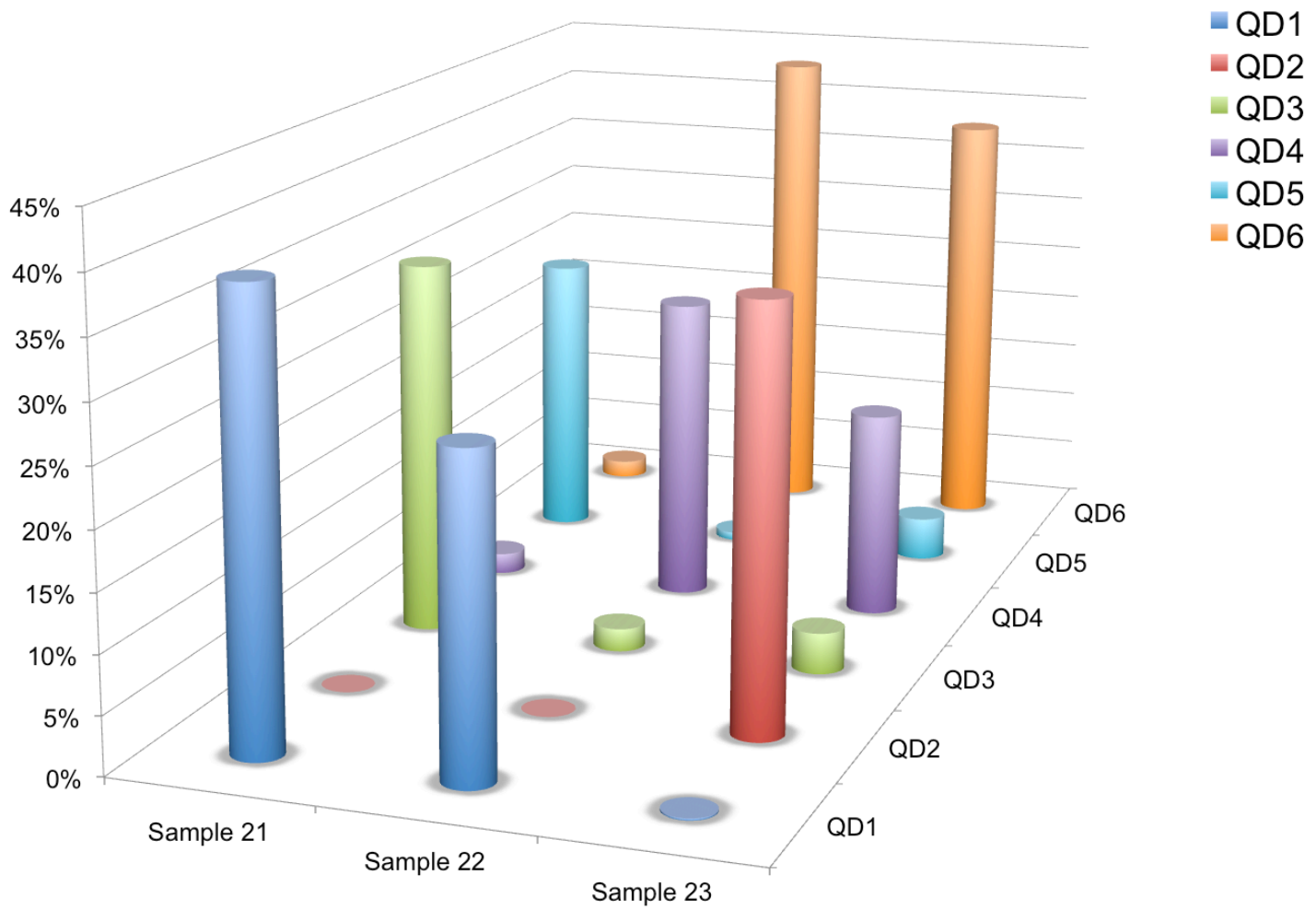

Figure 5.11(iii)

Figure 5.11 Quantum dot emission spectra deconvolution.

Emission spectra fitting results for samples with one (**i**), two (**ii**), and three (**iii**) equimolar populations of QDs. Bars represent the percentage share of signal for each QD identified in a sample. For confirmation of sample composition refer to **Table 5.3**.

Fluorescence detection on membrane

QDs 1-6 were scanned using the same Packard Bioscience BioChip dual laser scanner used for the microarray analysis in **Chapter 4**. It is important to determine which QDs can be detected using this hardware as it will likely be the instrument used for detection in future experiments. Scans of all 6 of the toluene-based QD stocks on both of the scanner's laser channels indicate that QD1 is not well detected on either channel, while QDs 3, 4 and 5 perform best on channel 1, and QD 6 performs best on channel 2 (**Figure 5.12)**. Detection of QDs 2-6 would be possible using this instrument, but assays would need to incorporate spatial multiplexing (e.g. a lateral flow strip with multiple analyte test lines) due to the discrete emission wavelength detection limitations of the scanner.

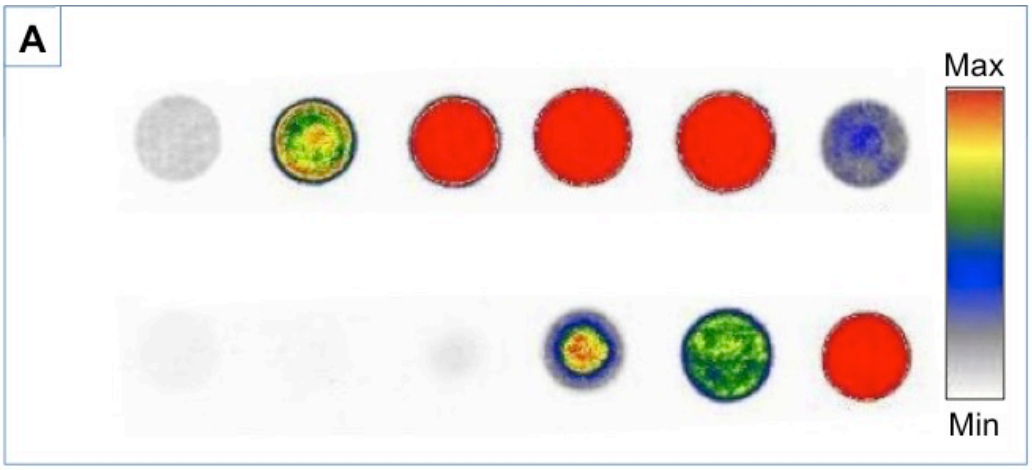

Figure 5.12 Detection of CdSe/ZnS QDs using dual channel BioChip Scanner.

[A] Comparison of QDs 1-6 hand-spotted on positively charged nylon membrane and scanned with dual channel scanner - channel 1 (Ex. 488 nm) shown top, and channel 2 (Ex. 561 nm) aligned below; fluorescence intensity meter shown right. QD1 is not well detected on either channel; QDs 3, 4 and 5 perform best on channel 1; QD 6 performs best on channel 2.

5.2.3 Photostability: QDs vs organic fluorophores

One quality of QDs that is regularly reported as a benefit for biological imaging is their superior photostability with greater resistance to photobleaching compared to organic dyes. To test this the effects of UV exposure on QD fluorescence was compared to rhodamine B isothiocyanate (RITC).

Comparison of fluorescence retention after UV-Vis exposure between QDs and organic fluorophores

Sets of QD3 and RITC were hand-spotted in triplicate on positively charged nylon membranes and exposed to UV-Vis light radiation in a CL1000 UV Cross Linker for varying durations. Both reagents exhibited a steady rate of photobleaching with increasing duration of UV-Vis exposure, but QD fluorescence declined at a slightly slower rate than that of RITC (**Figure 5.13**). To extend this the experiment was repeated with an additional time point and organic fluorophore, atto565-biotin. While all reagents again exhibited a steady rate of photobleaching with increasing duration of UV-Vis exposure, QD fluorescence declined at a slower rate than that of either organic fluorophore (**Figure 5.14**).

Effect of short duration UV exposure on QD fluorescence

While conducting these experiments, QD fluorescence was seen to increase upon very short (~30 seconds) exposure to high intensity UV light. This was investigated further in **Figure 5.15**. Briefly, QDs were scanned 3 times at 5 minute intervals and then subjected to 30 seconds high intensity UV exposure before being rescanned as before. This was repeated for a total of 6 sets of scans and 5 UV exposures. QD fluorescence was seen to steadily decrease over the course of each set of 3 scans as can be seen in **Figure 5.15 (Panel A)**, however fluorescence intensity rebounded back close to original values upon exposure to short duration high intensity UV. Mean background values remained constant throughout the experiment negating any contribution to fluorescence change by changes to the membrane surface. A gradual decrease in mean QD fluorescence of scan sets was observed over the course of the experiment, as shown in **Figure 5.15 (Panel B)**.

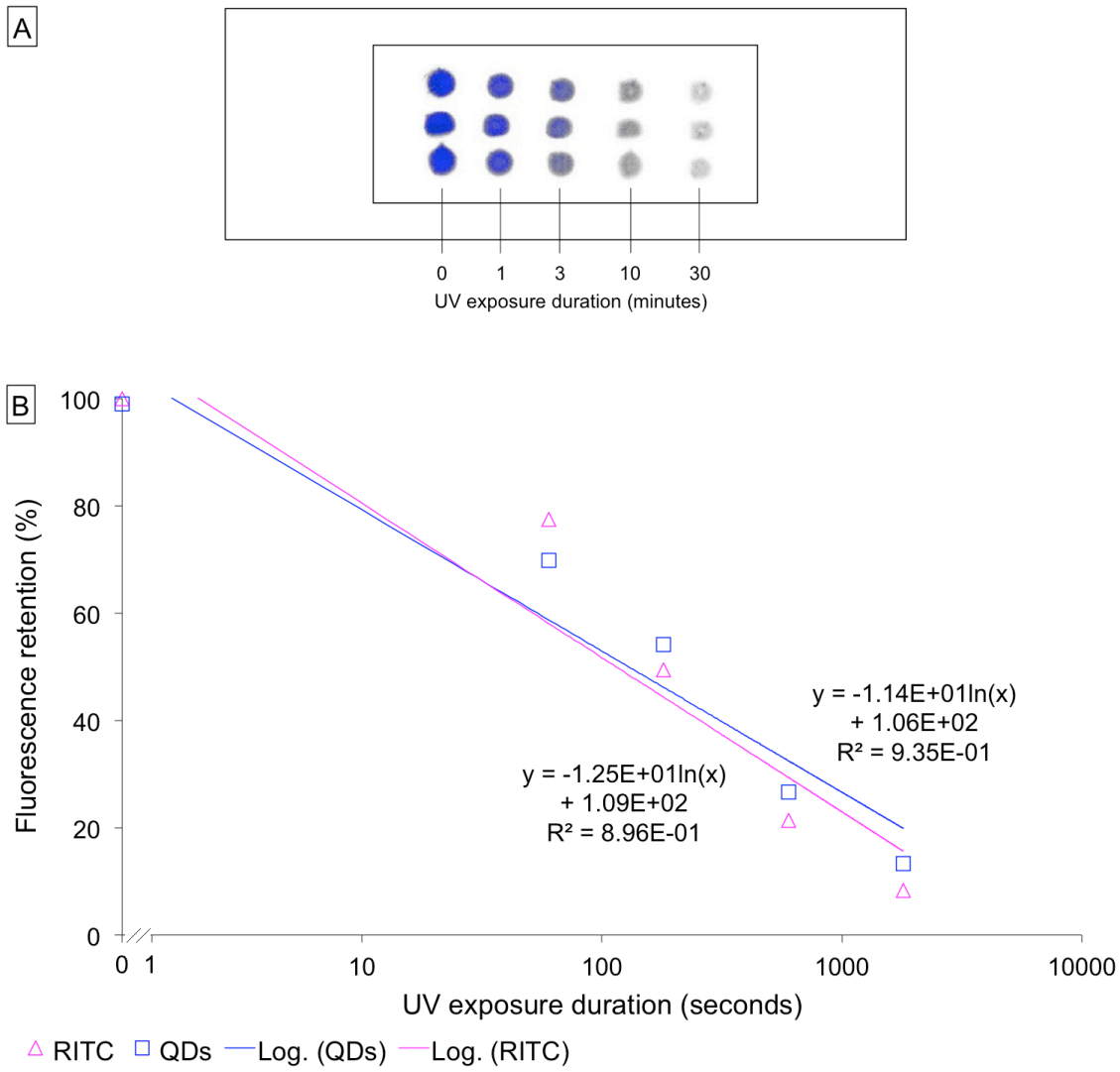

Figure 5.13 Photostability: QDs vs organic fluorophores (1)

[A] Scan image overlayed on slide diagram of 1 uL samples of QD3 hand-spotted in triplicate on positively charged nylon membrane and exposed to UV-Vis light radiation in a CL1000 UV Cross Linker for varying durations. Fluorescence steadily decreases with increasing exposure duration. A slide with matching RITC samples was also subjected to the same treatment (not shown). **[B]** Mean fluorescence of QDs and RITC samples plotted against UV-Vis exposure time-points. Both reagents exhibit a steady rate of photobleaching with increasing UV-Vis exposure, but with QD fluorescence declining at a slightly slower rate ($y = -1.14 \times 10^{1}$ for QDs vs $y = -1.25 \times 10^{1}$ for RITC).

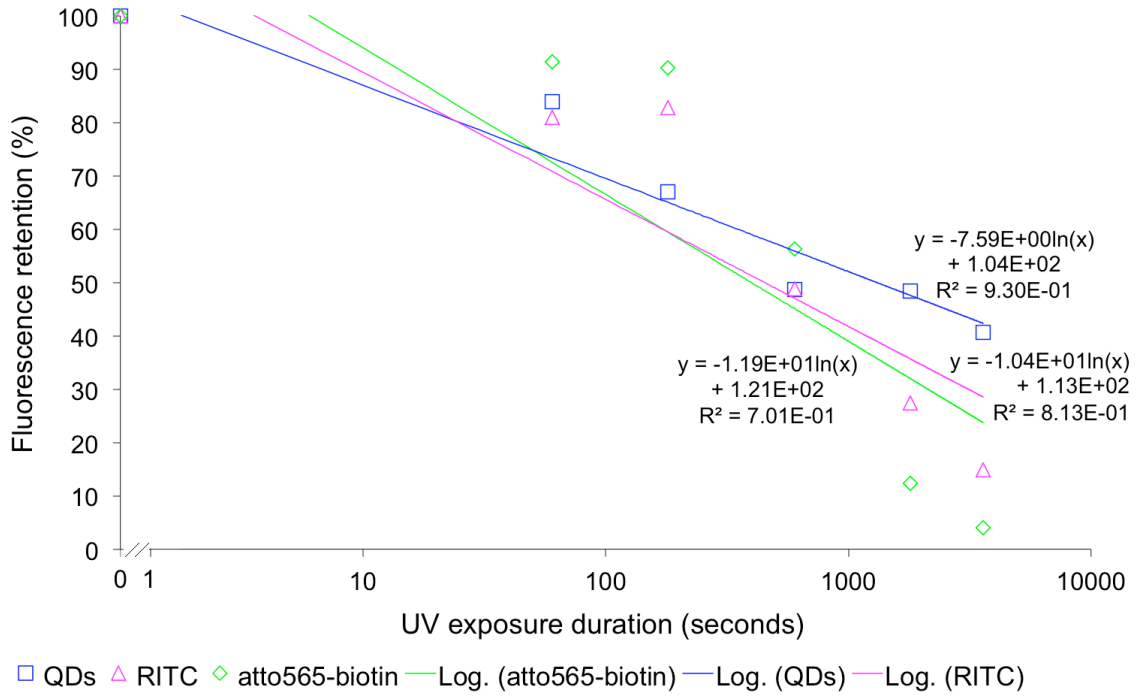

Figure 5.14 Photostability: QDs vs organic fluorophores (2)

Graph showing mean fluorescence remaining for QD3 and organic fluorophores (RITC, and atto-565-biotin) after exposure to UV-Vis radiation. QDs exhibit a slower rate of photobleaching when compared to the traditional organic dyes: y = -7.59 for QDs vs y = -1.04 x 10^1 for RITC vs y = -1.19 x 10^1 for atto565-biotin).

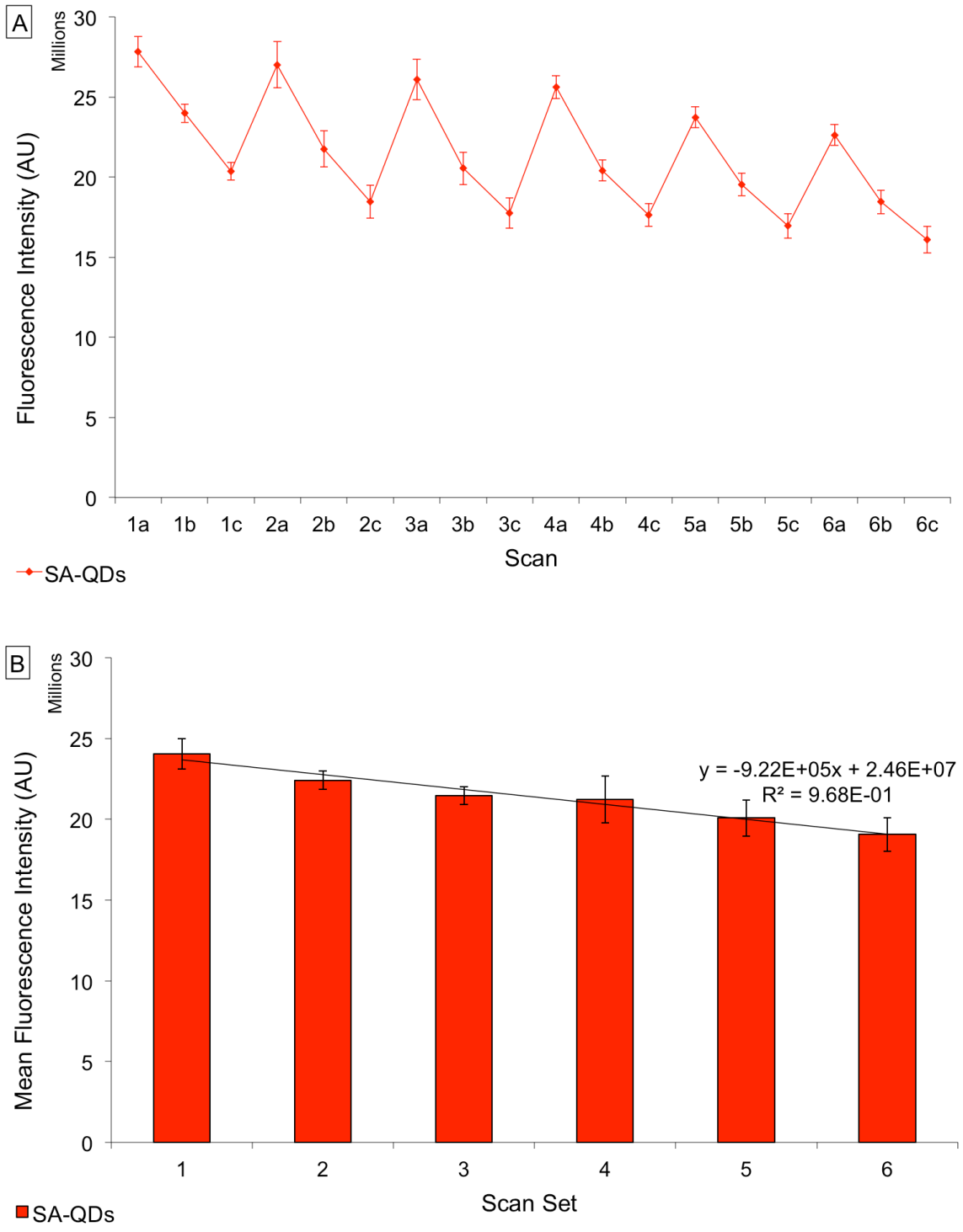

Figure 5.15 Effect of short duration UV exposure on QD fluorescence.

Hand-spotted SA-QD samples were scanned three times at five minute intervals and then exposed to 999,900 micro-Joules/cm^2 UV-Vis radiation for 30 seconds before being rescanned as before. This process was repeated for a total of six sets of scans and five UV-Vis exposures. Scan Set #1 is prior to any exposure. **[A]** shows mean fluorescence (from five spots) for each scan. Fluorescence values decline each time the QDs are scanned but rebound following UV exposure. **[B]** shows mean QD fluorescence averaged across each set of three scans. QD fluorescence shows a gradual decline over the course of the experiment (y = 9.22 x 105, R2 = 0.97).

5.3 Conclusions

1. GNPs were synthesised and conjugated to protein (BSA) with a clear red-shift of 7 nm at absorbance maximum observed between unconjugated GNPs and BSA-GNP conjugates (520 nm vs 527 nm). 0.1 mg BSA per 1 mL of GNPs was required to provide sufficient coverage of the particles and prevent aggregation upon the addition of salt.

2. Competitive GNP lateral flow test strips were created and used for the detection of diazepam (a benzodiazepine also known as Valium). Spiking of samples with diazepam resulted in competitive displacement of GNP-antibody conjugates for immobilised oxazepam and a visible reduction in intensity of GNPs at the test line.

3. QDs were evaluated for use in multiplexed assays. For excitation of the QDs stocks in solution an excitation wavelength of 380 nm provides a good compromise between relative emission intensity and avoidance of second order peaks that interfere with emission peaks. Emission maxima were determined for QDs 1-6 and confirmed to be within 5 nm of the values stated by the manufacturer.

4. Results from TEM imaging and subsequent size characterisation of six toluene-based QD stocks correlate closely with values supplied by the manufacturer (2.79 nm +/- 0.41 nm and 5.52 nm +/- 0.70 nm, for QD3 and QD6 respectively).

5. Spectral deconvolution was achieved for mixtures of up to 6 QD populations confirming the feasibility for QDs to provide spectral multiplexing in future assays.

6. QDs exhibited a slower rate of photobleaching when compared to traditional organic dyes, RITC and atto565-biotin ($y = -7.59$ for QDs vs $y = -1.04 \times 10^{1}$ for RITC vs $y = -1.19 \times 10^{1}$ for atto565-biotin). This is consistent with the wider literature on their properties and performance. Exposure to high-intensity UV-Vis radiation for short duration (30 seconds) led to an increase in QD fluorescence compared to the scan that preceded the exposure. Mean fluorescence values

from 3 scans still decrease with repeated, albeit short duration, exposure to UV-Vis radiation.

Chapter 6: IGF-1 Affinity Reagents

The aim of this chapter was to develop novel peptide affinity reagents against IGF-1 to overcome hurdles associated with traditional antibody-based affinity reagents.

The work seeks to determine if phage display can be used to generate these anti-IGF-1 reagents, and if so, how they compare to antibodies in terms of affinity and stability.

6.1 Generation of anti-IGF-1 peptides

6.1.1 Peptide binding on hydrogels

Novel anti-IGF-1 peptides were generated via phage display. The specific binding of these peptides to IGF-1 was confirmed using hydrogel-based fluorescence assays and insulin as negative control (**Figure 6.1**).

Competitive displacement assays using 100-fold excess of unlabelled anti-IGF-1 peptide resulted in an ~3 fold decrease in fluorescence intensity.

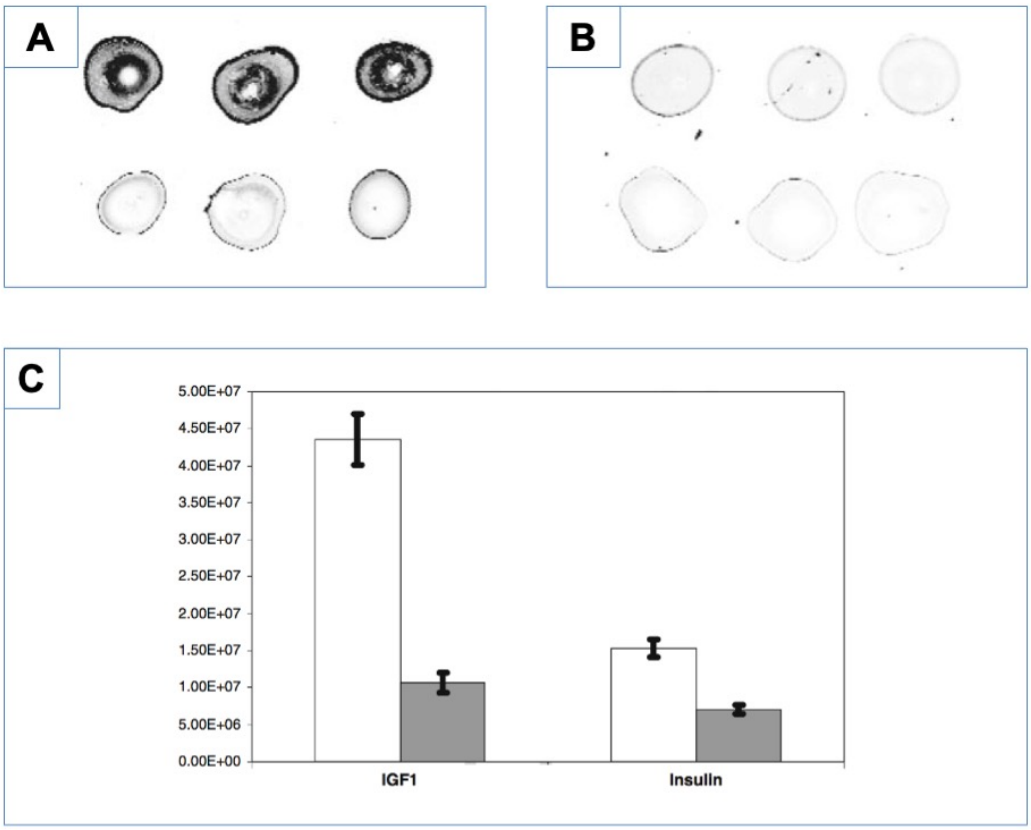

Figure 6.1 Peptide binding on hydrogels

[A] Peptide SALNTPN binds to IGF-1 (top row) but not to insulin (bottom row). **[B]** Same as **[A]** but in the presence of 100-fold excess of the unlabelled peptide SALNTPN. **[C]** Mean values of the fluorescence intensities for both scans (±stdev). Hydrogel work was carried out by group member, Anna Dulneva (Zhang *et al.*, 2010).

6.2 Binding characterisation of anti-IGF-1 affinity reagents.

Binding of the generated anti-IGF-1 peptides as well as commercial anti-IGF-1 antibodies were tested using enzyme-linked immunosorbent assays (ELISA), described in the following sections (6.2.1 and 6.2.2). An attempt was made to set up an assay suitable for both large anti-IGF-1 antibody and small anti-IGF-1 peptides, to help their comparison.

6.2.1 Binding characterisation of anti-IGF-1 antibodies

ELISA were used to compare binding characteristics of anti-IGF-1 antibodies and peptides. The ELISA formats for both antibody- and peptide-based anti-IGF-1 ELISAs are shown in **Figure 6.2**.

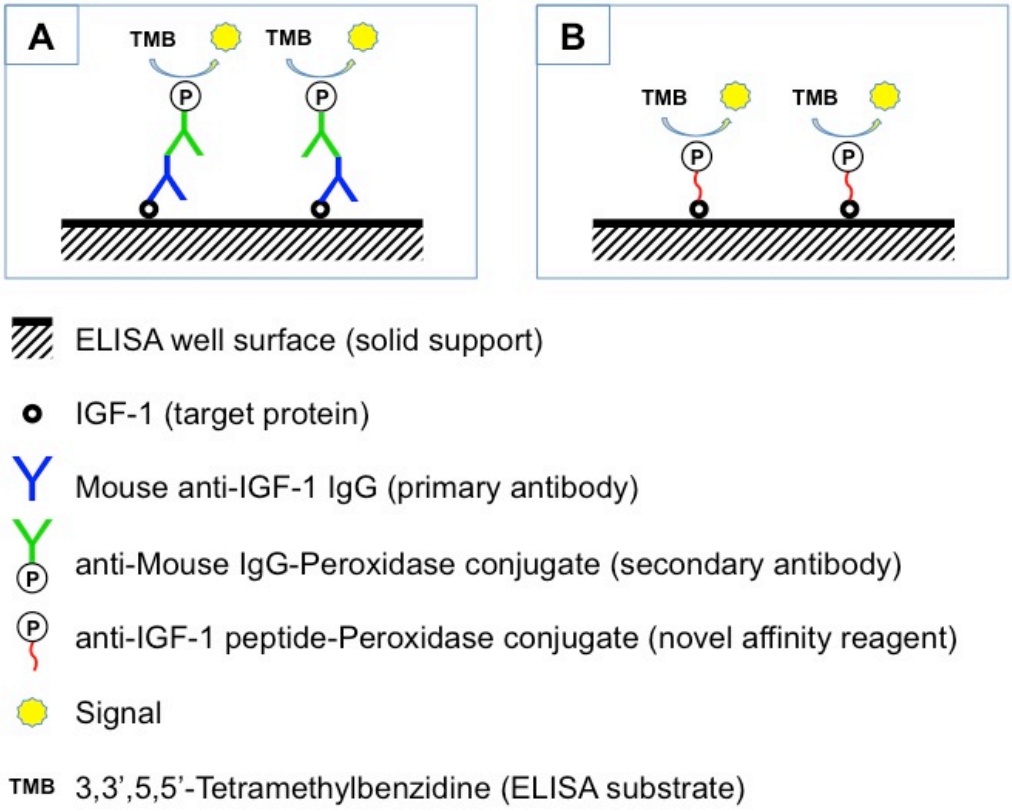

Figure 6.2 Anti-IGF-1 ELISAs: Antibody vs peptide affinity reagents

[A] Antibody-based sandwich ELISA for immobilised IGF-1. Mouse anti-IGF-1 IgG was used as a primary antibody, and rabbit anti-Mouse IgG conjugated to peroxidase as a secondary antibody. 3, 3', 5, 5' TMB was added as a substrate and reacted with the peroxidase enzyme to produce a coloured change indicating the detection of IGF-1. **[B]** Peptide-based direct ELISA. Anti-IGF-1 peptides were conjugated to peroxidase reducing the number of wash steps and negating the need for a secondary detection molecule.

ELISA optimisation and antibody kinetics

Optimisation of the anti-Mouse IgG secondary antibody was performed first. A secondary antibody dilution series indicated that dilutions of 1/3000 and below resulted in absorbance close to the upper limit of detection, and so a dilution of 1/5000 was selected for the subsequent experiments (**Figure 6.3**).

A time series for incubation of the secondary antibody with anti-IGF-1 monoclonal antibody immobilised in the ELISA wells ranging from 30 minutes to 18 hours showed there to be a positive correlation between incubation time and absorbance. A secondary antibody incubation time of 3 hours was chosen for subsequent experiments (**Figure 6.4**).

Optimisation of the anti-IGF-1 monoclonal antibody was then performed. A primary antibody log dilution series ranging from 1-10,000 ng/mL showed absorbance positively correlated with anti-IGF-1 concentration (**Figure 6.5**). While 100 ng/mL was seen to be at the upper detection limit of the absorbance reader, 500 ng/mL was selected for subsequent experiments on the basis that the secondary antibody dilution for this experiment was just 1/2000, not 1/5000 as intended from results of the previous optimisation step.

A time series for incubation of the primary antibody with immobilised IGF-1 in the ELISA wells ranging from 30 minutes to 18.5 hours showed there to be a positive correlation between incubation time and absorbance, with an equilibrium reached ~ 5 hours. A 5 hour incubation time for primary antibody was chosen for subsequent experiments (**Figure 6.6**).

Finally, a wash time series ranging from 1 to 9 hours in duration was performed to determine the primary antibody dissociation kinetics. Absorbance decreased with increasing wash time, however signal was very strong for all time-points. Absorbance results at 660 nm indicate k_d for the monoclonal anti-IGF-1 is 1.58×10^{-5} s^{-1} (**Figure 6.7**).

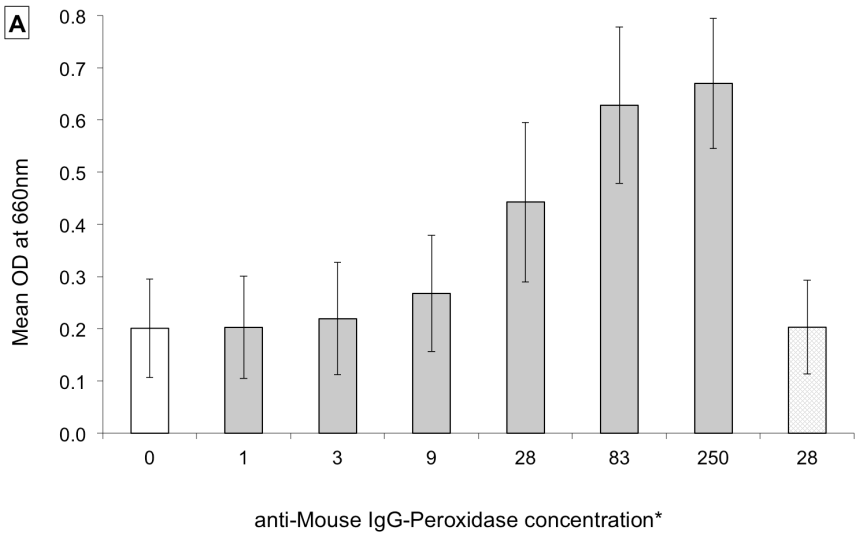
A
Mean OD at 660nm
0.0
0.1
0.2
0.3
0.4
0.5
0.6
0.7
0.8
0
1
3
9
28
83
250
28
anti-Mouse IgG-Peroxidase concentration*

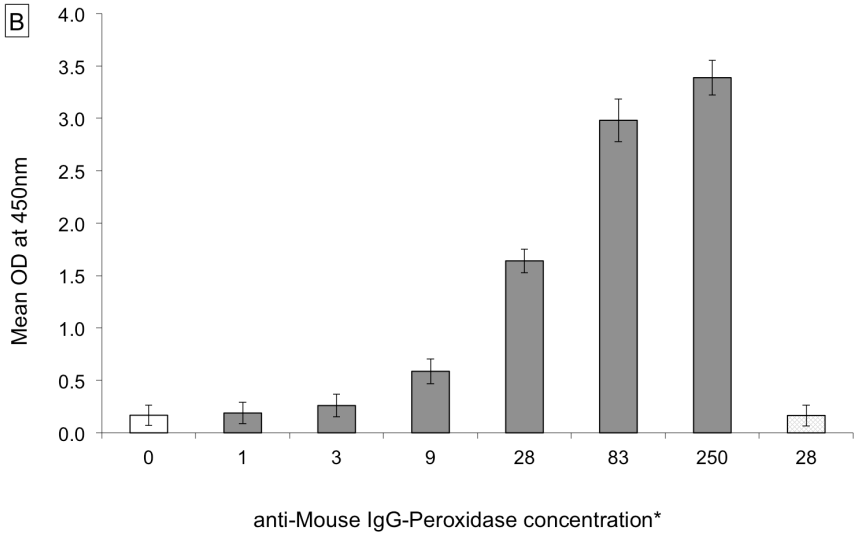
B
Mean OD at 450nm
0.0
0.5
1.0
1.5
2.0
2.5
3.0
3.5
4.0
0
1
3
9
28
83
250
28
anti-Mouse IgG-Peroxidase concentration*

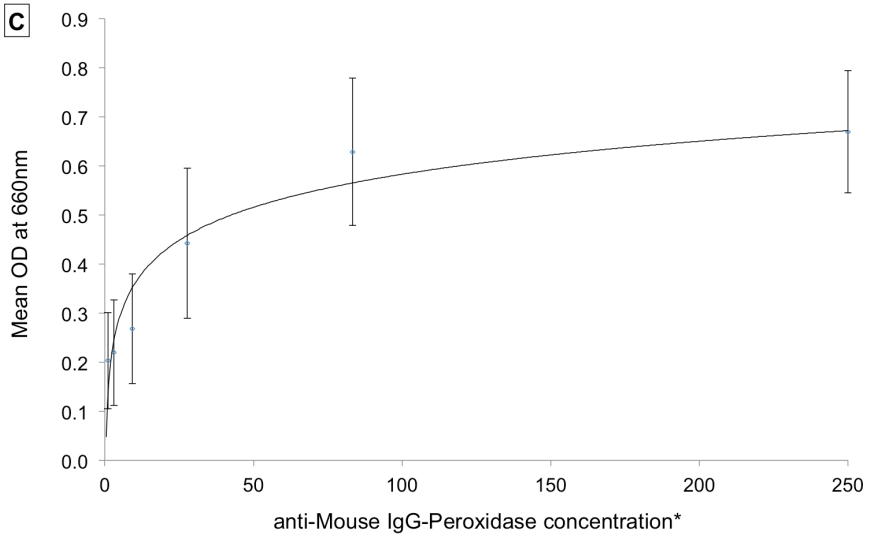
C
Mean OD at 660nm
0.0
0.1
0.2
0.3
0.4
0.5
0.6
0.7
0.8
0.9
0
50
100
150
200
250
anti-Mouse IgG-Peroxidase concentration*

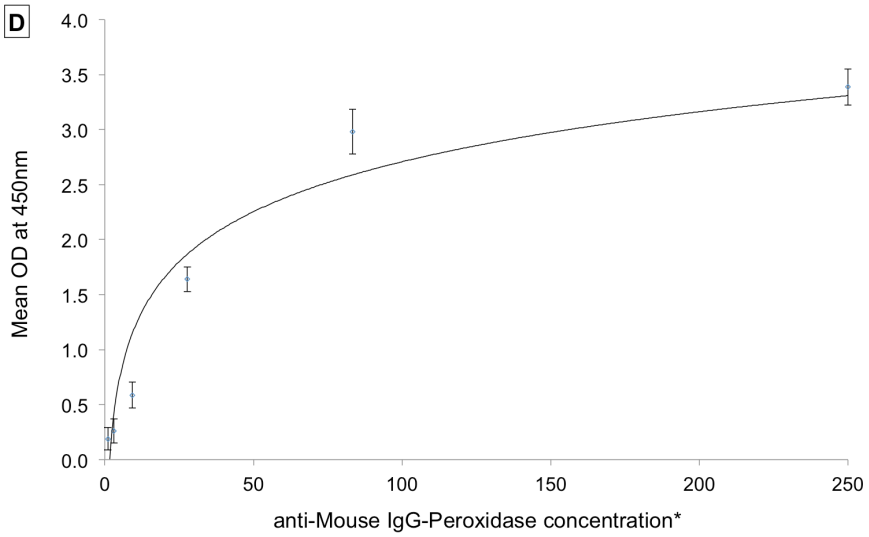
D
Mean OD at 450nm
0.0
0.5
1.0
1.5
2.0
2.5
3.0
3.5
4.0
0
50
100
150
200
250
anti-Mouse IgG-Peroxidase concentration*

Figure 6.3 Secondary antibody concentration optimisation.

Mouse anti-IGF-1 antibody (0.5 ug/mL) immobilised on ELISA well plates and assayed with rabbit anti-mouse IgG-peroxidase dilution range (*starting concentration unknown) for 2 hours 30 minutes. TOP – mean fluorescence at 660 nm (**A**) and 450 nm (**B**); n = 2 with values representing means of two wells; upper detection limit for absorbance is ~3-3.5 for measurements taken at 450 nm. Non-shaded bars represent anti-mouse IgG-peroxidase negative controls; criss-crossed bars represent anti-IGF-1 negative controls; error bars represent standard error of the mean (SEM) values (n = 2). Absorbance increases with increasing anti-mouse IgG-peroxidase concentration with 1/3,000 and 1/1,000 dilutions at detection limit of the absorbance reader. BOTTOM – Binding isotherms at 660 nm (**C**) and 450 nm (**D**). 1/5,000 dilution of anti-mouse IgG-peroxidase selected for association kinetics experiments.

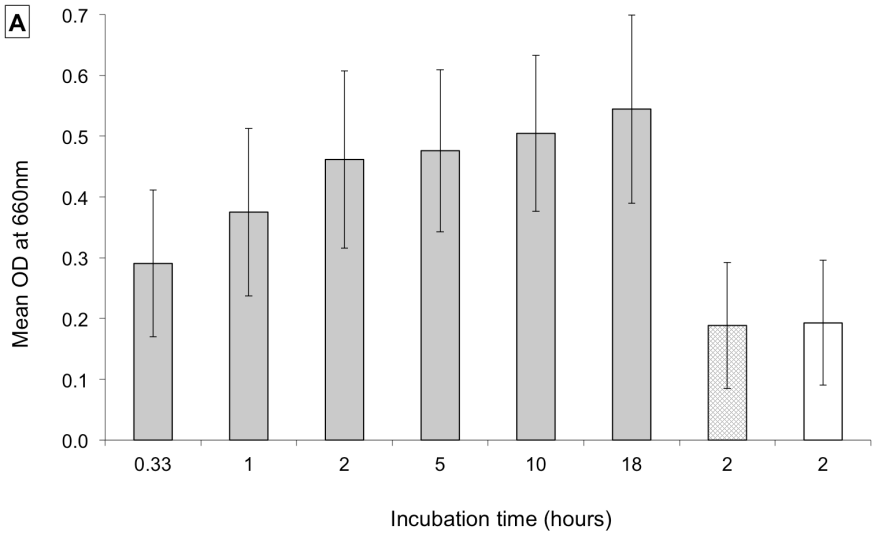
A
Mean OD at 660nm
0.7
0.6
0.5
0.4
0.3
0.2
0.1
0.0
0.33
1
2
5
10
18
2
2
Incubation time (hours)

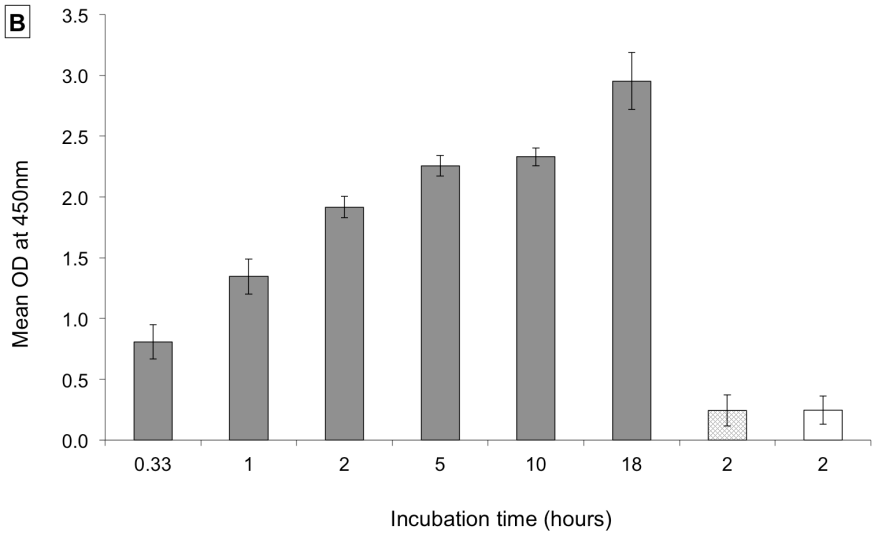
B
Mean OD at 450nm
3.5
3.0
2.5
2.0
1.5
1.0
0.5
0.0
0.33
1
2
5
10
18
2
2
Incubation time (hours)

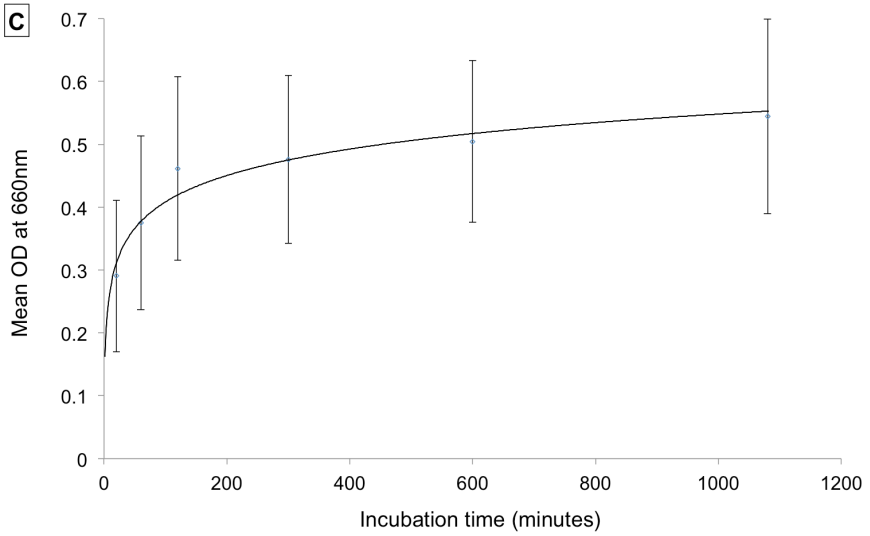
C
Mean OD at 660nm
0.7
0.6
0.5
0.4
0.3
0.2
0.1
0
0
200
400
600
800
1000
1200
Incubation time (minutes)

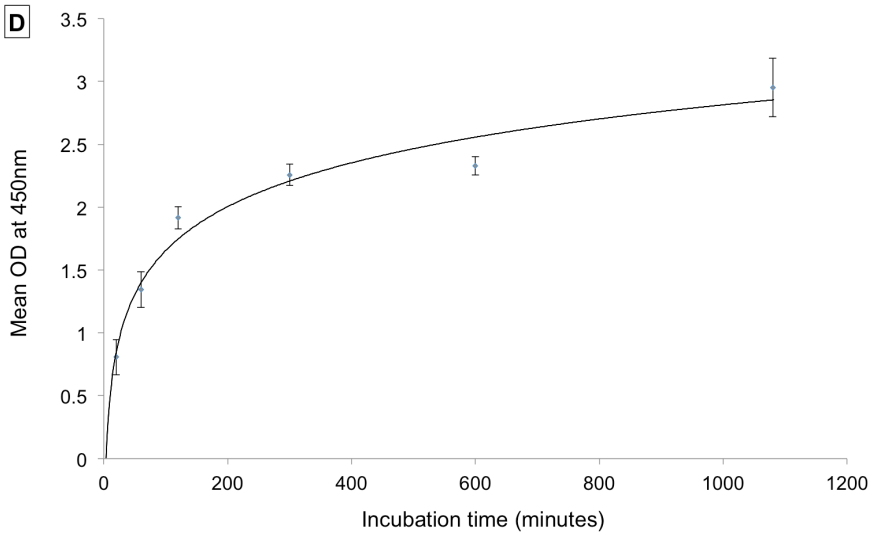
D
Mean OD at 450nm
3.5
3
2.5
2
1.5
1
0.5
0
0
200
400
600
800
1000
1200
Incubation time (minutes)

Figure 6.4 Secondary antibody association kinetics

Mouse anti-IGF-1 antibody (0.5 ug/mL) immobilised on ELISA well plates and assayed with rabbit anti-mouse IgG-peroxidase (1/5,000 dilution) for different incubation durations. TOP – mean fluorescence at 660 nm (**A**) and 450 nm (**B**); n = 2 with values representing means of two wells; upper detection limit for absorbance is ~3-3.5. Non-shaded bars represent anti-IGF-1 negative controls; criss-crossed bars represent anti-mouse IgG-peroxidase negative controls; error bars represent SEM values (n = 2). Absorbance increases with increasing incubation time. BOTTOM – Binding isotherms at 660 nm (**C**) and 450 nm (**D**). 3 hours selected for future incubations.

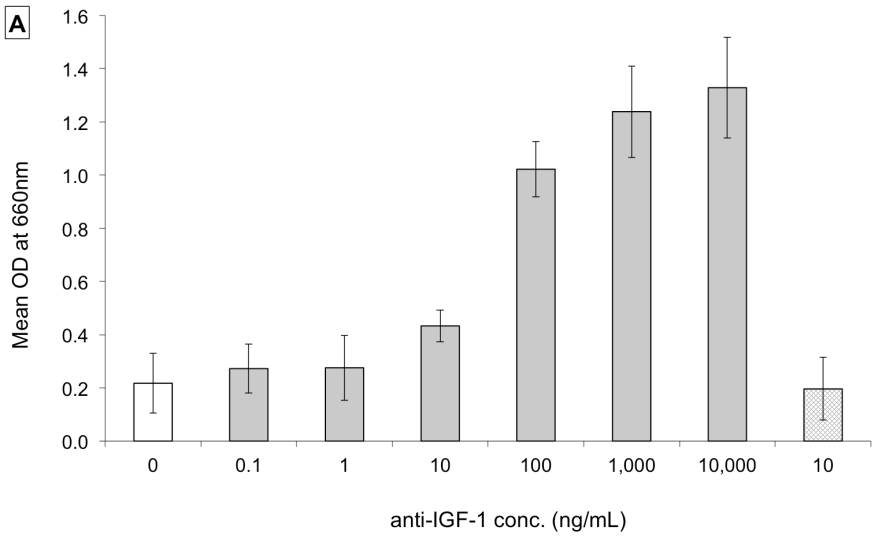
A
Mean OD at 660nm
1.6
1.4
1.2
1.0
0.8
0.6
0.4
0.2
0.0
0
0.1
1
10
100
1,000
10,000
10
anti-IGF-1 conc. (ng/mL)

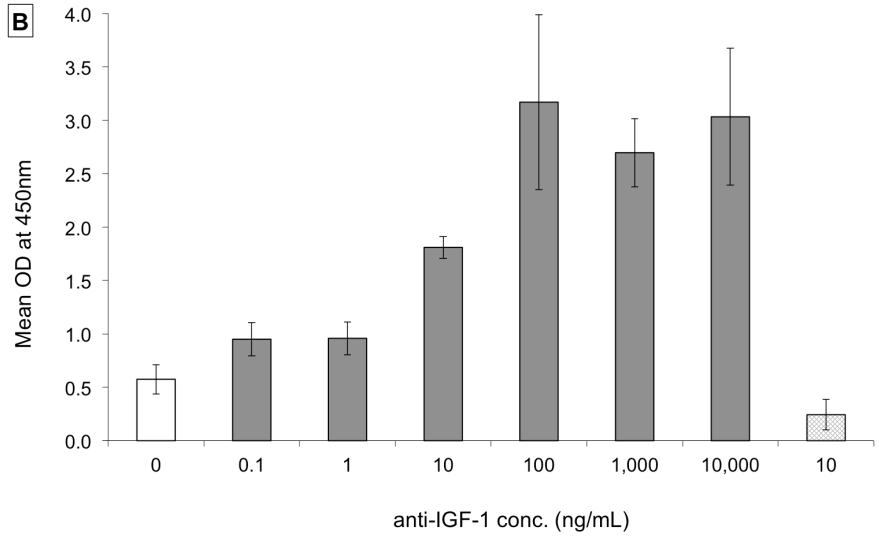
B
Mean OD at 450nm
4.0
3.5
3.0
2.5
2.0
1.5
1.0
0.5
0.0
0
0.1
1
10
100
1,000
10,000
10
anti-IGF-1 conc. (ng/mL)

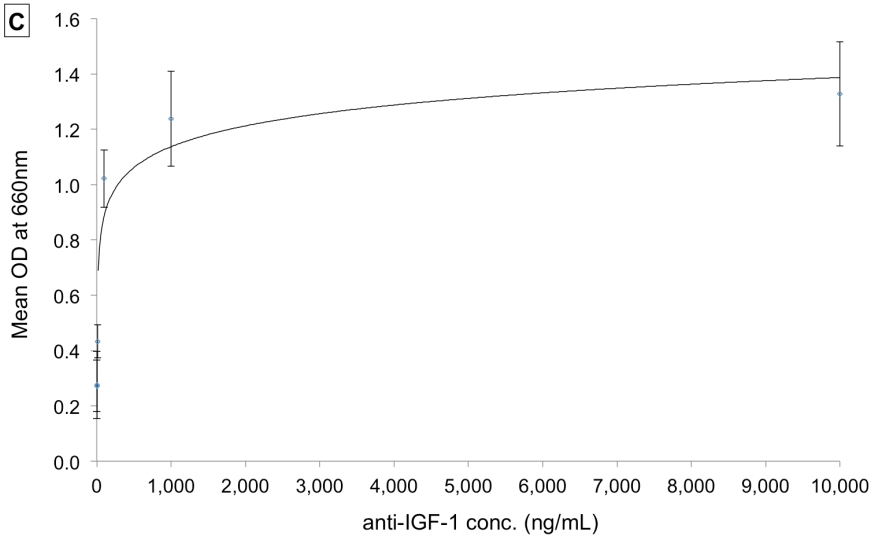
C
Mean OD at 660nm
1.6
1.4
1.2
1.0
0.8
0.6
0.4
0.2
0.0
0
1,000
2,000
3,000
4,000
5,000
6,000
7,000
8,000
9,000
10,000
anti-IGF-1 conc. (ng/mL)

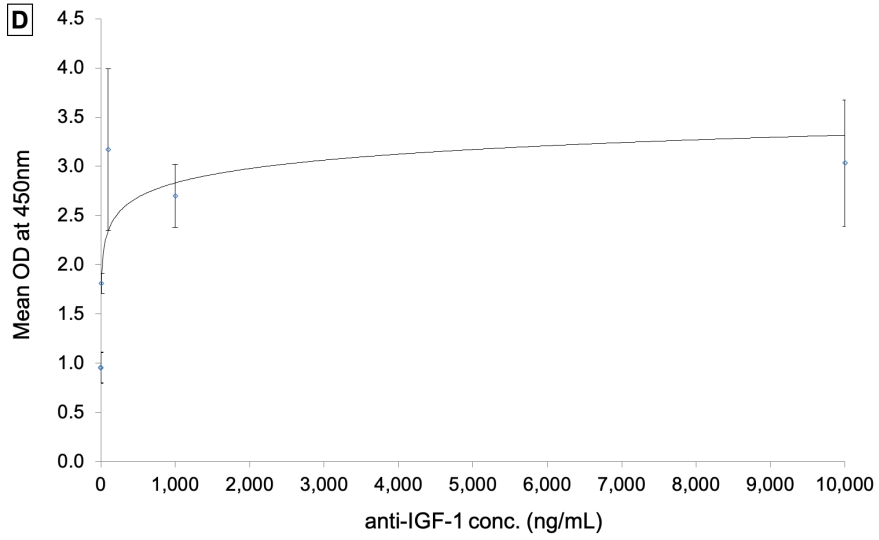
D
Mean OD at 450nm
4.5
4.0
3.5
3.0
2.5
2.0
1.5
1.0
0.5
0.0
0
1,000
2,000
3,000
4,000
5,000
6,000
7,000
8,000
9,000
10,000
anti-IGF-1 conc. (ng/mL)

Figure 6.5 Primary antibody concentration optimisation.

Log dilution series of mouse anti-IGF-1 antibody (1-10,000 ng/mL) immobilised on ELISA well plates and assayed with rabbit anti-mouse IgG-peroxidase (1,2000) for 3 hours. TOP – mean fluorescence at 660 nm (**A**) and 450 nm (**B**); n = 2 with values representing means of two wells; upper detection limit for absorbance is ~3-3.5 for measurements taken at 450nm. Non-shaded bars represent anti-IGF-1 negative controls; criss-crossed bars represent anti-mouse IgG-peroxidase negative controls; error bars represent SEM values (n = 2). Absorbance increases with increasing anti-IGF-1 concentration with 100 ng/mL at detection limit of the absorbance reader. BOTTOM – Binding isotherms at 660 nm (**C**) and 450 nm (**D**). 500 ng/mL of anti-IGF-1 selected for association kinetics experiments.

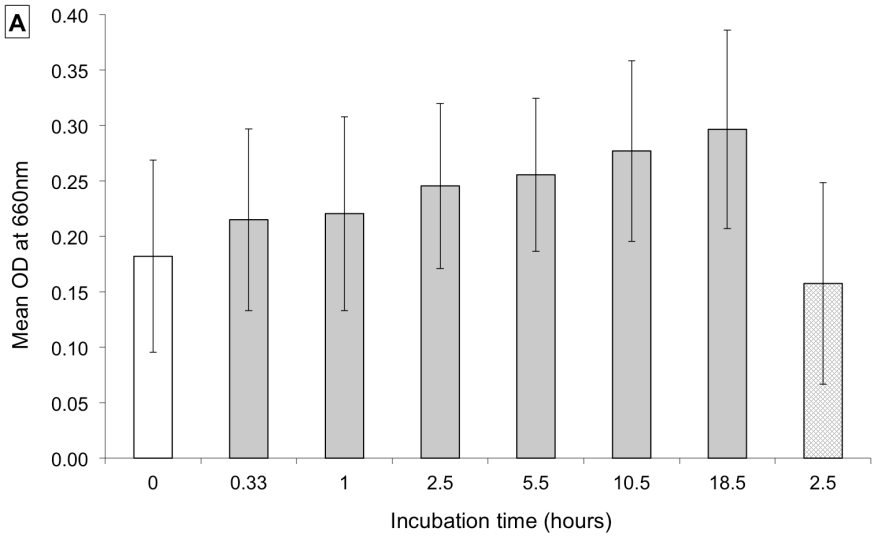
A
Mean OD at 660nm
0.40
0.35
0.30
0.25
0.20
0.15
0.10
0.05
0.00
0
0.33
1
2.5
5.5
10.5
18.5
2.5
Incubation time (hours)

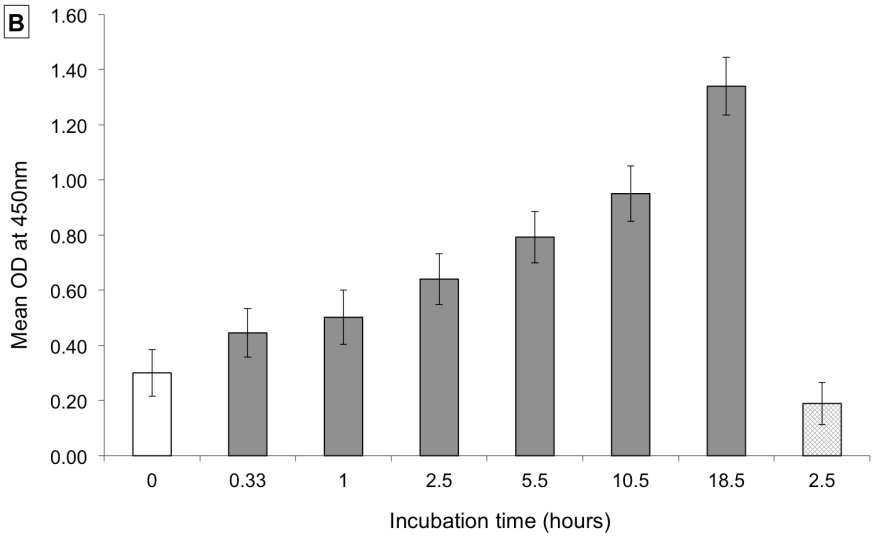
B
Mean OD at 450nm
1.60
1.40
1.20
1.00
0.80
0.60
0.40
0.20
0.00
0
0.33
1
2.5
5.5
10.5
18.5
2.5
Incubation time (hours)

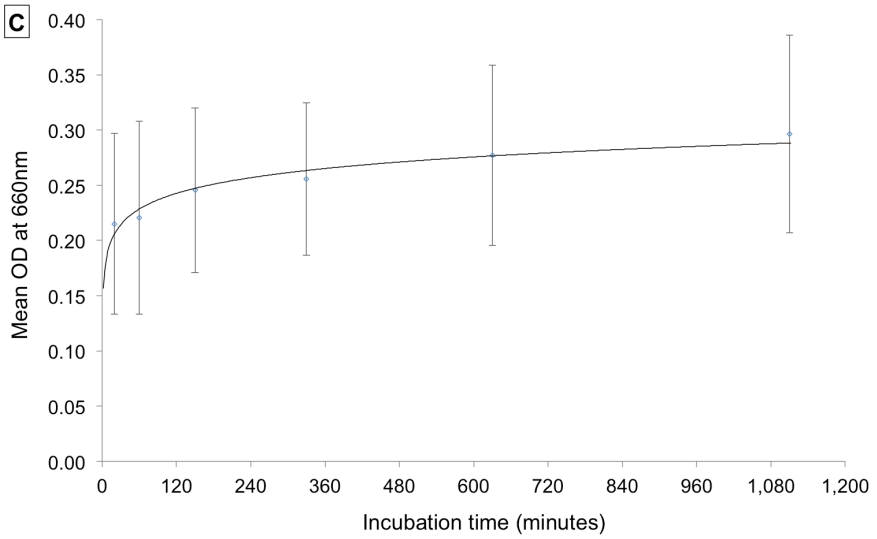
C
Mean OD at 660nm
0.40
0.35
0.30
0.25
0.20
0.15
0.10
0.05
0.00
0
120
240
360
480
600
720
840
960
1,080
1,200
Incubation time (minutes)

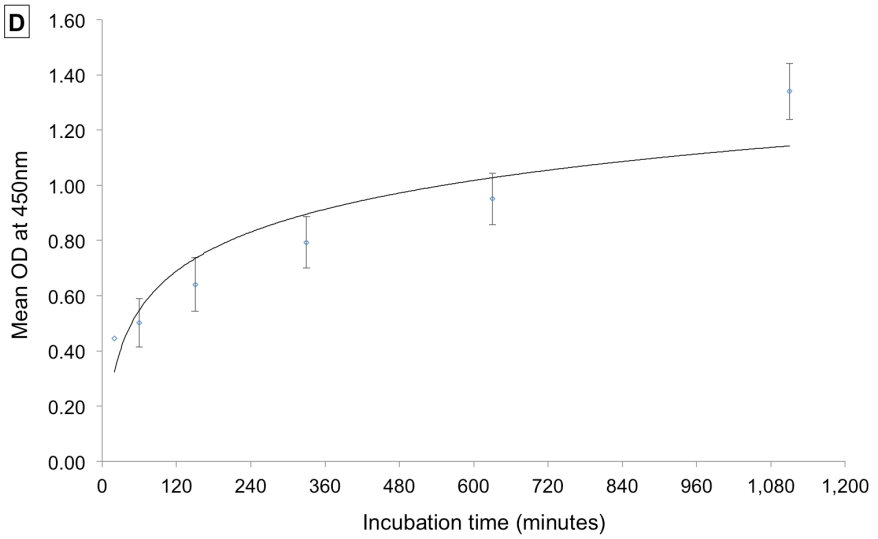
D
Mean OD at 450nm
1.60
1.40
1.20
1.00
0.80
0.60
0.40
0.20
0.00
0
120
240
360
480
600
720
840
960
1,080
1,200
Incubation time (minutes)

Figure 6.6 Primary antibody association kinetics.

IGF-1 (50 ng/mL) immobilised on ELISA well plates, incubated with mouse anti-IGF-1 antibody (500 ng/mL) for different durations, and assayed with rabbit anti-mouse IgG-peroxidase (1/5,000 dilution). TOP – mean fluorescence at 660 nm (**A**) and 450 nm (**B**); n = 2 with values representing means of two wells; upper detection limit for absorbance is ~3-3.5. Non-shaded bars represent anti-IGF-1 negative controls; criss-crossed bars represent anti-mouse IgG-peroxidase negative controls; error bars represent SEM values (n = 2). Absorbance increases with increasing incubation time and appears to reach equilibrium ~5 hours. BOTTOM – Binding isotherms at 660 nm (**C**) and 450 nm (**D**). 5 hours selected for future incubations.

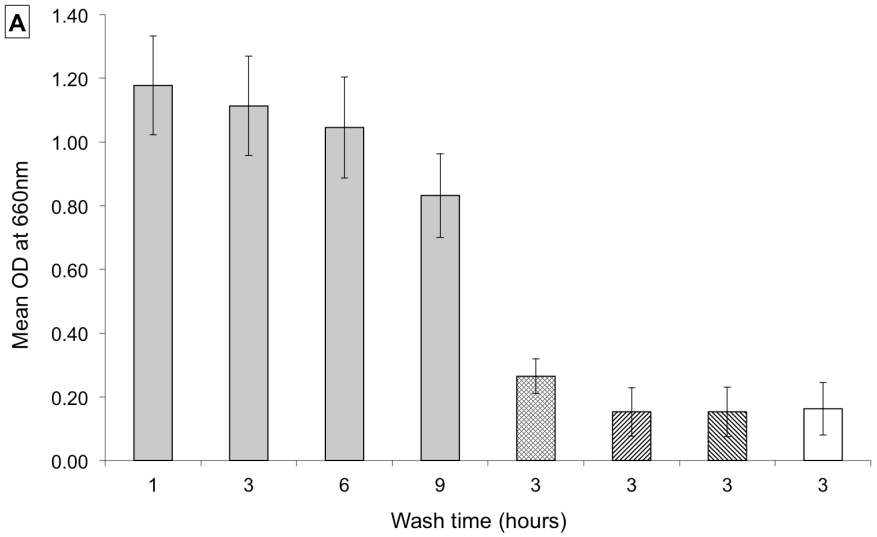
A
Mean OD at 660nm
1.40
1.20
1.00
0.80
0.60
0.40
0.20
0.00
1
3
6
9
3
3
3
3
Wash time (hours)

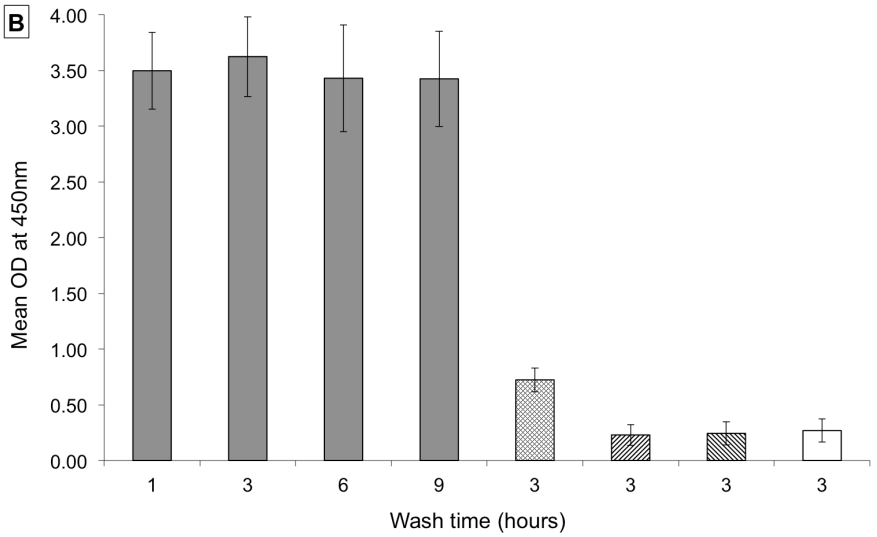
B
Mean OD at 450nm
4.00
3.50
3.00
2.50
2.00
1.50
1.00
0.50
0.00
1
3
6
9
3
3
3
3
Wash time (hours)

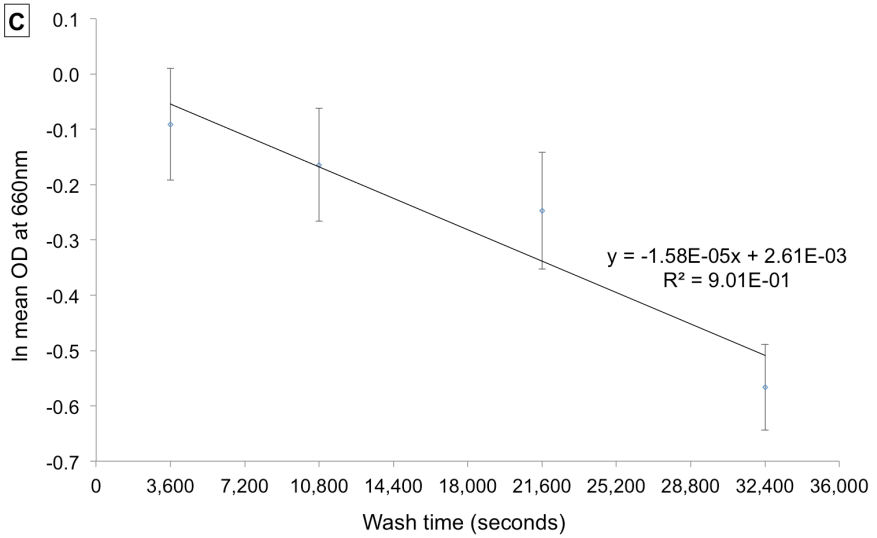
C
ln mean OD at 660nm
0.1
0.0
-0.1
-0.2
-0.3
-0.4
-0.5
-0.6
-0.7
y = -1.58E-05x + 2.61E-03
R² = 9.01E-01
0
3,600
7,200
10,800
14,400
18,000
21,600
25,200
28,800
32,400
36,000
Wash time (seconds)

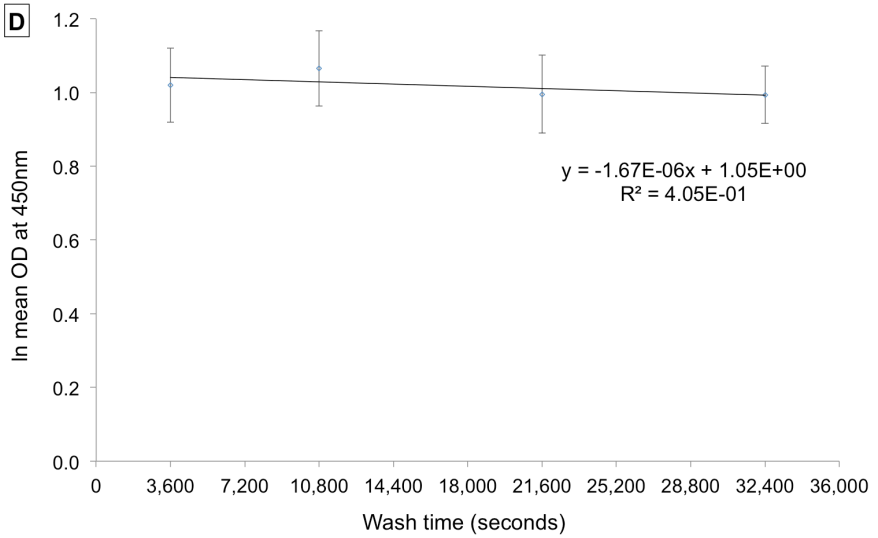
D
ln mean OD at 450nm
1.2
1.0
0.8
0.6
0.4
0.2
0.0
y = -1.67E-06x + 1.05E+00
R² = 4.05E-01
0
3,600
7,200
10,800
14,400
18,000
21,600
25,200
28,800
32,400
36,000
Wash time (seconds)

Figure 6.7 Primary antibody dissociation kinetics.

IGF-1 (100 ng/mL) immobilised on ELISA well plates, incubated with mouse anti-IGF-1 antibody (250 ng/mL) for a minimum of 8 hours before wash duration series, and finally assayed with rabbit anti-mouse IgG-peroxidase (1/5,000 dilution). TOP – mean fluorescence at 660 nm (**A**) and 450 nm (**B**); n = 2 with values representing means of two wells; upper detection limit for absorbance is ~3-3.5. Non-shaded bars represent IGF-1 negative controls; criss-crossed bars represent low pH reference wash samples; bars with hatchings to the right represent anti-mouse IgG-peroxidase negative controls; bars with hatchings to the left represent anti-IGF-1 negative controls; error bars represent SEM values (n = 2). Absorbance decreases with increasing wash time, but signal is very strong, especially for 450 nm results where values for wash times between 1 and 9 hours are at the limit of detection. BOTTOM – Log mean absorbance at 660 nm (**C**) and 450 nm (**D**). 660 nm results indicate k_d is 1.58×10^{-5} s^{-1}.

6.2.2 Binding characterisation of anti-IGF-1 peptides

Peroxidase labelling

Anti-IGF-1 peptides were conjugated to horseradish peroxidase to enable ELISA experiments. Peptide-peroxidase conjugates were purified from free peptide using buffer-exchanged Bio-Spin P30 spin columns as shown in the workflow in **Figure 6.8**.

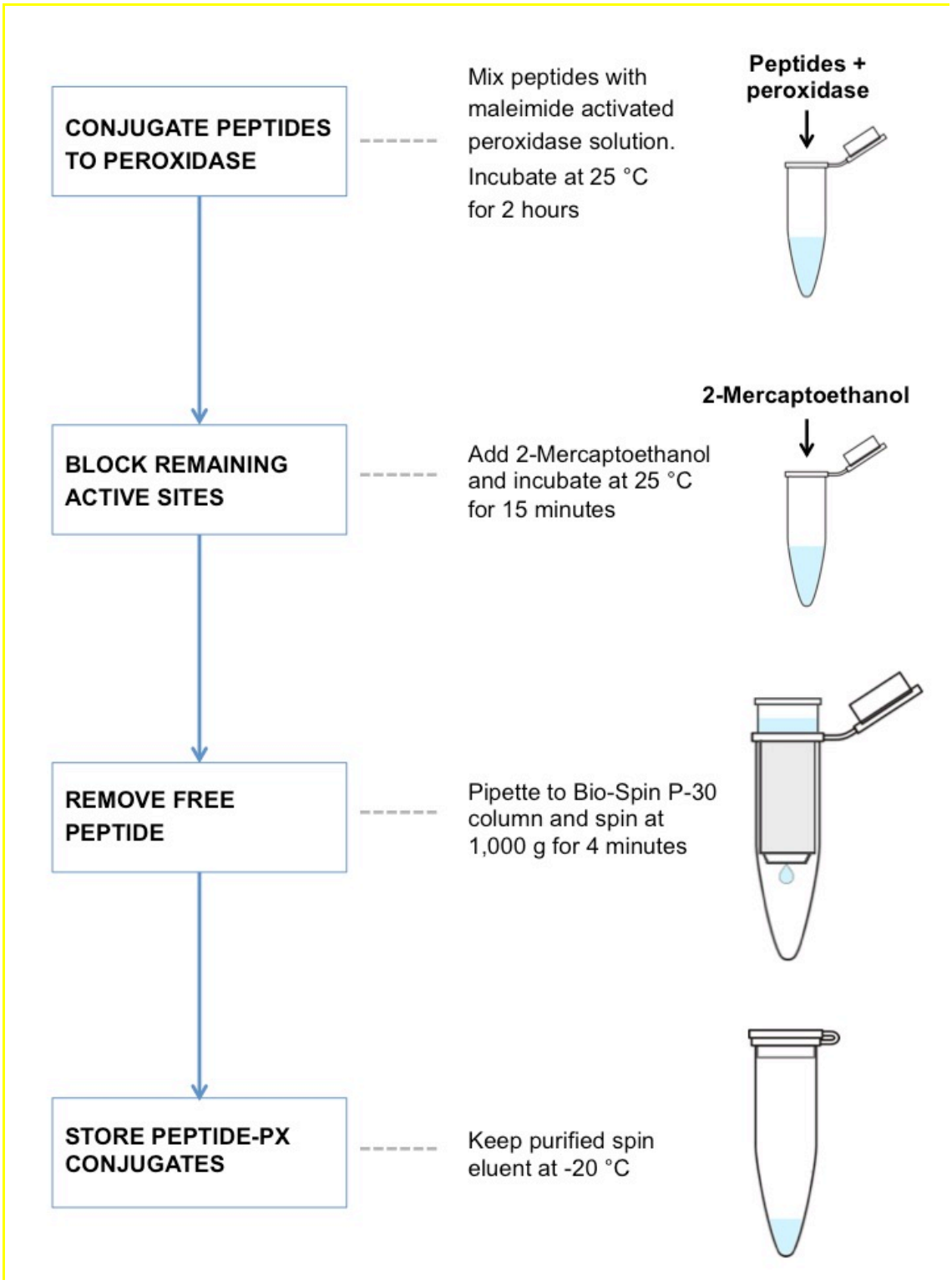

Figure 6.8 Workflow for peroxidase labelling of anti-IGF-1 peptides.

Anti-IGF-1 peptides were incubated with maleimide activated peroxidase solution. 2-Mercaptoethanol was then added to block any remaining active sites and after a short incubation period, mixtures were pipetted to Bio-Spin P-30 columns for purification of peptide-peroxidase conjugates from unbound peptide. Purified peroxidase-labelled peptides were then stored at -20 ºC.

Dissociation kinetics

Dissociation experiments using the anti-IGF-1 peptides were carried out with immobilised IGF-1 to compare their dissociation rates to that of the anti-IGF-1 antibody used in Section 6.2. Dissociation kinetics for peptide “N105” are shown in **Figure 6.9**, and dissociation rates for all anti-IGF-1 peptides from IGF-1 are summarised in **Table 6.1**.

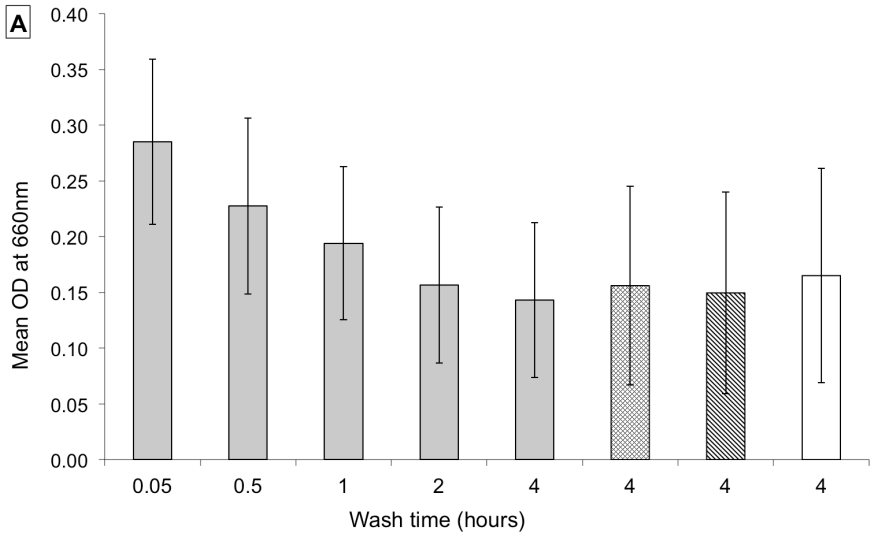
A
Mean OD at 660nm
0.40
0.35
0.30
0.25
0.20
0.15
0.10
0.05
0.00
0.05
0.5
1
2
4
4
4
4
Wash time (hours)

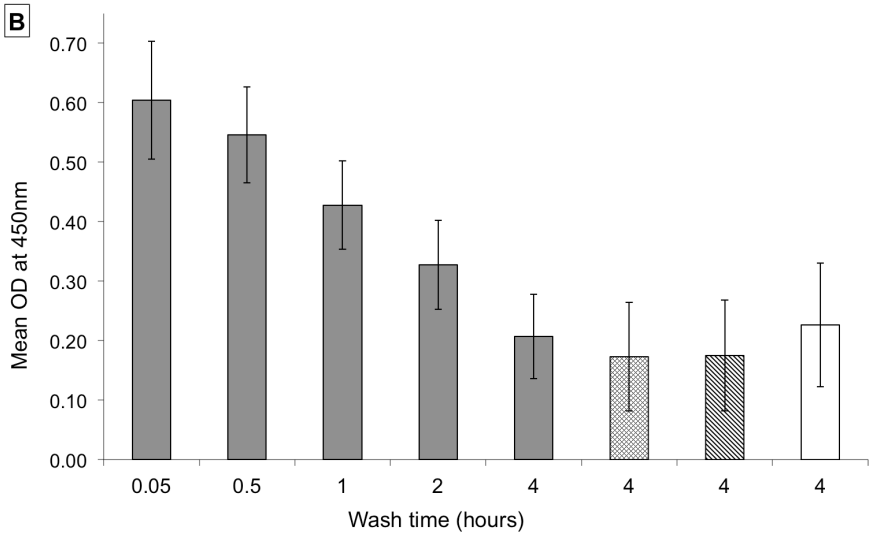
B
Mean OD at 450nm
0.70
0.60
0.50
0.40
0.30
0.20
0.10
0.00
0.05
0.5
1
2
4
4
4
4
Wash time (hours)

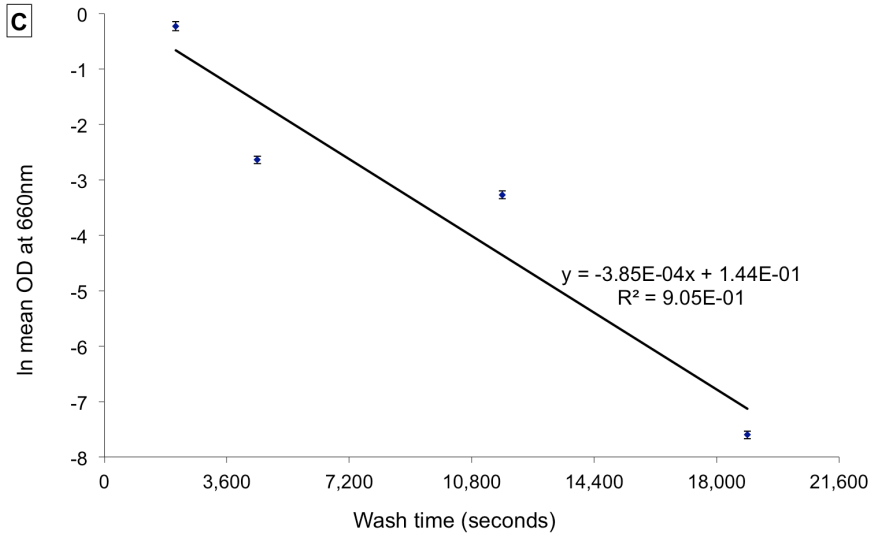
C
ln mean OD at 660nm
0
-1
-2
-3
-4
-5
-6
-7
-8
y = -3.85E-04x + 1.44E-01
R² = 9.05E-01
0
3,600
7,200
10,800
14,400
18,000
21,600
Wash time (seconds)

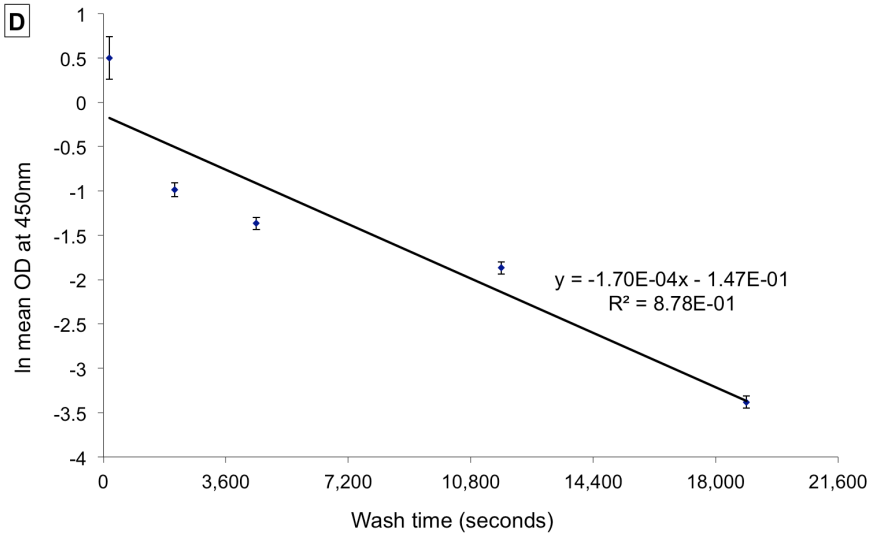
D
ln mean OD at 450nm
1
0.5
0
-0.5
-1
-1.5
-2
-2.5
-3
-3.5
-4
y = -1.70E-04x - 1.47E-01
R² = 8.78E-01
0
3,600
7,200
10,800
14,400
18,000
21,600
Wash time (seconds)

Figure 6.9 Anti-IGF-1 peptide dissociation kinetics.

IGF-1 (10 ug/mL) immobilised on ELISA well plates, incubated with anti-IGF-1 peptide-peroxidase ("N105", 1/1000 dilution) for a minimum of 4 hours before wash duration series. TOP – mean fluorescence at 660 nm (**A**) and 450 nm (**B**); n = 2 with values representing means of two wells; upper detection limit for absorbance is ~3-3.5. Non-shaded bars represent IGF-1 negative controls; criss-crossed bars represent low pH reference wash samples; bars with hatchings to the left represent anti-IGF-1 peptide-peroxidase negative controls; error bars represent SEM values (n = 2). Absorbance decreases with increasing wash time. BOTTOM – Log mean absorbance at 660 nm (**C**) and 450 nm (**D**). 450 nm results indicate k_d is -1.70×10^{-4} s^{-1}.

Table 6.1 Dissociation kinetics of anti-IGF-1 peptides from immobilised IGF-1.

Peptide Name	Sequence	Mean k_d (s^{-1})	SEM	No. of repeats
FAD105	GSALNTPNGSCSGSALNTPN	$-7.21E^{-5}$	$5.10E^{-5}$	2
N105	GSALNTPNGSGSC	$-1.26E^{-4}$	$2.73E^{-5}$	3
FAD106	GVLPHSRAGSCSGVLPHSRA	$-6.27E^{-5}$	$1.27E^{-5}$	2
FAD107	GTPVSTNQGSCSGTPVSTNQ	$-8.88E^{-5}$	$4.00E^{-5}$	2

6.3 Conclusions

1. Anti-IGF-1 peptides were generated via phage display, using phage display library that expresses a circularised (constrained) 7 amino acid long random peptide.

2. Synthetic peptides were shown to bind specifically to IGF-1 and not negative controls in fluorescence-based hydrogel assays.

3. Phage-derived peptides were conjugated to maleimide activated peroxidase and purified from unbound peptide using Bio-Spin P-30 spin columns.

4. The k_d of anti-IGF-1 peptides ranged from -1.26×10^{-4} s^{-1} (N105) to -8.88×10^{-5} s^{-1} (FAD107). This compares well to the dissociation rate measured for the monoclonal anti-IGF-1 antibody (1.58×10^{-5} s^{-1}).

5. In a separate study, the anti-IGF-1 peptides generated and described in this chapter, were shown to increase cell growth rates *in vitro* when added to a serum-free growth medium (data not shown).

Chapter 7: Final Discussion, Conclusions and Future Research Directions

7.1 Discussion

7.1.1 Anti-peptide affinity reagents and their applications

Target peptide selection involves choosing an appropriate protein target followed by the best peptide to be used as an antigen for generating affinity reagents against it. The expression patterns of particular proteins often provide a great deal of evidence as to the physiological state of a cell and an organism, providing strong markers and even therapeutic targets for diseases, or in the case of forensics, provide crucial information when profiling individuals from samples found at a crime scene. The 35 targets selected in Chapter 3 were chosen on the basis of decades' worth of research literature that reported on their quantitative expression profiles under different conditions as referenced. In essence, they were strongly pre-qualified by the body of evidence supporting their status as proven bio-markers across a broad range of conditions.

While the selection of the peptide for each marker was less obvious, it was still governed by sound immunogenic principles. The advantages of peptides over proteins in terms of stability and heterogeneity led to the decision to tryptically digest all proteins of interest. This had previously been reported as producing sufficiently hydrophilic peptides from nearly all human proteins (see **Table 1.8**), including very hydrophobic ones, and hydrophilicity of peptide antigens has been shown to correlate with their detection in affinity assays (Hopp, 1993; Soloviev & Finch, 2005). The predictability of these small peptide fragments in silico has the added advantage that such affinity reagents can be more easily generated via peptide synthesisers. To compare traditional tools to the peptide selection approach undertaken in Chapter 3, the antigenic peptide prediction tool from the Immunomedicine Group (Immunomedicine Group: Tools) was used to calculate immunogenicity scores for the 35 peptides chosen, results of which are shown in Table 7.1. In addition to antigen propensity, the number of antigenic determinants (epitopes) were also provided, though only 3 of the peptide sequences were predicted to contain one of these. When these results are plotted against antibody titres for the anti-peptide polyclonal antibodies generated via immunisation with the peptides there appears to be no correlation (**Figure 7.1**). This suggests that such traditional tools are not comprehensively capable in their ability to predict the immunogenicity of peptide sequences and that the approach demonstrated in Chapter 3 works because the majority of the antibodies did in fact display good titres. It should be noted that The Immunomedicine Group website does itself provide the disclaimer that the reported accuracy of their method is about 75%.

Table 7.1 ELISA titres and predicted immunogenicity scores for chosen peptide antigens

Antibody #	Target	ELISA (mean)[a]	Average antigen propensity	Predicted antigenic determinants
1	Myoglobin	**22,500**	**0.9711**	0
2	Tumour necrosis factor alpha	**37,500**	**1.0125**	0
3	C-reactive protein	**100,000**	**1.0560**	0
4	Fibrinogen (D Dimer)	**2,000**	**0.9989**	0
5	Fibrinogen (D Dimer)	**75,000**	**0.9642**	0
6	Fibrinogen (D Dimer)	**12,000**	**1.0115**	0
7	Interferon gamma	**212,500**	**1.0158**	0
8	Interleukin 1a	**60,000**	**1.0027**	0
9	Interleukin 1b	**300,000**	**1.0339**	**1**
10	Interleukin 2	**225,000**	**1.0353**	0
11	Interleukin 4	**2,000**	**1.0556**	0
12	Interleukin 6	**0**	**0.9915**	0
13	Interleukin 8	**400,000**	**1.0502**	0
14	Interleukin 10	**500,000**	**1.0428**	0
15	Beta-enolase	**500,000**	**1.0554**	**1**
16	E-selectin	**50,000**	**0.9414**	0
17	Fibronectin	**500,000**	**1.0118**	0
18	Haptoglobin	**25,000**	**1.0355**	0
19	Heat shock protein(s)	**15,000**	**1.0295**	0
20	Insulin-like growth factor I	**100,000**	**1.0079**	0
21	Leptin	**35,000**	**1.0534**	0
22	Prolactin	**15,000**	**0.9812**	0
23	Transforming growth factor-beta 1	**162,500**	**1.0385**	0
24	Transforming growth factor-beta 4	**300,000**	**1.0040**	0
25	Adiponectin	**60,000**	**1.0368**	0
26	Insulin	**22,500**	**1.0662**	0
27	Matrix metalloproteinase 1	**62,500**	**1.0229**	0
28	Matrix metalloproteinase 2	**15,000**	**0.9811**	0
29	Matrix metalloproteinase 3	**60,000**	**0.9795**	0
30	Matrix metalloproteinase 9	**15,000**	**1.0385**	0
31	Matrix metalloproteinase 11	**22,500**	**1.0861**	0
32	Prostate specific antigen	**20,000**	**1.0547**	0
33	Serum amyloid-A	**87,500**	**0.9975**	0
34	Sex hormone-binding globulin	**400,000**	**1.0668**	0
35	Pulmonary surfactant-associated protein A	**150,000**	**0.9773**	0

Average antigen propensity and antigenic determinants as predicted by one of the most popular online tools for the 35 peptide antigens chosen from tryptic digests of protein targets identified in Chapter 3.

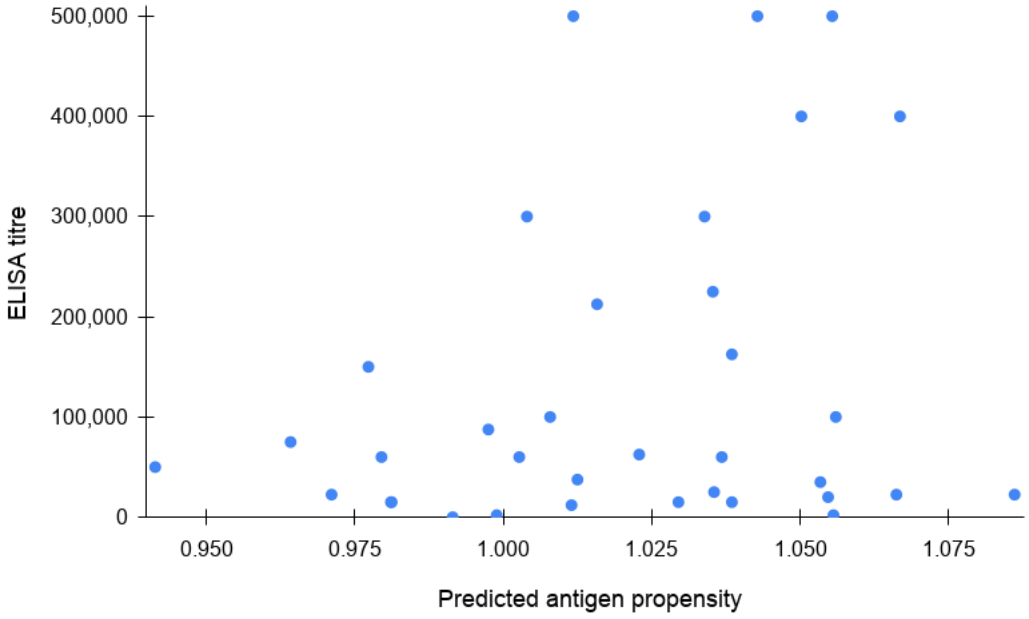

Figure 7.1 Scatter plot of ELISA titres vs predicted antigenicity

No apparent relationship between average antigen propensity scores as predicted by one of the leading online tools, and ELISA titre scores for the polyclonal antisera obtained from immunisation with the 35 chosen tryptic peptides chosen in Chapter 3.

7.1.2 Multiplexed affinity assays: spatial signal multiplexing using microarrays

Anti-peptide antibody microarrays

Competitive displacement assays provide practical benefits in terms of reduced sample preparation requirements and for multiplexing where they are favourable for measuring protein expression levels across a diverse range of concentrations. Challenges associated with the heterogeneity of protein targets justified the use of a peptide-based approach to the microarray methods investigated in this chapter.

Results from the competitive anti-peptide antibody microarrays showed strong intra-individual correlations among 3 of the 4 individuals from whom samples were taken (0.49 for Individual 1; 0.52 for Individual 3; 0.49 for Individual 4). These samples were taken before and after individuals received two alcohol treatments: after Treatment 1, three peptides were found to be up-regulated in all individuals (matrix metalloproteinase 1 & 2 and pulmonary surfactant-associated protein A), and three down-regulated (myoglobin, E-selectin, and transforming growth factor-beta 4); and after Treatment 2, beta-enolase was up-regulated, and interleukin 1b down-regulated, in all individuals. Although exact treatment conditions are unknown the results confirm the validity of anti-peptide microarrays for the detection of transient changes to the expression of target proteins in serum samples.

While microarrays surely allow for the miniaturisation and multiplexing of affinity based assays (in this case 33 anti-peptide antibodies and multiple control samples were arrayed in triplicate on an area of membrane measuring around 2 cm^2), and the choice of single label competitive displacement assays streamlined the procedures negating the need for repetitive labelling of experimental samples while also compensating for the heterogeneity of antibody affinities, they are not without their drawbacks. These issues will be discussed below.

Careful calibration of liquid chromatography column elution times was required prior to purification of the anti-peptide antibodies from the rabbit sera samples, and this process has several potential pitfalls. Firstly, the column parameters are not constant and thus variation in pump speed and flow rate may result in different elution times of the IgG fragment between sample runs. While this was overcome during calibration by making collections based on elution volume rather than time, the variability of the system still makes it prone to error. Simply widening the collection window must be balanced with

the undesired dilution and reduced purity of antibody that will result from doing so. 33 of the 35 sera samples were purified successfully but this was an extremely time-consuming and laborious process. Proteolytically digesting samples prior to analysis removes the need to preserve protein samples, however the purified polyclonal anti-peptide antibodies that are immobilised on the membrane are themselves proteins and prone to degradation.

Use of the Flexys robotic arrayer enables densely packed sample grids to be spotted on the membrane (6 5x5 grids on each membrane in this case). The pin heads themselves present another area of potential error as even tiny variation in pin-head size and shape can result in inconsistencies between antibody transfer to the membranes. This was minimised by printing trial transfers of dyes and selecting the 6 most homogeneous pins from a larger pool, however ten repeat transfers per spot were still necessary in order to increase reproducibility, greatly extending the duration of the printing process. Thorough pin-washing to avoid carry-over contamination between samples was also required and the number and duration of these washing stages considerably adds to the overall time required for array preparation. Maintaining a humid atmosphere within the arrayer enclosure was therefore critical to try and prevent samples drying out during the process, but there will inevitably be some variation between those printed at the very start of the procedure when all samples are fresh, and those printed last when samples, wash buffers, etc. have all been sat at above room temperature for the duration of the process.

The positively charged nylon membrane was chosen because it is a 3D porous substrate that allows for the antibodies to be immobilised with their binding epitopes accessible, and for its very high protein binding capacity which is suitable for the samples that resulted from liquid chromatography purification of IgG fractions from whole sera samples. While nylon is also less fragile than other porous 3D membrane substrates such as nitrocellulose, it is still prone to damage that can result in signal artefacts and must therefore be handled with extreme care. The large number of steps involved in the microarray procedure where the membranes must be handled such as blocking, multiple wash cycles, cross-linking, and mounting, mean that handling artefacts are almost inevitable (see **Figure 7.2**).

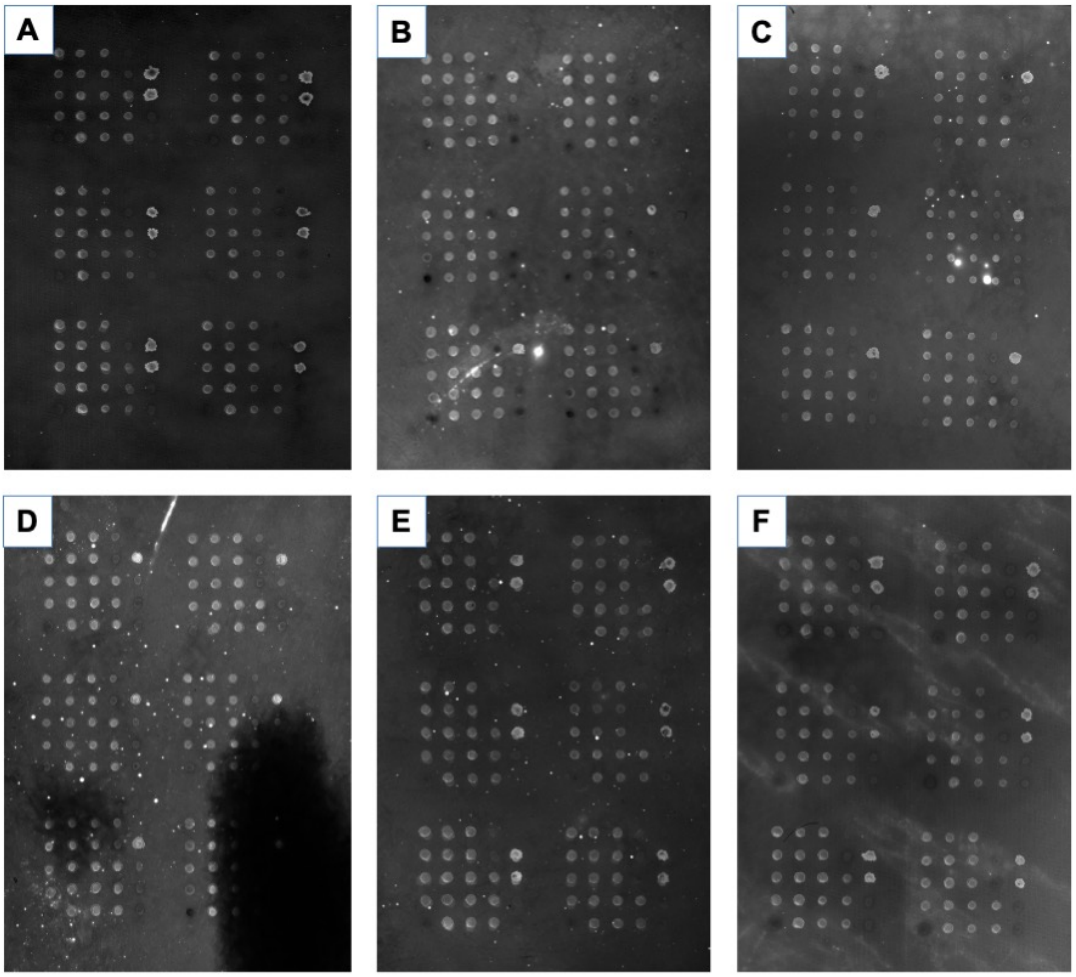

Figure 7.2 Artefacts and background heterogeneity of microarrays

Six scan images chosen to highlight the challenges involved with analysing microarray scans. **[A]** Relatively uniform background and minimal artefacts throughout. **[B]** Fluorescent streak artefact through grid bottom-left, and bright spot-sized artefact. **[C]** Cluster of 3 bright spot artefacts among grid centre-right. **[D]** Fluorescent streak artefact centre-top of the scan combined with a large dark zone bottom-right covering half of two grids. **[E]** Spattering of bright fluorescent artefacts through entire slide **[F]** No fluorescent artefacts but non-uniform streaky background throughout.

In this study, extensive efforts were made to remove the impact of fluorescent artefacts, minimise the effect of non-uniform backgrounds, eliminate non-specific binding, normalise signals pin-to-pin and membrane-to-membrane as well as apply grid quality score weighting in order to further refine the results (as per **Chapter 2.2.1**). With just 16 scan images, manual assessment was still feasible in order to investigate any unexpected results when required and check that obvious outliers had been suitably attended to, however this would prove far more challenging if this experiment was to be repeated with each sample analysed in triplicate. Larger studies with greater numbers of samples would result in substantially more data and make manual assessment entirely unfeasible.

Just as robotic techniques have provided improved efficiency and accuracy over manual processes, e.g. using the Flexsys arrayer in this experiment instead of hand spotting samples, the emerging field of artificial intelligence (AI) could help massively in processing the vast amount of data produced from microarray studies. Even with best efforts to design and refine automatic checkpoints on data as were made here, it is hard to imagine these can compare to those made by an AI with machine learning designed to remove artefacts, normalise results, and spot patterns. Such an evolution will undoubtedly improve dramatically not only the speed and accuracy of analysis, but also reveal more subtle and complex relationships that may otherwise go unseen.

Catto *et al.* (Catto *et al.*, 2010) used AI to identify a prognostic gene signature whose members reflect a variety of carcinogenic pathways that could identify progression in non-muscle-invasive bladder cancer. The motivation behind this AI-assisted study was the acknowledgement that while gene expression microarrays can reveal insights into disease biology and identify novel biomarkers, such experiments generate huge datasets that are extremely challenging to interpret. The group used AI and statistical analyses to identify progression-related genes in a microarray dataset (n=66 tumours, n=2800 genes). AI-selected genes were then investigated in a second cohort (n=262 tumours) using immunohistochemistry. AI identified 11 progression-associated genes (odds ratio [OR]: 0.70; 95% confidence interval [CI], 0.56-0.87; p=0.0004), and these were more discriminate than genes chosen using statistical analyses (OR: 1.24; 95% CI, 0.96-1.60; p=0.09). Commercial antibodies were then used to determine the expression of six AI-selected genes (LIG3, FAS, KRT18, ICAM1, DSG2, and BRCA2) that successfully identified tumour progression (concordance index: 0.66; log-rank test: p=0.01). AI-selected genes were more discriminate than pathologic criteria at determining progression (Cox multivariate analysis: p=0.01). The group concluded that AI and statistical analyses use different techniques of inference to determine gene-

phenotype associations and identify distinct prognostic gene signatures that are equally valid.

Microarray-based gene sequencing has been used in many studies to identify important signalling pathways that could impact the apthogenesis of pathogenesis of pulmonary arterial hypertension (PAH), a serious and progressive disease for which even the best therapies provide a 50% 5-year survival rate (Fessel *et al.*, 2013; Hemnes *et al.*, 2016; Hoffmann *et al.*, 2016). Such studies provide large quantity of data and in addition to the routine microarray data processing protocols of background noise reduction and normalisation, some differentially expressed signal data can often be ranked by their logarithmically transformed fold change values or by moderated t-statistic values. Low-expression genes are typically considered unreliable and discarded from the dataset manually (Mariani *et al.*, 2003; Aris *et al.*, 2004; Li *et al.*, 2005) or by filtering algorithms provided by software packages such as the Bioconductor (Aluru *et al.*, 2013; Chockalingam *et al.*, 2016) in an effort to further “de-noise” the data. Cui *et al.* (Cui *et al.*, 2019) hypothesised that some low-expression genes might function collectively and play a significant role in controlling the disease. Combining state-of-the-art machine learning and novel algorithms they demonstrated that clusters of small-expression genes could be extremely informative at predicting and differentiating different forms of PAH. Machine learning algorithms selected by the team included the Linear Discriminant Analysis (LDA), Support Vector Machine (SVM), and Artificial Neural Networks (ANN).

Neural Designer is a machine learning software that implements the Neural Networks technique and enables the discovery of intricate relationships and complex patterns from microarrays data. Alongside public databases for arrays including Array Express at the European Bioinformatics Institute and the NCBI´s Gene Expression Omnibus GEO, The Functional Genomics Data Society (FGED) has also led efforts to standardise microarray data sets so the researchers can more easily share common knowledge and compare experiments. Such collaborative efforts coupled with the advancements in AI and machine learning technology suggest a bright future lies ahead of microarrays.

However, despite their exceptional capacity for multiplexing, and compatibility with peptidomic protocols as demonstrated here with competitive assays of tryptically digested serum samples, the multiple complex steps and lengthy data processing involved make microarrays ill-suited to fulfilling the aims of this project. The anti-peptide antibodies used here also less than ideal in that they still need to be generated in animal hosts, purified from whole sera, and are prone to denaturing.

7.1.3 Multiplexing approaches to membrane and solution-based assays

The aim of this chapter was to explore lateral flow test devices as a simpler and more rapid alternative to microarrays.

One of the most common labelling reagents for lateral flow tests are GNPs (Banerjee & Jaiswal, 2018; Cheng *et al.*, 2019; Wen *et al.*, 2020) and these proved quick and easy to synthesise. The conjugation of protein to the GNPs was also straightforward, confirmed by a 7 nm red shift in the absorption maxima compared to non-conjugated particles. The amount of protein required to sufficiently block the surface and prevent aggregation was also determined with a salt-titration series.

Competitive GNP lateral flow test strips were then created and used for the successful detection of the benzodiazepine, diazepam (also known as Valium) in buffer and serum samples. Spiking of samples with diazepam resulted in competitive displacement of GNP-antibody conjugates for immobilised oxazepam (a key metabolite of most benzodiazepines) and a visible reduction in intensity of GNPs at the test line. These lateral flow strips were easier to produce compared to the microarrays produced in Chapter 3, and while specialist equipment allowed both formats to be produced in small scale batches, production of lateral flow test strips was significantly quicker. The membrane printing time in particular differs significantly to that of microarrays – whereas the batch of microarrays took hours to print, the lateral flow membranes took a matter of seconds to print, improving the reproducibility of the tests.

The results for these benzodiazepine tests were qualitative and each strip provided just a single result for a single analyte, compared to dozens of analytes in triplicate for each antibody microarray. To run samples in triplicate, multiple strips can be used as repeats, but in order to achieve multiplexity of analytes on a single strip, multiple test lines would need to be printed on the membrane. While this has been routinely done, there is a limit to just how many test lines a strip can practically accommodate in series. Tests that have pushed the limits on this approach include the simultaneous detection of four major nitrofuran metabolites in fish samples (Wang *et al.*, 2018), detection of five different contaminants that may exist simultaneously in drinking water (Xing *et al.*, 2015; Zhao *et al.*, 2016), and NG Biotech's NG-Test® CARBA 5, 15-minute lateral flow test for five most common carbapenemase enzymes produces by the bacteria of Enterobacterales and Pseudomonas aeruginosa (see **Figure 7.3 Panel A**), all of which use GNPs as the labelling reagent. Multiplexity via multiple strips in a single device has also been

demonstrated by way of a 10 strip “disc” where each strip tests for a unique epidemic foodborne pathogen (Zhao *et al.*, 2016) (see **Figure 7.3 Panel B**), and is now common among drugs of abuse testing, e.g. Prima’s multi-drug test permits simultaneous qualitative detection of amphetamine, methamphetamine, cocaine, morphine and THC in human urine with comparable detection limits to conventional single-analyte test strips.

In an attempt to harness the benefits of both formats, Taranova et al. created a “hybrid” strip consisting of 32 microarray spots in place of where a test-line would typically be positioned (Taranova *et al.*, 2013) (see **Figure 7.3 Panel C**). The group successfully used this approach for the simultaneous detection of four drugs of abuse, specifically morphine, amphetamine, methamphetamine, and benzoylecgonine (the major metabolite of cocaine) and concluded that the number of test spots could be increased to 100-150 with no changes to the printing procedure. A more recent extension of this was proposed in a collaboration between DCN and BioDot, and termed Symbolics. The approach combines lateral flow principles with arrayed reagents, with the name being derived from the ability to design the orientation of immobilised probes in formations of letters, symbols and such that the visible results intuitively symbolise outcomes (see **Figure 7.3 Panel D**). One of the major challenges with multiplexing lateral flow tests within a single strip is that flow rate through the membrane has been shown to decrease in a non-linear fashion with distance from the origin resulting in significantly different reaction times on the first line vs the last (Mansfield, 2009; Millipore, 2013) greatly impacting the ability to generate quantitative assays in multiplexed setups. While these issues can sometimes be overcome with careful optimisation of each capture reagent’s location on the strip (Bartosh *et al.*, 2020) and with the use of fields of dots instead of lines, it is perhaps this hike in complexity that has stifled the development of array-based lateral flow assays, and the uptake of Symbolics technology in the few years since it was introduced.

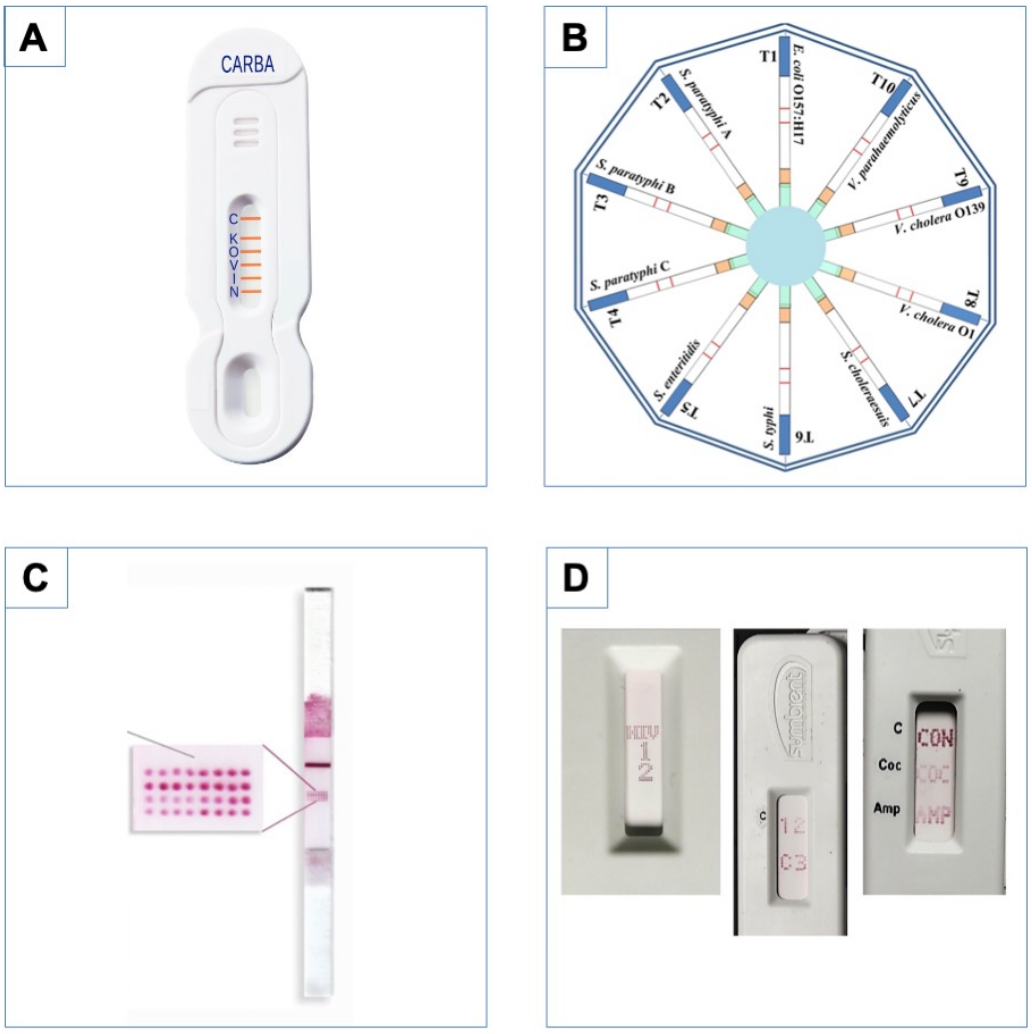

Figure 7.3 Approaches to multiplexing in lateral flow tests

Multiplexed approaches for lateral flow assays including: **[A]** Multiple test lines positioned in series on a single strip; **[B]** Multiple strips harnessed within a single test cassette permitting parallel testing; **[C]** Arrayed lines permitting multiplexing and repeats; **[D]** Symbolics, where capture reagents are arrays in patterns to provide visually intuitive results.

In order to try and overcome some of the limitations imposed on lateral flow tests due to spatial multiplexing with visual labels, QDs were investigated for their compatibility and potential to provide spectral multiplexing.

The size of unconjugated toluene-based QD stocks were first characterised as this is the primary feature underlying their emission profiles. Both the populations examined were found to closely match the measurements provided by the manufacturer (2.79 nm +/- 0.41 nm and 5.52 nm +/- 0.70 nm, for QD3 and QD6 respectively). Most importantly, low standard deviation for both should ensure narrow emission peaks due to close uniformity of particle sizes. Centre-to-centre measures should, in theory, provide the most accurate measurements for QD diameters as no particles can be closer than two radii from each other, however it became clear that the QDs were relatively widely dispersed and so diameter measurements were selected instead.

To quantitatively compare the narrowness of particle size the relative standard deviation (RSD) is usually applied (Segets, 2016). The RSD is defined as the standard deviation divided by the mean particle size, and “monodispersity” is considered to be achieved if RSD < 0.05, whereas “narrow” size distributions are found for RSD < 0.1. Applying this to the sizing results for the two populations of QDs examined, we see that the RSD is 0.15 and 1.3 for QD3 and QD6 respectively. However, these results should perhaps be viewed with caution given the relatively low sample size of just a few hundred from a population of millions of particles, and that these were manual measurements (albeit using Adobe Photoshop measure tool) based on hard to define “fuzzy” edges of particles on TEM images. A more automated approach that can distinguish particle boundaries as well as individual particles from aggregated particles, and that can be applied to larger data sets would provide greater accuracy (Segets *et al.*, 2012).

Single wavelength emission detection of multiple QDs is possible only when spatially separated (Figure 4ABA) but will not permit the detection of multiple QDs that are co-located. For this, scanning emission spectrum detection is required such that the emission at all wavelengths in a specified range can be determined. When measuring such emission spectra, a single excitation wavelength of 380 nm was used as it balanced the provision of strong excitation peaks and the avoidance of its second order diffraction peak at 760 nm interfering with the emission spectra of and of the QDs being used. The emission peaks were all found to be within 5 nm of those provided by the manufacturer, but scans were ultimately still necessary to obtain accurate full spectra for each of the individual stocks to aid in the deconvolution of signals derived from mixtures of two or more QD populations. Obtaining these unique spectral signatures that were

subsequently used as references when assigning the correct contribution of each to mixtures of multiple QD populations is the most critical step in the deconvolution of overlapping emission spectra (Spectral Imaging and Linear Unmixing | Nikon - microscopyu.com/techniques/confocal/spectral-imaging-and-linear-unmixing). Spectra from mixtures of 2, 3, 4, 5 and 6 QD populations were successfully resolved to reveal their individual components using a spectral unmixing algorithm where the minimum difference between the unknown spectra and the reference spectra for all possible mixtures of the reference spectra is calculated. This linear unmixing method relies on the assumption that the measured signal from each wavelength is linearly proportional to the percentage or concentration of that wavelength in the sample.

These results confirm that quantitative spectral multiplexing using QDs can be achieved using a single excitation wavelength coupled with scanning emission detection.

Photodegradation/bleaching of QDs

When compared to the traditional organic dyes RITC and atto565-biotin, QDs exhibited a slower rate of photobleaching. This is consistent with the wider literature on their properties and performance (Lee *et al.*, 2004; Resch-Genger *et al.*, 2008; Babu & Paira, 2017; Abdel-Salam *et al.*, 2020). However, an interesting observation was that while fluorescence appears to decrease with each laser scan, exposure to high-intensity UV-Vis radiation for short duration (30 seconds) led to an increase in QD fluorescence. Scanning appears to cause ~15% loss in fluorescence per scan at these settings, with a greater loss of fluorescence observed between the first and second scans (~18%) than between the second and third scans (~14%) of each set. Reduced fluorescence with repeated scans suggests the laser is in some way degrading the QDs, perhaps by causing defects to the surface and/or structure of the nanocrystals. Short, intense UV-vis exposure delivers a revival of fluorescence possibly due to broad excitation of the QDs, or because of a mild luminescence enhancement due to photoactivation via the UV-vis light. UV and visible light has been shown to induce chemical reactions on QDs surfaces, including the oxidation and decomposition of capping ligands, resulting in the formation of shells on the surface of a QD core (Carrillo-Carrión *et al.*, 2009) and used as a convenient and feasible way to enhance the fluorescence of QDs (Smyntyna *et al.*, 2014). More recently gamma radiation has been proposed as a more effective and efficient way to achieve this enhanced fluorescence at scale (Chang *et al.*, 2019). Even with their already superior qualities, it seems there is opportunity to further increase detection limits of QDs with a simple light treatment prior to measurement.

7.1.4 IGF-1 Affinity reagents

To overcome hurdles associated with traditional antibody-based affinity reagents, novel peptide affinity reagents against IGF-1 were generated via phage display. The binding of these peptides to IGF-1 was confirmed using hydrogel arrays, and ELISA after subsequent conjugation to maleimide activated peroxidase. K_{diss} of anti-IGF-1 peptides ranging from -1.26 x 10^{-4} s^{-1} (N105) to -8.88 x 10^{-5} (FAD107). This compares to 1.58 x 10^{-5} for the monoclonal anti-IGF-1 antibody.

The generated IGF-binding peptides were also tested *in vitro* for their effect on cell growth rates. Contrary to expectations, the anti-IGF-1 peptides, when added to the serum free growth medium that contained a small amount of IGF, failed to inhibit cellular proliferation and instead increased cell growth rates. Examining the literature on the wider IGF superfamily reveals a number of studies involving peptides that either directly or indirectly increase the potency of IGF-1 or have mitogenic effects themselves. Modified forms of the IGF-1 protein have been shown to have reduced affinity for the IGFBPs and as a result, increased potency (Tomas *et al.*, 1996). IGF-1 DES is a recombinant and truncated form of IGF-1 produced in E.coli and lacking the first three amino acids of the N-terminus of the full peptide and thus also known as IGF-1 Des(1-3), Des1-3, Des 1-3, Des (1-3), and IGF-1 (4-70). This small modification results in a ~10-fold increase in potency *in vivo* (Ballard *et al.*, 1996). Long arginine 3-IGF-1 (IGF-1 LR3) is another recombinant analogue of IGF-1 that has an arginine substitution at amino acid three, and an additional thirteen amino acids at its N-terminus. This modification results in a significantly longer half-life, much lower affinity for the IGFBPs and, consequently, around a 3-fold increase in potency (Tomas *et al.*, 1992). Binding of the novel anti-IGF-1 peptides could be conferring either or both of these effects on IGF-1 *in vitro*, resulting in the increased cell growth rates observed.

It could be possible that the peptides discovered increase the bioactivity of IGF-1 and/or themselves have a degree of bioactivity contributing to cell growth. Evidence has been reported for mitogenic effects from IGF-1 related peptides, or so called “E” peptides (Pfeffer *et al.*, 2009; Armakolas *et al.*, 2010; Kandalla *et al.*, 2011; Hede *et al.*, 2012). When IGF-1 is first synthesised, it is done so as one of three prohormones that are encoded by alternatively spliced IGF-1 mRNAs (proIGF-1Ea, proIGF-1Eb and proIGF-1Ec). All three proIGF-1s give rise to a common mature IGF-1 sequence but with different E-domains that are enzymatically cleaved. There is increasing evidence that these

cleaved E-peptides have themselves functional roles that are independent of IGF-1 receptor activation, including effects on proliferation and cell migration (Siegfried *et al.*, 1992; Kuo & Chen, 2002; Yang & Goldspink, 2002; Mills *et al.*, 2007). Pfeffer et al. (Pfeffer *et al.*, 2009) also found that Ea and Eb peptides also enhance the uptake of IGF-1 into cells, or possibly aid in the release of IGF-1 from IGFBPs, either directly or indirectly, enabling the mature IGF-1 ligand to bind to its receptor. Hede et al. (Hede *et al.*, 2012) also reported a tethering function for E peptides that could aid in maintaining concentrations of IGF-1 at their site of synthesis for more localised effects. The IGF-1 Ec peptide is also known as mechano-growth factor (MGF) and is up-regulated in exercised and damaged muscles, plays a neuroprotective role against ischemia, and contributes to the actions of IGF-1 to improve cardiac function and activate resident stem cell populations (Goldspink, 1996; Yang *et al.*, 1996, 1997; McKoy *et al.*, 1999; Burniston *et al.*, 2005; Dłużniewska *et al.*, 2005; Carpenter *et al.*, 2008; Kandalla *et al.*, 2011). Exogenous administration of synthetic Ec peptides have also been shown to possess bioactivity on human cell lines (Armakolas *et al.*, 2010; Milingos *et al.*, 2011; Philippou *et al.*, 2011).

The peptides could also be mimicking activity seen by other members of the IGFBP Superfamily. Insulin-like growth factor (IGF)-binding protein (IGFBP)-related proteins (IGFBP-rPs) are a group of 10 cysteine-rich proteins that share significant amino-terminal structural similarity with the conventional IGFBPs and are involved in diverse biological functions, including growth regulation. IGFBP-rP1 and IGFBP-rP2 have been reported to increase during senescence of the prostate epithelium and in response to growth inhibitors (TGF-β1 and atRA) suggesting they are likely to negatively regulate growth, however IGFBP-rP3's role as a growth stimulator and/or protooncogene has been reported after preferential expression in cancerous cells (López-Bermejo *et al.*, 2000). rhIGFBP-rP3 has been shown to bind IGF-1, IGF-2, and insulin with low affinity, and while synthesised by several malignant cell lines its ubiquitous presence in human biological fluids suggest it could be involved in the regulation of cell growth in non-malignant tissues too (Christine P. Burren *et al.*, 1999; Deshayes *et al.*, 2002).

Elsewhere phage-display derived anti-IGF-1 peptides have also been shown to have paradoxical effects, exhibiting both agonist and antagonist effects. IGF-F1-1 is a cyclic hexadecapeptide, sequence RNCFESFVAALRRCMYG-NH_2, that acts as a weak antagonist of IGF-1 binding to the IGF-1R, and to IGFBPs 2 and 3 by binding to the IGFBP-binding domain on IGF-1 (Deshayes *et al.*, 2002). Robinson & Rosenzweig (Robinson & Rosenzweig, 2006) demonstrated that it does not inhibit downstream signalling events triggered by IGF-1 however, and that it can also act as a mitogenic

agonist on its own, activating Akt phosphorylation, S-phase entry and [^{3}H]thymidine incorporation when added to MCF-7 cells alone. These agonistic effects could be due to IGF-F1-1 induced dissociation of extra cellular matrix (ECM) associated IGFBP-bound IGF-1, the possible binding of IGF-F1-1 to IGFBP2, or even possible crosstalk between the IGF-1R and alternative pathways that may be affected either directly or indirectly by the presence of the IGF-F1-1 peptide.

The growth stimulating effect observed for the anti-IGF-1 peptides reported here suggest the peptides may not block the hormone binding to relevant receptors, but perhaps play protective or carrier roles, increasing the bioavailability of the hormone and illustrate an important alternative mechanism of regulating IGF bioavailability. It would be important to identify whether the anti-IGF-1 peptides that contributed to the results seen in Chapter 5 have any mitogenic effects on cell in the absence of IGF-1, as has been observed in peptide agonists of the IGF-1 receptor (Beasley *et al.*, 2000) and indirectly as described above. If so, their IGF-1 independent effects would require further investigation to elucidate their exact mode of action. If not, it would suggest they are acting as a chaperone or cofactor, enhancing the IGF-1 mediated effects observed.

7.2 Conclusions

The initial work in this thesis sought to address the issue of assaying proteolytically or otherwise degraded specimens. Many such problems may be addressed by anti-peptide antibodies in conjunction with controlled proteolytic digestion of the samples prior to affinity assay. Such an approach was shown for the first time to be capable of quantitative detection of 33 protein targets in proteolytically treated serum, thus addressing the problems associated with sample degradation.

The microarray technology used to perform these assays proved compatible with the affinity peptidomics approach and adept at multiplexed detection. However, microarray based assays involve multiple complex steps and lengthy data processing and therefore lateral flow tests were explored as a simpler alternative.

Successful lateral flow tests were devised for the qualitative detection of the benzodiazepine diazepam, and while the setup utilised permitted just a single analyte to be tested per device, potential ways to multiplex these tests have been proposed in this discussion.

Spectral multiplexing has been explored. Accurate quantitative deconvolution of individual emission spectra from mixtures of up to 6 QDs was achieved demonstrating the potential for quantitative spectral multiplexing using these novel labelling reagents.

To this end the assays were used for assessing binding of antibodies (large molecular weight affinity reagents) to small peptides (from proteolytically digested targets). The next embodiment of the assay was used for testing low molecular weight affinity reagents (peptides) to large molecular weight targets (intact proteins). To develop peptide affinity reagents a recombinant approach utilising phage display rather than traditional poly/monoclonal antibody generation, produced peptide-based affinity reagents against IGF-1. These peptide affinity reagents demonstrated comparable dissociation rates to traditional antibodies, but also had the unexpected effect of increasing cell growth rates *in vitro*.

7.3 Future research directions

The present study has evaluated the feasibility of new affinity reagents and suitable technologies for application to multiplexed affinity assays geared towards quantitatively analysing a range of analytes. Methods developed in this thesis provide a basis from which further experimentation can be performed to integrate the methods, technologies and reagents into a platform capable of fulfilling the aims of this project, namely, to develop an assay system capable of quantitatively analysing a range of analytes, from “traditional” small molecule drugs, to peptide and protein markers the presence of which above or below certain thresholds, in isolation or combination, can provide crucial information to the user.

More recently, the range of QD reagents available has dramatically increased, led partly by the need for less toxic probes in cellular and *in vivo* studies (Zhu *et al.*, 2019). While toxicity is less of a concern in immunoassays, these emerging materials increase the chances of finding suitably compatible probes that are also more amenable to biomolecule conjugation. If spectral multiplexing on membranes can be achieved with emission deconvolution as this study proved possible in solution, then QD-based lateral flow strips with multiplexed capture lines would be a logical progression. Alternatively, spatial separation of probes via arrayed grids as described in this discussion provides another route for multiplexing lateral flow tests.

With regards to the anti-IGF-1 peptides, further testing is required to understand their binding specificity and mode of action in relation to their effect on cell growth rates. While not the focus of this study, their impact on the IGF-1 pathway means they have the potential to be useful peptide therapeutics.

Coupling phage-derived peptide affinity reagents to QDs should also be explored, as should the potential to produce anti-peptide peptide affinity reagents that could be applied to a peptidomics approach and truly combine the power and ease of recombinant affinity reagents with the robustness of the peptidomics approach explored at the start of this study which removes issues surrounding sample preservation.

7.4 Final Remarks

Throughout this study experiments and methods have been undertaken to establish a suitably robust method that is capable of quantitatively detecting multiple analytes of interest in a single, easy-to-use test kit. Some results of this study have already been published (Bailes & Soloviev, 2007, 2012; Soloviev *et al.*, 2007; Bailes *et al.*, 2009, 2012b, a,c; Ferrari *et al.*, 2010; Zhang *et al.*, 2010). While it is evident that more work needs to be conducted before this can ultimately be realised, progress has been made in the design and generation of novel affinity reagents, peptidomics, assays development, and multiplex capabilities of emerging labelling tools. Events in recent years, not least the ongoing investigations into claims of widespread state-sponsored doping schemes in sport and the COVID-19 pandemic of 2020 highlight the ever-growing requirement and importance and the impact of such tests across multiple frontiers.

References:

Abdel-Salam, M., Omran, B., Whitehead, K. & Baek, K.H. (2020) Superior properties and biomedical applications of microorganism-derived fluorescent quantum dots. *Molecules*, **25**, 4486.

Abdiche, Y., Malashock, D., Pinkerton, A. & Pons, J. (2008) Determining kinetics and affinities of protein interactions using a parallel real-time label-free biosensor, the Octet. *Analytical Biochemistry*, **377**, 209–217.

Abellan, R., Ventura, R., Pichini, S., Pascual, J.A., Pacifici, R., di Carlo, S., Bacosi, A., Seguar, J. & Zuccaro, P. (2005) Evaluation of immunoassays for the measurement of insulin-like growth factor-I and procollagen type III peptide, indirect biomarkers of recombinant human growth hormone misuse in sport. *Clinical Chemistry and Laboratory Medicine*, **43**, 75–85.

Afzaal, M. & O'Brien, P. (2006) Recent developments in II-VI and III-VI semiconductors and their applications in solar cells. *Journal of Materials Chemistry*, **16**, 1597–1602.

Agyei, D., Tsopmo, A. & Udenigwe, C.C. (2018) Bioinformatics and peptidomics approaches to the discovery and analysis of food-derived bioactive peptides. *Analytical and Bioanalytical Chemistry*, **410**, 3463–3472.

Ahlstedt, S., Kristoffersson, A., Pettersson, E. & Svärd, P.O. (1976) The Binding Properties of Rabbit Antibodies against Various Penicillins as Studied by Immunoprecipitation, Indirect Haemagglutination and Radiometric Immunoassay. *International Archives of Allergy and Immunology*, **51**, 145–155.

Akinfieva, O., Nabiev, I. & Sukhanova, A. (2013) New directions in quantum dot-based cytometry detection of cancer serum markers and tumor cells. *Critical Reviews in Oncology/Hematology*, **86**, 1–14.

Alexander, T.S. (2016) Human Immunodeficiency Virus Diagnostic Testing: 30 Years of Evolution. *Clinical and Vaccine Immunology*, **23**, 249–253.

Al-Harithy, R.N. (2004) Relationship of leptin concentration to gender, body mass index and age in Saudi adults. *Saudi Medical Journal*, **25**, 1086–1090.

Allen, N.E., Appleby, P.N., Davey, G.K. & Key, T.J. (2002) Lifestyle and nutritional determinants of bioavailable androgens and related hormones in British men. *Cancer Causes and Control*, **13**, 353–363.

Aluru, M., Zola, J., Nettleton, D. & Aluru, S. (2013) Reverse engineering and analysis of large genome-scale gene networks. *Nucleic Acids Research*, **41**, e24–e24.

van Amerongen, A., Wichers, J.H., Berendsen, L.B.J.M., Timmermans, A.J.M., Keizer, G.D., van Doorn, A.W.J., Bantjes, A. & van Gelder, W.M.J. (1993) Colloidal carbon particles as a new label for rapid immunochemical test methods: Quantitative computer image analysis of results. *Journal of Biotechnology*, **30**, 185–195.

Andryukov, B.G. (2020) Six decades of lateral flow immunoassay: From determining metabolic markers to diagnosing covid-19. *AIMS Microbiology*, **6**, 280–304.

Ang, S.H., Rambeli, M., Thevarajah, T.M., Alias, Y.B. & Khor, S.M. (2016) Quantitative, single-step dual measurement of hemoglobin A1c and total hemoglobin in human whole blood using a gold sandwich immunochromatographic assay for personalized medicine. *Biosensors and Bioelectronics*, **78**, 187–193.

Aris, V.M., Cody, M.J., Cheng, J., Dermody, J.J., Soteropoulus, P., Recce, M. & Tolias, P.P. (2004) Noise filtering and nonparametric analysis of microarray data underscores discriminating markers of oral, prostate, lung, ovarian and breast cancer. *BMC Bioinformatics*, **5**.

Armakolas, A., Philippou, A., Panteleakou, Z., Nezos, A., Sourla, A., Petraki, C. & Koutsilieris, M. (2010) Preferential expression of IGF-1Ec (MGF) transcript in cancerous tissues of human prostate: Evidence for a novel and autonomous growth factor activity of MGF E peptide in human prostate cancer cells. *The Prostate*, **70**, 1233–1242.

Ashare, A., Nymon, A.B., Doerschug, K.C., Morrison, J.M., Monick, M.M. & Hunninghake, G.W. (2008) Insulin-like growth factor-1 improves survival in sepsis via enhanced hepatic bacterial clearance. *American Journal of Respiratory and Critical Care Medicine*, **178**, 149–157.

Attili, B.S. & Suleiman, A.A. (1996) A piezoelectric immunosensor for the detection of cocaine. *Microchemical Journal*, **54**, 174–179.

Atzori, F., Traina, T.A., Ionta, M.T. & Massidda, B. (2009) Targeting insulin-like growth factor type 1 receptor in cancer therapy. *Targeted Oncology*, **4**, 255–266.

Autotest VIH - autotest-vih.eu/en/.

Babu, L.T. & Paira, P. (2017) Current Application of Quantum Dots (QD) in Cancer Therapy: A Review. *Mini-Reviews in Medicinal Chemistry*, **17**.

Bachelet, M., Pinot, F., Polla, R.I., Franois, D., Richard, M.J., Vayssier-Taussat, M. & Polla, B.S. (2002) Toxicity of cadmium in tobacco smoke: Protection by antioxidants and chelating resins. *Free Radical Research*, **36**, 99–106.

Bailes, J., Gazi, S., Ivanova, R. & Soloviev, M. (2012a) Effect of gold nanoparticle conjugation on the activity and stability of functional proteins. *Methods in Molecular Biology*, **906**, 89–99.

Bailes, J., Mayoss, S., Teale, P. & Soloviev, M. (2012b) Gold nanoparticle antibody conjugates for use in competitive lateral flow assays. *Methods in Molecular Biology*, **906**, 45–55.

Bailes, J., Milnthorpe, A., Smieszek, S. & Soloviev, M. (2012c) Rapley c09.tex Chip-Based Proteomics.

Bailes, J. & Soloviev, M. (2007) Affinity Peptidomics Approach to Protein Detection, Quantification, and Protein Affinity Assays: Application to Forensics and Biometrics. *Peptidomics: Methods and Applications*, 191–231.

Bailes, J. & Soloviev, M. (2012) The application of semiconductor quantum dots for enhancing peptide desorption, improving peak resolution and sensitivity of detection in matrix-assisted laser desorption/ionization (MALDI) mass spectrometry. *Methods in Molecular Biology*, **906**, 211–217.

Bailes, J., Vidal, L., Ivanov, D.A. & Soloviev, M. (2009) Quantum dots improve peptide detection in MALDI MS in a size dependent manner. *Journal of Nanobiotechnology*, **7**, 10.

Ballard, F.J., Wallace, J.C., Francis, G.L., Read, L.C. & Tomas, F.M. (1996) Des(1-3)IGF-I: A truncated form of insulin-like growth Factor-I. *International Journal of Biochemistry and Cell Biology*, **28**, 1085–1087.

Ballou, S.P. & Kushner, I. (1992) C-reactive protein and the acute phase response. *Advances in internal medicine*, **37**, 313–336.

Banerjee, R. & Jaiswal, A. (2018) Recent advances in nanoparticle-based lateral flow immunoassay as a point-of-care diagnostic tool for infectious agents and diseases. *Analyst*, **143**, 1970–1996.

Banta, S., Dooley, K. & Shur, O. (2013) Replacing antibodies: Engineering new binding proteins. *Annual Review of Biomedical Engineering*, **15**, 93–113.

Barry, R., Diggle, T., Terrett, J. & Soloviev, M. (2003) Competitive assay formats for high-throughput affinity arrays. *Journal of Biomolecular Screening*, **8**, 257–263.

Bartosh, A. v., Sotnikov, D. v., Hendrickson, O.D., Zherdev, A. v. & Dzantiev, B.B. (2020) Design of Multiplex Lateral Flow Tests: A Case Study for Simultaneous Detection of Three Antibiotics. *Biosensors*, **10**, 17.

Baserga, R. (1999) The IGF-I receptor in cancer research. *Experimental Cell Research*, **253**, 1–6.

le Basle, Y., Chennell, P., Tokhadze, N., Astier, A. & Sautou, V. (2020) Physicochemical Stability of Monoclonal Antibodies: A Review. *Journal of Pharmaceutical Sciences*, **109**, 169–190.

Bauer, M. & Patzelt, D. (2002) Evaluation of Mrna Markers for the Identification of Menstrual Blood. *Journal of Forensic Sciences*, **47**, 15560J.

Baum, R.P., Prasad, V., Müller, D., Schuchardt, C., Orlova, A., Wennborg, A., Tolmachev, V. & Feldwisch, J. (2010) Molecular imaging of HER2-expressing malignant tumors in breast cancer patients using synthetic 111In- or 68Ga-labeled Affibody molecules. *Journal of Nuclear Medicine*, **51**, 892–897.

Baumann, H. & Gauldie, J. (1994) The acute phase response. *Immunology Today*, **15**, 74–80.

Baxter, R.C. (1988) Characterization of the Acid-Labile Subunit of the Growth Hormone-Dependent Insulin-Like Growth Factor Binding Protein Complex. *Journal of Clinical Endocrinology and Metabolism*, **67**, 265–272.

Baxter, R.C. & Martin, J.L. (1986) Radioimmunoassay of growth hormone-dependent insulinlike growth factor binding protein in human plasma. *Journal of Clinical Investigation*, **78**, 1504–1512.

Bayley, H. (2006) Sequencing single molecules of DNA. *Current Opinion in Chemical Biology*, **10**, 628–637.

Beasley, J., Blume, A.J., SCHÄFFER, L., Pillutla, R., Brandt, J., Brissette, R., Spetzler, J., Cheng, W., Østergaard, S., Mandecki, W.S., Hansen, P.H., Ravera, M. & Hsiao, K.-C. (2000) Insulin and igf-1 receptor agonists and antagonists.

Belkina, A., Pihl, R. & Snyder-Cappione, J. (2017) *Evaluation of "Super Bright" Polymer Dyes in 13-16-color Human Immunophenotyping Panels*,.

Beltrand, J., Verkauskiene, R., Nicolescu, R., Sibony, O., Gaucherand, P., Chevenne, D., Claris, O. & Lévy-Marchal, C. (2008) Adaptive changes in neonatal hormonal and metabolic profiles induced by fetal growth restriction. *Journal of Clinical Endocrinology and Metabolism*, **93**, 4027–4032.

Berg, A.H., Combs, T.P., Du, X., Brownlee, M. & Scherer, P.E. (2001) The adipocyte-secreted protein Acrp30 enhances hepatic insulin action. *Nature Medicine*, **7**, 947–953.

Berlier, J.E., Rothe, A., Buller, G., Bradford, J., Gray, D.R., Filanoski, B.J., Telford, W.G., Yue, S., Liu, J., Cheung, C.Y., Chang, W., Hirsch, J.D., Beechem, J.M., Haugland, R.P. & Haugland, R.P. (2003) Quantitative Comparison of Long-wavelength Alexa Fluor Dyes to Cy Dyes: Fluorescence of the Dyes and Their Bioconjugates. *Journal of Histochemistry and Cytochemistry*, **51**, 1699–1712.

Bertelloni, S., Baroncelli, G.I., Dati, E., Ghione, S., Baldinotti, F., Toschi, B. & Simi, P. (2013) IGF-I generation test in prepubertal children with noonan syndrome due to mutations in the PTPN11 gene. *Hormones*, **12**, 86–92.

Betz, P., Nerlich, A., Wilske, J., Tübel, J., Wiest, I., Penning, R. & Eisenmenger, W. (1992) The time-dependent rearrangement of the epithelial basement membrane in human skin wounds -immunohistochemical localization of Collagen IV and VII. *International Journal Of Legal Medicine*, **105**, 93–97.

Bhalla, S., Verma, R., Kaur, H., Kumar, R., Usmani, S.S., Sharma, S. & Raghava, G.P.S. (2017) CancerPDF: A repository of cancer-associated peptidome found in human biofluids. *Scientific Reports*, **7**.

Bhasin, M., Singh, H. & Raghava, G.P.S. (2003) MHCBN: A comprehensive database of MHC binding and non-binding peptides. *Bioinformatics*, **19**, 665–666.

Bidlingmaier, M. & Freda, P.U. (2010) Measurement of human growth hormone by immunoassays: Current status, unsolved problems and clinical consequences. *Growth Hormone and IGF Research*, **20**, 19–25.

BioMedomics Inc. - biomedomics.com.

BioSure UK - biosure.co.uk.

Boersma, Y.L. & Plückthun, A. (2011) DARPins and other repeat protein scaffolds: Advances in engineering and applications. *Current Opinion in Biotechnology*, **22**, 849–857.

Brabant, G. & Wallaschofski, H. (2007) Normal levels of serum IGF-I: Determinants and validity of current reference ranges. *Pituitary*, **10**, 129–133.

Brea, A., Mosquera, D., Martín, E., Arizti, A., Cordero, J.L. & Ros, E. (2005) Nonalcoholic fatty liver disease is associated with carotid atherosclerosis: A case-control study. *Arteriosclerosis, Thrombosis, and Vascular Biology*, **25**, 1045–1050.

Brown, A.A. & Hu, F.B. (2001) Dietary modulation of endothelial function: Implications for cardiovascular disease. *American Journal of Clinical Nutrition*, **73**, 673–686.

Brus, L. (1991) Quantum crystallites and nonlinear optics. *Applied Physics A Solids and Surfaces*, **53**, 465–474.

Burkhalter, K.L., Horiuchi, K., Biggerstaff, B.J., Savage, H.M. & Nasci, R.S. (2014) Evaluation of a rapid analyte measurement platform and real-time reverse-transcriptase polymerase chain reaction assay west nile virus detection system in mosquito pools. *Journal of the American Mosquito Control Association*, **30**, 21–30.

Burniston, J.G., Chester, N., Clark, W.A., Tan, L.-B. & Goldspink, D.F. (2005) Dose-dependent apoptotic and necrotic myocyte death induced by the β2-adrenergic receptor agonist, clenbuterol. *Muscle & Nerve*, **32**, 767–774.

Burns, C., Rigsby, P., Moore, M. & Rafferty, B. (2009) The First International Standard for Insulin-like Growth Factor-1 (IGF-1) for immunoassay: Preparation and calibration in an international collaborative study. *Growth Hormone and IGF Research*, **19**, 457–462.

Cai, W., Shin, D.W., Chen, K., Gheysens, O., Cao, Q., Wang, S.X., Gambhir, S.S. & Chen, X. (2006) Peptide-labeled near-infrared quantum dots for imaging tumor vasculature in living subjects. *Nano Letters*, **6**, 669–676.

Cappa, Fintini, D., Brufani, C. & Cappa, M. (2009) Profile of mecasermin for the long-term treatment of growth failure in children and adolescents with severe primary IGF-1 deficiency. *Therapeutics and Clinical Risk Management*, **5**, 553–559.

Carpenter, V., Matthews, K., Devlin, G., Stuart, S., Jensen, J., Conaglen, J., Jeanplong, F., Goldspink, P., Yang, S.Y., Goldspink, G., Bass, J. & McMahon, C. (2008) Mechano-Growth Factor Reduces Loss of Cardiac Function in Acute Myocardial Infarction. *Heart Lung and Circulation*, **17**, 33–39.

Carrillo-Carrión, C., Cárdenas, S., Simonet, B.M. & Valcárcel, M. (2009) Quantum dots luminescence enhancement due to illumination with UV/Vis light. *Chemical Communications*, 5214–5226.

Carrio, A., Sampedro, C., Sanchez-Lopez, J.L., Pimienta, M. & Campoy, P. (2015) Automated low-cost smartphone-based lateral flow saliva test reader for drugs-of-abuse detection. *Sensors (Switzerland)*, **15**, 29569–29593.

Catto, J.W.F., Abbod, M.F., Wild, P.J., Linkens, D.A., Pilarsky, C., Rehman, I., Rosario, D.J., Denzinger, S., Burger, M., Stoehr, R., Knuechel, R., Hartmann, A. & Hamdy, F.C. (2010) The Application of Artificial Intelligence to Microarray Data: Identification of a Novel Gene Signature to Identify Bladder Cancer Progression. *European Urology*, **57**, 398–406.

Chan, J.M., Stampfer, M.J., Giovannucci, E., Gann, P.H., Ma, J., Wilkinson, P., Hennekens, C.H. & Pollak, M. (1998) Plasma insulin-like growth factor-I and prostate cancer risk: A prospective study. *Science*, **279**, 563–566.

Chan, W.C.W. & Nie, S. (1998) Quantum dot bioconjugates for ultrasensitive nonisotopic detection. *Science*, **281**, 2016–2018.

Chang, S., Wu, X., Lan, J., Li, Z., Zhang, X. & Zhang, H. (2019) γ-radiation enhanced luminescence of Thiol-capped quantum dots in aqueous solution. *Nanomaterials*, **9**, 506.

Chehab, F.F., Lim, M.E. & Lu, R. (1996) Correction of the sterility defect in homozygous obese female mice by treatment with the human recombinant leptin. *Nature Genetics*, **12**, 318–320.

Chen, B., Sun, Y., Niu, J., Jarugumilli, G.K. & Wu, X. (2018) Protein Lipidation in Cell Signaling and Diseases: Function, Regulation, and Therapeutic Opportunities. *Cell Chemical Biology*, **25**, 817–831.

Chen, C., Lewis, S.K., Voigt, L., Fitzpatrick, A., Plymate, S.R. & Weiss, N.S. (2005) Prostate carcinoma incidence in relation to prediagnostic circulating levels of insulin-like growth factor I, insulin-like growth factor binding protein 3, and insulin. *Cancer*, **103**, 76–84.

Chen, I.W., David, R., Maxon, H.R., Sperling, M. & Stein, E.A. (1980) Age-, sex-, and race-related differences in myoglobin concentrations in the serum of healthy persons. *Clinical Chemistry*, **26**, 1864–1868.

Cheng, N., Yang, Z., Wang, W., Wang, X., Xu, W. & Luo, Y. (2019) A Variety of Bio-nanogold in the Fabrication of Lateral Flow Biosensors for the Detection of Pathogenic Bacteria. *Current Topics in Medicinal Chemistry*, **19**, 2476–2493.

Chiellini, C., Santini, F., Marsili, A., Berti, P., Bertacca, A., Pelosini, C., Scartabelli, G., Pardini, E., López-Soriano, J., Centoni, R., Ciccarone, A.M., Benzi, L., Vitti, P., del Prato, S., Pinchera, A., Maffei, M., López-Soriano, J., Centoni, R., Ciccarone, A.M.,

Benzi, L., Vitti, P., del Prato, S., Pinchera, A. & Maffei, M. (2004) Serum haptoglobin: A novel marker of adiposity in humans. *Journal of Clinical Endocrinology and Metabolism*, **89**, 2678–2683.

Chockalingam, S., Aluru, M. & Aluru, S. (2016) Microarray Data Processing Techniques for Genome-Scale Network Inference from Large Public Repositories. *Microarrays*, **5**, 23.

Choe, M., Webber, K.O. & Pastan, I. (1994) B3(Fab)-PE38M: A Recombinant Immunotoxin in Which a Mutant Form of Pseudomonas Exotoxin Is Fused to the Fab Fragment of Monoclonal Antibody B3. *Cancer Research*, **54**.

Choi, D.H., Lee, S.K., Oh, Y.K., Bae, B.W., Lee, S.D., Kim, S., Shin, Y.B. & Kim, M.G. (2010) A dual gold nanoparticle conjugate-based lateral flow assay (LFA) method for the analysis of troponin I. *Biosensors and Bioelectronics*, **25**, 1999–2002.

Christine P. Burren, Wilson, E.M., Hwa, V., Oh, Y. & Rosenfeld, R.G. (1999) Binding Properties and Distribution of Insulin-Like Growth Factor Binding Protein-Related Protein 3 (IGFBP-rP3/NovH), an Additional Member of the IGFBP Superfamily [1]. *The Journal of Clinical Endocrinology & Metabolism*, **84**, 1096–1103.

Clark, R.A.F., DellaPelle, P., Manseau, E., Lanigan, J.M., Dvorak, H.F. & Colvin, R.B. (1982) Blood vessel fibronectin increases in conjunction with endothelial cell proliferation and capillary ingrowth during wound healing. *Journal of Investigative Dermatology*, **79**, 269–276.

Clearblue - clearblue.com.

Clemmons, D.R. (2011) Consensus statement on the standardization and evaluation of growth hormone and insulin-like growth factor assays. *Clinical Chemistry*, **57**, 555–559.

Clemmons, D.R. (2007) IGF-I assays: Current assay methodologies and their limitations. *Pituitary*, **10**, 121–128.

Clemmons, D.R. (2018) Role of igf-binding proteins in regulating igf responses to changes in metabolism. *Journal of Molecular Endocrinology*, **61**, T139–T169.

Cohen, J., Blethen, S., Kuntze, J., Smith, S.L., Lomax, K.G. & Mathew, P.M. (2014) Managing the child with severe primary insulin-like growth factor-1 deficiency (IGFD): IGFD diagnosis and management. *Drugs in R and D*, **14**, 25–29.

Colas, P., Cohen, B., Jessen, T., Grishina, I., McCoy, J. & Brent, R. (1996) Genetic selection of peptide aptamers that recognize and inhibit cyclin-dependent kinase 2. *Nature*, **380**, 548–550.

Cole, L.A. (2011) The utility of six over-the-counter (home) pregnancy tests. *Clinical Chemistry and Laboratory Medicine*, **49**, 1317–1322.

Conlon, J.M., Mechkarska, M. & Leprince, J. (2019) Peptidomic analysis in the discovery of therapeutically valuable peptides in amphibian skin secretions. *Expert Review of Proteomics*, **16**, 897–908.

Cooper, M.A., Dultsev, F.N., Minson, T., Ostanin, V.P., Abell, C. & Klenerman, D. (2001) Direct and sensitive detection of a human virus by rupture event scanning. *Nature Biotechnology*, **19**, 833–837.

Corstjens, P., Zuiderwijk, M., Brink, A., Li, S., Feindt, H., Niedbala, R.S. & Tanke, H. (2001) *Use of up-converting phosphor reporters in lateral-flow assays to detect specific nucleic acid sequences: A rapid, sensitive DNA test to identify human papillomavirus type 16 infection*. *Clinical Chemistry*, pp. 1885–1893. American Association for Clinical Chemistry Inc.

Costa, S., Sastre, P., Pérez, T., Tapia, I., Barrandeguy, M., Sánchez-Vizcaíno, J.M., Sánchez-Matamoros, A., Wigdorovitz, A., Sanz, A. & Rueda, P. (2016) Development and evaluation of a new lateral flow assay for simultaneous detection of antibodies against African Horse Sickness and Equine Infectious Anemia viruses. *Journal of Virological Methods*, **237**, 127–131.

Cox, K.L., Devanarayan, V., Kriauciunas, A., Manetta, J., Montrose, C. & Sittampalam, S. (2004) *Immunoassay Methods*, Eli Lilly & Company and the National Center for Advancing Translational Sciences.

van Craenenbroeck, E. & Engelborghs, Y. (2000) Fluorescence correlation spectroscopy: Molecular recognition at the single molecule level. *Journal of Molecular Recognition*, **13**, 93–100.

Craven, C., Fileger, M. & Woster, P. (2014) Demystifying Benzodiazepine Urine Drug Screen Results. *Practical Pain Management*, **14**, 3–9.

Cubbon, R.M., Kearney, M.T. & Wheatcroft, S.B. (2016) Endothelial IGF-1 Receptor Signalling in Diabetes and Insulin Resistance. *Trends in Endocrinology and Metabolism*, **27**, 96–104.

Cui, S., Wu, Q., West, J. & Bai, J. (2019) Machine learning-based microarray analyses indicate low-expression genes might collectively influence PAH disease. *PLoS Computational Biology*, **15**, e1007264.

Custom Rabbit Polyclonal Antibody Production Protocols | Thermo Fisher Scientific - thermofisher.com.

Daban, J.R., Bartolomé, S. & Samsó, M. (1991) Use of the hydrophobic probe Nile red for the fluorescent staining of protein bands in sodium dodecyl sulfate-polyacrylamide gels. *Analytical Biochemistry*, **199**, 169–174.

Dall, R., Longobardi, S., Ehrnborg, C., Keay, N., Rosén, T., Jørgensen, J.O.L.L., Cuneo, R.C., Boroujerdi, M.A., Cittadini, A., Napoli, R., Christiansen, J.S., Bengtsson, B.A., Sacca, L., Baxter, R.C., Basset, E.E. & Sönksen, P.H. (2000) The effect of four

weeks of supraphysiological growth hormone administration on the insulin-like growth factor axis women and men. *Journal of Clinical Endocrinology and Metabolism*, **85**, 4193–4200.

Darwish, I.A. (2006) Immunoassay Methods and their Applications in Pharmaceutical Analysis: Basic Methodology and Recent Advances. *International journal of biomedical science : IJBS*, **2**, 217–35.

Davey Smith, G., Greenwood, R., Gunnell, D., Sweetnam, P., Yarnell, J. & Elwood, P. (2001) Leg length, insulin resistance, and coronary heart disease risk: The Caerphilly study. *Journal of Epidemiology and Community Health*, **55**, 867–872.

Deshayes, K., Schaffer, M.L., Skelton, N.J., Nakamura, G.R., Kadkhodayan, S. & Sidhu, S.S. (2002) Rapid identification of small binding motifs with high-throughput phage display: Discovery of peptidic antagonists of IGF-1 function. *Chemistry and Biology*, **9**, 495–505.

Detekt Biomedical – idetekt.com.

DiaMondial - diamondial.com.

Dik, M.G., Pluijm, S.M.F., Jonker, C., Deeg, D.J.H., Lomecky, M.Z. & Lips, P. (2003) Insulin-like growth factor I (IGF-I) and cognitive decline in older persons. *Neurobiology of Aging*, **24**, 573–581.

Dillon, P.P., Manning, B.M., Daly, S.J., Killard, A.J. & O'Kennedy, R. (2003) Production of a recombinant anti-morphine-3-glucuronide single-chain variable fragment (scFv) antibody for the development of a "real-time" biosensor-based immunoassay. *Journal of Immunological Methods*, **276**, 151–161.

Dłużniewska, J., Sarnowska, A., Beręsewicz, M., Johnson, I., Srai, S.K.S., Ramesh, B., Goldspink, G., Górecki, D.C. & Zabłocka, B. (2005) A strong neuroprotective effect of the autonomous C-terminal peptide of IGF-1 Ec (MGF) in brain ischemia. *The FASEB Journal*, **19**, 1896–1898.

Drafts, B. (2001) Acoustic wave technology sensors. *IEEE Transactions on Microwave Theory and Techniques*, **49**, 795–802.

Dressler, J., Bachmann, L., Strejc, P., Koch, R. & Müller, E. (2000) Expression of adhesion molecules in skin wounds: Diagnostic value in legal medicine. *Forensic Science International*, **113**, 173–176.

Drygin, Y.F., Blintsov, A.N., Osipov, A.P., Grigorenko, V.G., Andreeva, I.P., Uskov, A.I., Varitsev, Y.A., Anisimov, B. v., Novikov, V.K. & Atabekov, J.G. (2009) High-sensitivity express immunochromatographic method for detection of plant infection by tobacco mosaic virus. *Biochemistry (Moscow)*, **74**, 986–993.

Du, J., Harding, G.L., Ogilvy, J.A., Dencher, P.R. & Lake, M. (1996) A study of Love-wave acoustic sensors. *Sensors and Actuators, A: Physical*, **56**, 211–219.

Durai, R., Yang, S.Y., Seifalian, A.M., Goldspink, G. & Winslet, M.C. (2007) Role of insulin-like growth factor binding protein-4 in prevention of colon cancer. *World Journal of Surgical Oncology*, **5**, 1–8.

E25Bio - e25bio.com.

Edouard, T., Grünenwald, S., Gennero, I., Salles, J.P. & Trauber, M. (2009) Prevalence of IGF1 deficiency in prepubertal children with isolated short stature. *European Journal of Endocrinology*, **161**, 43–50.

Ehmen, C., Medialdea-Carrera, R., Brown, D., de Filippis, A.M.B., de Sequeira, P.C., Nogueira, R.M.R., Brasil, P., Calvet, G.A., Blessmann, J., Mallmann, A., Sievertsen, J., Rackow, A., Schmidt-Chanasit, J., Emmerich, P., Schmitz, H., Deschermeier, C. & Mika, A. (2020) Accurate detection of Zika virus IgG using a novel immune complex binding ELISA. *Tropical Medicine & International Health*.

El-Manzalawy, Y., Dobbs, D. & Honavar, V. (2008) Predicting linear B-cell epitopes using string kernels. *Journal of Molecular Recognition*, **21**, 243–255.

Elmlinger, M.W., Zwirner, M. & Kühnel, W. (2005) Stability of insulin-like growth factor (IGF)-I and IGF binding protein (IGFBP)-3 measured by the IMMULITE® automated chemiluminescence assay system in different blood specimens. *Clinical Laboratory*, **51**, 145–152.

Emanuel, S.L., Engle, L.J., Chao, G., Zhu, R.R., Cao, C., Lin, Z., Yamniuk, A., Hosbach, J., Brown, J., Fitzpatrick, E., Gokemeijer, J., Morin, P., Morse, B., Carvajal, I.M., Fabrizio, D., Wright, M.C., das Gupta, R., Gosselin, M., Cataldo, D., Ryseck, R.P., Doyle, M.L., Wong, T.W., Camphausen, R.T., Cload, S.T., Marsh, H.N., Gottardis, M.M. & Furfine, E.S. (2011) A fibronectin scaffold approach to bispecific inhibitors of epidermal growth factor receptor and insulin-like growth factor-I receptor. *mAbs*, **3**, 38–48.

EP1320754B1 - Detection of peptides - Google Patents.

Ernst, S. & Simon, P. (2013) A quantitative approach for assessing significant improvements in elite sprint performance: Has IGF-1 entered the arena? *Drug Testing and Analysis*, **5**, 384–389.

Erotokritou-Mulligan, I., Bassett, E.E., Bartlett, C., Cowan, D., McHugh, C., Seah, R., Curtis, B., Wells, V., Harrison, K., Sönksen, P.H., Holt, R.I.G.G., Sönksen, P.H. & Holt, R.I.G.G. (2008) The effect of sports injury on insulin-like growth factor-I and type 3 procollagen: Implications for detection of growth hormone abuse in athletes. *Journal of Clinical Endocrinology and Metabolism*, **93**, 2760–2763.

Erotokritou-Mulligan, I., Bassett, E.E., Cowan, D.A., Bartlett, C., McHugh, C., Sönksen, P.H. & Holt, R.I.G. (2009) Influence of ethnicity on IGF-I and procollagen III peptide (P-III-P) in elite athletes and its effect on the ability to detect GH abuse. *Clinical Endocrinology*, **70**, 161–168.

Erotokritou-Mulligan, I., Guha, N., Stow, M., Bassett, E.E., Bartlett, C., Cowan, D.A., Sönksen, P.H. & Holt, R.I.G. (2012) The development of decision limits for the implementation of the GH-2000 detection methodology using current commercial insulin-like growth factor-I and amino-terminal pro-peptide of type III collagen assays. *Growth Hormone and IGF Research*, **22**, 53–58.

Evans, M.J., Livesey, J.H., Ellis, M.J. & Yandle, T.G. (2001) Effect of anticoagulants and storage temperatures on stability of plasma and serum hormones. *Clinical Biochemistry*, **34**, 107–112.

Expasy PeptideMass - web.expasy.org/peptide_mass/.

Exton, M.S., Krüger, T.H.C., Koch, M., Paulson, E., Knapp, W., Hartmann, U. & Schedlowski, M. (2001) Coitus-induced orgasm stimulates prolactin secretion in healthy subjects. *Psychoneuroendocrinology*, **26**, 287–294.

Fan, J., Cheng, Y. & Sun, M. (2020) Functionalized Gold Nanoparticles: Synthesis, Properties and Biomedical Applications. *Chemical Record*.

Favretto, D., Visentin, S., Stocchero, G., Vogliardi, S., Snenghi, R. & Montisci, M. (2018) Driving under the influence of drugs: Prevalence in road traffic accidents in Italy and considerations on per se limits legislation. *Traffic Injury Prevention*, **19**, 786–793.

Feng, H. & Qian, Z. (2018) Functional Carbon Quantum Dots: A Versatile Platform for Chemosensing and Biosensing. *The Chemical Record*, **18**, 491–505.

Feng, J., Wang, L., Dai, I., Harmon, T. & Bernert, J.T. (2007) Simultaneous determination of multiple drugs of abuse and relevant metabolites in urine by LC-MS-MS. *Journal of Analytical Toxicology*, **31**, 359–368.

Ferrari, E., Darios, F., Zhang, F., Niranjan, D., Bailes, J., Soloviev, M. & Davletov, B. (2010) Binary polypeptide system for permanent and oriented protein immobilization. *Journal of Nanobiotechnology*, **8**.

Ferrari, E. & Soloviev, M. (2020) *Nanoparticles in Biology and Medicine*, (ed. by E. Ferrari) and M. Soloviev) Springer US, New York, NY.

Fessel, J.P., Chen, X., Frump, A., Gladson, S., Blackwell, T., Kang, C., Johnson, J., Loyd, J.E., Hemnes, A., Austin, E. & West, J. (2013) Interaction between bone morphogenetic protein receptor type 2 and estrogenic compounds in pulmonary arterial hypertension. *Pulmonary Circulation*, **3**, 564–577.

Fettig, L.M. & Yee, D. (2020) *Advances in insulin-like growth factor biology and -directed cancer therapeutics*. *Advances in Cancer Research*, pp. 229–257. Academic Press Inc.

Fieguth, A., Feldbrügge, H., Gerich, T., Kleemann, W.J. & Tröger, H.D. (2003a) The time-dependent expression of fibronectin, MRP8, MRP14 and defensin in surgically treated human skin wounds. *Forensic Science International*, **131**, 156–161.

Fieguth, A., Franz, D., Lessig, R. & Kleemann, W.J. (2003b) Fatal trauma to the neck: Immunohistochemical study of local injuries. *Forensic Science International*, **135**, 218–225.

Fletcher, G., Mason, S., Terrett, J. & Soloviev, M. (2003) Self-assembly of proteins and their nucleic acids. *Journal of Nanobiotechnology*, **1**, 1–16.

Fletcher, L., Rider, C.C. & Taylor, C.B. (1976) Enolase isoenzymes. III. Chromatographic and immunological characteristics of rat brain enolase. *BBA - Enzymology*, **452**, 245–252.

Fliser, D., Wittke, S. & Mischak, H. (2005) Capillary electrophoresis coupled to mass spectrometry for clinical diagnostic purposes. *ELECTROPHORESIS*, **26**, 2708–2716.

Fodor, S.P., Rava, R.P., Huang, X.C., Pease, A.C., Holmes, C.P. & Adams, C.L. (1993) Multiplexed biochemical assays with biological chips. *Nature*, **364**, 555–556.

Földes-Papp, Z. (2007) "True" single-molecule molecule observations by fluorescence correlation spectroscopy and two-color fluorescence cross-correlation spectroscopy. *Experimental and Molecular Pathology*, **82**, 147–155.

Fredriksson, S., Gullberg, M., Jarvius, J., Olsson, C., Pietras, K., Gústafsdóttir, S.M., Östman, A. & Landegren, U. (2002) Protein detection using proximity-dependent DNA ligation assays. *Nature Biotechnology*, **20**, 473–477.

French, P.W., Penny, R., Laurence, J.A. & McKenzie, D.R. (2001) Mobile phones, heat shock proteins and cancer. *Differentiation*, **67**, 93–97.

Friedrich, N., Haring, R., Nauck, M., Lüdemann, J., Rosskopf, D., Spilcke-Liss, E., Felix, S.B., Dörr, M., Brabant, G., Völzke, H. & Wallaschofski, H. (2009) Mortality and serum insulin-like growth factor (IGF)-I and IGF binding protein 3 concentrations. *Journal of Clinical Endocrinology and Metabolism*, **94**, 1732–1739.

Froesch, E.R., Buergi, H., Ramseier, E.B., Bally, P. & Labhart, A. (1963) Antibody-suppressible And Nonsuppressible Insulin-like Activities In Human Serum And Their Physiologic Significance. An Insulin Assay With Adipose Tissue Of Increased Precision And Specificity. *The Journal of clinical investigation*, **42**, 1816–1834.

Frystyk, J., Freda, P. & Clemmons, D.R. (2010) The current status of IGF-I assays - A 2009 update. *Growth Hormone and IGF Research*, **20**, 8–18.

Fujita, M.Q., Zhu, B.L., Ishida, K., Quan, L., Oritani, S. & Maeda, H. (2002) Serum C-reactive protein levels in postmortem blood - An analysis with special reference to the cause of death and survival time. *Forensic Science International*, **130**, 160–166.

Fung, T.T., Rimm, E.B., Spiegelman, D., Rifai, N., Tofler, G.H., Willett, W.C. & Hu, F.B. (2001) Association between dietary patterns and plasma biomarkers of obesity and cardiovascular disease risk. *American Journal of Clinical Nutrition*, **73**, 61–67.

Garden, S.R. & Strachan, N.J.C. (2001) Novel colorimetric immunoassay for the detection of aflatoxin B1. *Analytica Chimica Acta*, **444**, 187–191.

Geißler, D. & Hildebrandt, N. (2016) Recent developments in Förster resonance energy transfer (FRET) diagnostics using quantum dots. *Analytical and Bioanalytical Chemistry*, **408**, 4475–4483.

Gera, N., Hussain, M. & Rao, B.M. (2013) Protein selection using yeast surface display. *Methods*, **60**, 15–26.

Gibriel, A.A.Y. (2012) Options available for labelling nucleic acid samples in dna microarray-based detection methods. *Briefings in Functional Genomics*, **11**, 311–318.

Gillespie, P.G. & Hudspeth, A.J. (1991) Chemiluminescence detection of proteins from single cells. *Proceedings of the National Academy of Sciences of the United States of America*, **88**, 2563–2567.

Girotti, S., Eremin, S., Montoya, A., Moreno, M.J., Caputo, P., D'Elia, M., Ripani, L., Romolo, F.S. & Maiolini, E. (2010) Development of a chemiluminescent ELISA and a colloidal gold-based LFIA for TNT detection. *Analytical and Bioanalytical Chemistry*, **396**, 687–695.

Girouard, L., Mandrekar, P., Catalano, D. & Szabo, G. (1998) Regulation of Monocyte Interleukin-12 Production by Acute Alcohol: A Role for Inhibition by Interleukin-10. *Alcoholism: Clinical and Experimental Research*, **22**, 211–216.

Giustina, A., Ambrosio, M.R., Beck Peccoz, P., Bogazzi, F., Cannavo', S., de Marinis, L., de Menis, E., Grottoli, S. & Pivonello, R. (2014) Use of Pegvisomant in acromegaly. An Italian Society of Endocrinology guideline. *Journal of Endocrinological Investigation*, **37**, 1017–1030.

Gizeli, E., Goddard, N.J., Lowe, C.R. & Stevenson, A.C. (1992) A Love plate biosensor utilising a polymer layer. *Sensors and Actuators: B. Chemical*, **6**, 131–137.

Gizeli, E., Liley, M., Lowe, C.R. & Vogel, H. (1997) Antibody Binding to a Functionalized Supported Lipid Layer: A Direct Acoustic Immunosensor. *Analytical Chemistry*, **69**, 4808–4813.

Gizeli, E., Stevenson, A.C., Goddard, N.J. & Lowe, C.R. (1993) *Acoustic Love plate sensors: comparison with other acoustic devices utilizing surface SH waves*,.

Goldman, E.R., Clapp, A.R., Anderson, G.P., Uyeda, H.T., Mauro, J.M., Medintz, I.L. & Mattoussi, H. (2004) Multiplexed Toxin Analysis Using Four Colors of Quantum Dot Fluororeagents. *Analytical Chemistry*, **76**, 684–688.

Goldspink, G. (1996) Muscle growth and muscle function: A molecular biological perspective. *Research in Veterinary Science*, **60**, 193–204.

González-Quintela, A., Dominguez-Santalla, M.J., Pérez, L.F., Vidal, C., Lojo, S. & Barrio, E. (2000) Influence of acute alcohol intake and alcohol withdrawal on circulating levels of IL-6, IL-8, IL-10 and IL-12. *Cytokine*, **12**, 1437–1440.

Gray, A., Bradbury, A.R.M., Knappik, A., Plückthun, A., Borrebaeck, C.A.K. & Dübel, S. (2020) Animal-free alternatives and the antibody iceberg. *Nature Biotechnology*, **38**, 1234–1239.

Green, M.R., Pastewka, J. v. & Peacock, A.C. (1973) Differential staining of phosphoproteins on polyacrylamide gels with a cationic carbocyanine dye. *Analytical Biochemistry*, **56**, 43–51.

Grellner, W. (2002) Time-dependent immunohistochemical detection of proinflammatory cytokines (IL-1β, IL-6, TNF-α) in human skin wounds. *Forensic Science International*, **130**, 90–96.

Grellner, W., Georg, T. & Wilske, J. (2000) Quantitative analysis of proinflammatory cytokines (IL-1β, IL-6, TNF-α) in human skin wounds. *Forensic Science International*, **113**, 251–264.

Grewal, Y.S., Shiddiky, M.J.A., Gray, S.A., Weigel, K.M., Cangelosi, G.A. & Trau, M. (2013) Label-free electrochemical detection of an entamoeba histolytica antigen using cell-free yeast-scFv probes. *Chemical Communications*, **49**, 1551–1553.

Grinnell, F. (1980) Fibroblast receptor for cell-substratum adhesion: Studies on the interaction of baby flamster kidney cells with latex beads coated by cold insoluble globulin (plasma fibronectin). *Journal of Cell Biology*, **86**, 104–112.

de Groof, F., Joosten, K.F.M.M., Janssen, J.A.M.J.L.M.J.L., de Kleijn, E.D., Hazelzet, J.A., Hop, W.C.J.J., Uitterlinden, P., van Doorn, J. & Hokken-Koelega, A.C.S.S. (2002) Acute stress response in children with meningococcal sepsis: Important differences in the growth hormone/insulin-like growth factor I axis between nonsurvivors and survivors. *Journal of Clinical Endocrinology and Metabolism*, **87**, 3118–3124.

Guha, N., Erotokritou-Mulligan, I., Bartlett, C., Nevitt, S.P., Francis, M., Bassett, E.E., Cowan, D.A., Sönksen, P.H. & Holt, R.I.G. (2014) Biochemical Markers of Insulin-Like Growth Factor-I Misuse in Athletes: The Response of Serum IGF-I, Procollagen Type III Amino-Terminal Propeptide, and the GH-2000 Score to the Administration of rhIGF-I/rhIGF Binding Protein-3 Complex. *The Journal of Clinical Endocrinology & Metabolism*, **99**, 2259–2268.

Gullberg, M., Gústafsdóttir, S.M., Schallmeiner, E., Jarvius, J., Bjarnegård, M., Betsholtz, C., Landegren, U. & Fredriksson, S. (2004) Cytokine detection by antibody-based proximity ligation. *Proceedings of the National Academy of Sciences of the United States of America*, **101**, 8420–8424.

Gusscott, S., Jenkins, C.E., Lam, S.H., Giambra, V., Pollak, M. & Weng, A.P. (2016) IGF1R derived PI3K/AKT signaling maintains growth in a subset of human T-cell acute lymphoblastic leukemias. *PLoS ONE*, **11**.

Gussenhoven, G.C., van der Hoorn, M.A., Goris, M.G., Terpstra, W.J., Hartskeerl, R.A., Mol, B.W., van Ingen, C.W. & Smits, H.L. (1997) LEPTO dipstick, a dipstick assay for detection of Leptospira-specific immunoglobulin M antibodies in human sera. *Journal of Clinical Microbiology*, **35**.

Haab, B.B., Dunham, M.J. & Brown, P.O. (2001) Protein microarrays for highly parallel detection and quantitation of specific proteins and antibodies in complex solutions. *Genome biology*, **2**, 1–13.

Haagsman, H.P. & van Golde, L.M.G. (1991) Synthesis and assembly of lung surfactant. *Annual Review of Physiology*, **53**, 441–464.

Hamdi, A. & Colas, P. (2012) Yeast two-hybrid methods and their applications in drug discovery. *Trends in Pharmacological Sciences*, **33**, 109–118.

Han, M., Gao, X., Su, J.Z. & Nie, S. (2001) Quantum-dot-tagged microbeads for multiplexed optical coding of biomolecules. *Nature Biotechnology*, **19**, 631–635.

Hanes, J. & Plückthun, A. (1997) In vitro selection and evolution of functional proteins by using ribosome display. *Proceedings of the National Academy of Sciences of the United States of America*, **94**, 4937–4942.

Hansen, J.A., Wang, J., Kawde, A.N., Xiang, Y., Gothelf, K. v. & Collins, G. (2006) Quantum-dot/aptamer-based ultrasensitive multi-analyte electrochemical biosensor. *Journal of the American Chemical Society*, **128**, 2228–2229.

Hartog, H., van der Graaf, W.T.A., Wesseling, J., van der Veer, E. & Boezen, H.M. (2008) Measurement of insulin-like growth factor-1 and insulin-like growth factor binding protein-3 after delayed separation of whole blood samples. *Clinical Biochemistry*, **41**, 636–639.

Hashiguchi, N., Ogura, H., Tanaka, H., Koh, T., Aoki, M., Shiozaki, T., Matsuoka, T., Shimazu, T. & Sugimoto, H. (2001) Enhanced expression of heat shock proteins in leukocytes from trauma patients. *Journal of Trauma - Injury, Infection and Critical Care*, **50**, 102–107.

Hede, M.S., Salimova, E., Piszczek, A., Perlas, E., Winn, N., Nastasi, T. & Rosenthal, N. (2012) E-Peptides Control Bioavailability of IGF-1. *PLoS ONE*, **7**, e51152.

Hedman, C.A., Frystyk, J., Lindström, T., Chen, J.-W.W., Flyvbjerg, A., Ørskov, H., Arnqvist, H.J., Lindström, T., Chen, J.-W.W., Flyvbjerg, A., Ørskov, H. & Arnqvist, H.J. (2004) Residual β-cell function more than glycemic control determines abnormalities of the insulin-like growth factor system in type 1 diabetes. *Journal of Clinical Endocrinology and Metabolism*, **89**, 6305–6309.

Hemnes, A.R., Zhao, M., West, J., Newman, J.H., Rich, S., Archer, S.L., Robbins, I.M., Blackwell, T.S., Cogan, J., Loyd, J.E., Zhao, Z., Gaskill, C., Jetter, C., Kropski, J.A., Majka, S.M. & Austin, E.D. (2016) Critical genomic networks and vasoreactive variants in idiopathic pulmonary arterial hypertension. *American Journal of Respiratory and Critical Care Medicine*, **194**, 464–475.

Hernández-Cueto, C., Vieira, D.N., Girela, E., Marques, E., Villanueva, E. & Sá, F.O. (1995) Diagnostic ability of D-dimer in the establishment of the vitality of wounds. *Forensic Science International*, **76**, 141–149.

Hines, M.A. & Guyot-Sionnest, P. (1996) Synthesis and characterization of strongly luminescing ZnS-capped CdSe nanocrystals. *Journal of Physical Chemistry*, **100**, 468–471.

Hirtz, M., Lyon, M., Feng, W., Holmes, A.E., Fuchs, H., Levkin, P.A. & Edu, -Michael Hirtz@kit (2013) Porous polymer coatings as substrates for the formation of high-fidelity micropatterns by quill-like pens. *Beilstein J. Nanotechnol*, **4**, 377–384.

Ho, J.A.A. & Huang, M.R. (2005) Application of a liposomal bioluminescent label in the development of a flow injection immunoanalytical system. *Analytical Chemistry*, **77**, 3431–3436.

Ho, J.A.A. & Wauchope, R.D. (2002) A strip liposome immunoassay for aflatoxin B1. *Analytical Chemistry*, **74**, 1493–1496.

Hochmeister, M.N., Budowle, B., Rudin, O., Gehrig, C., Borer, U., Thali, M. & Dirnhofer, R. (1999) Evaluation of Prostate-Specific Antigen (PSA) Membrane Test Assays for the Forensic Identification of Seminal Fluid. *Journal of Forensic Sciences*, **44**, 12042J.

Hoffmann, J., Wilhelm, J., Olschewski, A. & Kwapiszewska, G. (2016) Microarray analysis in pulmonary hypertension. *European Respiratory Journal*, **48**, 229–241.

Holt, R.I.G. (2009) Detecting growth hormone abuse in athletes. *Drug Testing and Analysis*, **1**, 426–433.

Holt, R.I.G., Bassett, E.E., Erotokritou-Mulligan, I., McHugh, C., Cowan, D., Bartlett, C. & Sönksen, P.H. (2009) Moving one step closer to catching the GH cheats: The GH-2004 experience. *Growth Hormone and IGF Research*, **19**, 346–351.

Holt, R.I.G., Erotokritou-Mulligan, I., McHugh, C., Bassett, E.E., Bartlett, C., Fityan, A., Bacon, J.L., Cowan, D.A. & Sönksen, P.H. (2010) The GH-2004 project: The response of IGF1 and type III pro-collagen to the administration of exogenous GH in non-Caucasian amateur athletes. *European Journal of Endocrinology*, **163**, 45–54.

Hopp, T.P. (1993) Retrospective: 12 years of antigenic determinant predictions, and more. *Peptide research*, **6**, 183–190.

Horáček, J.J., Garrett, S.D., Skládal, P. & Morgan, M.R.A.A. Characterization of the interactions between immobilized parathion and the corresponding recombinant scFv antibody using a piezoelectric biosensor. *Food and Agricultural Immunology*, **10**, 363–374.

Howarth, M., Takao, K., Hayashi, Y. & Ting, A.Y. (2005) Targeting quantum dots to surface proteins in living cells with biotin ligase. *Proceedings of the National Academy of Sciences of the United States of America*, **102**, 7583–7588.

Hu, J., Odom, T.W. & Lieber, C.M. (1999) Chemistry and physics in one dimension: Synthesis and properties of nanowires and nanotubes. *Accounts of Chemical Research*, **32**, 435–445.

Hwa, V., Oh, Y. & Rosenfeld, R.G. (1999) The Insulin-Like Growth Factor-Binding Protein (IGFBP) Superfamily*.

Hydrosense - hydrosense-legionella.com.

Ichikawa, T., Nakao, K., Hamasaki, K., Furukawa, R., Tsuruta, S., Ueda, Y., Taura, N., Shibata, H., Fujimoto, M., Toriyama, K. & Eguchi, K. (2007) Role of growth hormone, insulin-like growth factor 1 and insulin-like growth factor-binding protein 3 in development of non-alcoholic fatty liver disease. *Hepatology International*, **1**, 287–294.

Ishida, K., Zhu, B.L., Quan, L., Fujita, M.Q. & Maeda, H. (2000) Pulmonary surfactant-associated protein A levels in cadaveric sera with reference to the cause of death. *Forensic Science International*, **109**, 125–133.

Jain, A., Taghavian, O., Vallejo, D., Dotsey, E., Schwartz, D., Bell, F.G., Greef, C., Davies, D.H., Grudzien, J., Lee, A.P., Felgner, P.L. & Liang, L. (2016) Evaluation of quantum dot immunofluorescence and a digital CMOS imaging system as an alternative to conventional organic fluorescence dyes and laser scanning for quantifying protein microarrays. *PROTEOMICS*, **16**, 1271–1279.

Janssen, J.A.M.J.L., Stolk, R.P., Pols, H.A.P., Grobbee, D.E. & Lamberts, S.W.J. (1998) Serum total IGF-I, free IGF-I, and IGFBP-1 levels in an elderly population: Relation to cardiovascular risk factors and disease. *Arteriosclerosis, Thrombosis, and Vascular Biology*, **18**, 277–282.

Javad Khosravi, M., Papanastasiou-Diamandi, A. & Mistry, J. (1995) An ultrasensitive immunoassay for prostate-specific antigen based on conventional colorimetric detection. *Clinical Biochemistry*, **28**, 407–414.

Jayasena, S.D. (1999) Aptamers: An emerging class of molecules that rival antibodies in diagnostics. *Clinical Chemistry*, **45**, 1628–1650.

Ji, H., Chang, L., Zhao, J., Zhang, L., Jiang, X., Guo, F. & Wang, L. (2019) Evaluation of ELISA and CLIA for Treponema pallidum specific antibody detection in China: A multicenter study. *Journal of Microbiological Methods*, **166**.

Jones, J.D., Mogali, S. & Comer, S.D. (2012) Polydrug abuse: A review of opioid and benzodiazepine combination use. *Drug and Alcohol Dependence*, **125**, 8–18.

Jones, J.I. & Clemmons, D.R. (1995) Insulin-like growth factors and their binding proteins: Biological actions. *Endocrine Reviews*, **16**, 3–34.

Jones, T.J. & Hallworth, M.J. (1999) Postmortem prolactin as a marker of antemortem stress. *Journal of Clinical Pathology*, **52**, 749–751.

Jonsson, U., Fagerstam, L., Ivarsson, B., Johnsson, B., Karlsson, R., Lundh, K., Lofas, S., Persson, B., Roos, H., Ronnberg, I., Sjolander, S., Stenberg, E., Stahlberg, R., Urbaniczky, C., Ostlin, H. & Malmqvist, M. (1991) Real-time biospecific interaction analysis using surface plasmon resonance and a sensor chip technology. *BioTechniques*, **11**, 620–627.

Jousilahti, P., Salomaa, V., Rasi, V., Vahtera, E. & Palosuo, T. (2003) Association of markers of systemic inflammation, C reactive protein, serum amyloid A, and fibrinogen, with socioeconomic status. *Journal of Epidemiology and Community Health*, **57**, 730–733.

Julian, B.A., Wittke, S., Haubitz, M., Zürbig, P., Schiffer, E., McGuire, B.M., Wyatt, R.J. & Novak, J. (2007a) Urinary biomarkers of IgA nephropathy and other IgA-associated renal diseases. *World Journal of Urology*, **25**, 467–476.

Julian, B.A., Wittke, S., Novak, J., Good, D.M., Coon, J.J., Kellmann, M., Zürbig, P., Schiffer, E., Haubitz, M., Moldoveanu, Z., Calcatera, S.M., Wyatt, R.J., Sýkora, J., Sládková, E., Hes, O., Mischak, H. & McGuire, B.M. (2007b) Electrophoretic methods for analysis of urinary polypeptides in IgA-associated renal diseases. *ELECTROPHORESIS*, **28**, 4469–4483.

Juul, A., Scheike, T., Davidsen, M., Gyllenborg, J. & Jørgensen, T. (2002) Low serum insulin-like growth factor I is associated with increased risk of ischemic heart disease: A population-based case-control study. *Circulation*, **106**, 939–944.

Kaji, N., Tokeshi, M. & Baba, Y. (2007) Quantum dots for single bio-molecule imaging. *Analytical Sciences*, **23**, 21–24.

Kandalla, P.K., Goldspink, G., Butler-Browne, G. & Mouly, V. (2011) Mechano Growth Factor E peptide (MGF-E), derived from an isoform of IGF-1, activates human muscle progenitor cells and induces an increase in their fusion potential at different ages. *Mechanisms of Ageing and Development*, **132**, 154–162.

Kanefusa, K., Yoko, O., Fujiko, S., Atsuko, S., Kenji, M. & Yuro, T. (1983) Immunoassay of human muscle enolase subunit in serum: a novel marker antigen for muscle diseases. *Clinica Chimica Acta*, **131**, 75–85.

KATILA, H., CANTELL, K., APPELBERG, B. & RIMÓN, R. (1993) Is There a Seasonal Variation in the Interferon-Producing Capacity of Healthy Subjects? *Journal of Interferon Research*, **13**, 233–234.

Kato, H., Faria, T.N., Stannard, B., Roberts, C.T. & LeRoith, D. (1994) Essential role of tyrosine residues 1131, 1135, and 1136 of the insulin-like growth factor-I (IGF-I) receptor in IGF-I action. *Molecular Endocrinology*, **8**, 40–50.

Kay, B.K., Kasanov, J. & Yamabhai, M. (2001) Screening phage-displayed combinatorial peptide libraries. *Methods*, **24**, 240–246.

Keithley, R.B., Rosenthal, A.S., Essaka, D.C., Tanaka, H., Yoshimura, Y., Palcic, M.M., Hindsgaul, O. & Dovichi, N.J. (2013) Capillary electrophoresis with three-color fluorescence detection for the analysis of glycosphingolipid metabolism. *Analyst*, **138**, 164–170.

Kemp, S.F. (2009) Insulin-like growth factor-i deficiency in children with growth hormone insensitivity: Current and future treatment options. *BioDrugs*, **23**, 155–163.

Kemp, S.F. (2007) Mecasermin rinfabate. *Drugs of Today*, **43**, 149–155.

Kemp, S.F., Fowlkes, J.L. & Thrailkill, K.M. (2006) Efficacy and safety of mecasermin rinfabate. *Expert Opinion on Biological Therapy*, **6**, 533–538.

Kempeni, J. (1999) Preliminary results of early clinical trials with the fully human anti-TNFα monoclonal antibody D2E7. *Annals of the Rheumatic Diseases*, **58**, I70–I72.

Kesavaraju, B., Farajollahi, A., Lampman, R.L., Hutchinson, M., Krasavin, N.M., Graves, S.E. & Dickson, S.L. (2012) Evaluation of a rapid analyte measurement platform for west nile virus detection based on united states mosquito control programs. *American Journal of Tropical Medicine and Hygiene*, **87**, 359–363.

Khaodhiar, L., Ling, P.R., Blackburn, G.L. & Bistrian, B.R. (2004) Serum levels of interleukin-6 and C-reactive protein correlate with body mass index across the broad range of obesity. *Journal of Parenteral and Enteral Nutrition*, **28**, 410–415.

Khosravi, J., Diamandi, A., Bodani, U., Khaja, N. & Krishna, R.G. (2005) Pitfalls of immunoassay and sample for IGF-I: Comparison of different assay methodologies using various fresh and stored serum samples. *Clinical Biochemistry*, **38**, 659–666.

Kiang, J.G. & Tsokos, G.C. (1998) Heat shock protein 70 kDa: Molecular biology, biochemistry, and physiology. *Pharmacology and Therapeutics*, **80**, 183–201.

Koczula, K.M. & Gallotta, A. (2016) Lateral flow assays. *Essays in Biochemistry*, **60**, 111–120.

Kovacs, G. & Venema, A. (1992) Theoretical comparison of sensitivities of acoustic shear wave modes for (bio)chemical sensing in liquids. *Applied Physics Letters*, **61**, 639–641.

Kowal-Vern, A., Walenga, J.M., Hoppensteadt, D., Sharp-Pucci, M. & Gamelli, R.L. (1994) Interleukin-2 and interleukin-6 in relation to burn wound size in the acute phase of thermal injury. *Journal of the American College of Surgeons*, **178**, 357–362.

Krajcik, R.A., Borofsky, N.D., Massardo, S. & Orentreich, N. (2002) Insulin-like growth factor I (IGF-I), IGF-binding proteins, and breast cancer. *Cancer Epidemiology Biomarkers and Prevention*, **11**, 1566–1573.

Krebs, A., Wallaschofski, H., Spilcke-Liss, E., Kohlmann, T., Brabant, G., Völzke, H. & Nauck, M. (2008) Five commercially available insulin-like growth factor I (IGF-I) assays in comparison to the former Nichols Advantage IGF-I in a growth hormone treated population. *Clinical Chemistry and Laboratory Medicine*, **46**, 1776–1783.

Krupanidhi, S. Therapeutic Proteins through Phage Display-A Brilliant Technique for its Simplicity. *Indian Journal of Pharmaceutical Education and Research*, **53**.

Kuchroo, V.K. & Nicholson, L.B. (2003) Fast and feel good? *Nature*, **422**, 27–28.

Kuemmerle, J.F. (2012) *Growth Factors in the Gastrointestinal Tract*. *Physiology of the Gastrointestinal Tract*, pp. 199–277. Academic Press.

Kuo, Y.H. & Chen, T.T. (2002) Novel activities of pro-IGF-I E peptides: Regulation of morphological differentiation and anchorage-independent growth in human neuroblastoma cells. *Experimental Cell Research*, **280**, 75–89.

Kurek, R., Tunn, U.W., Eckart, O., Aumüller, G., Wong, J. & Renneberg, H. (2000) The significance of serum levels of insulin-like growth factor-1 in patients with prostate cancer. *BJU International*, **85**, 125–129.

Kurien, B.T. & Hal Scofield, R. (2015) *Western blotting: An introduction*. *Western Blotting: Methods and Protocols*, pp. 17–30. Springer New York.

Kuroki, Y., Takahashi, H., Fukada, Y., Mikawa, M., Inagawa, A., Fujimoto, S. & Akino, T. (1985) Two-site “simultaneous” immunoassay with monoclonal antibodies for the determination of surfactant apoproteins in human amniotic fluid. *Pediatric Research*, **19**, 1017–1020.

de La Cruzs, V.F., Lalq, A.A. & Mccutchan, T.F. (1988) Immunogenicity and epitope mapping of foreign sequences via genetically engineered filamentous phage. *THE JOURNAL OF BIOLOGICAL CHEMISTRY*, **263**, 4318–4322.

Lacey, J. v., Hsing, A.W., Fillmore, C.M., Hoffman, S., Helzlsouer, K.J. & Comstock, G.W. (2001) Null association between insulin-like growth factors, insulin-like growth factor-binding proteins, and prostate cancer in a prospective study. *Cancer Epidemiology Biomarkers and Prevention*, **10**, 1101–1102.

Lam, R.W., Song, C. & Yatham, L.N. (2004) Does neuroimmune dysfunction mediate seasonal mood changes in winter depression? *Medical Hypotheses*, **63**, 567–573.

Laron, Z. & Werner, H. (2020) Laron syndrome – A historical perspective. *Reviews in Endocrine and Metabolic Disorders*.

Larsson, C., Bramfeldt, H., Wingren, C., Borrebaeck, C. & Höök, F. (2005) Gravimetric antigen detection utilizing antibody-modified lipid bilayers. *Analytical Biochemistry*, **345**, 72–80.

Latosinska, A., Siwy, J., Mischak, H. & Frantzi, M. (2019) Peptidomics and proteomics based on CE-MS as a robust tool in clinical application: The past, the present, and the future. *Electrophoresis*, **40**, 2294–2308.

Laughlin, G.A., Barrett-Connor, E., Criqui, M.H. & Kritz-Silverstein, D. (2004) The Prospective Association of Serum Insulin-Like Growth Factor I (IGF-I) and IGF-Binding Protein-1 Levels with All Cause and Cardiovascular Disease Mortality in Older Adults: The Rancho Bernardo Study. *The Journal of Clinical Endocrinology & Metabolism*, **89**, 114–120.

Le, T.T., Chang, P., Benton, D.J., McCauley, J.W., Iqbal, M. & Cass, A.E.G. (2017) Dual Recognition Element Lateral Flow Assay Toward Multiplex Strain Specific Influenza Virus Detection. *Analytical Chemistry*, **89**, 6781–6786.

Lebofsky, R. & Bensimon, A. (2003) Single DNA molecule analysis: Applications of molecular combing. *Briefings in Functional Genomics and Proteomics*, **1**, 385–396.

Lee, C., Levin, A. & Branton, D. (1987) Copper staining: A five-minute protein stain for sodium dodecyl sulfate-polyacrylamide gels. *Analytical Biochemistry*, **166**, 308–312.

Lee, L.Y., Ong, S.L., Hu, J.Y., Ng, W.J., Feng, Y., Tan, X. & Wong, S.W. (2004) Use of semiconductor quantum dots for photostable immunofluorescence labeling of Cryptosporidium parvum. *Applied and Environmental Microbiology*, **70**, 5732–5736.

Lee, P.Y., Low, T.Y. & Jamal, R. (2019) *Probing the endogenous peptidomes of cancer for biomarkers: A new endeavor*. *Advances in Clinical Chemistry*, pp. 67–89. Academic Press Inc.

Lekishvili, T. & Campbell, J.J. (2018) Rapid comparative immunophenotyping of human mesenchymal stromal cells by a modified fluorescent cell barcoding flow cytometric assay. *Cytometry Part A*, **93**, 905–915.

Leonard, P., Hearty, S., Brennan, J., Dunne, L., Quinn, J., Chakraborty, T. & O'Kennedy, R. (2003) Advances in biosensors for detection of pathogens in food and water. *Enzyme and Microbial Technology*, **32**, 3–13.

Li, X., Kim, J., Zhou, J., Gu, W. & Quigg, R. (2005) Use of signal thresholds to determine significant changes in microarray data analyses. *Genetics and Molecular Biology*, **28**, 191–200.

Li, Z., Yi, Y., Luo, X., Xiong, N., Liu, Y., Li, S., Sun, R., Wang, Y., Hu, B., Chen, W., Zhang, Y., Wang, J., Huang, B., Lin, Y., Yang, J., Cai, W., Wang, X., Cheng, J., Chen, Z., Sun, K., Pan, W., Zhan, Z., Chen, L. & Ye, F. (2020) Development and clinical application of a rapid IgM-IgG combined antibody test for SARS-CoV-2 infection diagnosis. *Journal of Medical Virology*, **92**, 1518–1524.

Lian, Y., Ge, M. & Pan, X.M. (2014) EPMLR: Sequence-based linear B-cell epitope prediction method using multiple linear regression. *BMC Bioinformatics*, **15**, 1–6.

Liao, J.Y. & Li, H. (2010) Lateral flow immunodipstick for visual detection of aflatoxin B1 in food using immuno-nanoparticles composed of a silver core and a gold shell. *Microchimica Acta*, **171**, 289–295.

Longcope, C., Feldman, H.A., McKinlay, J.B. & Araujo, A.B. (2000) Diet and Sex Hormone-Binding Globulin. *The Journal of Clinical Endocrinology & Metabolism*, **85**, 293–296.

Lönnberg, M. & Carlsson, J. (2001) Quantitative detection in the attomole range for immunochromatographic tests by means of a flatbed scanner. *Analytical Biochemistry*, **293**, 224–231.

López-Bermejo, A., Buckway, C.K., Devi, G.R., Hwa, V., Plymate, S.R., Oh, Y. & Rosenfeld, R.G. (2000) Characterization of Insulin-Like Growth Factor-Binding Protein-Related Proteins (IGFBP-rPs) 1, 2, and 3 in Human Prostate Epithelial Cells: Potential Roles for IGFBP-rP1 and 2 in Senescence of the Prostatic Epithelium*. *Endocrinology*, **141**, 4072–4080.

López-Calderero, I., Chávez, E.S. & García-Carbonero, R. (2010) The insulin-like growth factor pathway as a target for cancer therapy. *Clinical and Translational Oncology*, **12**, 326–338.

Lopez-Garcia, E., Schulze, M.B., Fung, T.T., Meigs, J.B., Rifai, N., Manson, J.A.E. & Hu, F.B. (2004) Major dietary patterns are related to plasma concentrations of markers of inflammation and endothelial dysfunction. *The American journal of clinical nutrition*, **80**, 1029–1035.

Lorey, S., Fiedler, E., Kunert, A., Nerkamp, J., Lange, C., Fiedler, M., Bosse-Doenecke, E., Meysing, M., Gloser, M., Rundfeldt, C., Rauchhaus, U., Hänssgen, I., Göttler, T., Steuernagel, A., Fiedler, U. & Haupts, U. (2014) Novel ubiquitin-derived high affinity binding proteins with tumor targeting properties. *Journal of Biological Chemistry*, **289**, 8493–8507.

Lu, R.M., Hwang, Y.C., Liu, I.J., Lee, C.C., Tsai, H.Z., Li, H.J. & Wu, H.C. (2020) Development of therapeutic antibodies for the treatment of diseases. *Journal of Biomedical Science*, **27**, 1–30.

Lygren, T., Schjerling, P., Jacobsen, S., Berg, L.C., Nielsen, M.O., Langberg, H. & Thomsen, P.D. (2013) Validation of the IDS Octeia ELISA for the determination of insulin-like growth factor 1 in equine serum and tendon tissue extracts. *Veterinary Clinical Pathology*, **42**, 184–189.

Magambo, K.A., Kalluvya, S.E., Kapoor, S.W., Seni, J., Chofle, A.A., Fitzgerald, D.W. & Downs, J.A. (2014) Utility of urine and serum lateral flow assays to determine the prevalence and predictors of cryptococcal antigenemia in HIV-positive outpatients beginning antiretroviral therapy in Mwanza, Tanzania. *Journal of the International AIDS Society*, **17**.

Major, J.M., Laughlin, G.A., Kritz-Silverstein, D., Wingard, D.L. & Barrett-Connor, E. (2010) Insulin-like growth factor-I and cancer mortality in older men. *Journal of Clinical Endocrinology and Metabolism*, **95**, 1054–1059.

Mäkiranta, J., Verho, J., Lekkala, J. & Matintupa, N. (2006) *Novel measurement method for magnetic particles*. *Annual International Conference of the IEEE Engineering in Medicine and Biology - Proceedings*, pp. 4598–4601. Conf Proc IEEE Eng Med Biol Soc.

Mäkiranta, J.J. & Lekkala, J.O. (2005) *Modeling and simulation of magnetic nanoparticle sensor*. *Annual International Conference of the IEEE Engineering in Medicine and Biology - Proceedings*, pp. 1256–1259. Institute of Electrical and Electronics Engineers Inc.

Mansfield, M.A. (2009) *Nitrocellulose Membranes for Lateral Flow Immunoassays: A Technical Treatise*. *Lateral Flow Immunoassay*, pp. 1–19. Humana Press.

Mantzoros, C.S., Tzonou, A., Signorello, L.B., Stampfer, M., Trichopoulos, D. & Adami, H.O. (1997) Insulin like growth factor 1 in relation to prostate cancer and benign prostatic hyperplasia. *British Journal of Cancer*, **76**, 1115–1118.

Marballi, K., Genabai, N.K., Blednov, Y.A., Harris, R.A. & Ponomarev, I. (2016) Alcohol consumption induces global gene expression changes in VTA dopaminergic neurons. *Genes, Brain and Behavior*, **15**, 318–326.

Mariani, T.J., Budhraja, V., Mecham, B.H., Gu, C.C., Watson, M.A. & Sadovsky, Y. (2003) A variable fold change threshold determines significance for expression microarrays. *The FASEB journal : official publication of the Federation of American Societies for Experimental Biology*, **17**, 321–323.

Massart, C. & Poirier, J.Y. (2006) Serum insulin-like growth factor-I measurement in the follow-up of treated acromegaly: Comparison of four immunoassays. *Clinica Chimica Acta*, **373**, 176–179.

Mastrandrea, L.D., Wactawski-Wende, J., Donahue, R.P., Hovey, K.M., Clark, A. & Quattrin, T. (2008) Young women with type 1 diabetes have lower bone mineral density that persists over time. *Diabetes Care*, **31**, 1729–1735.

Matsuda, H., Seo, Y. & Takahama, K. (1999) A sandwich enzyme immunoassay for human muscle-specific β-enolase and its application for the determination of skeletal muscle injury. *Forensic Science International*, **99**, 197–208.

McKoy, G., Ashley, W., Mander, J., Yu Yang, S., Williams, N., Russell, B. & Goldspink, G. (1999) Expression of insulin growth factor-1 splice variants and structural genes in rabbit skeletal muscle induced by stretch and stimulation. *Journal of Physiology*, **516**, 583–592.

Mendlovic, S., Mozes, E., Eilat, E., Doron, A., Lereya, J., Zakuth, V. & Spirer, Z. (1999) Immune activation in non-treated suicidal major depression. *Immunology Letters*, **67**, 105–108.

Messingham, K.A.N., Heinrich, S.A., Schilling, E.M. & Kovacs, E.J. (2002) Interleukin-4 Treatment Restores Cellular Immunity After Ethanol Exposure and Burn Injury. *Alcoholism: Clinical and Experimental Research*, **26**, 519–526.

Messmer, B.T., Benham, C.J. & Thaler, D.S. (2000) Sequential determination of ligands binding to discrete components in heterogeneous mixtures by iterative panning and blocking (IPAB). *Journal of Molecular Biology*, **296**, 821–832.

Metzger, J., Schanstra, J.P. & Mischak, H. (2009) Capillary electrophoresis-mass spectrometry in urinary proteome analysis: Current applications and future developments. *Analytical and Bioanalytical Chemistry*, **393**, 1431–1442.

Meyer, F., Galan, P., Douville, P., Bairati, I., Kegle, P., Bertrais, S., Czernichow, S. & Hercberg, S. (2005) A prospective study of the insulin-like growth factor axis in relation with prostate cancer in the SU.VI.MAX trial. *Cancer Epidemiology Biomarkers and Prevention*, **14**, 2269–2272.

Miles, M.F. (1995) Alcohol's Effects on Gene Expression. *Alcohol health and research world*, **19**, 237–245.

Milingos, D.S., Philippou, A., Armakolas, A., Papageorgiou, E., Sourla, A., Protopapas, A., Liapi, A., Antsaklis, A., Mastrominas, M. & Koutsilieris, M. (2011) Insulinlike growth factor-1Ec (MGF) expression in eutopic and ectopic endometrium: Characterization of the MGF E-peptide actions in vitro. *Molecular Medicine*, **17**, 21–28.

Millipore (2013) *Rapid Lateral Flow Test Strips: Considerations for Product Development*, EMD Millipore Corporation, Billerica.

Mills, P., Lafrenière, J.F., Benabdallah, B.F., el Fahime, E.M. & Tremblay, J.P. (2007) A new pro-migratory activity on human myogenic precursor cells for a synthetic peptide within the E domain of the mechano growth factor. *Experimental Cell Research*, **313**, 527–537.

Mimasaka, S., Hashiyada, M., Nata, M. & Funayama, M. (2001) Correlation between Serum IL-6 Levels and Death: Usefulness in Diagnosis of "Traumatic Shock"? *The Tohoku Journal of Experimental Medicine*, **193**, 319–324.

Mintz, C.S. & Crea, R. (2013) Protein scaffolds: The next generation of protein therapeutics? *BioProcess International*.

Miyaishi, S., Kitao, T., Yamamoto, Y., Ishizu, H., Matsumoto, T., Mizutani, Y., Heinemann, A. & Puschel, K. (1996) Identification of menstrual blood by the simultaneous determination of FDP-D dimer and myoglobin contents. *Japanese Journal of Legal Medicine*, **50**, 400–403.

Molnar, J., Gelder, F.B., Zong Lai, M., Siefring, G.E., Bruce Credo, R. & Lorand, L. (1978) *OPSONIC FUNCTION OF PLASMA F1BRONECTIN Purification of Opsonically Active Human and Rat Cold-Insoluble Globulin (Plasma Fibronectin)1*,.

Moock, J., Albrecht, C., Friedrich, N., Völzke, H., Nauck, M., Koltowska-Haggström, M., Kohlmann, T. & Wallaschofski, H. (2009) Health-related quality of life and IGF-1 in GH-deficient adult patients on GH replacement therapy: Analysis of the German KIMS data and the Study of Health in Pomerania. *European Journal of Endocrinology*, **160**, 17–24.

Moorthy, J., Mensing, G.A., Kim, D., Mohanty, S., Eddington, D.T., Tepp, W.H., Johnson, E.A. & Beebe, D.J. (2004) Microfluidic tectonics platform: A colorimetric, disposable botulinum toxin enzyme-linked immunosorbent assay system. *Electrophoresis*, **25**, 1705–1713.

Moreno, M.D.L., Cebolla, Á., Munõz-Suano, A., Carrillo-Carrion, C., Comino, I., Pizarro, Á., León, F., Rodríguez-Herrera, A. & Sousa, C. (2017) Detection of gluten immunogenic peptides in the urine of patients with coeliac disease reveals transgressions in the gluten-free diet and incomplete mucosal healing. *Gut*, **66**, 250–257.

Morris, J.K., George, L.M., Wu, T. & Wald, N.J. (2006) Insulin-like growth factors and cancer: No role in screening. Evidence from the BUPA study and meta-analysis of prospective epidemiological studies. *British Journal of Cancer*, **95**, 112–117.

Muller, A.F., Kopchick, J.J., Flyvbjerg, A. & van der Lely, A.J. (2004) Growth hormone receptor antagonists. *Journal of Clinical Endocrinology and Metabolism*, **89**, 1503–1511.

Murphy, N., Knuppel, A., Papadimitriou, N., Martin, R.M., Tsilidis, K.K., Smith-Byrne, K., Fensom, G., Perez-Cornago, A., Travis, R.C., Key, T.J. & Gunter, M.J. (2020) Insulin-like growth factor-1, insulin-like growth factor-binding protein-3, and breast cancer risk: observational and Mendelian randomization analyses with ∼430 000 women. *Annals of Oncology*, **31**, 641–649.

Myrtle, J. & Ivor, L. (1989) *Measurement of PSA in Serum by two immunometric Methods (Hybritech Tandem-R/Tandem-E PSA)*. *Clinical Aspects of Prostate Cancer* (ed. by W. Catalona), pp. 161–171. Elsevier, New York.

Nguyen, H., Park, J., Kang, S. & Kim, M. (2015) Surface Plasmon Resonance: A Versatile Technique for Biosensor Applications. *Sensors*, **15**, 10481–10510.

Niedbala, R.S., Feindt, H., Kardos, K., Vail, T., Burton, J., Bielska, B., Li, S., Milunic, D., Bourdelle, P. & Vallejo, R. (2001) Detection of analytes by immunoassay using Up-Converting Phosphor Technology. *Analytical Biochemistry*, **293**, 22–30.

Niemelä, O., Parkkila, S., Koll, M. & Preedy, V.R. (2002) Generation of protein adducts with malondialdehyde and acetaldehyde in muscles with predominantly type I or

type II fibers in rats exposed to ethanol and the acetaldehyde dehydrogenase inhibitor cyanamide. *American Journal of Clinical Nutrition*, **76**, 668–674.

Niewiarowski, S., Regoeczi, E. & Mustard, J.F. (1972) Adhesion of Fibroblasts to Polymerizing Fibrin and Retraction of Fibrin Induced by Fibroblasts. *Experimental Biology and Medicine*, **140**, 199–204.

Niu, K., Zheng, X., Huang, C., Xu, K., Zhi, Y., Shen, H. & Jia, N. (2014) A colloidal gold nanoparticle-based immunochromatographic test strip for rapid and convenient detection of staphylococcus aureus. *Journal of Nanoscience and Nanotechnology*, **14**, 5151–5156.

Nixon, A.E., Sexton, D.J. & Ladner, R.C. (2014) Drugs derived from phage display from candidate identification to clinical practice. *mAbs*, **6**, 73–85.

Noren, K.A. & Noren, C.J. (2001) Construction of high-complexity combinatorial phage display peptide libraries. *Methods*, **23**, 169–178.

Ochs, D.C., McConkey, E.H. & Sammons, D.W. (1981) Silver Stains for proteins in polyacerylamide gels: A comparison of six methods. *Electrophoresis*, **2**, 304–307.

O'Gara, P.T., Kushner, F.G., Ascheim, D.D., Casey, D.E., Chung, M.K., de Lemos, J.A., Ettinger, S.M., Fang, J.C., Fesmire, F.M., Franklin, B.A., Granger, C.B., Krumholz, H.M., Linderbaum, J.A., Morrow, D.A., Newby, L.K., Ornato, J.P., Ou, N., Radford, M.J., Tamis-Holland, J.E., Tommaso, C.L., Tracy, C.M., Woo, Y.J. & Zhao, D.X. (2013) 2013 ACCF/AHA guideline for the management of st-elevation myocardial infarction: A report of the American college of cardiology foundation/american heart association task force on practice guidelines. *Journal of the American College of Cardiology*, **61**, 78–140.

Owers-Narhi, J.A., Hua, L., Rosenfeld, Q.X., Arakawa, R., Rohde, T., Prestrelski, M., Lauren, S., Stoney, S., Tsai, K.S. & Weiss, L.A. (1993) *Role of Native Disulfide Bonds in the Structure and Activity of Insulin-like Growth Factor 1: Genetic Models of Protein-Folding Intermediates1"*,.

Paccou, J., Dewailly, J. & Cortet, B. (2012) Reduced levels of serum IGF-1 is related to the presence of osteoporotic fractures in male idiopathic osteoporosis. *Joint Bone Spine*, **79**, 78–82.

Page, J.H., Ma, J., Pollak, M., Manson, J.A.E. & Hankinson, S.E. (2008) Plasma insulinlike growth factor 1 and binding-protein 3 and risk of myocardial infarction in women: A prospective study. *Clinical Chemistry*, **54**, 1682–1688.

Page, L.E., Zhang, X., Tyrakowski, C.M., Ho, C.T. & Snee, P.T. (2016) Synthesis and characterization of DNA-quantum dot conjugates for the fluorescence ratiometric detection of unlabelled DNA. *Analyst*, **141**, 6251–6258.

Palerme, J.S., Lamperelli, E., Gagne, J., Cazlan, C., Zhang, M. & Olds, J.E. (2019) Seroprevalence of Leptospira spp., Toxoplasma gondii, and Dirofilaria immitis in Free-Roaming Cats in Iowa. *Vector-Borne and Zoonotic Diseases*, **19**, 193–198.

Palmqvist, R., Hallmans, G., Rinaldi, S., Biessy, C., Stenling, R., Riboli, E. & Kaaks, R. (2002) Plasma insulin-like growth factor 1, insulin-like growth factor binding protein 3, and risk of colorectal cancer: A prospective study in northern Sweden. *Gut*, **50**, 642–646.

Pavlov, V., Xiao, Y., Shlyahovsky, B. & Willner, I. (2004) Aptamer-functionalized Au nanoparticles for the amplified optical detection of thrombin. *Journal of the American Chemical Society*, **126**, 11768–11769.

Pearce, L., Oddie, G., Coia, G., Kortt, A., Hudson, P. & Lilley, G. (1997) Linear gene fusions of antibody fragments with streptavidin can be linked to biotin labelled secondary molecules to form bispecific reagents. *IUBMB Life*, **42**, 1179–1188.

Pease, A.C., Solas, D., Sullivan, E.J., Cronin, M.T., Holmes, C.P. & Fodor, S.P.A. (1994) Light-generated oligonucleotide arrays for rapid DNA sequence analysis. *Proceedings of the National Academy of Sciences of the United States of America*, **91**, 5022–5026.

Pennington, M.W., Czerwinski, A. & Norton, R.S. (2018) Peptide therapeutics from venom: Current status and potential. *Bioorganic and Medicinal Chemistry*, **26**, 2738–2758.

Petrikkos, G.L., Christofilopoulou, S.A., Tentolouris, N.K., Charvalos, E.A., Kosmidis, C.J. & Daikos, G.L. (2005) Value of measuring serum procalcitonin, C-reactive protein, and mannan antigens to distinguish fungal from bacterial infections. *European Journal of Clinical Microbiology and Infectious Diseases*, **24**, 272–275.

Pfäffle, R. & Kiess, W. (2020) *Gh and igf-1 replacement in children*. *Handbook of Experimental Pharmacology*, pp. 67–86. Springer.

Pfeffer, L.A., Brisson, B.K., Lei, H. & Barton, E.R. (2009) The insulin-like growth factor (IGF)-I E-peptides modulate cell entry of the mature IGF-I protein. *Molecular Biology of the Cell*, **20**, 3810–3817.

Philippou, A., Armakolas, A., Panteleakou, Z., Pissimissis, N., Nezos, A., Theos, A., Kaparelou, M., Armakolas, N., Pneumaticos, S. & Koutsilieris, M. (2011) IGF1Ec expression in MG-63 human osteoblast-like osteosarcoma cells. *undefined*.

Pohanka, M. (2017) Quantum Dots in the Therapy: Current Trends and Perspectives. *Mini-Reviews in Medicinal Chemistry*, **17**, 650–656.

Portilho, M.M., Moraes, L. de, Kikuti, M., Nascimento, L.C.J., Reis, M.G., Boaventura, V.S., Khouri, R. & Ribeiro, G.S. (2020) Accuracy of the Zika IgM antibody capture enzyme-linked immunosorbent assay from the centers for disease control and

prevention (CDC Zika MAC-ELISA) for diagnosis of zika virus infection. *Diagnostics*, **10**.

Posthuma-Trumpie, G.A., Korf, J. & van Amerongen, A. (2009) Lateral flow (immuno)assay: Its strengths, weaknesses, opportunities and threats. A literature survey. *Analytical and Bioanalytical Chemistry*, **393**, 569–582.

Postlethwaite, A.E., Keski-Oja, J., Balian, G. & Kang, A.H. (1981) Induction of fibroblast chemotaxis by fibronectin. Localization of the chemotactic region to a 140,000-molecular weight non-gelatin-binding fragment. *Journal of Experimental Medicine*, **153**, 494–499.

Powrie, J.K., Bassett, E.E., Rosen, T., Jørgensen, J.O., Napoli, R., Sacca, L., Christiansen, J.S., Bengtsson, B.A. & Sönksen, P.H. (2007) Detection of growth hormone abuse in sport. *Growth Hormone and IGF Research*, **17**, 220–226.

Predicted Antigenic Peptides | Immunomedicine Group - imed.med.ucm.es/Tools/antigenic.pl.

Price, V.H. (2003) Therapy of alopecia areata: On the cusp and in the future. *Journal of Investigative Dermatology Symposium Proceedings*, **8**, 207–211.

Qiagen ESEQuant - lateralflowreader.com.

Quarmby, V. & Quan, C. (1999) How much insulin-like growth factor-I (IGF-I) circulates?: impact of standardization on IGF-I assay accuracy. *Developments in biological standardization*, **97**, 111–118.

Quidel Triage Cardiac Panel | Quidel.

Ragland, W.L., Pace, J.L. & Kemper, D.L. (1974) Fluorometric scanning of fluorescamine-labeled proteins in polyacrylamide gels. *Analytical Biochemistry*, **59**, 24–33.

Raja, A., Riedel Machicao, A., Morrissey, A.B., Jacobs, M.R. & Daniel, T.M. (1988) Specific detection of Mycobacterium tuberculosis in radiometric cultures by using an immunoassay for antigen 5. *Journal of Infectious Diseases*, **158**, 468–470.

Rammensee, H.G., Bachmann, J., Emmerich, N.P.N., Bachor, O.A. & Stevanović, S. (1999) SYFPEITHI: Database for MHC ligands and peptide motifs. *Immunogenetics*, **50**, 213–219.

RCSB PDB - 1BQT: Three-dimensional Structure Of Human Insulin-like Growth Factor-I (IGF-I) Determined By 1H-NMR And Distance Geometry, 6 Structures.

Reiter, Y., Brinkmann, U., Webber, K.O., Jung, S.H., Lee, B. & Pastan, I. (1994) Engineering interchain disulfide bonds into conserved framework regions of fv fragments: Improved biochemical characteristics of recombinant immunotoxins containing disulfide-stabilized Fv. *Protein Engineering, Design and Selection*, **7**, 697–704.

Resch-Genger, U., Grabolle, M., Cavaliere-Jaricot, S., Nitschke, R. & Nann, T. (2008) Quantum dots versus organic dyes as fluorescent labels. *Nature Methods*, **5**, 763–775.

Reverdatto, S., Burz, D. & Shekhtman, A. (2015) Peptide Aptamers: Development and Applications. *Current Topics in Medicinal Chemistry*, **15**, 1082–1101.

Richter, A., Eggenstein, E. & Skerra, A. (2014) Anticalins: Exploiting a non-Ig scaffold with hypervariable loops for the engineering of binding proteins. *FEBS Letters*, **588**, 213–218.

Rider, C.C. & Taylor, C.B. (1974) Enolase isoenzymes in rat tissues: Electrophoretic, chromatographic, immunological and kinetic properties. *BBA - Protein Structure*, **365**, 285–300.

Rinderknecht, E. & Humbel, R.E. (1976) Polypeptides with nonsuppressible insulin like and cell growth promoting activities in human serum: isolation, chemical characterization, and some biological properties of forms I and II. *Proceedings of the National Academy of Sciences of the United States of America*, **73**, 2365–2369.

Robinson, S.A. & Rosenzweig, S.A. (2006) Paradoxical effects of the phage display-derived peptide antagonist IGF-F1-1 on insulin-like growth factor-1 receptor signaling. *Biochemical Pharmacology*, **72**, 53–61.

Rodgers, B.D., Roalson, E.H. & Thompson, C. (2008) Phylogenetic analysis of the insulin-like growth factor binding protein (IGFBP) and IGFBP-related protein gene families. *General and Comparative Endocrinology*, **155**, 201–207.

Romanov, V., Davidoff, S.N., Miles, A.R., Grainger, D.W., Gale, B.K. & Brooks, B.D. (2014) A critical comparison of protein microarray fabrication technologies. *Analyst*, **139**, 1303–1326.

Ronald T. LaBorde (2000) Immunochromatographic assay method and apparatus.

Rongen, H.A.H., Hoetelmans, R.M.W., Bult, A. & van Bennekom, W.P. (1994a) Chemiluminescence and immunoassays. *Journal of Pharmaceutical and Biomedical Analysis*, **12**, 433–462.

Rongen, H.A.H., Hoetelmans, R.M.W., Bult, A. & van Bennekom, W.P. (1994b) Chemiluminescence and immunoassays. *Journal of Pharmaceutical and Biomedical Analysis*, **12**, 433–462.

Root, D.D. & Reisler, E. (1989) Copper iodide staining of protein blots on nitrocellulose membranes. *Analytical Biochemistry*, **181**, 250–253.

Rosenbloom, A.L. (2009) Mecasermin (recombinant human insulin-like growth factor I). *Advances in Therapy*, **26**, 40–54.

Rosenbloom, A.L. (2007) Recombinant Human Insulin-Like Growth Factor I (rhIGF-I) and rhIGF-I/rhIGF-Binding-Protein-3: New Growth Treatment Options? *Journal of Pediatrics*, **150**, 7–11.

Rowlands, M.A., Gunnell, D., Harris, R., Vatten, L.J., Holly, J.M.P. & Martin, R.M. (2009) Circulating insulin-like growth factor peptides and prostate cancer risk: A systematic review and meta-analysis. *International Journal of Cancer*, **124**, 2416–2429.

Ruckert, R., Lindner, G., Bulfone-Paus, S. & Paus, R. (2000) High-dose proinflammatory cytokines induce apoptosis of hair bulb keratinocytes in vivo. *British Journal of Dermatology*, **143**, 1036–1039.

Ruhl, C.E., Everhart, J.E., Ding, J., Goodpaster, B.H., Kanaya, A.M., Simonsick, E.M., Tylavsky, F.A. & Harris, T.B. (2004) Serum leptin concentrations and body adipose measures in older black and white adults. *American Journal of Clinical Nutrition*, **80**, 576–583.

Ryan, M.H., Petrone, D., Nemeth, J.F., Barnathan, E., Björck, L. & Jordan, R.E. (2008) Proteolysis of purified IgGs by human and bacterial enzymes in vitro and the detection of specific proteolytic fragments of endogenous IgG in rheumatoid synovial fluid. *Molecular Immunology*, **45**, 1837–1846.

Saha, S., Bhasin, M. & Raghava, G.P.S. (2005) Bcipep: A database of B-cell epitopes. *BMC Genomics*, **6**, 79.

Saha, S. & Raghava, G.P.S. (2007) Prediction methods for B-cell epitopes. *Methods in molecular biology (Clifton, N.J.)*, **409**, 387–394.

Sakai, G., Saiki, T., Uda, T., Miura, N. & Yamazoe, N. (1995) Selective and repeatable detection of human serum albumin by using piezoelectric immunosensor. *Sensors and Actuators: B. Chemical*, **24**, 134–137.

Salmon, W.D. & Daughaday, W.H. (1957) A hormonally controlled serum factor which stimulates sulfate incorporation by cartilage in vitro. *The Journal of Laboratory and Clinical Medicine*, **49**, 825–836.

Sano, T., Kurotobi, S., Matsuzaki, K., Yamamoto, T., Maki, I., Miki, K., Kogaki, S. & Hara, J. (2007) Prediction of non-responsiveness to standard high-dose gamma-globulin therapy in patients with acute Kawasaki disease before starting initial treatment. *European Journal of Pediatrics*, **166**, 131–137.

Santolaria, F., Pérez-Cejas, A., Alemán, M.R., González-Reimers, E., Milena, A., de la Vega, M.J., Martínez-Riera, A. & Gómez-Rodríguez, M.A. (2003) Low serum leptin levels and malnutrition in chronic alcohol misusers hospitalized by somatic complications. *Alcohol and Alcoholism*, **38**, 60–66.

Sato, A., Nishimura, S., Ohkubo, T., Kyogoku, Y., Koyama, S., Kobayashi, M., Yasuda, T. & Kobayashi, Y. (1993) Three-dimensional structure of human insulin-like growth factor-I (IGF-I) determined by 1H-NMR and distance geometry. *International Journal of Peptide and Protein Research*, **41**, 433–440.

SATO, A., NISHIMURA, S., OHKUBO, T., KYOGOKU, Y., KOYAMA, S., KOBAYASHI, M., YASUDA, T. & KOBAYASHI, Y. (1993) Three-dimensional structure of human

insulin-like growth factor-I (IGF-I) determined by 1H-NMR and distance geometry. *International Journal of Peptide and Protein Research*, **41**, 433–440.

Schönfeld, D., Matschiner, G., Chatwell, L., Trentmann, S., Gille, H., Hülsmeyer, M., Brown, N., Kaye, P.M., Schlehuber, S., Hohlbaum, A.M. & Skerra, A. (2009) An engineered lipocalin specific for CTLA-4 reveals a combining site with structural and conformational features similar to antibodies. *Proceedings of the National Academy of Sciences of the United States of America*, **106**, 8198–8203.

Schrader, M. & Schulz-Knappe, P. (2001) Peptidomics technologies for human body fluids. *Trends in Biotechnology*, **19**, 55–60.

Schramm, E.C., Staten, N.R., Zhang, Z., Bruce, S.S., Kellner, C., Atkinson, J.P., Kyttaris, V.C., Tsokos, G.C., Petri, M., Sander Connolly, E. & Olson, P.K. (2015) A quantitative lateral flow assay to detect complement activation in blood. *Analytical Biochemistry*, **477**, 78–85.

Schulte, I., Tammen, H., Selle, H. & Schulz-Knappe, P. (2005) Peptides in body fluids and tissues as markers of disease. *Expert Review of Molecular Diagnostics*, **5**, 145–157.

Scrivener, E., Barry, R., Platt, A., Calvert, R., Masih, G., Hextall, P., Soloviev, M. & Terrett, J. (2003) Peptidomics: A new approach to affinity protein microarrays. *Proteomics*, **3**, 122–128.

Segets, D. (2016) Analysis of Particle Size Distributions of Quantum Dots: From Theory to Application. *KONA Powder and Particle Journal*, **33**, 48–62.

Segets, D., Lucas, J.M., Klupp Taylor, R.N., Scheele, M., Zheng, H., Alivisatos, A.P. & Peukert, W. (2012) Determination of the quantum dot band gap dependence on particle size from optical absorbance and transmission electron microscopy measurements. *ACS Nano*, **6**, 9021–9032.

Servat, A., Robardet, E. & Cliquet, F. (2019) An inter-laboratory comparison to evaluate the technical performance of rabies diagnosis lateral flow assays. *Journal of Virological Methods*, **272**.

Shearer, W.T., Lee, B.N., Cron, S.G., Rosenblatt, H.M., Smith, E.O., Lugg, D.J., Nickolls, P.M., Sharp, R.M., Rollings, K. & Reuben, J.M. (2002) Suppression of human anti-inflammatory plasma cytokines IL-10 and IL-1RA with elevation of proinflammatory cytokine IFN-γ during the isolation of the Antarctic winter. *Journal of Allergy and Clinical Immunology*, **109**, 854–857.

Shibata, Y., Tsukazaki, T., Hirata, K., Xin, C. & Yamaguchi, A. (2004) Role of a new member of IGFBP superfamily, IGFBP-rP10, in proliferation and differentiation of osteoblastic cells. *Biochemical and Biophysical Research Communications*, **325**, 1194–1200.

van Sickle, B.J., Simmons, J., Hall, R., Raines, M., Ness, K. & Spagnoli, A. (2009) Increased circulating IL-8 is associated with reduced IGF-1 and related to poor metabolic control in adolescents with type 1 diabetes mellitus. *Cytokine*, **48**, 290–294.

Siegfried, J.M., Kasprzyk, P.G., Treston, A.M., Mulshine, J.L., Quinn, K.A. & Cuttitta, F. (1992) A mitogenic peptide amide encoded within the E peptide domain of the insulin-like growth factor IB prohormone. *Proceedings of the National Academy of Sciences of the United States of America*, **89**, 8107–8111.

Silverman, J., Lu, Q., Bakker, A., To, W., Duguay, A., Alba, B.M., Smith, R., Rivas, A., Li, P., Le, H., Whitehorn, E., Moore, K.W., Swimmer, C., Perlroth, V., Vogt, M., Kolkman, J. & Stemmer, W.P.C. (2005) Multivalent avimer proteins evolved by exon shuffling of a family of human receptor domains. *Nature Biotechnology*, **23**, 1556–1561.

Sinha, M.K., Ohannesian, J.P., Heiman, M.L., Kriauciunas, A., Stephens, T.W., Magosin, S., Marco, C. & Caro, J.F. (1996) Nocturnal rise of leptin in lean, obese, and non-insulin-dependent diabetes mellitus subjects. *Journal of Clinical Investigation*, **97**, 1344–1347.

Sirolli, V., Pieroni, L., di Liberato, L., Urbani, A. & Bonomini, M. (2020) Urinary peptidomic biomarkers in kidney diseases. *International Journal of Molecular Sciences*, **21**.

Sjögren, K., Liu, J.L., Blad, K., Skrtic, S., Vidal, O., Wallenius, V., Leroith, D., Törnell, J., Isaksson, O.G.P., Jansson, J.O. & Ohlsson, C. (1999) Liver-derived insulin-like growth factor I (IGF-I) is the principal source of IGF-I in blood but is not required for postnatal body growth in mice. *Proceedings of the National Academy of Sciences of the United States of America*, **96**, 7088–7092.

Smyntyna, V., Semenenko, B., Skobeeva, V. & Malushin, N. (2014) Photoactivation of luminescence in CdS nanocrystals. *Beilstein Journal of Nanotechnology*, **5**, 355–359.

Soloviev, M., Bailes, J., Salata, N. & Finch, P. (2007) *Protein Profiling for Forensic and Biometric Applications*. *Molecular Forensics* (ed. by R. Rapley) and D. Whitehouse), pp. 197–220. John Wiley & Sons, Ltd, UK.

Soloviev, M., Barry, R. & Terrett, J. (2005) *Chip Based Proteomics Technology*. *Molecular Analysis and Genome Discovery*, pp. 217–249. John Wiley & Sons, Ltd, Chichester, UK.

Soloviev, M. & Finch, P. (2005) Peptidomics, current status. *Journal of Chromatography B: Analytical Technologies in the Biomedical and Life Sciences*, **815**, 11–24.

Sönksen, P. (2009) The International Olympic Committee (IOC) and GH-2000. *Growth Hormone and IGF Research*, **19**, 341–345.

de Soyza, K. (1991) Evaluation of an enzyme linked immunosorbent assay (ELISA) method for ABO and Lewis typing of body fluids in forensic samples. *Forensic Science International*, **52**, 65–76.

Spectral Imaging and Linear Unmixing | Nikon - microscopyu.com/techniques/confocal/spectral-imaging-and-linear-unmixing.

Stattin, P., Rinaldi, S., Biessy, C., Stenman, U.H., Hallmans, G. & Kaaks, R. (2004) High levels of circulating insulin-like growth factor-I increase prostate cancer risk: A prospective study in a population-based nonscreened cohort. *Journal of Clinical Oncology*, **22**, 3104–3112.

Steinberg, T.H., Jones, L.J., Haugland, R.P. & Singer, V.L. (1996) SYPRO orange and SYPRO red protein gel stains: One-step fluorescent staining of denaturing gels for detection of nanogram levels of protein. *Analytical Biochemistry*, **239**, 223–237.

Su, X., Robelek, R., Wu, Y., Wang, G. & Knoll, W. (2004) Detection of Point Mutation and Insertion Mutations in DNA Using a Quartz Crystal Microbalance and MutS, a Mismatch Binding Protein. *Analytical Chemistry*, **76**, 489–494.

SureScreen Diagnostics - surescreen.com.

Szabo, G., Mandrekar, P., Dolganiuc, A., Catalano, D. & Kodys, K. (2001) Reduced Alloreactive T-Cell Activation After Alcohol Intake is Due to Impaired Monocyte Accessory Cell Function and Correlates With Elevated IL-10, IL-13, and Decreased IFNgamma Levels. *Alcoholism: Clinical and Experimental Research*, **25**, 1766–1772.

Szabo, G., Verma, B.K., Rasi, M.F. a & Catalano, D.E. (1992) Induction of transforming growth factor-beta and prostaglandin E2 production by ethanol in human monocytes. *Journal of Leukocyte Biology*, **52**, 602–610.

Takagahara, T. & Takeda, K. (1992) Theory of the quantum confinement effect on excitons in quantum dots of indirect-gap materials. *Physical Review B*, **46**, 15578–15581.

Talbot, D.N. & Yphantis, D.A. (1971) Fluorescent monitoring of SDS gel electrophoresis. *Analytical Biochemistry*, **44**, 246–253.

Tammemagi, M.C., Frank, J.W., LeBlanc, M. & Artsob, H. (1995) Intra- and interlaboratory reproducibility of an ELISA serological test for Lyme disease. *Canadian Journal of Infectious Diseases*, **6**, 90–95.

Tang, D., Sauceda, J.C., Lin, Z., Ott, S., Basova, E., Goryacheva, I., Biselli, S., Lin, J., Niessner, R. & Knopp, D. (2009) Magnetic nanogold microspheres-based lateral-flow immunodipstick for rapid detection of aflatoxin B2 in food. *Biosensors and Bioelectronics*, **25**, 514–518.

Tanimoto, K., Hizuka, N., Fukuda, I., Takano, K. & Hanafusa, T. (2008) The influence of age on the GH-IGF1 axis in patients with acromegaly. *European Journal of Endocrinology*, **159**, 375–379.

Taranova, N.A., Byzova, N.A., Zaiko, V. v., Starovoitova, T.A., Vengerov, Y.Y., Zherdev, A. v. & Dzantiev, B.B. (2013) Integration of lateral flow and microarray technologies for multiplex immunoassay: Application to the determination of drugs of abuse. *Microchimica Acta*, **180**, 1165–1172.

Taylor, S.I., Barr, V. & Reitman, M. (1996) Does leptin contribute to diabetes caused by obesity? *Science*, **274**, 1151–1152.

Tekesin, I., Anderer, G., Hellmeyer, L., Stein, W., Kühnert, M. & Schmidt, S. (2004) Assessment of fetal lung development by quantitative ultrasonic tissue characterization: a methodical study. *Prenatal Diagnosis*, **24**, 671–676.

Terazono, H., Anzai, Y., Soloviev, M. & Yasuda, K. (2010) Labelling of live cells using fluorescent aptamers: Binding reversal with DNA nucleases. *Journal of Nanobiotechnology*, **8**, 8.

Theodorescu, D., Fliser, D., Wittke, S., Mischak, H., Krebs, R., Walden, M., Ross, M., Eltze, E., Bettendorf, O., Wulfing, C. & Semjonow, A. (2005) Pilot study of capillary electrophoresis coupled to mass spectrometry as a tool to define potential prostate cancer biomarkers in urine. *Electrophoresis*, **26**, 2797–2808.

Theodorescu, D., Wittke, S., Ross, M.M., Walden, M., Conaway, M., Just, I., Mischak, H. & Frierson, H.F. (2006) Discovery and validation of new protein biomarkers for urothelial cancer: A prospective analysis. *Lancet Oncology*, **7**, 230–240.

Thomas, A.J., Davis, S., Morris, C., Jackson, E., Harrison, R. & O'Brien, J.T. (2005) Increase in interleukin-1β in late-life depression. *American Journal of Psychiatry*, **162**, 175–177.

Thompson, M., Arthur, C.L. & Dhaliwal, G.K. (1986) Liquid-Phase Piezoelectric and Acoustic Transmission Studies of Interfacial Immunochemistry. *Analytical Chemistry*, **58**, 1206–1209.

Tirumalai, R.S., Chan, K.C., Prieto, D.R.A., Issaq, H.J., Conrads, T.P. & Veenstra, T.D. (2003) Characterization of the low molecular weight human serum proteome. *Molecular & cellular proteomics : MCP*, **2**, 1096–1103.

Tolcher, A.W., Sweeney, C.J., Papadopoulos, K., Patnaik, A., Chiorean, E.G., Mita, A.C., Sankhala, K., Furfine, E., Gokemeijer, J., Iacono, L., Eaton, C., Silver, B.A. & Mita, M. (2011) Phase I and pharmacokinetic study of CT-322 (BMS-844203), a targeted adnectin inhibitor of VEGFR-2 based on a domain of human fibronectin. *Clinical Cancer Research*, **17**, 363–371.

Tomas, F.M., Knowles, S.E., Owens, P.C., Chandler, C.S., Francis, G.L., Read, L.C. & Ballard, F.J. (1992) Insulin-like growth factor-I (IGF-I) and especially IGF-I variants are anabolic in dexamethasone-treated rats. *Biochemical Journal*, **282**, 91–97.

Tomas, F.M., Lemmey, A.B., Read, L.C. & Ballard, F.J. (1996) Superior potency of infused IGF-I analogue which bind poorly to IGF-binding proteins is maintained when administered by injection. *Journal of Endocrinology*, **150**, 77–84.

Torrance, L., Ziegler, A., Pittman, H., Paterson, M., Toth, R. & Eggleston, I. (2006) Oriented immobilisation of engineered single-chain antibodies to develop biosensors for virus detection. *Journal of Virological Methods*, **134**, 164–170.

Trautinger, F. (2001) Heat shock proteins in the photobiology of human skin. *Journal of Photochemistry and Photobiology B: Biology*, **63**, 70–77.

Travia, R., Watts, E., Fensom, G., Perez-Cornago, A., Knuppel, A., Allen, N., Gunter, M., Martin, R., Byrne, K.S., Murphy, N., Tsilidis, K. & Key, T. (2019) *Serum hormones and prostate cancer incidence and mortality in UK Biobank [abstract]*. *NCRI Cancer Conference*,.

Tsokos, M., Reichelt, U., Jung, R., Nierhaus, A. & Püschel, K. (2001) Interleukin-6 and C-reactive protein serum levels in sepsis-related fatalities during the early postmortem period. *Forensic Science International*, **119**, 47–56.

Tsumoto, K., Shinoki, K., Kondo, H., Uchikawa, M., Juji, T. & Kumagai, I. (1998) Highly efficient recovery of functional single-chain Fv fragments from inclusion bodies overexpressed in Escherichia coli by controlled introduction of oxidizing reagent - Application to a human single-chain Fv fragment. *Journal of Immunological Methods*, **219**, 119–129.

Tuerk, C. & Gold, L. (1990) Systematic evolution of ligands by exponential enrichment: RNA ligands to bacteriophage T4 DNA polymerase. *Science*, **249**, 505–510.

UniProtKB.

Ünsal, E., Köksal, D., Selim Yurdakul, A., Atikcan, Ş. & Cinaz, P. (2005) Analysis of insulin like growth factor 1 and insulin like growth factor binding protein 3 levels in bronchoalveolar lavage fluid and serum of patients with lung cancer. *Respiratory Medicine*, **99**, 559–565.

Urusov, A.E., Zherdev, A. v. & Dzantiev, B.B. (2019) Towards lateral flow quantitative assays: Detection approaches. *Biosensors*, **9**.

US20020055186A1 - Detection of peptides - Google Patents.

Vasques, G.A., Andrade, N.L.M., Correa, F.A. & Jorge, A.A.L. (2019) Update on new GH-IGF axis genetic defects. *Archives of Endocrinology and Metabolism*, **63**, 608–617.

Vatten, L.J., Holly, J.M., Gunnell, D. & Tretli, S. (2008) Nested case-control study of the association of circulating levels of serum insulin-like growth factor I and insulin-like

growth factor binding protein 3 with breast cancer in young women in Norway. *Cancer Epidemiology Biomarkers and Prevention*, **17**, 2097–2100.

Verma, S., Venkatesh, V., Kumar, R., Kashyap, S., Kumar, M., Maurya, A.K., Dhole, T.N. & Singh, M. (2019) Etiological agents of diarrhea in hospitalized pediatric patients with special emphasis on diarrheagenic Escherichia coli in North India. *Journal of Laboratory Physicians*, **11**, 068–074.

Vermeulen, A., Kaufman, J.M. & Giagulli, V.A. (1996) Influence of some biological indexes on sex hormone-binding globulin and androgen levels in aging or obese males. *The Journal of Clinical Endocrinology & Metabolism*, **81**, 1821–1826.

Vircell - vircell.com.

Vita, R., Zarebski, L., Greenbaum, J.A., Emami, H., Hoof, I., Salimi, N., Damle, R., Sette, A. & Peters, B. (2009) The Immune Epitope Database 2.0. *Nucleic Acids Research*, **38**, D854–D862.

Voura, E.B., Jaiswal, J.K., Mattoussi, H. & Simon, S.M. (2004) Tracking metastatic tumor cell extravasation with quantum dot nanocrystals and fluorescence emission-scanning microscopy. *Nature Medicine*, **10**, 993–998.

Vu, T.Q., Lam, W.Y., Hatch, E.W. & Lidke, D.S. (2015) Quantum dots for quantitative imaging: from single molecules to tissue. *Cell and Tissue Research*, **360**, 71–86.

Wallace, J.D., Cuneo, R.C., Baxter, R., Ørskov, H., Keay, N., Pentecost, C., Dall, R., Rosén, T., Jørgensen, J.O., Cittadini, A., Longobardi, S., Sacca, L., Christiansen, J.S., Bengtsson, B.-Å. & Sönksen, P.H. (1999) Responses of the Growth Hormone (GH) and Insulin-Like Growth Factor Axis to Exercise, GH Administration, and GH Withdrawal in Trained Adult Males: A Potential Test for GH Abuse in Sport [1]. *The Journal of Clinical Endocrinology & Metabolism*, **84**, 3591–3601.

Wallace, J.D., Cuneo, R.C., Lundberg, P.A., Rosén, T., Jørgensen, J.O.L., Longobardi, S., Keay, N., Sacca, L., Christiansen, J.S., Bengtsson, B.-A. & Sönksen, P.H. (2000) Responses of Markers of Bone and Collagen Turnover to Exercise, Growth Hormone (GH) Administration, and GH Withdrawal in Trained Adult Males1. *The Journal of Clinical Endocrinology & Metabolism*, **85**, 124–133.

Wang, Q., Liu, Y., Wang, M., Chen, Y. & Jiang, W. (2018) A multiplex immunochromatographic test using gold nanoparticles for the rapid and simultaneous detection of four nitrofuran metabolites in fish samples. *Analytical and Bioanalytical Chemistry*, **410**, 223–233.

Wang, S.H., Zhang, J. bin, Zhang, Z.P., Zhou, Y.F., Yang, R.F., Chen, J., Guo, Y.C., You, F. & Zhang, X.E. (2006) Construction of single chain variable fragment (ScFv) and BiscFv-alkaline phosphatase fusion protein for detection of Bacillus Anthracis. *Analytical Chemistry*, **78**, 997–1004.

Ward, E.S. (1992) Antibody engineering: the use of *Escherichia coli* as an expression host. *The FASEB Journal*, **6**, 2422–2427.

Weidle, U.H., Auer, J., Brinkmann, U., Georges, G. & Tiefenthaler, G. (2013) The emerging role of new protein scaffold-based agents for treatment of cancer. *Cancer Genomics and Proteomics*, **10**, 155–168.

Wen, T., Huang, C., Shi, F.J., Zeng, X.Y., Lu, T., Ding, S.N. & Jiao, Y.J. (2020) Development of a lateral flow immunoassay strip for rapid detection of IgG antibody against SARS-CoV-2 virus. *Analyst*, **145**, 5345–5352.

Werner, H., Sarfstein, R., Nagaraj, K. & Laron, Z. (2020) Laron Syndrome Research Paves the Way for New Insights in Oncological Investigation. *Cells*, **9**.

Westman, M.E., Paul, A., Malik, R., McDonagh, P., Ward, M.P., Hall, E. & Norris, J.M. (2016) Seroprevalence of feline immunodeficiency virus and feline leukaemia virus in Australia: risk factors for infection and geographical influences (2011–2013). *Journal of Feline Medicine and Surgery Open Reports*, **2**, 205511691664638.

Weyer, C., Funahashi, T., Tanaka, S., Hotta, K., Matsuzawa, Y., Pratley, R.E. & Tataranni, P.A. (2001) Hypoadiponectinemia in Obesity and Type 2 Diabetes: Close Association with Insulin Resistance and Hyperinsulinemia. *The Journal of Clinical Endocrinology & Metabolism*, **86**, 1930–1935.

W.H.P.M. Inc. - whpm.com.

Willets, K.A., Nishimura, S.Y., Schuck, P.J., Twieg, R.J. & Moerner, W.E. (2005) Nonlinear optical chromophores as nanoscale emitters for single-molecule spectroscopy. *Accounts of Chemical Research*, **38**, 549–556.

Wilson, C.M. (1979) Studies and critique of amido black 10B, Coomassie blue R, and fast green FCF as stains for proteins after polyacrylamide gel electrophoresis. *Analytical Biochemistry*, **96**, 263–278.

Wilson, D.S., Keefe, A.D. & Szostak, J.W. (2001) The use of mRNA display to select high-affinity protein-binding peptides. *Proceedings of the National Academy of Sciences of the United States of America*, **98**, 3750–3755.

Winter, G. (2019) Harnessing Evolution to Make Medicines (Nobel Lecture). *Angewandte Chemie - International Edition*, **58**, 14438–14445.

WO2002025287A3 - Detection of peptides - Google Patents.

Woodson, K., Tangrea, J.A., Pollak, M., Copeland, T.D., Taylor, P.R., Virtamo, J. & Albanes, D. (2003) Serum insulin-like growth factor I: Tumor marker or etiologic factor? A prospective study of prostate cancer among Finnish men. *Cancer Research*, **63**, 3991–3994.

Wu, A.H.B., Smith, A., Christenson, R.H., Murakami, M.M. & Apple, F.S. (2004) Evaluation of a point-of-care assay for cardiac markers for patients suspected of acute myocardial infarction. *Clinica Chimica Acta*, **346**, 211–219.

Wu, X., Liu, H., Liu, J., Haley, K.N., Treadway, J.A., Larson, J.P., Ge, N., Peale, F. & Bruchez, M.P. (2003) Immunofluorescent labeling of cancer marker Her2 and other cellular targets with semiconductor quantum dots. *Nature Biotechnology*, **21**, 41–46.

Wu, X., Song, Z., Zhai, X., Zuo, L., Mei, X., Xiang, R., Kang, Z., Zhou, L. & Wang, H. (2019) Simultaneous and visual detection of infectious bronchitis virus and Newcastle disease virus by multiple LAMP and lateral flow dipstick. *Poultry Science*, **98**, 5401–5411.

Wurch, T., Pierré, A. & Depil, S. (2012) Novel protein scaffolds as emerging therapeutic proteins: From discovery to clinical proof-of-concept. *Trends in Biotechnology*, **30**, 575–582.

Xia, X., Xu, Y., Zhao, X. & Li, Q. (2009) Lateral flow immunoassay using europium chelate-loaded silica nanoparticles as labels. *Clinical Chemistry*, **55**, 179–182.

Xing, C., Liu, L., Song, S., Feng, M., Kuang, H. & Xu, C. (2015) Ultrasensitive immunochromatographic assay for the simultaneous detection of five chemicals in drinking water. *Biosensors and Bioelectronics*, **66**, 445–453.

Yahaya, M.L., Zakaria, N.D., Noordin, R. & Abdul Razak, K. (2020) Development of rapid gold nanoparticles based lateral flow assays for simultaneous detection of Shigella and Salmonella genera. *Biotechnology and Applied Biochemistry*.

Yakar, S., Liu, J.L.I., Stannard, B., Butler, A., Accili, D., Sauer, B. & Leroith, D. (1999) Normal growth and development in the absence of hepatic insulin-like growth factor I. *Proceedings of the National Academy of Sciences of the United States of America*, **96**, 7324–7329.

Yalow, R.S. & Yalow, A.A. (1980) The physics of radioimmunoassay. *Transactions of the New York Academy of Sciences*, **40**, 253–266.

Yang, S., Alnaqeeb, M., Simpson, H. & Goldspink, G. (1997) Changes in muscle fibre type, muscle mass and IGF-I gene expression in rabbit skeletal muscle subjected to stretch. *Journal of Anatomy*, **190**, 613–622.

Yang, S., Alnaqeeb, M., Simpson, H. & Goldspink, G. (1996) Cloning and characterization of an IGF-1 isoform expressed in skeletal muscle subjected to stretch. *Journal of Muscle Research and Cell Motility*, **17**, 487–495.

Yang, S.Y. & Goldspink, G. (2002) Different roles of the IGF-I Ec peptide (MGF) and mature IGF-I in myoblast proliferation and differentiation. *FEBS Letters*, **522**, 156–160.

Yang, Y., Liang, S., Li, Y., Gao, F., Cao, Y., Zhao, X., Gao, G. & Li, L. (2019) Effects of early administration of insulin-like growth factor-1 on cognitive function in septic encephalopathy. *Neuropsychiatric Disease and Treatment*, **15**, 323–337.

Yannakoulia, M., Yiannakouris, N., Blüher, S., Matalas, A.-L., Klimis-Zacas, D. & Mantzoros, C.S. (2003) Body Fat Mass and Macronutrient Intake in Relation to Circulating Soluble Leptin Receptor, Free Leptin Index, Adiponectin, and Resistin Concentrations in Healthy Humans. *The Journal of Clinical Endocrinology & Metabolism*, **88**, 1730–1736.

Yeh, F.L., Lin, W.L. & Shen, H.D. (2000) Changes in circulating levels of an anti-inflammatory cytokine interleukin 10 in burned patients. *Burns*, **26**, 454–459.

Yeh, F.L., Shen, H.D. & Fang, R.H. (2002) Deficient transforming growth factor β and interleukin-10 responses contribute to the septic death of burned patients. *Burns*, **28**, 631–637.

Ylera, F., Harth, S., Waldherr, D., Frisch, C. & Knappik, A. (2013) Off-rate screening for selection of high-affinity anti-drug antibodies. *Analytical Biochemistry*, **441**, 208–213.

Yoon, C.H., Cho, J.H., Oh, H. il, Kim, M.J., Lee, C.W., Choi, J.W. & Paek, S.H. (2003) Development of a membrane strip immunosensor utilizing ruthenium as an electro-chemiluminescent signal generator. *Biosensors and Bioelectronics*, **19**, 289–296.

Young, B., Gleeson, M. & Cripps, A.W. (1991) C-reactive protein: A critical review. *Pathology*, **23**, 118–124.

Young, L., Jernigan, R.L. & Covell, D.G. (1994) A role for surface hydrophobicity in protein-protein recognition. *Protein Science*, **3**, 717–729.

Yu, H., Mistry, J., Nicar, M.J., Khosravi, M.J., Diamandis, A., van Doorn, J. & Juul, A. (1999) Insulin-like growth factors (IGF-I, free IGF-I, and IGF-II) and insulin- like growth factor binding proteins (IGFBP-2, IGFBP-3, IGFBP-6, and ALS) in blood circulation. *Journal of Clinical Laboratory Analysis*, **13**, 166–172.

Yu, Y., Mitchell, S., Lynaugh, H., Brown, M., Paul Nobrega, R., Zhi, X., Sun, T., Caffry, I., Cao, Y., Yang, R., Burnina, I., Xu, Y. & Estep, P. (2016) Understanding fortebio's sensors for high-throughput kinetic and epitope screening for purified antibodies and yeast culture supernatant. *Journal of Biomolecular Screening*, **21**, 88–95.

Yukawa, H. & Baba, Y. (2017) In Vivo Fluorescence Imaging and the Diagnosis of Stem Cells Using Quantum Dots for Regenerative Medicine. *Analytical Chemistry*, **89**, 2671–2681.

Zahnd, C., Kawe, M., Stumpp, M.T., de Pasquale, C., Tamaskovic, R., Nagy-Davidescu, G., Dreier, B., Schibli, R., Binz, H.K., Waibel, R. & Plückthun, A. (2010) Efficient tumor targeting with high-affinity designed ankyrin repeat proteins: Effects of affinity and molecular size. *Cancer Research*, **70**, 1595–1605.

Zampelas, A., Panagiotakos, D.B., Pitsavos, C., Chrysohoou, C. & Stefanadis, C. (2004) Associations between coffee consumption and inflammatory markers in healthy persons: The ATTICA study. *American Journal of Clinical Nutrition*, **80**, 862–867.

Zhai, H., Yao, Y. & Lu, L. (1999) The relationship between tissue tumor necrosis factor-alpha(TNF-alpha) mRNA expression and gut-derived endotoxemia in rats after thermal injury. *Zhonghua zheng xing shao shang wai ke za zhi = Zhonghua zheng xing shao shang waikf [i.e. waike] zazhi = Chinese journal of plastic surgery and burns / [Chung-hua cheng hsing shao shang wai k'o tsa chih pien chi wei yüan hui pien chi]*, **15**, 424–427.

Zhang, F., Dulneva, A., Bailes, J. & Soloviev, M. (2010) Affinity peptidomics: Peptide selection and affinity capture on hydrogels and microarrays. *Methods in molecular biology (Clifton, N.J.)*, **615**, 313–344.

Zhang, N., Ahsan, M.H., Purchio, A.F. & West, D.B. (2005) Serum Amyloid A-Luciferase Transgenic Mice: Response to Sepsis, Acute Arthritis, and Contact Hypersensitivity and the Effects of Proteasome Inhibition. *The Journal of Immunology*, **174**, 8125–8134.

Zhang, Y., Proenca, R., Maffei, M., Barone, M., Leopold, L. & Friedman, J.M. (1994) Positional cloning of the mouse obese gene and its human homologue. *Nature*, **372**, 425–432.

Zhao, Y., Wang, H., Zhang, P., Sun, C., Wang, X., Wang, X., Yang, R., Wang, C. & Zhou, L. (2016) Rapid multiplex detection of 10 foodborne pathogens with an up-converting phosphor technology-based 10-channel lateral flow assay. *Scientific Reports*, **6**, 1–8.

Zheng, X., Baker, H. & Hancock, W.S. (2006) Analysis of the low molecular weight serum peptidome using ultrafiltration and a hybrid ion trap-Fourier transform mass spectrometer. *Journal of Chromatography A*, **1120**, 173–184.

Zhou, D., Munster, A. & Winchurch, R.A. (1991) Pathologic concentrations of interleukin 6 inhibit T cell responses via induction of activation of TGF-β. *The FASEB Journal*, **5**, 2582–2585.

Zhou, D.X., Zhao, Y., Baker, J.A., Gu, Q., Hamre, K.M., Yue, J., Jones, B.C., Cook, M.N. & Lu, L. (2017) The effect of alcohol on the differential expression of cluster of differentiation 14 gene, associated pathways, and genetic network. *PLOS ONE*, **12**, e0178689.

Zhu, B.L., Ishida, K., Quan, L., Li, D.R., Taniguchi, M., Fujita, M.Q., Maeda, H. & Tsuji, T. (2002) Pulmonary immunohistochemistry and serum levels of a surfactant-associated protein A in fatal drowning. *Legal Medicine*, **4**, 1–6.

Zhu, B.L., Ishida, K., Quan, L., Taniguchi, M., Oritani, S., Kamikodai, Y., Fujita, M.Q. & Maeda, H. (2001) Post-mortem urinary myoglobin levels with reference to the causes of death. *Forensic Science International*, **115**, 183–188.

Zhu, C., Chen, Z., Gao, S., Goh, B.L., Samsudin, I. bin, Lwe, K.W., Wu, Y., Wu, C. & Su, X. (2019) Recent advances in non-toxic quantum dots and their biomedical applications. *Progress in Natural Science: Materials International*, **29**, 628–640.

Ziganshin, R.H., Kovalchuk, S.I. & Azarkin, I. v. (2019) *Peptidomic workflow applied to cerebrospinal fluid analysis*. *Methods in Molecular Biology*, pp. 111–118. Humana Press Inc.

Zimmerli, L.U., Schiffer, E., Zürbig, P., Good, D.M., Kellmann, M., Mouls, L., Pitt, A.R., Coon, J.J., Schmieder, R.E., Peter, K.H., Mischak, H., Kolch, W., Delles, C. & Dominiczak, A.F. (2008) Urinary proteomic biomarkers in coronary artery disease. *Molecular and Cellular Proteomics*, **7**, 290–298.

Zitzmann, M. & Nieschlag, E. (2001) Testosterone levels in healthy men and the relation to behavioural and physical characteristics: Facts and constructs. *European Journal of Endocrinology*, **144**, 183–197.

Zuiderwijk, M., Tanke, H.J., Niedbala, R.S. & Corstjens, P.L.A.M. (2003) An amplification-free hybridization-based DNA assay to detect Streptococcus pneumoniae utilizing the up-converting phosphor technology. *Clinical Biochemistry*, **36**, 401–403.

Zürbig, P. & Mischak, H. (2008) Capillary electrophoresis coupled to mass spectrometry for biomarker discovery and diagnosis of kidney diseases. *Contributions to Nephrology*, **160**, 107–126.

Appendix:

Publications

Photostability of Semiconductor Quantum Dots in Response to UV Exposure

Bailes, J.

Nanoparticles in Biology and Medicine. Methods in Molecular Biology 2020; 2118:343-349. doi: 10.1007/978-1-0716-0319-2_25.

Abstract:

The interest in quantum dots (QDs) and their popularity in life science applications stems from their high photostability and unique optical properties such as superior light absorption. Photostability of semiconductor QDs is reportedly higher than that of organic dyes, but QDs may also be affected by light exposure. The outcome of such exposure may depend on many experimental factors, can lead to either an increase or decrease in the photoluminescent efficiency of QDs and is difficult to predict. QDs may therefore require experimental testing for their photostability especially prior to quantitative applications. A simple QD testing procedure described here showed a substantial degree of photobleaching when exposed to UV; nevertheless, the rate of change was noticeably lower than that measured for traditional organic dyes, as expected. The procedure reported is also applicable to traditional organic dyes and allows for quantitative comparisons to be conducted.

Affinity peptidomics and the selection of protein markers for the early non-invasive detection of breast cancer

Alsaidi, Y., **Bailes, J.** & Soloviev, M.

Poster: ELRIG Drug Discovery 2016 - Liverpool, United Kingdom,

Effect of gold nanoparticle conjugation on the activity and stability of functional proteins

Bailes, J., Gazi, S., Ivanova, R. & Soloviev, M.

Nanoparticles in Biology and Medicine. Methods in Molecular Biology 2012; 906:89-99. doi: 10.1007/978-1-61779-953-2_7.

Abstract:

Immobilization of functional proteins such as enzymes on solid surfaces produces a variety of effects ranging from the reversal and strong inhibition to the enhancement of protein stability and function. Such effects are protein-dependent and are affected by the physical and chemical properties of the surfaces. Functional consequences of protein immobilization on the surface of gold nanoparticles (AuNPs) are protein-dependent and require thorough investigation using suitable functional tests. However, traditional approaches to making control samples, i.e., immobilized protein vs. protein in solution in absence of any nanoparticles do not provide sufficiently identical reaction conditions and complicate interpretation of the results. This report provides advice and methods for preparing AuNP-conjugated preparations generally suitable for studying the effects of immobilization on the activity and stability of different functional proteins. We use bovine catalase to illustrate our approach, but the methods are easily adaptable to any other enzyme or protein. The AuNP-immobilized enzyme showed increased stability at elevated temperatures compared to the same enzyme in solution.

Gold nanoparticle antibody conjugates for use in competitive lateral flow assays

Bailes, J., Mayoss, S., Teale, P. & Soloviev, M.

Methods in Molecular Biology 2012; 906:45-55. doi: 10.1007/978-1-61779-953-2_4.

Abstract:

Gold nanoparticles (GNPs) are widely used in a variety of biomedical diagnostic assays and for imaging. Their popularity stems from key properties such as their low toxicity and high extinction coefficients, as well as straightforward synthesis methods that allow GNPs to be produced quickly and inexpensively. Here we describe the use of GNPs for visual detection in a lateral flow assay using benzodiazepine affinity assay to illustrate the methods.

The Application of Semiconductor Quantum Dots for Enhancing Peptide Desorption, Improving Peak Resolution and Sensitivity of Detection in Matrix-Assisted Laser Desorption/Ionization (MALDI) Mass Spectrometry

Bailes, J., Soloviev, M.

Methods in Molecular Biology 2012; 906:211-7. doi: 10.1007/978-1-61779-953-2_16.

Abstract:

The interest in quantum dots (QD) and a number of reported life sciences applications increased dramatically over the last decade. The popularity of QDs stems from better photostability, higher extinction -co-efficients, and unique optical properties such as superior light absorption. Here we report methods for improving matrix-assisted laser desorption/ionization desorption of crude tryptic protein digests by using CdSe/ZnS QDs. The addition of QDs to the matrix improves the signal-to-noise ratio, peak quality and increases the number of detected peptides and the overall sequence coverage.

Chip-Based Proteomics

Bailes, J., Milnthorpe, A., Smieszek, S. & Soloviev, M.

Molecular Analysis and Genome Discovery 2011; Rapley, R. & Harbron, S. (eds.). 2nd ed. p. 193-218 Ch.9

Abstract:

Characterization of the complement of expressed proteins from a single genome is a central focus of the evolving field of proteomics. Monitoring the expression and properties of a large number of proteins provides important information about the physiological state of a cell and an organism. A cell can express a large number of different proteins and the expression profile (the number of proteins expressed and their expression levels) varies in different cell types, explaining why different cells perform different functions. The central concept of modern proteomics is ‘multiplexing’, or a simultaneous analysis of all proteins in a defined protein population. However, since one genome produces many proteomes and the number of expressed genes in a single cell may exceed 10000, the characterization of thousands of proteins to evaluate proteomes ideally requires a high-throughput, automated process. This is why new improved methods for high-throughput protein identification and quantitation were needed. Many such technologies have been developed recently, led by advances in the electronics industry and more recently by the successes of the DNA chip-based technologies.

Serum Proteomics in the Diagnosis and Treatment of Haematological Malignancies

Smieszek, S., **Bailes, J.** & Soloviev, M.

Current Proteomics 2010; 7, 3, p. 195-208

Abstract:

Application of serum proteomics and peptidomics to the field of haematological malignancies can lead to an in depth understanding of the evolution of leukemogenesis, offering potential for early diagnosis, individualized and molecularly specific treatments, and disease surveillance through the monitoring of protein signatures. Currently, the limited understanding of aetiology prevents curative treatments for haematological malignancies. Until recently, the primary focus was on cytogenetics. Gene expression profiling and metaphase karyotyping has been done extensively, yet the lack of correlation between transcript and protein has limited the comprehensiveness of these approaches. Transcriptomics has dominated the field with significant emphasis being placed upon SNP genotyping, copy number variation analysis, DNA sequencing and methylation profiling. However, the integration of the existing knowledge with proteomics is needed to discover the molecular mechanisms of haematological malignancies and for the development of diagnostic tests. Proteomic analysis allows for direct assessment of the expressed, modified and degraded proteins. The Human Serum and Plasma Proteome Projects coupled with advancing technologies with increased sensitivity and throughput are beginning to produce productive breakthroughs including new markers for the detection of early stages of leukaemias and lymphomas. This review summarizes recent research efforts in the field of haematological malignancies, and examines relevant high throughput proteomic technologies, limitations, and pathophysiological background. A broader perspective on candidates for marker panels for the detection of malignant transformations is discussed.

Affinity peptidomics: Peptide selection and affinity capture on hydrogels and microarrays

Zhang, F., Dulneva, A., **Bailes, J.** & Soloviev, M.

Methods In Molecular Biology 2010; 615:313-44. doi: 10.1007/978-1-60761-535-4_23.

Introduction:

Affinity peptidomics relies on the successfully proven approach used widely in mass-spectrometry-based protein analysis, where protein samples are proteolytically digested prior to the analysis. Unlike traditional proteomic analyses, affinity peptidomics employs affinity detection instead of, or in addition to, the mass-spectrometry detection. Affinity peptidomics, therefore, bridges the gap between protein microarrays and mass spectrometry and can be used for the detection, identification and quantification of endogenous or proteolytic peptides on microarrays and by MALDI-MS. Phage display technology is a widely applicable generic molecular display method suitable for studying protein-protein or protein-peptide interactions and the development of recombinant affinity reagents. Phage display complements the affinity peptidomics approach when the latter is used, e.g. to characterise a repertoire of antigenic determinants of polyclonal, monoclonal antibodies or other recombinantly obtained affinity reagents or in studying protein-protein interactions. 3D materials such as membrane-based porous substrates and acrylamide hydrogels provide convenient alternatives and are superior to many 2D surfaces in maintaining protein conformation and minimising non-specific interactions. Hydrogels have been found to be advantageous in performing antibody affinity assays and peptide-binding assays. Here we report a range of peptide selection and peptide-binding assays used for the detection, quantification or validation of peptide targets using array-based techniques and fluorescent or MS detection.

Binary polypeptide system for permanent and oriented protein immobilization

Ferrari, E., Darios, F., Zhang, F., Niranjan, D., **Bailes, J.**, Soloviev, M. & Davletov, B.
Journal of Nanobiotechnology 2010 May 12;8:9. doi: 10.1186/1477-3155-8-9.

Abstract:
BACKGROUND: Many techniques in molecular biology, clinical diagnostics and biotechnology rely on binary affinity tags. The existing tags are based on either small molecules (e.g., biotin/streptavidin or glutathione/GST) or peptide tags (FLAG, Myc, HA, Strep-tag and His-tag). Among these, the biotin-streptavidin system is most popular due to the nearly irreversible interaction of biotin with the tetrameric protein, streptavidin. The major drawback of the stable biotin-streptavidin system, however, is that neither of the two tags can be added to a protein of interest via recombinant means (except for the Strep-tag case) leading to the requirement for chemical coupling.
RESULTS: Here we report a new immobilization system which utilizes two monomeric polypeptides which self-assemble to produce non-covalent yet nearly irreversible complex which is stable in strong detergents, chaotropic agents, as well as in acids and alkali. Our system is based on the core region of the tetra-helical bundle known as the SNARE (soluble N-ethylmaleimide-sensitive factor attachment protein receptor) complex. This irreversible protein attachment system (IPAS) uses either a shortened syntaxin helix and fused SNAP25-synaptobrevin or a fused syntaxin-synaptobrevin and SNAP25 allowing a two-component system suitable for recombinant protein tagging, capture and immobilization. We also show that IPAS is suitable for use with traditional beads and chromatography, planar surfaces and BIAcore, gold nanoparticles and for protein-protein interaction in solution.
CONCLUSIONS: IPAS offers an alternative to chemical cross-linking, streptavidin-biotin system and to traditional peptide affinity tags and can be used for a wide range of applications in nanotechnology and molecular sciences.

Quantum dots improve peptide detection in MALDI MS in a size dependent manner

Bailes, J., Vidal, L., Ivanov, D. A. & Soloviev, M.

Journal of Nanobiotechnology 2009 Dec 31;7:10. doi: 10.1186/1477-3155-7-10.

Abstract:

Laser Desorption Ionization Mass Spectrometry employs matrix which is co-crystallised with the analyte to achieve "soft ionization" that is the formation of ions without fragmentation. A variety of matrix-free and matrix-assisted LDI techniques and matrices have been reported to date. LDI has been achieved using ultra fine metal powders (UFMPs), desorption ionisation on silicon (DIOS), sol-gel assisted laser desorption/ionization (SGALDI), as well as with common MALDI matrices such as 2,5-dihydroxy benzoic acid (DHB), 3,5-dimethoxy-4-hydroxycinnamic acid (SA), alpha-cyano-4-hydroxycinnamic acid (CHCA) to name a few. A variety of matrix additives have been shown to improve matrix assisted desorption, including silicon nanowires (SiNW), carbon nanotubes (CNT), metal nanoparticles and nanodots. To our knowledge no evidence exists for the application of highly fluorescent CdSe/ZnS quantum dots to enhance MALDI desorption of biological samples. Here we report that although CdSe/ZnS quantum dots on their own cannot substitute matrix in MALDI-MS, their presence has a moderately positive effect on MALDI desorption, improves the signal-to-noise ratio, peak quality and increases the number of detected peptides and the overall sequence coverage.

Affinity peptidomics approach to protein detection, quantification, and protein affinity assays: Application to forensics and biometrics

Bailes, J. & Soloviev M.

Peptidomics: Methods and Applications 2008; Soloviev, M., Shaw, C. & Andrén P. (eds.). UK: John Wiley & Sons, Ltd, p. 1931-231 Ch.10

Introduction:

Deciphering the proteome is a huge undertaking that involves not only the identification of the proteins themselves but also all their varying isoforms that result from numerous post-translational modifications. Learning how these proteins interact with each other coupled with the causes and effects of changes to their expression patterns is critical for progress in numerous areas, not least in disease research and biomarker and drug discovery. Single protein assays have been proposed for forensic analysis before, but so far such bioassays were limited mostly to PCR-based DNA "fingerprinting". Furthermore, no technical capabilities existed until very recently for achieving highly parallel and quantitative analysis of proteins and especially for scene-of-crime assays. In order to tackle such challenges, researchers require technology capable of quantitatively assaying complex protein samples. Such technologies ideally possess a number of desirable features: high-throughput, speed, accuracy and reproducibility, and increasingly sort after, the ability to multiplex so that multiple different targets can be tested simultaneously.

Protein profiling for forensic and biometric applications

Soloviev M., **Bailes, J.**, Salata N. & Finch P.

Molecular Forensics 2007 Rapley, R. & Whitehouse, D. (eds.). UK: John Wiley & Sons, Ltd, p. 197-220 Ch.13

Introduction:

This Chapter evaluates the usability of known protein markers for quantitative protein profiling assays applicable to forensic and biometric applications. We will discuss the use of Competitive Displacement Assays (CDA) and Peptidomics technology in the design of multiplex protein assays for lab-based and potentially scene-of-crime applications. CDA embody the most accurate multiplex protein affinity assay system to date, applicable to a wide range of protein profiling applications. The Peptidomics technology is the most generic and multiplatform-compatible affinity assay system to date, applicable for protein identification, quantification and expression profiling. It relies on proteolytic protein digestion, requires only the availability of small peptide fragment(s) and is therefore capable of a reliable analysis of denatured, partially-degraded proteins and protein fragments. Protein microarrays and peptidomics are combined in a single system capable of simple yet quantitative protein analysis from real samples (i.e. imperfectly stored, partially degraded samples, scene of crime applications etc).

Selection of tryptic peptide antigens

Myoglobin

A

MYOGLOBIN
154 a.a.
UniProtKB ID: **P02144**

MGLSDGEWQL VLNVWGKVEA DIPGHGQEVL
IRLFKGHPET LEKFDKFKHL KSEDEMKASE
DLKKHGATVL TALGGILKKK GHHEAEIKPL
AQSHATKHKI PVKYLEFISE CIIQVLQSKH
PGDFGADAQG AMNKALELFR KDMASNYKEL
GFQG

Kyte & Doolittle Score: -0.48

B

Mass	Position	Sequence
1800.93	2–17	GLSDGEWQLVLNVWGK
1632.87	18–32	VEADIPGHGQEVLIR
407.27	33–35	LFK
910.46	36–43	GHPETLEK
409.21	44–46	FDK
294.18	47–48	FK
397.26	49–51	HLK
738.30	52–57	SEDEMK
662.34	58–63	ASEDLK
147.11	64–64	K
1350.81	65–78	HGATVLTALGGILK
147.11	79–79	K
147.11	80–80	K
1853.96	81–97	GHHEAEIKPLAQSHATK
284.17	98–99	HK
456.32	100–103	IPVK
1913.01	104–119	YLEFISECIIQVLQSK
1515.66	**120–134**	**HPGDFGADAQGAMNK**
748.44	135–140	ALELFR
147.11	141–141	K
828.36	142–148	DMASNYK
650.31	149–154	ELGFQG

D

PEPTIDE ANTIGEN

Tryptic peptide:
HPGDFGADAQGAMNK

Synthetic peptide:
Biotin-CGDFGADAQGAMNK

Hydrophilicity change:
-0.012

C

	A	C	D	E	F	G	H	I	J	K	L	M	N	O	P	Q	R	S	T	U	V
	seq into the cells below	RANK	SET RANGE	9	16	Read K&D	RANK	Amino acid positions with individual K&D scores shown below. do not hcnage the table o													
	to 1000 rows with gaps	all peptides	PEP LENGTH	Suitable				1	2	3	4	5	6	7	8	9	10	11	12	13	1
3	GLSDGEWQLVLNVWGK	16	16		YES	-0.12	2	-0.40	3.80	-0.80	-3.50	-0.40	-3.50	-0.90	-3.50	3.80	4.20	3.80	-3.50	4.20	-0.9
4	VEADIPGHGQEVLIR	17	15		YES	-0.07	3	4.20	-3.50	1.80	-3.50	4.50	-1.60	-0.40	-3.20	-0.40	-3.50	-3.50	4.20	3.80	4.5
5	LFK	21	3		NO			3.80	2.80	-3.90											
6	GHPETLEK	7	8		NO			-0.40	-3.20	-1.60	-3.50	-0.70	3.80	-3.50	-3.90						
7	FDK	8	3		NO			2.80	-3.50	-3.90											
8	FK	14	2		NO			2.80	-3.90												
9	HLK	10	3		NO			-3.20	3.80	-3.90											
10	SEDEMK	6	6		NO			-0.80	-3.50	-3.50	-3.50	1.90	-3.90								
11	ASEDLK	12	6		NO			1.80	-0.80	-3.50	-3.50	3.80	-3.90								
12	K	1	1		NO			-3.90													
13	HGATVLTALGGILK	22	14		YES	1.00	5	-3.20	-0.40	1.80	-0.70	4.20	3.80	-0.70	1.80	3.80	-0.40	-0.40	4.50	3.80	-3.9
14	K	1	1		NO			-3.90													
15	K	1	1		NO			-3.90													
16	GHHEAEIKPLAQSHATK	11	17		NO			-0.40	-3.20	-3.20	-3.50	1.80	-3.50	4.50	-3.90	-1.60	3.80	1.80	-3.50	-0.80	-3.2
17	HK	5	2		NO			-3.20	-3.90												
18	IPVK	20	4		NO			4.50	-1.60	4.20	-3.90										
19	YLEFISECIIQVLQSK	18	16		YES	0.61	4	-1.30	3.80	-3.50	2.80	4.50	-0.80	-3.50	2.50	4.50	4.50	-3.50	4.20	3.80	-3.5
20	HPGDFGADAQGAMNK	13	15		YES	-0.92	1	-3.20	-1.60	-0.40	-3.50	2.80	-0.40	1.80	-3.50	1.80	-3.50	-0.40	1.80	1.90	-3.5
21	ALELFR	19	6		NO			1.80	3.80	-3.50	3.80	2.80	-4.50								
22	K	1	1		NO			-3.90													
23	DMASNYK	9	7		NO			-3.50	1.90	1.80	-0.80	-3.50	-1.30	-3.90							
24	ELGFQG	15	6		NO			-3.50	3.80	-0.40	2.80	-3.50	-0.40								
25																					

Tumour necrosis factor alpha

A

TUMOUR NECROSIS FACTOR ALPHA
233 a.a.
UniProtKB ID: **P01375**

MSTESMIRDV ELAEEALPKK TGGPQGSRRC
LFLSLFSFLI VAGATTLFCL LHFGVIGPQR
EEFPRDLSLI SPLAQAVRSS SRTPSDKPVA
HVVANPQAEG QLQWLNRRAN ALLANGVELR
DNQLVVPSEG LYLIYSQVLF KGQGCPSTHV
LLTHTISRIA VSYQTKVNLL SAIKSPCQRE
TPEGAEAKPW YEPIYLGGVF QLEKGDRLSA
EINRPDYLDF AESGQVYFGI IAL

Kyte & Doolittle Score: -0.05

B

Mass	Position	Sequence
954.44	1–8	MSTESMIR
1213.63	9–19	DVELAEEALPK
147.11	20–20	K
759.37	21–28	TGGPQGSR
175.12	29–29	R
3383.84	30–60	CLFLSLFSFLIVAGATTLFCLLHFGVIGPQR
677.33	61–65	EEFPR
1382.80	66–78	DLSLISPLAQAVR
436.22	79–82	SSSR
2755.43	**83–107**	**TPSDKPVAHVVANPQAEGQLQWLNR**
175.12	108–108	R
1240.70	109–120	ANALLANGVELR
2425.30	121–141	DNQLVVPSEGLYLIYSQVLFK
1806.93	142–158	GQGCPSTHVLLTHTISR
909.50	159–166	IAVSYQTK
857.55	167–174	VNLLSAIK
590.27	175–179	SPCQR
2851.42	180–204	ETPEGAEAKPWYEPIYLGGVFQLEK
347.17	205–207	GDR
2901.47	208–233	LSAEINRPDYLDFAESGQVYFGIIAL
954.44	1–8	MSTESMIR
1213.63	9–19	DVELAEEALPK

D

PEPTIDE ANTIGEN

Tryptic peptide:
QAEGQLQWLNR

Synthetic peptide:
Biotin-CGQAEGQLQWLNR

Hydrophilicity change:
+0.860

C

	A	B	C	D	E	F	G	H	I	J	K	L	M	N	O	P	Q
	Paste seq into the cells below	Read the K&D	RANK	SET RANGE	9	16	Read K&D	RANK	Amino acid positions with individual K&D scores shown								
	Up to 1000 rows with gaps	score below	all peptides	PEP LENGTH		Suitable			1	2	3	4	5	6	7	8	
3	MSTESMIR	-0.25	14	8		NO			1.90	-0.80	-0.70	-3.50	-0.80	1.90	4.50	-4.50	
4	DVELAEEALPK	-0.37	12	11		YES	-0.37	2	-3.50	4.20	-3.50	3.80	1.80	-3.50	-3.50	1.80	3.8
5	K	-3.90	3	1		NO			-3.90								
6	TGGPQGSR	-1.54	8	8		NO			-0.70	-0.40	-0.40	-1.60	-3.50	-0.40	-0.80	-4.50	
7	R	-4.50	1	1		NO			-4.50								
8	CLFLSLFSFLIVAGATTLFCLLHFGVIGF	1.60	22	31		NO			2.50	3.80	2.80	3.80	-0.80	3.80	2.80	-0.80	2.8
9	EEFPR	-2.06	5	5		NO			-3.50	-3.50	2.80	-1.60	-4.50				
10	DLSLISPLAQAVR	0.69	20	13		YES	0.69	5	-3.50	3.80	-0.80	3.80	4.50	-0.80	-1.60	3.80	1.8
11	SSSR	-1.73	6	4		NO			-0.80	-0.80	-0.80	-4.50					
12	TPSDKPVAHVVANPQAEGQLQWLNR	-0.72	10	25		NO			-0.70	-1.60	-0.80	-3.50	-3.90	-1.60	4.20	1.80	-3.2
13	R	-4.50	1	1		NO			-4.50								
14	ANALLANGVELR	0.47	19	12		YES	0.47	4	1.80	-3.50	1.80	3.80	3.80	1.80	-3.50	-0.40	4.2
15	DNQLVVPSEGLYLIYSQVLFK	0.36	18	21		NO			-3.50	-3.50	-3.50	3.80	4.20	4.20	-1.60	-0.80	-3.5
16	GQGCPSTHVLLTHTISR	-0.10	15	17		NO			-0.40	-3.50	-0.40	2.50	-1.60	-0.80	-0.70	-3.20	4.2
17	IAVSYQTK	0.04	16	8		NO			4.50	1.80	4.20	-0.80	-1.30	-3.50	-0.70	-3.90	
18	VNLLSAIK	1.24	21	8		NO			4.20	-3.50	3.80	3.80	-0.80	1.80	4.50	-3.90	
19	SPCQR	-1.58	7	5		NO			-0.80	-1.60	2.50	-3.50	-4.50				
20	ETPEGAEAKPWYEPIYLGGVFQLEK	-0.65	11	25		NO			-3.50	-0.70	-1.60	-3.50	-0.40	1.80	-3.50	1.80	-3.5
21	GDR	-2.80	4	3		NO			-0.40	-3.50	-4.50						
22	LSAEINRPDYLDFAESGQVYFGIIAL	0.31	17	26		NO			3.80	-0.80	1.80	-3.50	4.50	-3.50	-4.50	-1.60	-3.5
23	TPSDKPVAHVVANP	-0.30	13	14		YES	-0.30	3	-0.70	-1.60	-0.80	-3.50	-3.90	-1.60	4.20	1.80	-3.2
24	QAEGQLQWLNR	-1.26	9	11		YES	-1.26	1	-3.50	1.80	-3.50	-0.40	-3.50	3.80	-3.50	-0.90	3.8

Fibrinogen A

A

FIBRINOGEN A
866 a.a.
UniProtKB ID: **P02671**

MFSMRIVCLV LSVVGTAWTA DSGEGDFLAE GGGVRGPRVV
ERHQSACKDS DWPFCSDEDW NYKCPSGCRM KGLIDEVNQD
FTNRINKLKN SLFEYQKNNK DSHSLTTNIM EILRGDFSSA
NNRDNTYNRV SEDLRSRIEV LKRKVIEKVQ HIQLLQKNVR
AQLVDMKRLE VDIDIKIRSC RGSCSRALAR EVDLKDYEDQ
QKQLEQVIAK DLLPSRDRQH LPLIKMKPVP DLVPGNFKSQ
LQKVPPEWKA LTDMPQMRME LERPGGNEIT RGGSTSYGTG
SETESPRNPS SAGSWNSGSS GPGSTGNRNP GSSGTGGTAT
WKPGSSGPGS TGSWNSGSSG TGSTGNQNPG SPRPGSTGTW
NPGSSERGSA GHWTSESSVS GSTGQWHSES GSFRPDSPGS
GNARPNNPDW GTFEEVSGNV SPGTRREYHT EKLVTSKGDK
ELRTGKEKVT SGSTTTTRRS CSKTVTKTVI GPDGHKEVTK
EVVTSEDGSD CPEAMDLGTL SGIGTLDGFR HRHPDEAAFF
DTASTGKTFP GFFSPMLGEF VSETESRGSE SGIFTNTKES
SSHHPGIAEF PSRGKSSSYS KQFTSSTSYN RGDSTFESKS
YKMADEAGSE ADHEGTHSTK RGHAKSRPVR DCDDVLQTHP
SGTQSGIFNI KLPGSSKIFS VYCDQETSLG GWLLIQQRMD
GSLNFNRTWQ DYKRGFGSLN DEGEGEFWLG NDYLHLLTQR
GSVLRVELED WAGNEAYAEY HFRVGSEAEG YALQVSSYEG
TAGDALIEGS VEEGAEYTSH NNMQFSTFDR DADQWEENCA
EVYGGGWWYN NCQAANLNGI YYPGGSYDPR NNSPYEIENG
VVWVSFRGAD YSLRAVRMKI RPLVTQ

Kyte & Doolittle Score: -0.82

B

Mass	Position	Sequence
488.31	145-148	VIEK
1106.67	149-157	VQHIQLLQK
388.23	158-160	NVR
804.43	161-167	AQLVDMK
175.12	168-168	R
944.53	169-176	LEVDIDIK
288.20	177-178	IR
365.16	179-181	SCR
509.21	182-186	GSCSR
430.28	187-190	ALAR
603.33	191-195	EVDLK
925.39	**196-202**	**DYEDQQK**
928.55	203-210	QLEQVIAK
700.40	211-216	DLLPSR
290.15	217-218	DR
848.54	219-225	QHLPLIK
1441.79	226-238	MKPVPDLVPGNFK
603.35	239-243	SQLQK
755.41	244-249	VPPEWK
1062.51	250-258	ALTDMPQMR
1501.74	259-271	MELERPGGNEITR
488.31	145-148	VIEK

D

PEPTIDE ANTIGEN

Tryptic peptide:
DYEDQQK

Synthetic peptide:
Biotin-CGDYEDQQK

Hydrophilicity change:
+1.467

C

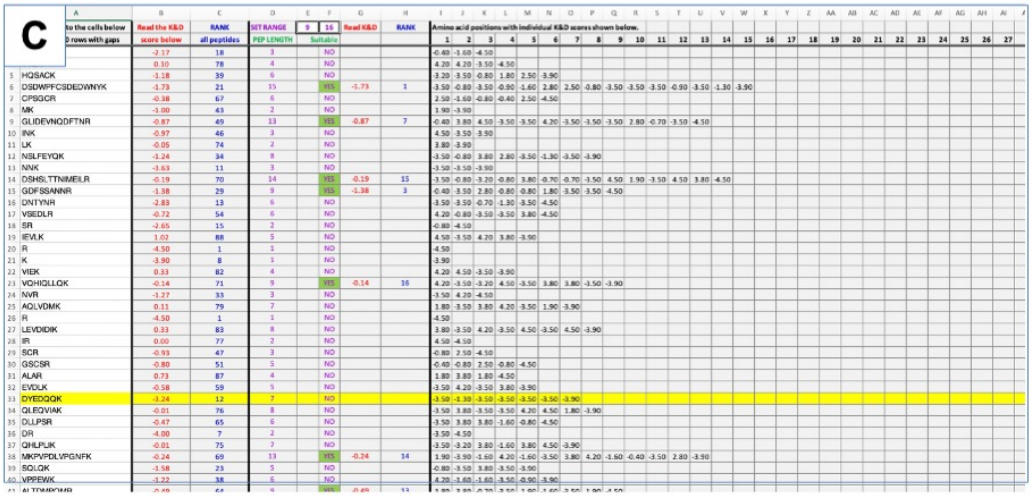

Fibrinogen B

A

FIBRINOGEN B
491 a.a.
UniProtKB ID: **P02675**

MKRMVSWSFH KLKTMKHLLL LLLCVFLVKS QGVNDNEEGF
FSARGHRPLD KKREEAPSLR PAPPPISGGG YRARPAKAAA
TQKKVERKAP DAGGCLHADP DLGVLCPTGC QLQEALLQQE
RPIRNSVDEL NNNVEAVSQT SSSSFQYMYL LKDLWQKRQK
QVKDNENVVN EYSSELEKHQ LYIDETVNSN IPTNLRVLRS
ILENLRSKIQ KLESDVSAQM EYCRTPCTVS CNIPVVSGKE
CEEIIRKGGE TSEMYLIQPD SSVKPYRVYC DMNTENGGWT
VIQNRQDGSV DFGRKWDPYK QGFGNVATNT DGKNYCGLPG
EYWLGNDKIS QLTRMGPTEL LIEMEDWKGD KVKAHYGGFT
VQNEANKYQI SVNKYRGTAG NALMDGASQL MGENRTMTIH
NGMFFSTYDR DNDGWLTSDP RKQCSKEDGG GWWYNRCHAA
NPNGRYYWGG QYTWDMAKHG TDDGVVWMNW KGSWYSMRKM
SMKIRPFFPQ Q

Kyte & Doolittle Score: -0.76

B

Mass	Position	Sequence
717.43	329-334	ISQLTR
1691.80	335-348	MGPTELLIEMEDWK
319.16	349-351	GDK
246.18	352-353	VK
1535.72	354-367	AHYGGFTVQNEANK
851.46	368-374	YQISVNK
338.18	375-376	YR
1892.86	377-395	GTAGNALMDGASQLMGENR
1820.81	396-410	TMTIHNGMFFSTYDR
1275.56	**411-421**	**DNDGWLTSDPR**
147.11	422-422	K
465.21	423-426	QCSK
1239.52	427-436	EDGGGWWYNR
939.42	437-445	CHAANPNGR
1668.72	446-458	YYWGGQYTWDMAK
1544.70	459-471	HGTDDGVVWMNWK
886.39	472-478	GSWYSMR
147.11	479-479	K
496.23	480-483	MSMK
1032.56	484-491	IRPFFPQQ
717.43	329-334	ISQLTR
1691.80	335-348	MGPTELLIEMEDWK

D

PEPTIDE ANTIGEN

Tryptic peptide:
DNDGWLTSDPR

Synthetic peptide:
Biotin-CGDNDGWLTSDPR

Hydrophilicity change:
+1.530

C

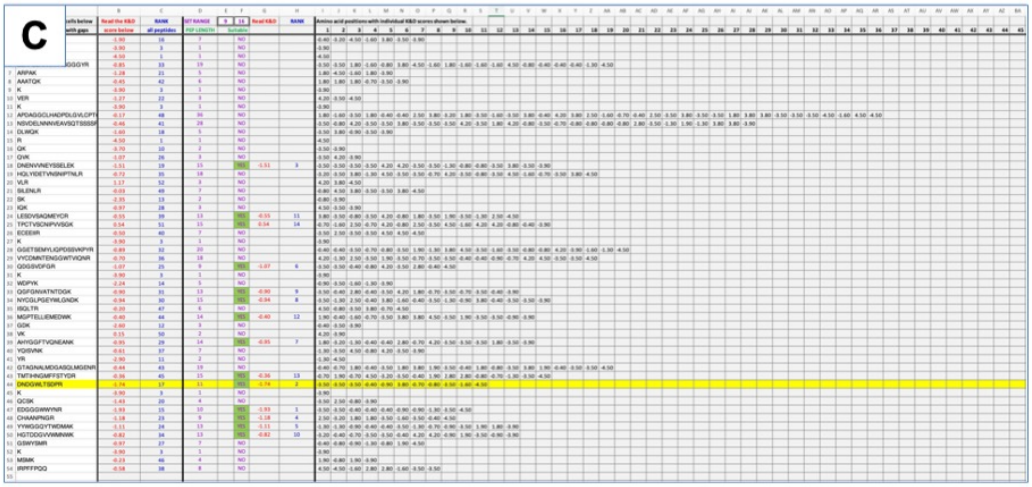

Fibrinogen G

A

FIBRINOGEN G

437 a.a.

UniProtKB ID: **A0A140VJJ6**

MSWSLHPRNL ILYFYALLFL SSTCVAYVAT RDNCCILDER
FGSYCPTTCG IADFLSTYQT KVDKDLQSLE DILHQVENKT
SEVKQLIKAI QLTYNPDESS KPNMIDAATL KSRKMLEEIM
KYEASILTHD SSIRYLQEIY NSNNQKIVNL KEKVAQLEAQ
CQEPCKDTVQ IHDITGKDCQ DIANKGAKQS GLYFIKPLKA
NQQFLVYCEI DGSGNGWTVF QKRLDGSVDF KKNWIQYKEG
FGHLSPTGTT EFWLGNEKIH LISTQSAIPY ALRVELEDWN
GRTSTADYAM FKVGPEADKY RLTYAYFAGG DAGDAFDGFD
FGDDPSDKFF TSHNGMQFST WDNDNDKFEG NCAEQDGSGW
WMNKCHAGHL NGVYYQGGTY SKASTPNGYD NGIIWATWKT
RWYSMKKTTM KIIPFNRLTI GEGQQHHLGG AKQAGDV

Kyte & Doolittle Score: -0.54

B

Mass	Position	Sequence
609.34	27-31	YVATR
1080.44	32-40	DNCCILDER
2303.04	41-61	FGSYCPTTCGIADFLSTYQT K
361.21	62-64	VDK
1780.91	65-79	DLQSLEDILHQVENK
563.30	80-84	TSEVK
501.34	85-88	QLIK
2520.27	89-111	AIQLTYNPDESSKPNMIDAA TLK
262.15	112-113	SR
147.11	114-114	K
893.45	115-121	MLEEIMK
1491.74	122-134	YEASILTHDSSIR
1513.73	**135-146**	**YLQEIYNSNNQK**
586.39	147-151	IVNLK
276.16	152-153	EK
1446.67	154-166	VAQLEAQCQEPCK
1226.64	167-177	DTVQIHDITGK
906.40	178-185	DCQDIANK
275.17	186-188	GAK
1293.76	189-199	QSGLYFIKPLK
2604.22	200-222	ANQQFLVYCEIDGSGNGWTV FQK
175.12	223-223	R

D

PEPTIDE ANTIGEN

Tryptic peptide:

YLQEIYNSNNQK

Synthetic peptide:

Biotin-CGYLQEIYNSNNQK

Hydrophilicity change:

+1.747

C

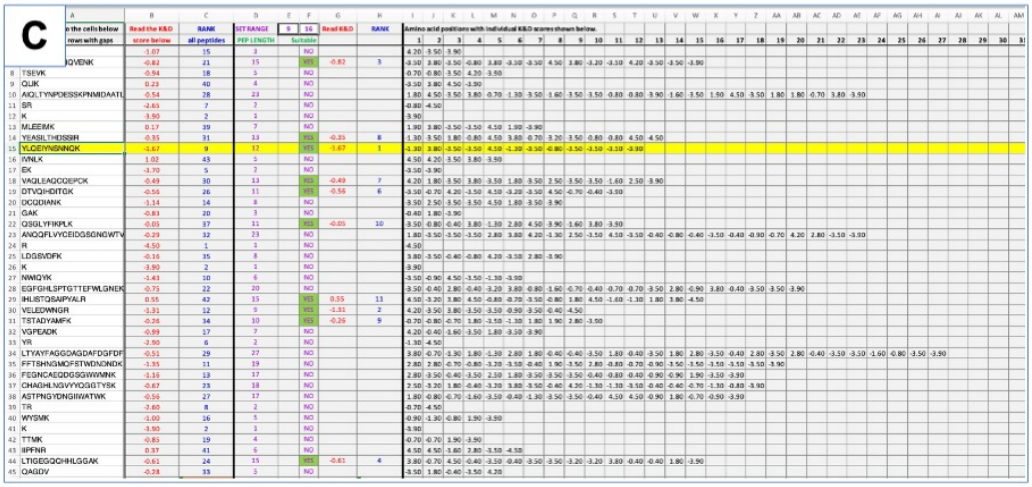

C-reactive protein

A

C-REACTIVE PROTEIN
224 a.a.
UniProtKB ID: **P2741**

MEKLLCFLVL TSLSHAFGQT DMSRKAFVFP
KESDTSYVSL KAPLTKPLKA FTVCLHFYTE
LSSTRGYSIF SYATKRQDNE ILIFWSKDIG
YSFTVGGSEI LFEVPEVTVA PVHICTSWES
ASGIVEFWVD GKPRVRKSLK KGYTVGAEAS
IILGQEQDSF GGNFEGSQSL VGDIGNVNMW
DFVLSPDEIN TIYLGGPFSP NVLNWRALKY
EVQGEVFTKP QLWP

Kyte & Doolittle Score: -0.03

B

Mass	Position	Sequence
1931.97	1-17	MGLSDGEWQLVLNVWGK
1632.87	18-32	VEADIPGHGQEVLIR
407.27	33-35	LFK
910.46	36-43	GHPETLEK
409.21	44-46	FDK
294.18	47-48	FK
397.26	49-51	HLK
738.30	52-57	SEDEMK
662.34	58-63	ASEDLK
147.11	64-64	K
1350.81	65-78	HGATVLTALGGILK
147.11	79-79	K
147.11	80-80	K
1853.96	81-97	GHHEAEIKPLAQSHATK
284.17	98-99	HK
456.32	100-103	IPVK
1913.01	104-119	YLEFISECIIQVLQSK
1515.66	120-134	HPGDFGADAQGAMNK
748.44	135-140	ALELFR
147.11	141-141	K
828.36	142-148	DMASNYK
650.31	149-154	ELGFQG

D

PEPTIDE ANTIGEN

Tryptic peptide:
ESDTSYVSLK

Synthetic peptide:
Biotin-CGESDTSYVSLK

Hydrophilicity change:
+0.401

C

	A	B	C	D	E	F	G	H	I	J	K	L
	ste seq into the cells below	Read the K&D	RANK	SET RANGE	9	16	Read K&D	RANK	Amino acid positions with			
2	Up to 1000 rows with gaps	score below	all peptides	PEP LENGTH		Suitable			1	2	3	4
3	QTDMSR	-1.85	5	6		NO			-3.50	-0.70	-3.50	1.90
4	K	-3.90	2	1		NO			-3.90			
5	AFVFPK	1.02	17	6		NO			1.80	2.80	4.20	2.80
6	ESDTSYVSLK	-0.73	6	10		YES	-0.73	1	-3.50	-0.80	-3.50	-0.70
7	APLTKPLK	-0.29	10	8		NO			1.80	-1.60	3.80	-0.70
8	AFTVCLHFYTELSSTR	0.34	15	16		YES	0.34	5	1.80	2.80	-0.70	4.20
9	GYSIFSYATK	-0.01	13	10		YES	-0.01	4	-0.40	-1.30	-0.80	4.50
10	R	-4.50	1	1		NO			-4.50			
11	QDNEILIFWSK	-0.36	8	11		YES	-0.36	3	-3.50	-3.50	-3.50	-3.50
12	DIGYSFTVGGSEILFEVPEVTV	0.29	14	47		NO			-3.50	4.50	-0.40	-1.30
13	VR	-0.15	11	2		NO			4.20	-4.50		
14	K	-3.90	2	1		NO			-3.90			
15	SLK	-0.30	9	3		NO			-0.80	3.80	-3.90	
16	K	-3.90	2	1		NO			-3.90			
17	GYTVGAEASIILGQEQDSFGG	-0.06	12	65		NO			-0.40	-1.30	-0.70	4.20
18	ALK	0.57	16	3		NO			1.80	3.80	-3.90	
19	YEVQGEVFTKPQLWP	-0.63	7	15		YES	-0.63	2	-1.30	-3.50	4.20	-3.50

Interferon gamma

A

INTERFERON GAMMA
166 a.a.
UniProtKB ID: **P01579**

MKYTSYILAF QLCIVLGSLG CYCQDPYVKE
AENLKKYFNA GHSDVADNGT LFLGILKNWK
EESDRKIMQS QIVSFYFKLF KNFKDDQSIQ
KSVETIKEDM NVKFFNSNKK KRDDFEKLTN
YSVTDLNVQR KAIHELIQVM AELSPAAKTG
KRKRSQMLFR GRRASQ

Kyte & Doolittle Score: -0.58

B

Mass	Position	Sequence
749.38	24–29	QDPYVK
703.36	30–35	EAENLK
147.11	36–36	K
2252.13	37–57	YFNAGHSDVADNGTLFLGILK
447.24	58–60	NWK
635.26	61–65	EESDR
147.11	66–66	K
1490.77	67–78	IMQSQIVSFYFK
407.27	79–81	LFK
408.22	82–84	NFK
833.40	**85–91**	**DDQSIQK**
676.39	92–97	SVETIK
735.33	98–103	EDMNVK
756.37	104–109	FFNSNK
147.11	110–110	K
147.11	111–111	K
175.12	112–112	R
653.28	113–117	DDFEK
1522.79	118–130	LTNYSVTDLNVQR
147.11	131–131	K
1820.99	132–148	AIHELIQVMAELSPAAK
305.18	149–151	TGK

D

PEPTIDE ANTIGEN

Tryptic peptide:
DDQSIQK

Synthetic peptide:
Biotin-CGDDQSIQK

Hydrophilicity change:
+0.767

C

	A	B	C	D	E	F	G	H	I	J	K	L	M	N	O	P	Q	R	S	T	U	V	W	X
	eq into the cells below	Read the K&D	RANK	SET RANGE	7	16	Read K&D	RANK	Amino acid positions with individual K&D scores shown below.															
	1000 rows with gaps	score below	all peptides	PEP LENGTH		Suitable			1	2	3	4	5	6	7	8	9	10	11	12	13	14	15	16
3	QDPYVK	-1.60	15	6		NO			-3.50	-3.50	-1.60	-1.30	4.20	-3.90										
4	EAENLK	-1.47	17	6		NO			-3.50	1.80	-3.50	-3.50	3.80	-3.90										
5	K	-3.90	4	1		NO			-3.90															
6	YFNAGHSDVADNGTLFLGILK	0.20	24	21		NO			-1.30	2.80	-3.50	1.80	-0.40	-3.20	-0.80	-3.50	4.20	1.80	-3.50	-3.50	-0.40	-0.70	3.80	2.80
7	NWK	-2.77	11	3		NO			-3.50	-0.90	-3.90													
8	EESDR	-3.16	10	5		NO			-3.50	-3.50	-0.80	-3.50	-4.50											
9	K	-3.90	4	1		NO			-3.90															
10	IMQSQIVSFYFK	0.58	25	12		YES	0.58	3	4.50	1.90	-3.50	-0.80	-3.50	4.50	4.20	-0.80	2.80	-1.30	2.80	-3.90				
11	LFK	0.90	27	3		NO			3.80	2.80	-3.90													
12	NFK	-1.53	16	3		NO			-3.50	2.80	-3.90													
13	DDQSIQK	-2.03	13	7		YES	-2.03	1	-3.50	-3.50	-3.50	-0.80	4.50	-3.50	-3.90									
14	SVETIK	-0.03	23	6		NO			-0.80	4.20	-3.50	-0.70	4.50	-3.90										
15	EDMNVK	-1.38	18	6		NO			-3.50	-3.50	1.90	-3.50	4.20	-3.90										
16	FFNSNK	-1.02	19	6		NO			2.80	2.80	-3.50	-0.80	-3.50	-3.90										
17	K	-3.90	4	1		NO			-3.90															
18	K	-3.90	4	1		NO			-3.90															
19	R	-4.50	1	1		NO			-4.50															
20	DDFEK	-2.32	12	5		NO			-3.50	-3.50	2.80	-3.50	-3.90											
21	LTNYSVTDLNVQR	-0.46	20	13		YES	-0.46	2	3.80	-0.70	-3.50	-1.30	-0.80	4.20	-0.70	-3.50	3.80	-3.50	4.20	-3.50	-4.50			
22	K	-3.90	4	1		NO			-3.90															
23	AIHELIQVMAELSPAAK	0.58	26	17		NO			1.80	4.50	-3.20	-3.50	3.80	4.50	-3.50	4.20	1.90	1.80	-3.50	3.80	-0.80	-1.60	1.80	1.80
24	TGK	-1.67	14	3		NO			-0.70	-0.40	-3.90													
25	R	-4.50	1	1		NO			-4.50															
26	K	-3.90	4	1		NO			-3.90															
27	R	-4.50	1	1		NO			-4.50															
28	SQMLFR	-0.05	22	6		NO			-0.80	-3.50	1.90	3.80	2.80	-4.50										
29	G	-0.40	21	1		NO			-0.40															

Interleukin 1a

A

INTERLEUKIN 1a
271 a.a.
UniProtKB ID: **P01583**

MAKVPDMFED LKNCYSENEE DSSSIDHLSL
NQKSFYHVSY GPLHEGCMDQ SVSLSISETS
KTSKLTFKES MVVVATNGKV LKKRRLSLSQ
SITDDDLEAI ANDSEEEIIK PRSAPFSFLS
NVKYNFMRII KYEFILNDAL NQSIIRANDQ
YLTAAALHNL DEAVKFDMGA YKSSKDDAKI
TVILRISKTQ LYVTAQDEDQ PVLLKEMPEI
PKTITGSETN LLFFWETHGT KNYFTSVAHP
NLFIATKQDY WVCLAGGPPS ITDFQILENQ
A

Kyte & Doolittle Score: -0.34

B

Mass	Position	Sequence
1196.63	113-123	SAPFSFLSNVK
730.33	124-128	YNFMR
373.28	129-131	IIK
1808.95	132-146	YEFILNDALNQSIIR
2057.03	147-165	ANDQYLTAAALHNLDEAVK
831.37	166-172	FDMGAYK
321.18	173-175	SSK
448.20	176-179	DDAK
714.49	180-185	ITVILR
347.23	186-188	ISK
1961.02	189-205	TQLYVTAQDEDQPVLLK
843.43	**206-212**	**EMPEIPK**
2182.08	213-231	TITGSETNLLFFWETHGTK
1822.95	232-247	NYFTSVAHPNLFIATK
2665.26	248-271	QDYWVCLAGGPPSITDFQILENQA
1196.63	113-123	SAPFSFLSNVK
730.33	124-128	YNFMR
373.28	129-131	IIK
1808.95	132-146	YEFILNDALNQSIIR
2057.03	147-165	ANDQYLTAAALHNLDEAVK
831.37	166-172	FDMGAYK
321.18	173-175	SSK

D

PEPTIDE ANTIGEN

Tryptic peptide:
EMPEIPK

Synthetic peptide:
Biotin-CGEMPEIPK

Hydrophilicity change:
+0.285

C

	A	B	C	D	E	F	G	H	I	J
	aste seq into the cells below	Read the K&D	RANK	SET RANGE	7	16	Read K&D	RANK	Amino aci	
2	Up to 1000 rows with gaps	score below	all peptides	PEP LENGTH		Suitable			1	
3	SAPFSFLSNVK	0.36	13	11		YES	0.36	5	-0.80	1.8
4	YNFMR	-0.92	4	5		NO			-1.30	-3.5
5	IIK	1.70	14	3		NO			4.50	4.5
6	YEFILNDALNQSIIR	0.11	11	15		YES	0.11	3	-1.30	-3.5
7	ANDQYLTAAALHNLDEAVK	-0.29	8	19		NO			1.80	-3.5
8	FDMGAYK	-0.37	6	7		YES	-0.37	2	2.80	-3.5
9	SSK	-1.83	2	3		NO			-0.80	-0.8
10	DDAK	-2.28	1	4		NO			-3.50	-3.5
11	ITVILR	1.97	15	6		NO			4.50	-0.7
12	ISK	-0.07	10	3		NO			4.50	-0.8
13	TQLYVTAQDEDQPVLLK	-0.45	5	17		NO			-0.70	-3.5
14	EMPEIPK	-1.10	3	7		YES	-1.10	1	-3.50	1.9
15	TITGSETNLLFFWETHGTK	-0.31	7	19		NO			-0.70	4.5
16	NYFTSVAHPNLFIATK	0.16	12	16		YES	0.16	4	-3.50	-1.3
17	QDYWVCLAGGPPSITDFQILE	-0.10	9	24		NO			-3.50	-3.5

Interleukin 1b

A

INTERLEUKIN 1b
269 a.a.
UniProtKB ID: **P01584**

MAEVPELASE MMAYYSGNED DLFFEADGPK
QMKCSFQDLD LCPLDGGIQL RISDHHYSKG
FRQAASVVVA MDKLRKMLVP CPQTFQENDL
STFFPFIFEE EPIFFDTWDN EAYVHDAPVR
SLNCTLRDSQ QKSLVMSGPY ELKALHLQGQ
DMEQQVVFSM SFVQGEESND KIPVALGLKE
KNLYLSCVLK DDKPTLQLES VDPKNYPKKK
MEKRFVFNKI EINNKLEFES AQFPNWYIST
SQAENMPVFL GGTKGGQDIT DFTMQFVSS

Kyte & Doolittle Score: -0.42

B

Mass	Position	Sequence
442.28	117-120	APVR
806.42	121-127	SLNCTLR
605.29	128-132	DSQQK
1223.63	133-143	SLVMSGPYELK
3181.46	144-171	ALHLQGQDMEQQVVFSMSFVQGEESNDK
810.54	172-179	IPVALGLK
276.16	180-181	EK
1052.58	182-190	NLYLSCVLK
1584.81	**191-204**	**DDKPTLQLESVDPK**
521.27	205-208	NYPK
147.11	209-209	K
147.11	210-210	K
407.20	211-213	MEK
175.12	214-214	R
654.36	215-219	FVFNK
730.41	220-225	IEINNK
3291.57	226-254	LEFESAQFPNWYISTSQAENMPVFLGGTK
1632.72	255-269	GGQDITDFTMQFVSS
442.28	117-120	APVR
806.42	121-127	SLNCTLR
605.29	128-132	DSQQK
1223.63	133-143	SLVMSGPYELK

D

PEPTIDE ANTIGEN

Tryptic peptide:
DDKPTLQLESVDPK

Synthetic peptide:
Biotin-CGDDKPTLQLESVDPK

Hydrophilicity change:
+0.586

C

	A	B	C	D	E	F	G	H	I	J	K	L	M
1	ste seq into the cells below	Read the K&D	RANK	SET RANGE	9	16	Read K&D	RANK	Amino acid positions with individ				
2	Up to 1000 rows with gaps	score below	all peptides	PEP LENGTH		Suitable			1	2	3	4	5
3	APVR	-0.02	13	4		NO			1.80	-1.60	4.20	-4.50	
4	SLNCTLR	0.09	14	7		NO			-0.80	3.80	-3.50	2.50	-0.70
5	DSQQK	-3.04	5	5		NO			-3.50	-0.80	-3.50	-3.50	-3.90
6	SLVMSGPYELK	0.13	15	11		YES	0.13	3	-0.80	3.80	4.20	1.90	-0.80
7	ALHLQGQDMEQQVVFSMSFV	-0.62	10	28		NO			1.80	3.80	-3.20	3.80	-3.50
8	IPVALGLK	1.53	18	8		NO			4.50	-1.60	4.20	1.80	3.80
9	EK	-3.70	4	2		NO			-3.50	-3.90			
10	NLYLSCVLK	0.96	17	9		YES	0.96	4	-3.50	3.80	-1.30	3.80	-0.80
11	DDKPTLQLESVDPK	-1.30	8	14		YES	-1.30	1	-3.50	-3.50	-3.90	-1.60	-0.70
12	NYPK	-2.58	6	4		NO			-3.50	-1.30	-1.60	-3.90	
13	K	-3.90	2	1		NO			-3.90				
14	K	-3.90	2	1		NO			-3.90				
15	MEK	-1.83	7	3		NO			1.90	-3.50	-3.90		
16	R	-4.50	1	1		NO			-4.50				
17	FVFNK	0.48	16	5		NO			2.80	4.20	2.80	-3.50	-3.90
18	IEINNK	-0.90	9	6		NO			4.50	-3.50	4.50	-3.50	-3.50
19	LEFESAQFPNWYISTSQAENM	-0.28	11	29		NO			3.80	-3.50	2.80	-3.50	-0.80
20	GGQDITDFTMQFVSS	-0.11	12	15		YES	-0.11	2	-0.40	-0.40	-3.50	-3.50	4.50

Interleukin 2

A

INTERLEUKIN 2
153 a.a.
UniProtKB ID: **P60568**

MYRMQLLSCI ALSLALVTNS APTSSSTKKT
QLQLEHLLLD LQMILNGINN YKNPKLTRML
TFKFYMPKKA TELKHLQCLE EELKPLEEVL
NLAQSKNFHL RPRDLISNIN VIVLELKGSE
TTFMCEYADE TATIVEFLNR WITFCQSIIS
TLT

Kyte & Doolittle Score: -0.01

B

Mass	Position	Sequence
778.39	21-28	APTSSSTK
147.11	29-29	K
2724.48	30-52	TQLQLEHLLLDLQMILNGINNYK
358.21	53-55	NPK
389.25	56-58	LTR
639.35	59-63	MLTFK
685.34	64-68	FYMPK
147.11	69-69	K
561.32	70-74	ATELK
2563.34	75-96	HLQCLEEELKPLEEVLNLAQSK
939.53	**97-103**	**NFHLRPR**
1582.94	104-117	DLISNINVIVLELK
2627.16	118-140	GSETTFMCEYADETATIVEFLNR
1512.78	141-153	WITFCQSIISTLT

D

PEPTIDE ANTIGEN

Tryptic peptide:
NFHLRPR

Synthetic peptide:
Biotin-CGNFHLRPR

Hydrophilicity change:
+0.948

C

	A	B	C	D	E	F	G	H	I
	aste seq into the cells below	Read the K&D	RANK	SET RANGE	7	16	Read K&D	RANK	Ami
2	Up to 1000 rows with gaps	score below	all peptides	PEP LENGTH		Suitable			
3	APTSSSTK	-0.94	5	8		YES	-0.94	2	1.8
4	K	-3.90	1	1		NO			-3.9
5	TQLQLEHLLLDLQMILNGINNY	0.00	11	23		NO			-0.7
6	NPK	-3.00	3	3		NO			-3.5
7	LTR	-0.47	7	3		NO			3.8
8	MLTFK	0.78	12	5		NO			1.9
9	FYMPK	-0.42	9	5		NO			2.8
10	K	-3.90	1	1		NO			-3.9
11	ATELK	-0.50	6	5		NO			1.8
12	HLQCLEEELKPLEEVLNLAQSK	-0.46	8	22		NO			-3.2
13	NFHLRPR	-1.53	4	7		YES	-1.53	1	-3.5
14	DLISNINVIVLELK	1.04	13	14		YES	1.04	3	-3.5
15	GSETTFMCEYADETATIVEFL	-0.20	10	23		NO			-0.4
16	WITFCQSIISTLT	1.12	14	13		YES	1.12	4	-0.9

Interleukin 4

A

INTERLEUKIN 4
153 a.a.
UniProtKB ID: **P05112**

MGLTSQLLPP LFFLLACAGN FVHGHKCDIT
LQEIIKTLNS LTEQKTLCTE LTVTDIFAAS
KNTTEKETFC RAATVLRQFY SHHEKDTRCL
GATAQQFHRH KQLIRFLKRL DRNLWGLAGL
NSCPVKEANQ STLENFLERL KTIMREKYSK
CSS

Kyte & Doolittle Score: -0.30

B

Mass	Position	Sequence
284.17	25-26	HK
1175.63	27-36	CDITLQEIIK
1033.55	37-45	TLNSLTEQK
1712.88	46-61	TLCTELTVTDIFAASK
592.29	62-66	NTTEK
655.29	67-71	ETFCR
630.39	72-77	AATVLR
1075.50	**78-85**	**QFYSHHEK**
391.19	86-88	DTR
1231.60	89-99	CLGATAQQFHR
284.17	100-101	HK
529.35	102-105	QLIR
407.27	106-108	FLK
175.12	109-109	R
403.23	110-112	LDR
1471.77	113-126	NLWGLAGLNSCPVK
1550.74	127-139	EANQSTLENFLER
260.20	140-141	LK
520.29	142-145	TIMR
276.16	146-147	EK
397.21	148-150	YSK
296.09	151-153	CSS

D

PEPTIDE ANTIGEN

Tryptic peptide:
QFYSHHEK

Synthetic peptide:
Biotin-CGQFYSHHEK

Hydrophilicity change:
+1.155

C

	A	B	C	D	E	F	G	H	I	J	K	L	M	N	O	P	Q	R
	e seq into the cells below	Read the K&D	RANK	SET RANGE	7	16	Read K&D	RANK	Amino acid positions with individual K&D scores shown below.									
	to 1000 rows with gaps	score below	all peptides	PEP LENGTH		Suitable			1	2	3	4	5	6	7	8	9	10
3	HK	-3.55	3	2		NO			-3.20	-3.90								
4	CDITLQEIIK	0.47	19	10		YES	0.47	6	2.50	-3.50	4.50	-0.70	3.80	-3.50	-3.50	4.50	4.50	-3.90
5	TLNSLTEQK	-1.00	11	9		YES	-1.00	3	-0.70	3.80	-3.50	-0.80	3.80	-0.70	-3.50	-3.50	-3.90	
6	TLCTELTVTDIFAASK	0.67	20	16		YES	0.67	7	-0.70	3.80	2.50	-0.70	-3.50	3.80	-0.70	4.20	-0.70	-3.50
7	NTTEK	-2.46	6	5		NO			-3.50	-0.70	-0.70	-3.50	-3.90					
8	ETFCR	-0.68	12	5		NO			-3.50	-0.70	2.80	2.50	-4.50					
9	AATVLR	1.07	22	6		NO			1.80	1.80	-0.70	4.20	3.80	-4.50				
10	QFYSHHEK	-2.08	7	8		YES	-2.08	1	-3.50	2.80	-1.30	-0.80	-3.20	-3.20	-3.50	-3.90		
11	DTR	-2.90	5	3		NO			-3.50	-0.70	-4.50							
12	CLGATAQQFHR	-0.28	13	11		YES	-0.28	4	2.50	3.80	-0.40	1.80	-0.70	1.80	-3.50	-3.50	2.80	-3.20
13	HK	-3.55	3	2		NO			-3.20	-3.90								
14	QLIR	0.08	15	4		NO			-3.50	3.80	4.50	-4.50						
15	FLK	0.90	21	3		NO			2.80	3.80	-3.90							
16	R	-4.50	1	1		NO			-4.50									
17	LDR	-1.40	9	3		NO			3.80	-3.50	-4.50							
18	NLWGLAGLNSCPVK	0.35	18	14		YES	0.35	5	-3.50	3.80	-0.90	-0.40	3.80	1.80	-0.40	3.80	-3.50	-0.80
19	EANQSTLENFLER	-1.14	10	13		YES	-1.14	2	-3.50	1.80	-3.50	-3.50	-0.80	-0.70	3.80	-3.50	-3.50	2.80
20	LK	-0.05	14	2		NO			3.80	-3.90								
21	TIMR	0.30	16	4		NO			-0.70	4.50	1.90	-4.50						
22	EK	-3.70	2	2		NO			-3.50	-3.90								
23	YSK	-2.00	8	3		NO			-1.30	-0.80	-3.90							
24	CSS	0.30	17	3		NO			2.50	-0.80	-0.80							

Interleukin 6

A

INTERLEUKIN 6
212 a.a.
UniProtKB ID: **P05231**

MNSFSTSAFG PVAFSLGLLL VLPAAFPAPV
PPGEDSKDVA APHRQPLTSS ERIDKQIRYI
LDGISALRKE TCNKSNMCES SKEALAENNL
NLPKMAEKDG CFQSGFNEET CLVKIITGLL
EFEVYLEYLQ NRFESSEEQA RAVQMSTKVL
IQFLQKKAKN LDAITTPDPT TNASLLTKLQ
AQNQWLQDMT THLILRSFKE FLQSSLRALR
QM

Kyte & Doolittle Score: -0.27

B

Mass	Position	Sequence
828.41	30–37	VPPGEDSK
765.40	38–44	DVAAPHR
917.47	45–52	QPLTSSER
375.22	53–55	IDK
416.26	56–58	QIR
1120.64	59–68	YILDGISALR
147.11	69–69	K
594.26	70–74	ETCNK
885.34	75–82	SNMCESSK
1325.71	83–94	EALAENNLNLPK
478.23	95–98	MAEK
1776.76	99–114	DGCFQSGFNEETCLVK
2213.19	115–132	IITGLLEFEVYLEYLQNR
1082.47	133–141	FESSEEQAR
764.40	142–148	AVQMSTK
988.62	149–156	VLIQFLQK
147.11	157–157	K
218.15	158–159	AK
1986.04	160–178	NLDAITTPDPTTNASLLTK
2209.15	179–196	LQAQNQWLQDMTTHLILR
381.21	197–199	SFK
979.52	200–207	EFLQSSLR

D

PEPTIDE ANTIGEN

Tryptic peptide:
FESSEEQAR

Synthetic peptide:
Biotin-CGFESSEEQAR

Hydrophilicity change:
+0.947

C

	A	B	C	D	E	F	G	H	I	J	K	L	M	N	O	P	Q	R	S	T
	seq into the cells below	Read the K&D	RANK	SET RANGE	7	16	Read K&D	RANK	Amino acid positions with individual K&D scores shown below.											
	o 1000 rows with gaps	score below	all peptides	PEP LENGTH		Suitable			1	2	3	4	5	6	7	8	9	10	11	12
3	VPPGEDSK	-1.39	6	8		YES	-1.39	3	4.20	-1.60	-1.60	-0.40	-3.50	-3.50	-0.80	-3.90				
4	DVAAPHR	-0.71	13	7		YES	-0.71	5	-3.50	4.20	1.80	1.80	-1.60	-3.20	-4.50					
5	QPLTSSER	-1.45	5	8		YES	-1.45	2	-3.50	-1.60	3.80	-0.70	-0.80	-0.80	-3.50	-4.50				
6	IDK	-0.97	10	3		NO			4.50	-3.50	-3.90									
7	QIR	-1.17	7	3		NO			-3.50	4.50	-4.50									
8	YILDGISALR	0.79	23	10		YES	0.79	10	-1.30	4.50	3.80	-3.50	-0.40	4.50	-0.80	1.80	3.80	-4.50		
9	K	-3.90	1	1		NO			-3.90											
10	ETCNK	-1.82	3	5		NO			-3.50	-0.70	2.50	-3.50	-3.90							
11	SNMCESSK	-1.11	8	8		YES	-1.11	4	-0.80	-3.50	1.90	2.50	-3.50	-0.80	-0.80	-3.90				
12	EALAENNLNLPK	-0.67	14	12		YES	-0.67	6	-3.50	1.80	3.80	1.80	-3.50	-3.50	-3.50	3.80	-3.50	3.80	-1.60	-3.90
13	MAEK	-0.93	11	4		NO			1.90	1.80	-3.50	-3.90								
14	DGCFQSGFNEETCLVK	-0.32	18	16		YES	-0.32	8	-3.50	-0.40	2.50	2.80	-3.50	-0.80	-0.40	2.80	-3.50	-3.50	-3.50	-0.70
15	IITGLLEFEVYLEYLQNR	0.31	21	18		NO			4.50	4.50	-0.70	-0.40	3.80	3.80	-3.50	2.80	-3.50	4.20	-1.30	3.80
16	FESSEEQAR	-1.72	4	9		YES	-1.72	1	2.80	-3.50	-0.80	-0.80	-3.50	-3.50	-3.50	1.80	-4.50			
17	AVQMSTK	-0.14	20	7		YES	-0.14	9	1.80	4.20	-3.50	1.90	-0.80	-0.70	-3.90					
18	VLIQFLQK	1.03	24	8		YES	1.03	11	4.20	3.80	4.50	-3.50	2.80	3.80	-3.50	-3.90				
19	K	-3.90	1	1		NO			-3.90											
20	AK	-1.05	9	2		NO			1.80	-3.90										
21	NLDAITTPDPTTNASLLTK	-0.31	19	19		NO			-3.50	3.80	-3.50	1.80	4.50	-0.70	-0.70	-1.60	-3.50	-1.60	-0.70	-0.70
22	LQAQNQWLQDMTTHLILR	-0.42	16	18		NO			3.80	-3.50	1.80	-3.50	-3.50	-3.50	-0.90	3.80	-3.50	-3.50	1.90	-0.70
23	SFK	-0.63	15	3		NO			-0.80	2.80	-3.90									
24	EFLQSSLR	-0.34	17	8		YES	-0.34	7	-3.50	2.80	3.80	-3.50	-0.80	-0.80	3.80	-4.50				
25	ALR	0.37	22	3		NO			1.80	3.80	-4.50									
26	QM	-0.80	12	2		NO			-3.50	1.90										

Interleukin 8

A

INTERLEUKIN 8
99 a.a.
UniProtKB ID: **P10145**

MTSKLAVALL AAFLISAALC EGAVLPRSAK
ELRCQCIKTY SKPFHPKFIK ELRVIESGPH
CANTEIIVKL SDGRELCLDP KENWVQRVVE
KFLKRAENS

Kyte & Doolittle Score: -0.02

B

Mass	Position	Sequence
741.43	21-27	EGAVLPR
305.18	28-30	SAK
417.25	31-33	ELR
594.27	34-38	CQCIK
1104.58	**39-47**	**TYSKPFHPK**
407.27	48-50	FIK
417.25	51-53	ELR
1709.89	54-69	VIESGPHCANTEIIVK
547.28	70-74	LSDGR
817.41	75-81	ELCLDPK
831.41	82-87	ENWVQR
474.29	88-91	VVEK
407.27	92-94	FLK
175.12	95-95	R
420.17	96-99	AENS

D

PEPTIDE ANTIGEN

Tryptic peptide:
TYSKPFHPK

Synthetic peptide:
Biotin-CGTYSKPFHPK

Hydrophilicity change:
+1.081

C

	A	B	C	D	E	F	G	H	I	J
	aste seq into the cells below	Read the K&D	RANK	SET RANGE	9	16	Read K&D	RANK	Amino acid p	
2	Up to 1000 rows with gaps	score below	all peptides	PEP LENGTH		Suitable			1	2
3	EGAVLPR	-0.03	10	7		NO			-3.50	-0.40
4	SAK	-0.97	8	3		NO			-0.80	1.80
5	ELR	-1.40	5	3		NO			-3.50	3.80
6	CQCIK	0.42	13	5		NO			2.50	-3.50
7	TYSKPFHPK	-1.58	3	9		YES	-1.58	1	-0.70	-1.30
8	FIK	1.13	15	3		NO			2.80	4.50
9	ELR	-1.40	5	3		NO			-3.50	3.80
10	VIESGPHCANTEIIVK	0.32	12	16		YES	0.32	2	4.20	4.50
11	LSDGR	-1.08	7	5		NO			3.80	-0.80
12	ELCLDPK	-0.34	9	7		NO			-3.50	3.80
13	ENWVQR	-1.95	2	6		NO			-3.50	-3.50
14	VVEK	0.25	11	4		NO			4.20	4.20
15	FLK	0.90	14	3		NO			2.80	3.80
16	R	-4.50	1	1		NO			-4.50	
17	AENS	-1.50	4	4		NO			1.80	-3.50

Interleukin 10

A

INTERLEUKIN 10
178 a.a.
UniProtKB ID: **P22301**

MHSSALLCCL VLLTGVRASP GQGTQSENSC
THFPGNLPNM LRDLRDAFSR VKTFFQMKDQ
LDNLLLKESL LEDFKGYLGC QALSEMIQFY
LEEVMPQAEN QDPDIKAHVN SLGENLKTLR
LRLRRCHRFL PCENKSKAVE QVKNAFNKLQ
EKGIYKAMSE FDIFINYIEA YMTMKIRN

Kyte & Doolittle Score: -0.35

B

Mass	Position	Sequence
2572.17	19–42	SPGQGTQSENSCTHFPGNLPNMLR
403.23	43–45	DLR
595.28	46–50	DAFSR
246.18	51–52	VK
801.40	53–58	TFFQMK
1071.60	59–67	DQLDNLLLK
980.49	68–75	ESLLEDFK
3559.64	76–106	GYLGCQALSEMIQFYLEEVMPQAENQDPDIK
1181.63	**107–117**	**AHVNSLGENLK**
389.25	118–120	TLR
288.20	121–122	LR
288.20	123–124	LR
175.12	125–125	R
415.19	126–128	CHR
850.41	129–135	FLPCENK
234.14	136–137	SK
673.39	138–143	AVEQVK
593.30	144–148	NAFNK
517.30	149–152	LQEK
480.28	153–156	GIYK
2317.06	157–175	AMSEFDIFINYIEAYMTMK
288.20	176–177	IR

D

PEPTIDE ANTIGEN

Tryptic peptide:
AHVNSLGENLK

Synthetic peptide:
Biotin-CGAHVNSLGENLK

Hydrophilicity change:
-0.115

C

	A	B	C	D	E	F	G	H	I	J	K	L	M	N	O	P	Q	R	S
	seq into the cells below	Read the K&D	RANK	SET RANGE	9	16	Read K&D	RANK	Amino acid positions with individual K&D scores shown below.										
	to 1000 rows with gaps	score below	all peptides	PEP LENGTH		Suitable			1	2	3	4	5	6	7	8	9	10	11
3	SPGQGTQSENSCTHFPGNLF	-0.99	8	24		NO			-0.80	-1.60	-0.40	-3.50	-0.40	-0.70	-3.50	-0.80	-3.50	-3.50	-0.80
4	DLR	-1.40	6	3		NO			-3.50	3.80	-4.50								
5	DAFSR	-0.84	9	5		NO			-3.50	1.80	2.80	-0.80	-4.50						
6	VK	0.15	22	2		NO			4.20	-3.90									
7	TFFQMK	-0.10	20	6		NO			-0.70	2.80	2.80	-3.50	1.90	-3.90					
8	DQLDNLLLK	-0.30	17	9		YES	-0.30	2	-3.50	-3.50	3.80	-3.50	-3.50	3.80	3.80	3.80	-3.90		
9	ESLLEDFK	-0.60	10	8		NO			-3.50	-0.80	3.80	3.80	-3.50	-3.50	2.80	-3.90			
10	GYLGCQALSEMIQFYLEEVMF	-0.40	14	31		NO			-0.40	-1.30	3.80	-0.40	2.50	-3.50	1.80	3.80	-0.80	-3.50	1.90
11	AHVNSLGENLK	-0.47	12	11		YES	-0.47	1	1.80	-3.20	4.20	-3.50	-0.80	3.80	-0.40	-3.50	-3.50	3.80	-3.90
12	TLR	-0.47	13	3		NO			-0.70	3.80	-4.50								
13	LR	-0.35	15	2		NO			3.80	-4.50									
14	LR	-0.35	15	2		NO			3.80	-4.50									
15	R	-4.50	1	1		NO			-4.50										
16	CHR	-1.73	5	3		NO			2.50	-3.20	-4.50								
17	FLPCENK	-0.49	11	7		NO			2.80	3.80	-1.60	2.50	-3.50	-3.50	-3.90				
18	SK	-2.35	3	2		NO			-0.80	-3.90									
19	AVEQVK	-0.12	19	6		NO			1.80	4.20	-3.50	-3.50	4.20	-3.90					
20	NAFNK	-1.26	7	5		NO			-3.50	1.80	2.80	-3.50	-3.90						
21	LQEK	-1.78	4	4		NO			3.80	-3.50	-3.50	-3.90							
22	GIYK	-0.28	18	4		NO			-0.40	4.50	-1.30	-3.90							
23	AMSEFDIFINYIEAYMTMK	0.34	23	19		NO			1.80	1.90	-0.80	-3.50	2.80	-3.50	4.50	2.80	4.50	-3.50	-1.30
24	IR	0.00	21	2		NO			4.50	-4.50									
25	N	-3.50	2	1		NO			-3.50										

Beta-enolase

A

BETA-ENOLASE
434 a.a.
UniProtKB ID: **P13929**

MAMQKIFARE ILDSRGNPTV EVDLHTAKGR FRAAVPSGAS
TGIYEALELR DGDKGRYLGK GVLKAVENIN NTLGPALLQK
KLSVVDQEKV DKFMIELDGT ENKSKFGANA ILGVSLAVCK
AGAAEKGVPL YRHIADLAGN PDLILPVPAF NVINGGSHAG
NKLAMQEFMI LPVGASSFKE AMRIGAEVYH HLKGVIKAKY
GKDATNVGDE GGFAPNILEN NEALELLKTA IQAAGYPDKV
VIGMDVAASE FYRNGKYDLD FKSPDDPARH ITGEKLGELY
KSFIKNYPVV SIEDPFDQDD WATWTSFLSG VNIQIVGDDL
TVTNPKRIAQ AVEKKACNCL LLKVNQIGSV TESIQACKLA
QSNGWGVMVS HRSGETEDTF IADLVVGLCT GQIKTGAPCR
SERLAKYNQL MRIEEALGDK AIFAGRKFRN PKAK

Kyte & Doolittle Score: -0.19

B

Mass	Position	Sequence
477.25	2–5	AMQK
506.31	6–9	IFAR
732.39	10–15	EILDSR
1380.71	**16–28**	**GNPTVEVDLHTAK**
232.14	29–30	GR
322.19	31–32	FR
1804.94	33–50	AAVPSGASTGIYEALELR
434.19	51–54	DGDK
232.14	55–56	GR
480.28	57–60	YLGK
416.29	61–64	GVLK
1694.94	65–80	AVENINNTLGPALLQK
147.11	81–81	K
917.49	82–89	LSVVDQEK
361.21	90–92	VDK
1296.61	93–103	FMIELDGTENK
234.14	104–105	SK
1462.81	106–120	FGANAILGVSLAVCK
546.29	121–126	AGAAEK
704.41	127–132	GVPLYR
3021.59	133–162	HIADLAGNPDLILPVPAFNVINGGSHAGN K
1868.96	163–179	LAMQEFMILPVGASSFK

D

PEPTIDE ANTIGEN

Tryptic peptide:
GNPTVEVDLHTAK

Synthetic peptide:
Biotin-CGNPTVEVDLHTAK

Hydrophilicity change:
+0.128

C

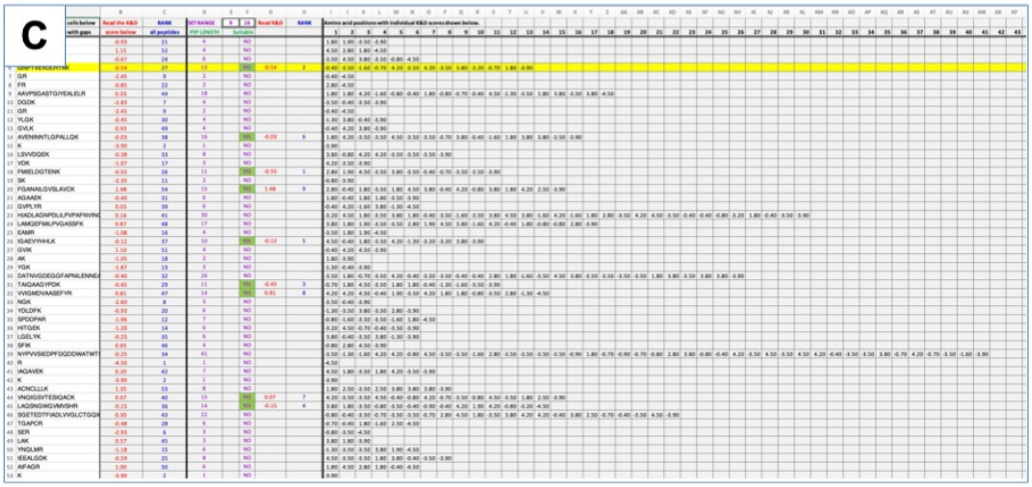

E-selectin

A

E-SELECTIN
610 a.a.
UniProtKB ID: **P16581**

MIASQFLSAL TLVLLIKESG AWSYNTSTEA MTYDEASAYC
QQRYTHLVAI QNKEEIEYLN SILSYSPSYY WIGIRKVNNV
WVWVGTQKPL TEEAKNWAPG EPNNRQKDED CVEIYIKREK
DVGMWNDERC SKKKLALCYT AACTNTSCSG HGECVETINN
YTCKCDPGFS GLKCEQIVNC TALESPEHGS LVCSHPLGNF
SYNSSCSISC DRGYLPSSME TMQCMSSGEW SAPIPACNVV
ECDAVTNPAN GFVECFQNPG SFPWNTTCTF DCEEGFELMG
AQSLQCTSSG NWDNEKPTCK AVTCRAVRQP QNGSVRCSHS
PAGEFTFKSS CNFTCEEGFM LQGPAQVECT TQGQWTQQIP
VCEAFQCTAL SNPERGYMNC LPSASGSFRY GSSCEFSCEQ
GFVLKGSKRL QCGPTGEWDN EKPTCEAVRC DAVHQPPKGL
VRCAHSPIGE FTYKSSCAFS CEEGFELHGS TQLECTSQGQ
WTEEVPSCQV VKCSSLAVPG KINMSCSGEP VFGTVCKFAC
PEGWTLNGSA ARTCGATGHW SGLLPTCEAP TESNIPLVAG
LSAAGLSLLT LAPFLLWLRK CLRKAKKFVP ASSCQSLESD
GSYQKPSYIL

Kyte & Doolittle Score: -0.41

B

Mass	Position	Sequence
2605.06	22-43	WSYNTSTEAMTYDEASAYCQQR
1186.66	44-53	YTHLVAIQNK
2695.33	54-75	EEIEYLNSILSYSPSYYWIGIR
147.11	76-76	K
2198.16	77-95	VNNVWVWVGTQKPLTEEAK
1154.53	**96-105**	**NWAPGEPNNR**
275.17	106-107	QK
1226.56	108-117	DEDCVEIYIK
175.12	118-118	R
276.16	119-120	EK
1121.47	121-129	DVGMWNDER
337.15	130-132	CSK
147.11	133-133	K
147.11	134-134	K
3170.34	135-164	LALCYTAACTNTSCSGHGECVETINNYTCK
923.43	165-173	CDPGFSGLK
4186.80	174-212	CEQIVNCTALESPEHGSLVCSHPLGNFSYNS SCSISCDR
9540.98	213-300	GYLPSSMETMQCMSSGEWSAPIPACNVVECD AVTNPANGFVECFQNPGSFPWNTTCTFDCEE GFELMGAQSLQCTSSGNWDNEKPTCK
549.28	301-305	AVTCR
345.22	306-308	AVR
885.45	309-316	QPQNGSVR
1310.58	317-328	CSHSPAGEFTFK

D

PEPTIDE ANTIGEN

Tryptic peptide:
NWAPGEPNNR

Synthetic peptide:
Biotin-CGNWAPGEPNNR

Hydrophilicity change:
+1.294

C

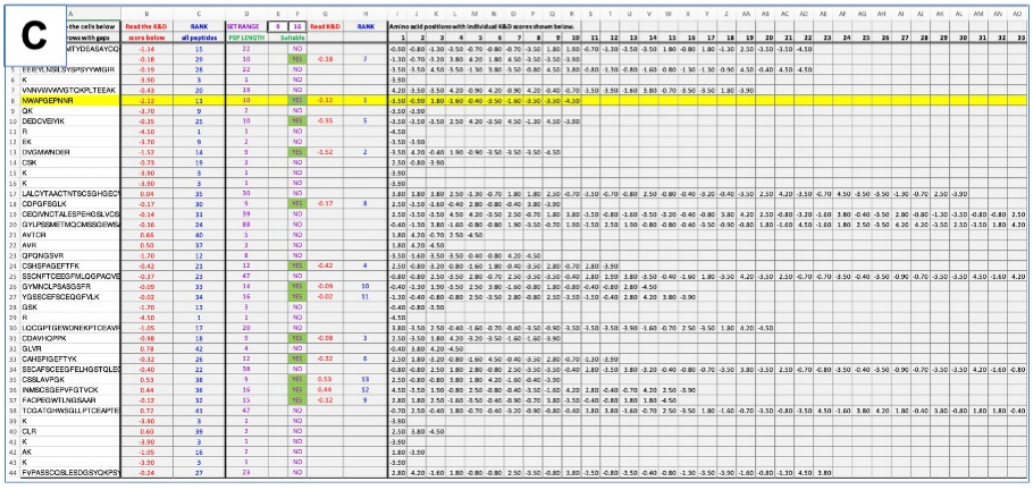

Fibronectin

A

FIBRONECTIN

2477 a.a.

UniProtKB ID: **P02751**

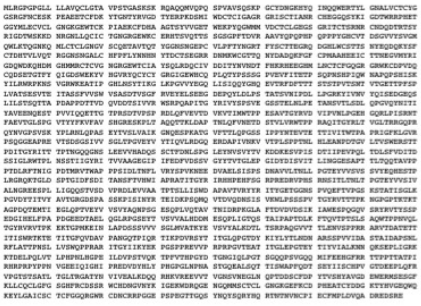

Kyte & Doolittle Score: -0.51

B

Mass	Position	Sequence
2775.32	32–57	QAQQMVQPQSPVAVSQSKPGCYDNGK
1401.67	58–67	HYQINQQWER
1677.77	68–83	TYLGNALVCTCYGGSR
1933.79	84–100	GFNCESKPEAEETCFDK
874.41	101–107	YTGNTYR
1064.54	108–116	VGDTYERPK
1527.64	117–130	DSMIWDCTCIGAGR
232.14	131–132	GR
877.46	133–140	ISCTIANR
1008.42	141–149	CHEGGQSYK
747.38	150–155	IGDTWR
2063.95	156–174	RPHETGGYMLECVCLGNGK
1261.62	175–185	GEWTCKPIAEK
4070.73	186–222	CFDHAAGTSYVVGETWEKPYQGWMMVDCT CLGEGSGR
680.34	223–228	ITCTSR
289.16	229–230	NR
851.33	231–237	CNDQDTR
526.26	238–241	TSYR
806.40	242–248	IGDTWSK
147.11	249–249	K
404.19	250–252	DNR
1348.65	253–265	GNLLQCICTGNGR

D

PEPTIDE ANTIGEN

Tryptic peptide:

HYQINQQWER

Synthetic peptide:

Biotin-CGHYQINQQWER

Hydrophilicity change:

+1.219

C

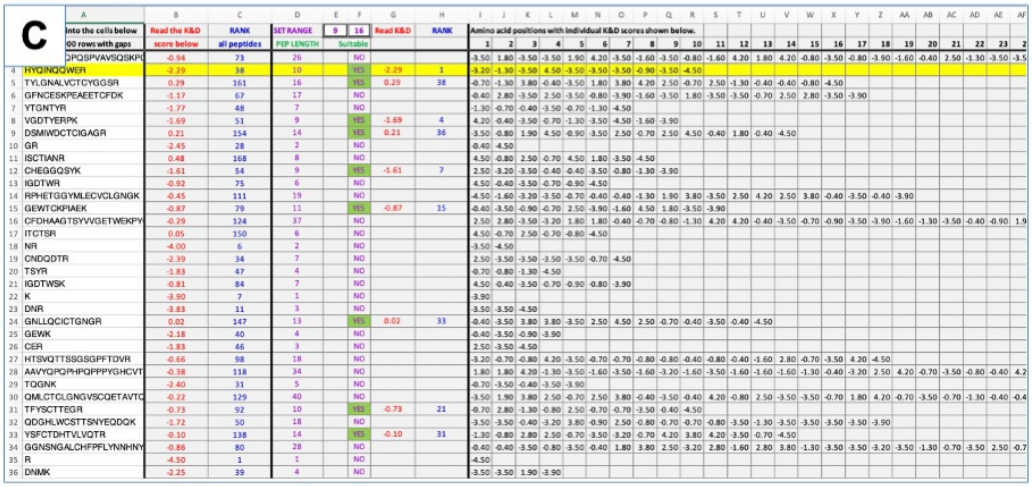

	Into the cells below	Read the K&D	RANK	SET RANGE	9	16	Read K&D	RANK	Amino acid positions with individual K&D scores shown below.																								
	00 rows with gaps	score below	all peptides	PEP LENGTH		Suitable			1	2	3	4	5	6	7	8	9	10	11	12	13	14	15	16	17	18	19	20	21	22	23	2
	QPQSPVAVSQSKPG	-0.94	73	26		NO			-3.50	1.80	-3.50	-3.50	1.90	4.20	-3.50	-1.60	-3.50	-0.80	-1.60	4.20	1.80	4.20	-0.80	-3.50	-0.80	-3.90	-1.60	-0.40	2.50	-1.30	-3.50	-3.5
4	HYQINQQWER	-2.29	38	10		YES	-2.29	1	-3.20	-1.30	-3.50	4.50	-3.50	-3.50	-3.50	-0.90	-3.50	-4.50														
5	TYLGNALVCTCYGGSR	0.29	161	16		YES	0.29	38	-0.70	-1.30	3.80	-0.40	-3.50	1.80	3.80	4.20	2.50	-0.70	2.50	-1.30	-0.40	-0.40	-0.80	-4.50								
6	GFNCESKPEAEETCFDK	-1.17	67	17		NO			-0.40	2.80	-3.50	2.50	-3.50	-0.80	-3.90	-1.60	-3.50	1.80	-3.50	-3.50	-0.70	2.50	2.80	-3.50	-3.90							
7	YTGNTYR	-1.77	48	7		NO			-1.30	-0.70	-0.40	-3.50	-0.70	-1.30	-4.50																	
8	VGDTYERPK	-1.69	51	9		YES	-1.69	4	4.20	-0.40	-3.50	-0.70	-1.30	-3.50	-4.50	-1.60	-3.90															
9	DSMIWDCTCIGAGR	0.21	154	14		YES	0.21	36	-3.50	-0.80	1.90	4.50	-0.90	-3.50	2.50	-0.70	2.50	4.50	-0.40	1.80	-0.40	-4.50										
10	GR	-2.45	28	2		NO			-0.40	-4.50																						
11	ISCTIANR	0.48	168	8		NO			4.50	-0.80	2.50	-0.70	4.50	1.80	-3.50	-4.50																
12	CHEGGQSYK	-1.61	54	9		YES	-1.61	7	2.50	-3.20	-3.50	-0.40	-0.40	-3.50	-0.80	-1.30	-3.90															
13	IGDTWR	-0.92	75	6		NO			4.50	-0.40	-3.50	-0.70	-0.90	-4.50																		
14	RPHETGGYMLECVCLGNGK	-0.45	111	19		NO			-4.50	-1.60	-3.20	-3.50	-0.70	-0.40	-0.40	-1.30	1.90	3.80	-3.50	2.50	4.20	2.50	3.80	-0.40	-3.50	-0.40	-3.90					
15	GEWTCKPIAEK	-0.87	79	11		YES	-0.87	15	-0.40	-3.50	-0.90	-0.70	2.50	-3.90	-1.60	4.50	1.80	-3.50	-3.90													
16	CFDHAAGTSYVVGETWEKPY	-0.29	124	37		NO			2.50	2.80	-3.50	-3.20	1.80	1.80	-0.40	-0.70	-0.80	-1.30	4.20	4.20	-0.40	-3.50	-0.70	-0.90	-3.50	-3.90	-1.60	-1.30	-3.50	-0.40	-0.90	1.9
17	ITCTSR	0.05	150	6		NO			4.50	-0.70	2.50	-0.70	-0.80	-4.50																		
18	NR	-4.00	6	2		NO			-3.50	-4.50																						
19	CNDQDTR	-2.39	34	7		NO			2.50	-3.50	-3.50	-3.50	-0.70	-4.50																		
20	TSYR	-1.83	47	4		NO			-0.70	-0.80	-1.30	-4.50																				
21	IGDTWSK	-0.81	84	7		NO			4.50	-0.40	-3.50	-0.70	-0.90	-0.80	-3.90																	
22	K	-3.90	7	1		NO			-3.90																							
23	DNR	-3.83	11	3		NO			-3.50	-3.50	-4.50																					
24	GNLLQCICTGNGR	0.02	147	13		YES	0.02	33	-0.40	-3.50	3.80	3.80	-3.50	2.50	4.50	2.50	-0.70	-0.40	-3.50	-0.40	-4.50											
25	GEWK	-2.18	40	4		NO			-0.40	-3.50	-0.90	-3.90																				
26	CER	-1.83	46	3		NO			2.50	-3.50	-4.50																					
27	HTSVQTTSSGSGPFTDVR	-0.66	98	18		NO			-3.20	-0.70	-0.80	4.20	-3.50	-0.70	-0.70	-0.80	-0.80	-0.40	-0.80	-0.40	-1.60	2.80	-0.70	-3.50	4.20	-4.50						
28	AAVYQPQPHPQPPPYGHCVT	-0.38	118	34		NO			1.80	1.80	4.20	-1.30	-3.50	-1.60	-3.50	-1.60	-3.20	-1.60	-3.50	-1.60	-1.60	-1.60	-1.30	-0.40	-3.20	2.50	4.20	-0.70	-3.50	-0.80	-0.40	4.2
29	TQGNK	-2.40	31	5		NO			-0.70	-3.50	-0.40	-3.50	-3.90																			
30	QMLCTCLGNGVSCQETAVTC	-0.22	129	40		NO			-3.50	1.90	3.80	2.50	-0.70	2.50	3.80	-0.40	-3.50	-0.40	4.20	-0.80	2.50	-3.50	-3.50	-0.70	1.80	4.20	-0.70	-3.50	-0.70	-1.30	-0.40	-0.4
31	TFYSCTTEGR	-0.73	92	10		YES	-0.73	21	-0.70	2.80	-1.30	-0.80	2.50	-0.70	-0.70	-3.50	-0.40	4.50														
32	QDGHLWCSTTSNYEQDQK	-1.72	50	18		NO			-3.50	-3.50	-0.40	-3.20	3.80	-0.90	2.50	-0.80	-0.70	-0.70	-0.80	-3.50	-1.30	-3.50	-3.50	-3.50	-3.50	-3.90						
33	YSFCTDHTVLVQTR	-0.10	138	14		YES	-0.10	31	-1.30	-0.80	2.80	2.50	-0.70	-3.50	-3.20	-0.70	4.20	3.80	4.20	-3.50	-0.70	-4.50										
34	GGNSNGALCHFPFLYNNHNY	-0.86	80	28		NO			-0.40	-0.40	-3.50	-0.80	-3.50	-0.40	1.80	3.80	2.50	-3.20	2.80	-1.60	2.80	3.80	-1.30	-3.50	-3.50	-3.20	-3.50	-1.30	-0.70	-3.50	2.50	-0.7
35	R	-4.50	1	1		NO			-4.50																							
36	DNMK	-2.25	39	4		NO			-3.50	-3.50	1.90	-3.90																				

Haptoglobin

A

HAPTOGLOBIN
406 a.a.
UniProtKB ID: **P00738**

MSALGAVIAL LLWGQLFAVD SGNDVTDIAD
DGCPKPPEIA HGYVEHSVRY QCKNYYKLRT
EGDGVYTLND KKQWINKAVG DKLPECEADD
GCPKPPEIAH GYVEHSVRYQ CKNYYKLRTE
GDGVYTLNNE KQWINKAVGD KLPECEAVCG
KPKNPANPVQ RILGGHLDAK GSFPWQAKMV
SHHNLTTGAT LINEQWLLTT AKNLFLNHSE
NATAKDIAPT LTLYVGKKQL VEIEKVVLHP
NYSQVDIGLI KLKQKVSVNE RVMPICLPSK
DYAEVGRVGY VSGWGRNANF KFTDHLKYVM
LPVADQDQCI RHYEGSTVPE KKTPKSPVGV
QPILNEHTFC AGMSKYQEDT CYGDAGSAFA
VHDLEEDTWY ATGILSFDKS CAVAEYGVYV
KVTSIQDWVQ KTIAEN

Kyte & Doolittle Score: -0.42

B

Mass	Position	Sequence
895.47	154–161	NPANPVQR
923.53	162–170	ILGGHLDAK
920.46	171–178	GSFPWQAK
2679.39	179–202	MVSHHNLTTGATLINEQWLLTTAK
1458.73	203–215	NLFLNHSENATAK
1290.73	216–227	DIAPTLTLYVGK
147.11	228–228	K
858.49	229–235	QLVEIEK
1795.01	236–251	VVLHPNYSQVDIGLIK
260.20	252–253	LK
275.17	254–255	QK
703.37	256–261	VSVNER
987.54	262–270	VMPICLPSK
809.38	271–277	DYAEVGR
980.49	278–286	VGYVSGWGR
593.30	287–291	NANFK
760.40	292–297	FTDHLK
1650.80	298–311	YVMLPVADQDQCIR
1146.54	**312–321**	**HYEGSTVPEK**
147.11	322–322	K
345.21	323–325	TPK
2115.04	326–345	SPVGVQPILNEHTFCAGMSK

D

PEPTIDE ANTIGEN

Tryptic peptide:
HYEGSTVPEK

Synthetic peptide:
Biotin-CGHYEGSTVPEK

Hydrophilicity change:
+0.629

C

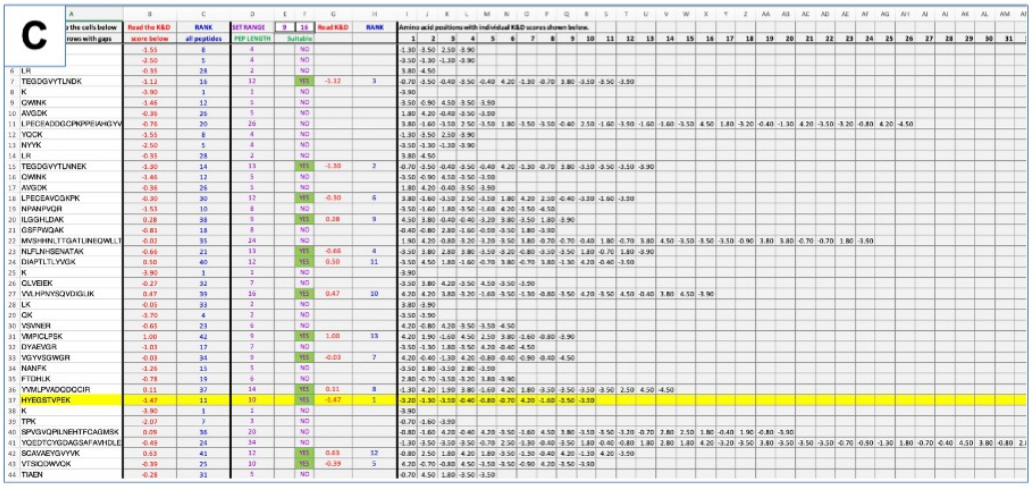

Heat shock protein(s)

A

HEAT SHOCK PROTEIN(s)
641 a.a.
UniProtKB ID: **P0DMV8**

MAKAAAIGID LGTTYSCVGV FQHGKVEIIA NDQGNRTTPS
YVAFTDTERL IGDAAKNQVA LNPQNTVFDA KRLIGRKFGD
PVVQSDMKHW PFQVINDGDK PKVQVSYKGE TKAFYPEEIS
SMVLTKMKEI AEAYLGYPVT NAVITVPAYF NDSQRQATKD
AGVIAGLNVL RIINEPTAAA IAYGLDRTGK GERNVLIFDL
GGGTFDVSIL TIDDGIFEVK ATAGDTHLGG EDFDNRLVNH
FVEEFKRKHK KDISQNKRAV RRLRTACERA KRTLSSSTQA
SLEIDSLFEG IDFYTSITRA RFEELCSDLF RSTLEPVEKA
LRDAKLDKAQ IHDLVLVGGS TRIPKVQKLL QDFFNGRDLN
KSINPDEAVA YGAAVQAAIL MGDKSENVQD LLLLDVAPLS
LGLETAGGVM TALIKRNSTI PTKQTQIFTT YSDNQPGVLI
QVYEGERAMT KDNNLLGRFE LSGIPPAPRG VPQIEVTFDI
DANGILNVTA TDKSTGKANK ITITNDKGRL SKEEIERMVQ
EAEKYKAEDE VQRERVSAKN ALESYAFNMK SAVEDEGLKG
KISEADKKKV LDKCQEVISW LDANTLAEKD EFEHKRKELE
QVCNPIISGL YQGAGGPGPG GFGAQGPKGG SGSGPTIEEV
D

Kyte & Doolittle Score: -0.38

B

Mass	Position	Sequence
218.15	2-3	AK
2208.11	4-25	AAAIGIDLGTTYSCVGVFQHGK
1228.63	26-36	VEIIANDQGNR
1487.70	**37-49**	**TTPSYVAFTDTER**
687.40	50-56	LIGDAAK
1658.85	57-71	NQVALNPQNTVFDAK
175.12	72-72	R
458.31	73-76	LIGR
147.11	77-77	K
1222.58	78-88	FGDPVVQSDMK
1680.85	89-102	HWPFQVINDGDKPK
723.40	103-108	VQVSYK
434.22	109-112	GETK
1614.81	113-126	AFYPEEISSMVLTK
278.15	127-128	MK
3001.49	129-155	EIAEAYLGYPVTNAVITVPAYFNDSQR
447.26	156-159	QATK
1197.69	160-171	DAGVIAGLNVLR
1687.90	172-187	IINEPTAAAIAYGLDR
305.18	188-190	TGK
361.18	191-193	GER
2897.52	194-220	NVLIFDLGGGTFDVSILTIDDGIFEVK

D

PEPTIDE ANTIGEN

Tryptic peptide:
TTPSYVAFTDTER

Synthetic peptide:
Biotin-CTTPSYVAFTDTER

Hydrophilicity change:
+0.095

C

Insulin growth-like factor 1

A

IGF-1
153 a.a.
UniProtKB ID: Q5U743

MGKISSLPTQ LFKCCFCDFL KVKMHTMSSS
HLFYLALCLL TFTSSATAGP ETLCGAELVD
ALQFVCGDRG FYFNKPTGYG SSSRRAPQTG
IVDECCFRSC DLRRLEMYCA PLKPAKSARS
VRAQRHTDMP KTQKEVHLKN ASRGSAGNKN
YRM

Kyte & Doolittle Score: -0.27

B

Massa	Position	Sequence
2193.03	49-69	GPETLCGAELVDALQFVCGDR
1667.78	**70-84**	**GFYFNKPTGYGSSSR**
175.12	85-85	R
1438.65	86-98	APQTGIVDECCFR
593.27	99-103	SCDLR
175.12	104-104	R
1363.71	105-116	LEMYCAPLKPAK
333.19	117-119	SAR
361.22	120-122	SVR
374.21	123-125	AQR
728.34	126-131	HTDMPK
376.22	132-134	TQK
625.37	135-139	EVHLK
447.23	140-143	NASR
533.27	144-149	GSAGNK
452.23	150-152	NYR
150.06	153-153	M

D

PEPTIDE ANTIGEN

Tryptic peptide:
GFYFNKPTGYGSSSR

Synthetic peptide:
Biotin-CGFYFNKPTGYGSSSR

Hydrophilicity change:
+0.498

C

	A	B	C	D	E	F	G	H	I	J	K	L
	ste seq into the cells below	Read the K&D	RANK	SET RANGE	9	16	Read K&D	RANK	Amino acid positions with in			
2	Up to 1000 rows with gaps	score below	all peptides	PEP LENGTH		Suitable			1	2	3	4
3	GPETLCGAELVDALQFVCGDI	0.27	16	21		NO			-0.40	-1.60	-3.50	-0.70
4	GFYFNKPTGYGSSSR	-0.99	10	15		YES	-0.99	1	-0.40	2.80	-1.30	2.80
5	R	-4.50	1	1		NO			-4.50			
6	APQTGIVDECCFR	0.05	15	13		YES	0.05	3	1.80	-1.60	-3.50	-0.70
7	SCDLR	-0.50	12	5		NO			-0.80	2.50	-3.50	3.80
8	R	-4.50	1	1		NO			-4.50			
9	LEMYCAPLKPAK	-0.02	14	12		YES	-0.02	2	3.80	-3.50	1.90	-1.30
10	SAR	-1.17	9	3		NO			-0.80	1.80	-4.50	
11	SVR	-0.37	13	3		NO			-0.80	4.20	-4.50	
12	AQR	-2.07	5	3		NO			1.80	-3.50	-4.50	
13	HTDMPK	-1.83	6	6		NO			-3.20	-0.70	-3.50	1.90
14	TQK	-2.70	4	3		NO			-0.70	-3.50	-3.90	
15	EVHLK	-0.52	11	5		NO			-3.50	4.20	-3.20	3.80
16	NASR	-1.75	7	4		NO			-3.50	1.80	-0.80	-4.50
17	GSAGNK	-1.20	8	6		NO			-0.40	-0.80	1.80	-0.40
18	NYR	-3.10	3	3		NO			-3.50	-1.30	-4.50	
19	M	1.90	17	1		NO			1.90			

Leptin

A

LEPTIN
167 a.a.
UniProtKB ID: **P41159**

MHWGTLCGFL WLWPYLFYVQ AVPIQKVQDD
TKTLIKTIVT RINDISHTQS VSSKQKVTGL
DFIPGLHPIL TLSKMDQTLA VYQQILTSMP
SRNVIQISND LENLRDLLHV LAFSKSCHLP
WASGLETLDS LGGVLEASGY STEVVALSRL
QGSLQDMLWQ LDLSPGC

Kyte & Doolittle Score: +0.13

B

Mass	Position	Sequence
584.38	22-26	VPIQK
705.34	27-32	VQDDTK
474.33	33-36	TLIK
589.37	37-41	TIVTR
1415.71	**42-54**	**INDISHTQSVSSK**
275.17	55-56	QK
1921.12	57-74	VTGLDFIPGLHPILTLSK
2082.04	75-92	MDQTLAVYQQILTSMPSR
1527.81	93-105	NVIQISNDLENLR
1142.66	106-115	DLLHVLAFSK
3504.73	116-149	SCHLPWASGLETLDSLGGVLEASGYSTE VVALSR
2003.96	150-167	LQGSLQDMLWQLDLSPGC

D

PEPTIDE ANTIGEN

Tryptic peptide:
INDISHTQSVSSK

Synthetic peptide:
Biotin-CINDISHTQSVSSK

Hydrophilicity change:
+0.545

C

	A	B	C	D	E	F	G
1	Paste seq into the cells below	Read the K&D	RANK	SET RANGE	9	16	Read K&D
2	Up to 1000 rows with gaps	score below	all peptides	PEP LENGTH		Suitable	
3	VPIQK	-0.06	6	5		NO	
4	VQDDTK	-1.82	2	6		NO	
5	TLIK	0.93	12	4		NO	
6	TIVTR	0.56	9	5		NO	
7	INDISHTQSVSSK	-0.64	3	13		YES	-0.64
8	QK	-3.70	1	2		NO	
9	VTGLDFIPGLHPILTLSK	0.80	10	18		NO	
10	MDQTLAVYQQILTSMPSR	-0.14	5	18		NO	
11	NVIQISNDLENLR	-0.42	4	13		YES	-0.42
12	DLLHVLAFSK	0.88	11	10		YES	0.88
13	SCHLPWASGLETLDSLGGVLE	0.29	8	34		NO	
14	LQGSLQDMLWQLDLSPGC	0.06	7	18		NO	

Prolactin

A

PROLACTIN
227 a.a.
UniProtKB ID: **P01236**

MNIKGSPWKG SLLLLLVSNL LLCQSVAPLP
ICPGGAARCQ VTLRDLFDRA VVLSHYIHNL
SSEMFSEFDK RYTHGRGFIT KAINSCHTSS
LATPEDKEQA QQMNQKDFLS LIVSILRSWN
EPLYHLVTEV RGMQEAPEAI LSKAVEIEEQ
TKRLLEGMEL IVSQVHPETK ENEIYPVWSG
LPSLQMADEE SRLSAYYNLL HCLRRDSHKI
DNYLKLLKCR IIHNNNC

Kyte & Doolittle Score: -0.23

B

Mass	Position	Sequence
954.52	29–38	LPICPGGAAR
719.39	39–44	CQVTLR
665.33	45–49	DLFDR
2453.18	50–70	AVVLSHYIHNLSSEMFSEFDK
175.12	71–71	R
633.31	72–76	YTHGR
565.33	77–81	GFITK
1673.78	82–97	AINSCHTSSLATPEDK
1104.51	**98–106**	**EQAQQMNQK**
1275.77	107–117	DFLSLIVSILR
1742.89	118–131	SWNEPLYHLVTEVR
1273.65	132–143	GMQEAPEAILSK
1046.54	144–152	AVEIEEQTK
175.12	153–153	R
1923.03	154–170	LLEGMELIVSQVHPETK
2550.18	171–192	ENEIYPVWSGLPSLQMADEESR
1465.76	193–204	LSAYYNLLHCLR
175.12	205–205	R
486.23	206–209	DSHK
765.41	210–215	IDNYLK
373.28	216–218	LLK
278.13	219–220	CR

D

PEPTIDE ANTIGEN

Tryptic peptide:
EQAQQMNQK

Synthetic peptide:
Biotin-CGEQAQQMNQK

Hydrophilicity change:
+1.508

C

	A	B	C	D	E	F	G	H	I	J	K	L	M	N	O	P	Q	R	S
	seq into the cells below	Read the K&D	RANK	SET RANGE	9	16	Read K&D	RANK	Amino acid positions with individual K&D scores shown below.										
	to 1000 rows with gaps	score below	all peptides	PEP LENGTH		Suitable			1	2	3	4	5	6	7	8	9	10	11
3	LPICPGGAAR	0.59	21	10		YES	0.59	7	3.80	-1.60	4.50	2.50	-1.60	-0.40	-0.40	1.80	1.80	-4.50	
4	CQVTLR	0.30	18	6		NO			2.50	-3.50	4.20	-0.70	3.80	-4.50					
5	DLFDR	-0.98	8	5		NO			-3.50	3.80	2.80	-3.50	-4.50						
6	AVVLSHYIHNLSSEMFSEFDK	0.05	16	21		NO			1.80	4.20	4.20	3.80	-0.80	-3.20	-1.30	4.50	-3.20	-3.50	3.80
7	R	-4.50	1	1		NO			-4.50										
8	YTHGR	-2.02	6	5		NO			-1.30	-0.70	-3.20	-0.40	-4.50						
9	GFITK	0.46	20	5		NO			-0.40	2.80	4.50	-0.70	-3.90						
10	AINSCHTSSLATPEDK	-0.54	12	16		YES	-0.54	3	1.80	4.50	-3.50	-0.80	2.50	-3.20	-0.70	-0.80	-0.80	3.80	1.80
11	EQAQQMNQK	-2.36	5	9		YES	-2.36	1	-3.50	-3.50	1.80	-3.50	-3.50	1.90	-3.50	-3.50	-3.90		
12	DFLSLIVSILR	1.62	23	11		YES	1.62	8	-3.50	2.80	3.80	-0.80	3.80	4.50	4.20	-0.80	4.50	3.80	-4.50
13	SWNEPLYHLVTEVR	-0.54	13	14		YES	-0.54	4	-0.80	-0.90	-3.50	-3.50	-1.60	3.80	-1.30	-3.20	3.80	4.20	-0.70
14	GMQEAPEAILSK	-0.28	15	12		YES	-0.28	5	-0.40	1.90	-3.50	-3.50	1.80	-1.60	-3.50	1.80	4.50	3.80	-0.80
15	AVEIEEQTK	-0.90	9	9		YES	-0.90	2	1.80	4.20	-3.50	4.50	-3.50	-3.50	-3.50	-0.70	-3.90		
16	R	-4.50	1	1		NO			-4.50										
17	LLEGMELIVSQVHPETK	0.09	17	17		NO			3.80	3.80	-3.50	-0.40	1.90	-3.50	3.80	4.50	4.20	-0.80	-3.50
18	ENEIYPVWSGLPSLQMADEES	-0.78	10	22		NO			-3.50	-3.50	-3.50	4.50	-1.30	-1.60	4.20	-0.90	-0.80	-0.40	3.80
19	LSAYYNLLHCLR	0.41	19	12		YES	0.41	6	3.80	-0.80	1.80	-1.30	-1.30	-3.50	3.80	3.80	-3.20	2.50	3.80
20	R	-4.50	1	1		NO			-4.50										
21	DSHK	-2.85	4	4		NO			-3.50	-0.80	-3.20	-3.90							
22	IDNYLK	-0.65	11	6		NO			4.50	-3.50	-3.50	-1.30	3.80	-3.90					
23	LLK	1.23	22	3		NO			3.80	3.80	-3.90								
24	CR	-1.00	7	2		NO			2.50	-4.50									
25	IIHNNNC	-0.31	14	7		NO			4.50	4.50	-3.20	-3.50	-3.50	-3.50	2.50				

Transforming growth factor beta 1

A

TRANSFORMING GROWTH FACTOR BETA 1

390 a.a.

UniProtKB ID: **P01137**

MPPSGLRLLL LLLPLLWLLV LTPGRPAAGL
STCKTIDMEL VKRKRIEAIR GQILSKLRLA
SPPSQGEVPP GPLPEAVLAL YNSTRDRVAG
ESAEPEPEPE ADYYAKEVTR VLMVETHNEI
YDKFKQSTHS IYMFFNTSEL REAVPEPVLL
SRAELRLLRL KLKVEQHVEL YQKYSNNSWR
YLSNRLLAPS DSPEWLSFDV TGVVRQWLSR
GGEIEGFRLS AHCSCDSRDN TLQVDINGFT
TGRRGDLATI HGMNRPFLLL MATPLERAQH
LQSSRHRRAL DTNYCFSSTE KNCCVRQLYI
DFRKDLGWKW IHEPKGYHAN FCLGPCPYIW
SLDTQYSKVL ALYNQHNPGA SAAPCCVPQA
LEPLPIVYYV GRKPKVEQLS NMIVRSCKCS

Kyte & Doolittle Score: -0.31

B

Mass	Position	Sequence
1650.81	229-243	DNTLQVDINGFTTGR
175.12	244-244	R
2566.36	245-267	GDLATIHGMNRPFLLLMATPLER
926.48	268-275	AQHLQSSR
312.18	276-277	HR
175.12	278-278	R
1478.65	279-291	ALDTNYCFSSTEK
594.25	292-296	NCCVR
954.50	297-303	QLYIDFR
147.11	304-304	K
618.32	305-309	DLGWK
809.43	310-315	WIHEPK
2663.21	316-338	GYHANFCLGPCPYIWSLDTQYSK
3623.85	339-372	VLALYNQHNPGASAAPCCVPQALEPLPI VYYVGR
372.26	373-375	KPK
1188.64	**376-385**	**VEQLSNMIVR**
337.15	386-388	SCK
209.06	389-390	CS

D

PEPTIDE ANTIGEN

Tryptic peptide:

VEQLSNMIVR

Synthetic peptide:

Biotin-CGEQLSNMIVR

Hydrophilicity change:

-0.375

C

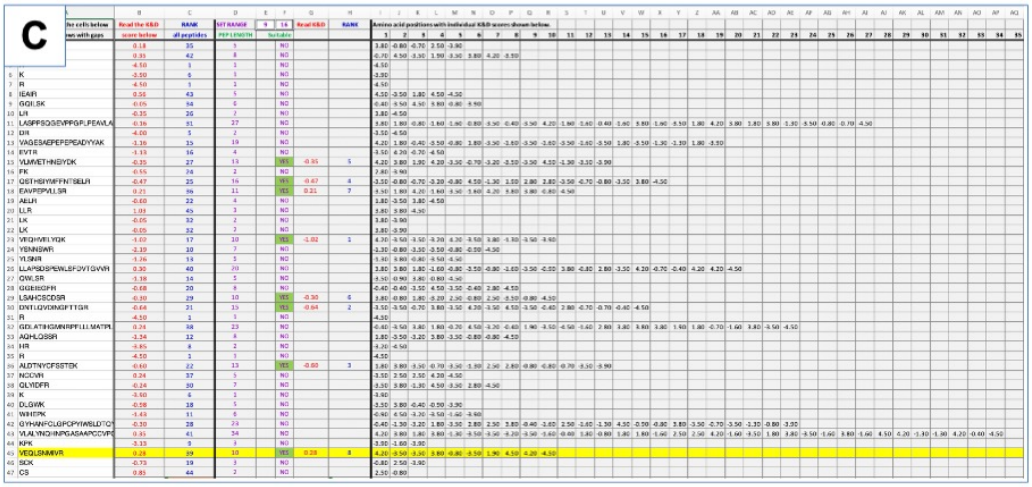

Transforming growth factor beta 4

A

TRANSFORMING GROWTH FACTOR BETA 4

366 a.a.

UniProtKB ID: **A1NY82**

MWPLWLCWAL WVLPLAGPGA ALTEEQLLGS
LLRQLQLSEV PVLDRADMEK LVIPAHVRAQ
YVVLLRRSHG DRSRGKRFSQ SFREVAGRFL
ASEASTHLLV FGMEQRLPPN SELVQAVLRL
FQEPVPKAAL HRHGRLSPRS AQARVTVEWL
RVRDDGSNRT SLIDSRLVSV HESGWKAFDV
TEAVNFWQQL SRPRQPLLLQ VSVQREHLGP
LASGAHKLVR FASQGAPAGL GEPQLELHTL
DLRDYGAQGD CDPEAPMTEG TRCCRQEMYI
DLQGMKWAKN WVLEPPGFLA YECVGTCQQP
PEALAFNWPF LGPRQCIASE TASLPMIVSI
KEGGRTRPQV VSLPNMRVQK CSCASDGALV
PRRLQP

Kyte & Doolittle Score: -0.23

B

Mass	Position	Sequence
472.29	136-139	LSPR
532.28	140-144	SAQAR
902.51	145-151	VTVEWLR
274.19	152-153	VR
663.27	154-159	DDGSNR
791.43	160-166	TSLIDSR
1141.60	167-176	LVSVHESGWK
2164.09	177-194	AFDVTEAVNFWQQLSRPR
1280.77	195-205	QPLLLQVSVQR
1216.64	206-217	EHLGPLASGAHK
387.27	218-220	LVR
2420.26	221-243	FASQGAPAGLGEPQLELHTLDLR
2012.80	244-262	DYGAQGDCDPEAPMTEGTR
381.14	263-265	CCR
1355.63	**266-276**	**QEMYIDLQGMK**
404.23	277-279	WAK
3946.91	280-314	NWVLEPPGFLAYECVGTCQQPPEALAFN WPFLGPR
1790.94	315-331	QCIASETASLPMIVSIK
418.20	332-335	EGGR
1397.77	336-347	TRPQVVSLPNMR
472.29	136-139	LSPR
532.28	140-144	SAQAR

D

PEPTIDE ANTIGEN

Tryptic peptide:

QEMYIDLQGMK

Synthetic peptide:

Biotin-CGQEMYIDLQGMK

Hydrophilicity change:

+0.188

C

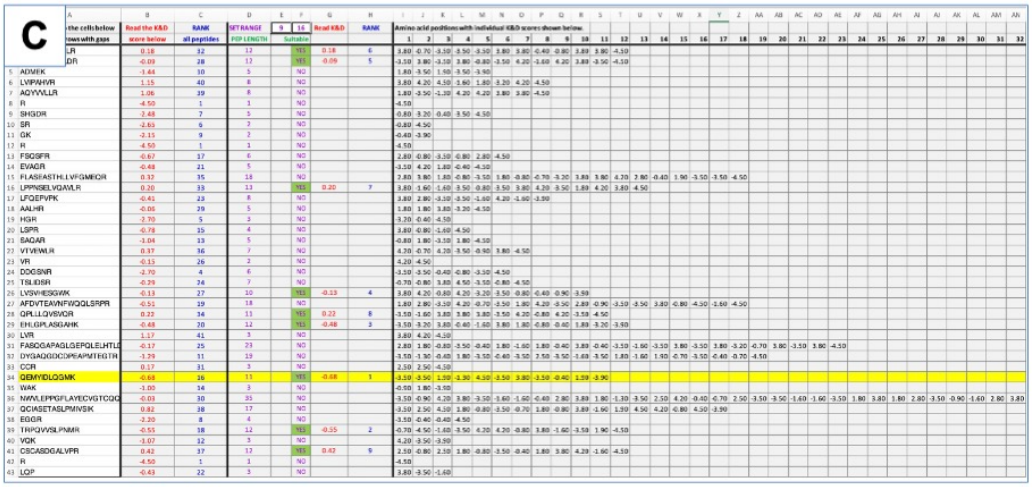

Adiponectin

A

ADIPONECTIN
244 a.a.
UniProtKB ID: **A8K660**

MLLLGAVLLL LALPGHDQET TTQGPGVLLP
LPKGACTGWM AGIPGHPGHN GAPGRDGRDG
TPGEKGEKGD PGLIGPKGDI GETGVPGAEG
PRGFPGIQGR KGEPGEGAYV YRSAFSVGLE
TYVTIPNMPI RFTKIFYNQQ NHYDGSTGKF
HCNIPGLYYF AYHITVYMKD VKVSLFKKDK
AMLFTYDQYQ ENNVDQASGS VLLHLEVGDQ
VWLQVYGEGE RNGLYADNDN DSTFTGFLLY
HDTN

Kyte & Doolittle Score: -0.41

B

Mass	Position	Sequence
1678.94	18–33	QETTTQGPGVLLPLPK
2100.96	34–55	GACTGWMAGIPGHPGHNGAPGR
347.17	56–58	DGR
703.33	59–65	DGTPGEK
333.18	66–68	GEK
853.48	69–77	GDPGLIGPK
1411.68	78–92	GDIGETGVPGAEGPR
831.45	93–100	GFPGIQGR
147.11	101–101	K
1197.55	**102–112**	**GEPGEGAYVYR**
2095.09	113–131	SAFSVGLETYVTIPNMPIR
395.23	132–134	FTK
1771.80	135–149	IFYNQQNHYDGSTGK
2480.19	150–169	FHCNIPGLYYFAYHITVYMK
361.21	170–172	DVK
593.37	173–177	VSLFK
147.11	178–178	K
262.14	179–180	DK
4701.22	181–221	AMLFTYDQYQENNVDQASGSVLLHLEVGDQVWLQVYGEGER
2607.13	222–244	NGLYADNDNDSTFTGFLLYHDTN

D

PEPTIDE ANTIGEN

Tryptic peptide:
GEPGEGAYVYR

Synthetic peptide:
Biotin-CGEPGEGAYVYR

Hydrophilicity change:
+0.290

C

	A	B	C	D	E	F	G	H	I	J	K	L	M	N	O
	te seq into the cells below	Read the K&D	RANK	SET RANGE	9	16	Read K&D	RANK	Amino acid positions with individual K&D scores						
	p to 1000 rows with gaps	score below	all peptides	PEP LENGTH		Suitable			1	2	3	4	5	6	7
3	QETTTQGPGVLLPLPK	-0.41	16	16		YES	-0.41	4	-3.50	-3.50	-0.70	-0.70	-0.70	-3.50	-0.40
4	GACTGWMAGIPGHPGHNGA	-0.42	14	22		NO			-0.40	1.80	2.50	-0.70	-0.40	-0.90	1.90
5	DGR	-2.80	4	3		NO			-3.50	-0.40	-4.50				
6	DGTPGEK	-2.00	6	7		NO			-3.50	-0.40	-0.70	-1.60	-0.40	-3.50	-3.90
7	GEK	-2.60	5	3		NO			-0.40	-3.50	-3.90				
8	GDPGLIGPK	-0.39	17	9		YES	-0.39	5	-0.40	-3.50	-1.60	-0.40	3.80	4.50	-0.40
9	GDIGETGVPGAEGPR	-0.69	11	15		YES	-0.69	3	-0.40	-3.50	4.50	-0.40	-3.50	-0.70	-0.40
10	GFPGIQGR	-0.44	13	8		NO			-0.40	2.80	-1.60	-0.40	4.50	-3.50	-0.40
11	K	-3.90	1	1		NO			-3.90						
12	GEPGEGAYVYR	-0.99	9	11		YES	-0.99	2	-0.40	-3.50	-1.60	-0.40	-3.50	-0.40	1.80
13	SAFSVGLETYVTIPNMPIR	0.44	19	19		NO			-0.80	1.80	2.80	-0.80	4.20	-0.40	3.80
14	FTK	-0.60	12	3		NO			2.80	-0.70	-3.90				
15	IFYNQQNHYDGSTGK	-1.48	7	15		YES	-1.48	1	4.50	2.80	-1.30	-3.50	-3.50	-3.50	-3.50
16	FHCNIPGLYYFAYHITVYMK	0.36	18	20		NO			2.80	-3.20	2.50	-3.50	4.50	-1.60	-0.40
17	DVK	-1.07	8	3		NO			-3.50	4.20	-3.90				
18	VSLFK	1.22	20	5		NO			4.20	-0.80	3.80	2.80	-3.90		
19	K	-3.90	1	1		NO			-3.90						
20	DK	-3.70	3	2		NO			-3.50	-3.90					
21	AMLFTYDQYQENNVDQASGS	-0.42	15	41		NO			1.80	1.90	3.80	2.80	-0.70	-1.30	-3.50
22	NGLYADNDNDSTFTGFLLYH	-0.81	10	23		NO			-3.50	-0.40	3.80	-1.30	1.80	-3.50	-3.50

Insulin

A

INSULIN
110 a.a.
UniProtKB ID: **P01308**

MALWMRLLPL LALLALWGPD PAAAFVNQHL
CGSHLVEALY LVCGERGFFY TPKTRREAED
LQVGQVELGG GPGAGSLQPL ALEGSLQKRG
IVEQCCTSIC SLYQLENYCN

Kyte & Doolittle Score: +0.19

B

Mass	Position	Sequence
2487.23	25-46	FVNQHLCGSHLVEALYLVCGER
859.43	47-53	GFFYTPK
120.07	54-54	T
2383.01	**90-110**	**GIVEQCCTSICSLYQLENYCN**

D

PEPTIDE ANTIGEN

Tryptic peptide:
CSLYQLENYCN

Synthetic peptide:
Biotin-CSLYQLENYAN

Hydrophilicity change:
+0.693

C

	A	B	C	D	E	F	G	H	I	J	K	L	M	N	O	P	Q	R	S
1	Paste seq into the cells below	Read the K&D	RANK	SET RANGE	9	16	Read K&D	RANK	Amino acid positions with individual K&D scores shown below.										
2	Up to 1000 rows with gaps	score below	all peptides	PEP LENGTH		Suitable			1	2	3	4	5	6	7	8	9	10	11
3	FVNQHLCGSHLVEALYLVCGE	0.44	6	22		NO			2.80	4.20	-3.50	-3.50	-3.20	3.80	2.50	-0.40	-0.80	-3.20	3.80
4	GFFYTPK	-0.33	3	7		NO			-0.40	2.80	2.80	-1.30	-0.70	-1.60	-3.90				
5	T	-0.70	1	1		NO			-0.70										
6	GIVEQCCTSICSLYQLENYCN	0.21	4	21		NO			-0.40	4.50	4.20	-3.50	-3.50	2.50	2.50	-0.70	-0.80	4.50	2.50
7	GIVEQCCTSICSLYQLENYCN	0.21	4	21		NO			-0.40	4.50	4.20	-3.50	-3.50	2.50	2.50	-0.70	-0.80	4.50	2.50
8	CSLYQLENYCN	-0.44	2	11		YES	-0.44	1	2.50	-0.80	3.80	-1.30	-3.50	3.80	-3.50	-3.50	-1.30	2.50	-3.50
9																			
10																			
11																			
12																			
13																			
14																			
15																			
16																			
17																			
18																			
19																			
20																			
21																			
22																			

Matrix metalloproteinases 1

A

MATRIX METALLOPROTEINASE 1

469 a.a.

UniProtKB ID: **Q53FK3**

MHSFPPLLLL LFWGVVSHSF PATLETQEQD VDLVQKYLEK
YYNLKNDGRQ VEKRRNSGPV VEKLKQMQEF FGLKVTGKPD
AETLKVMKQP RCGVPDVAQF VLTEGNPRWE QTHLTYRIEN
YTPDLPRADV DHAIEKAFQL WSNVTPLTFT KVSEGQADIM
ISFVRGDHRD NSPFDGPGGN LAHAFQPGPG IGGDAHFDED
ERWTNNFREY NLHRVAAHEL GHSLGLSHST DIGALMYPSY
TFSGDVQLAQ DDIDGIQAIY GRSQNPVQPI GPQTPKACDS
KLTFDAITTI RGEVMFFKDR FYMRTNPFYP EVELNFISVF
WPQLPNGLEA AYEFADRDEV RFFKGNKYWA VQGQNVLHGY
PKDIYSSFGF PRTVKHIDAA LSEENTGKTY FFVANKYWRY
DEYKRSMDPG YPKMIAHDFP GIGHKVDAVF MKDGFFYFFH
GTRQYKFDPK AKRILTLQKA NSWFNCRKN

Kyte & Doolittle Score: -0.57

B

Mass	Position	Sequence
2185.08	18–36	HSFPATLETQEQDVDLVQK
552.30	37–40	YLEK
700.37	41–45	YYNLK
461.21	46–49	NDGR
503.28	50–53	QVEK
175.12	54–54	R
175.12	55–55	R
829.44	56–63	NSGPVVEK
260.20	64–65	LK
1127.56	66–74	QMQEFFGLK
1158.64	75–85	VTGKPDAETLK
377.22	86–88	VMK
400.23	89–91	QPR
1801.89	92–108	CGVPDVAQFVLTEGNPR
1233.60	**109–117**	**WEQTHLTYR**
1217.62	118–127	IENYTPDLPR
997.49	128–136	ADVDHAIEK
1752.93	137–151	AFQLWSNVTPLTFTK
1551.78	152–165	VSEGQADIMISFVR
484.23	166–169	GDHR
3393.48	170–202	DNSPFDGPGGNLAHAFQPGPGIGGDAHFDEDER
837.40	203–208	WTNNFR

D

PEPTIDE ANTIGEN

Tryptic peptide:

WEQTHLTYR

Synthetic peptide:

Biotin-CGWEQTHLTYR

Hydrophilicity change:

+0.560

C

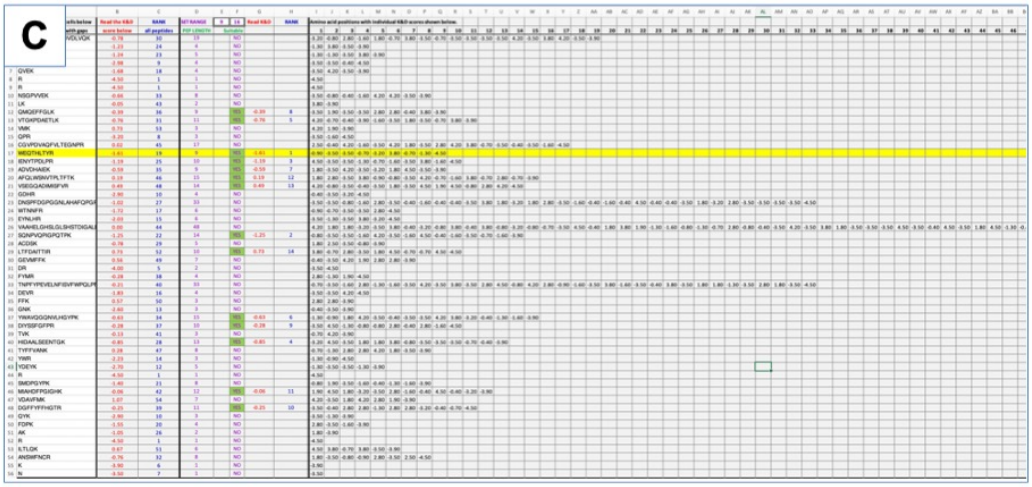

Matrix metalloproteinases 2

A

MATRIX METALLOPROTEINASE 2

660 a.a.

UniProtKB ID: **P08253**

MEALMARGAL TGPLRALCLL GCLLSHAAAA PSPIIKFPGD
VAPKTDKELA VQYLNTFYGC PKESCNLFVL KDTLKKMQKF
FGLPQTGDLD QNTIETMRKP RCGNPDVANY NFFPRKPKWD
KNQITYRIIG YTPDLDPETV DDAFARAFQV WSDVTPLRFS
RIHDGEADIM INFGRWEHGD GYPFDGKDGL LAHAFAPGTG
VGGDSHFDDD ELWTLGEGQV VRVKYGNADG EYCKFPFLFN
GKEYNSCTDT GRSDGFLWCS TTYNFEKDGK YGFCPHEALF
TMGGNAEGQP CKFPFRFQGT SYDSCTTEGR TDGYRWCGTT
EDYDRDKKYG FCPETAMSTV GGNSEGAPCV FPFTFLGNKY
ESCTSAGRSD GKMWCATTAN YDDDRKWGFC PDQGYSLFLV
AAHEFGHAMG LEHSQDPGAL MAPIYTYTKN FRLSQDDIKG
IQELYGASPD IDLGTGPTPT LGPVTPEICK QDIVFDGIAQ
IRGEIFFFKD RFIWRTVTPR DKPMGPLLVA TFWPELPEKI
DAVYEAPQEE KAVFFAGNEY WIYSASTLER GYPKPLTSLG
LPPDVQRVDA AFNWSKNKKT YIFAGDKFWR YNEVKKKMDP
GFPKLIADAW NAIPDNLDAV VDLQGGGHSY FFKGAYYLKL
ENQSLKSVKF GSIKSDWLGC

Kyte & Doolittle Score: -0.45

B

Mass	Position	Sequence
843.41	110–115	YNFFPR
372.26	116–118	KPK
448.22	119–121	WDK
794.42	122–127	NQITYR
2108.02	128–146	IIGYTPDLDPETVDDAFAR
1418.74	147–158	AFQVWSDVTPLR
409.22	159–161	FSR
1587.76	162–175	IHDGEADIMINFGR
1407.60	**176–187**	**WEHGDGYPFDGK**
3638.71	188–222	DGLLAHAFAPGTGVGGDSHFDDDELWTLGEG QVVR
246.18	223–224	VK
1119.44	225–234	YGNADGEYCK
969.52	235–242	FPFLFNGK
1145.45	243–252	EYNSCTDTGR
1797.78	253–267	SDGFLWCSTTYNFEK
319.16	268–270	DGK
2357.01	271–292	YGFCPHEALFTMGGNAEGQPCK
566.31	293–296	FPFR
1551.64	297–310	FQGTSYDSCTTEGR
611.28	311–315	TDGYR
1245.48	316–325	WCGTTEDYDR
262.14	326–327	DK

D

PEPTIDE ANTIGEN

Tryptic peptide:

WEHGDGYPFDGK

Synthetic peptide:

Biotin-CGWEHGDGYPFDGK

Hydrophilicity change:

+0.818

C

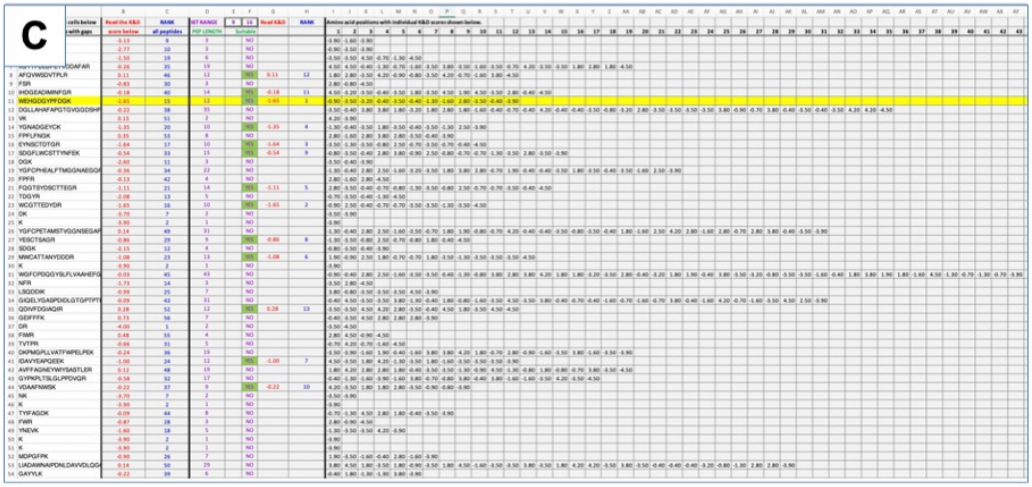

Matrix metalloproteinases 3

A

MATRIX METALLOPROTEINASE 3

477 a.a.

UniProtKB ID: **P08254**

MKSLPILLLL CVAVCSAYPL DGAARGEDTS MNLVQKYLEN
YYDLKKDVKQ FVRRKDSGPV VKKIREMQKF LGLEVTGKLD
SDTLEVMRKP RCGVPDVGHF RTFPGIPKWR KTHLTYRIVN
YTPDLPKDAV DSAVEKALKV WEEVTPLTFS RLYEGEADIM
ISFAVREHGD FYPFDGPGNV LAHAYAPGPG INGDAHFDDD
EQWTKDTTGT NLFLVAAHEI GHSLGLFHSA NTEALMYPLY
HSLTDLTRFR LSQDDINGIQ SLYGPPPDSP ETPLVPTEPV
PPEPGTPANC DPALSFDAVS TLRGEILIFK DRHFWRKSLR
KLEPELHLIS SFWPSLPSGV DAAYEVTSKD LVFIFKGNQF
WAIRGNEVRA GYPRGIHTLG FPPTVRKIDA AISDKEKNKT
YFFVEDKYWR FDEKRNSMEP GFPKQIAEDF PGIDSKIDAV
FEEFGFFYFF TGSSQLEFDP NAKKVTHTLK SNSWLNC

Kyte & Doolittle Score: -0.39

B

Mass	Position	Sequence
881.51	350-356	DLVFIFK
991.51	357-364	GNQFWAIR
574.29	365-369	GNEVR
563.29	370-374	AGYPR
1294.73	375-386	GIHTLGFPPTVR
147.11	387-387	K
832.44	388-395	IDAAISDK
276.16	396-397	EK
261.16	398-399	NK
1048.50	400-407	TYFFVEDK
524.26	408-410	YWR
538.25	411-414	FDEK
175.12	415-415	R
1006.47	**416-424**	**NSMEPGFPK**
1319.65	425-436	QIAEDFPGIDSK
3152.46	437-463	IDAVFEEFGFFYFFTGSSQLEFDPNAK
147.11	464-464	K
698.42	465-470	VTHTLK
823.34	471-477	SNSWLNC

D

PEPTIDE ANTIGEN

Tryptic peptide:

NSMEPGFPK

Synthetic peptide:

Biotin-CGNSMEPGFPK

Hydrophilicity change:

+0.387

C

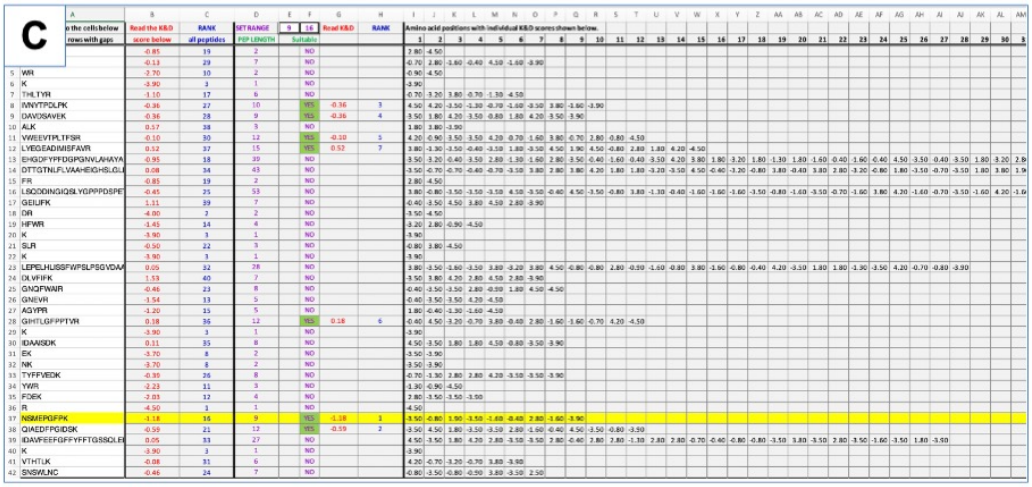

Matrix metalloproteinases 9

A

MATRIX METALLOPROTEINASE 9

707 a.a.

UniProtKB ID: **P14780**

MSLWQPLVLV LLVLGCCFAA PRQRQSTLVL FPGDLRTNLT
DRQLAEEYLY RYGYTRVAEM RGESKSLGPA LLLLQKQLSL
PETGELDSAT LKAMRTPRCG VPDLGRFQTF EGDLKWHHHN
ITYWIQNYSE DLPRAVIDDA FARAFALWSA VTPLTFTRVY
SRDADIVIQF GVAEHGDGYP FDGKDGLLAH AFPPGPGIQG
DAHFDDDELW SLGKGVVVPT RFGNADGAAC HFPFIFEGRS
YSACTTDGRS DGLPWCSTTA NYDTDDRFGF CPSERLYTQD
GNADGKPCQF PFIFQGQSYS ACTTDGRSDG YRWCATTANY
DRDKLFGFCP TRADSTVMGG NSAGELCVFP FTFLGKEYST
CTSEGRGDGR LWCATTSNFD SDKKWGFCPD QGYSLFLVAA
HEFGHALGLD HSSVPEALMY PMYRFTEGPP LHKDDVNGIR
HLYGPRPEPE PRPPTTTTPQ PTAPPTVCPT GPPTVHPSER
PTAGPTGPPS AGPTGPPTAG PSTATTVPLS PVDDACNVNI
FDAIAEIGNQ LYLFKDGKYW RFSEGRGSRP QGPFLIADKW
PALPRKLDSV FEERLSKKLF FFSGRQVWVY TGASVLGPRR
LDKLGLGADV AQVTGALRSG RGKMLLFSGR RLWRFDVKAQ
MVDPRSASEV DRMFPGVPLD THDVFQYREK AYFCQDRFYW
RVSSRSELNQ VDQVGYVTYD ILQCPED

Kyte & Doolittle Score: -0.39

B

Mass	Position	Sequence
2350.10	163-184	DADIVIQFGVAEHGDGYPFDGK
3175.51	185-214	DGLLAHAFPPGPGIQGDAHFDDDELWSLGK
727.45	215-221	GVVVPTR
1955.89	222-239	FGNADGAACHFPFIFEGR
1060.44	240-249	SYSACTTDGR
2016.82	250-267	SDGLPWCSTTANYDTDDR
942.41	268-275	FGFCPSER
3515.56	276-307	LYTQDGNADGKPCQFPFIFQGQSYSACTTDGR
597.26	308-312	SDGYR
1200.51	313-322	WCATTANYDR
262.14	323-324	DK
940.47	325-332	LFGFCPTR
2448.16	333-356	ADSTVMGGNSAGELCVFPFTFLGK
1132.46	357-366	EYSTCTSEGR
404.19	367-370	GDGR
1487.65	371-383	LWCATTSNFDSDK
147.11	384-384	K
4512.10	385-424	WGFCPDQGYSLFLVAAHEFGHALGLDHSSVPEALMYPMYR
1025.54	**425-433**	**FTEGPPLHK**
788.39	434-440	DDVNGIR

D

PEPTIDE ANTIGEN

Tryptic peptide:

FTEGPPLHK

Synthetic peptide:

Biotin-CGFTEGPPLHK

Hydrophilicity change:

+0.169

C

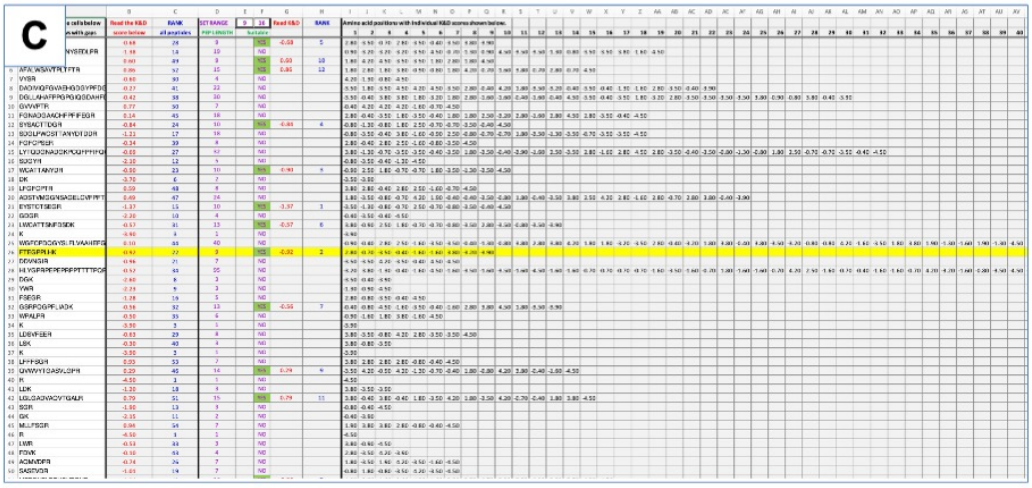

Matrix metalloproteinases 11

A

MATRIX METALLOPROTEINASE 11

488 a.a.

UniProtKB ID: **P24347**

MAPAAWLRSA AARALLPPML LLLLQPPPLL ARALPPDAHH
LHAERRGPQP WHAALPSSPA PAPATQEAPR PASSLRPPRC
GVPDPSDGLS ARNRQKRFVL SGGRWEKTDL TYRILRFPWQ
LVQEQVRQTM AEALKVWSDV TPLTFTEVHE GRADIMIDFA
RYWHGDDLPF DGPGGILAHA FFPKTHREGD VHFDYDETWT
IGDDQGTDLL QVAAHEFGHV LGLQHTTAAK ALMSAFYTFR
YPLSLSPDDC RGVQHLYGQP WPTVTSRTPA LGPQAGIDTN
EIAPLEPDAP PDACEASFDA VSTIRGELFF FKAGFVWRLR
GGQLQPGYPA LASRHWQGLP SPVDAAFEDA QGHIWFFQGA
QYWVYDGEKP VLGPAPLTEL GLVRFPVHAA LVWGPEKNKI
YFFRGRDYWR FHPSTRRVDS PVPRRATDWR GVPSEIDAAF
QDADGYAYFL RGRLYWKFDP VKVKALEGFP RLVGPDFFGC
AEPANTFL

Kyte & Doolittle Score: -0.33

B

Mass	Position	Sequence
735.41	98-104	FVLSGGR
462.23	105-107	WEK
768.39	108-113	TDLTYR
401.29	114-116	ILR
1429.76	**117-127**	**FPWQLVQEQVR**
891.46	128-135	QTMAEALK
1972.98	136-152	VWSDVTPLTFTEVHEGR
1051.52	153-161	ADIMIDFAR
2557.23	162-184	YWHGDDLPFDGPGGILAHAFFPK
413.23	185-187	THR
4737.21	188-230	EGDVHFDYDETWTIGDDQGTDLLQVAAHE FGHVLGLQHTTAAK
1206.60	231-240	ALMSAFYTFR
1265.58	241-251	YPLSLSPDDCR
1825.93	252-267	GVQHLYGQPWPTVTSR
3849.85	268-305	TPALGPQAGIDTNEIAPLEPDAPPDACEA SFDAVSTIR
887.47	306-312	GELFFFK
735.39	313-318	AGFVWR
288.20	319-320	LR
1414.74	321-334	GGQLQPGYPALASR
5592.78	335-384	HWQGLPSPVDAAFEDAQGHIWFFQGAQYW VYDGEKPVLGPAPLTELGLVR
1450.78	385-397	FPVHAALVWGPEK
261.16	398-399	NK

D

PEPTIDE ANTIGEN

Tryptic peptide:

FPWQLVQEQVR

Synthetic peptide:

Biotin-CGFPWQLVQEQVR

Hydrophilicity change:

-0.032

C

	A	B	C	D	E	F	G	H	I	J	K	L	M	N	O	P	Q	R	S	T	U	V	W	X	Y	Z	AA	AB	AC	AD	AE	AF	AG	AH	AI
1	to the cells below	Read the K&D	RANK	SET RANGE	9	16	Read K&D	RANK	Amino acid positions with individual K&D scores shown below.																											
2	0 rows with gaps	score below	all peptides	PEP LENGTH		Suitable			1	2	3	4	5	6	7	8	9	10	11	12	13	14	15	16	17	18	19	20	21	22	23	24	25	26	27
3		0.67	34	7		NO			2.80	4.20	3.80	-0.80	-0.40	-0.40	-4.50																				
4		-2.77	5	3		NO			-0.90	-3.50	-3.90																								
5	TDLTYR	-1.15	11	6		NO			-0.70	-3.50	3.80	-0.70	-1.30	-4.50																					
6	ILR	1.27	37	3		NO			4.50	3.80	-4.50																								
7	FPWQLVQEQVR	-0.55	15	11		YES	-0.55	3	2.80	-1.60	-0.90	-3.50	3.80	4.20	-3.50	-3.50	-3.50	4.20	-4.50																
8	QTMAEALK	-0.29	21	8		NO			-3.50	-0.70	1.90	1.80	-3.50	1.80	3.80	-3.90																			
9	VWSDVTPLTFTEVHEGR	-0.28	22	17		NO			4.20	-0.90	-0.80	3.50	4.20	-0.70	-1.60	3.80	-0.70	2.80	-0.70	-3.50	4.20	3.20	3.50	-0.40	-4.50										
10	ADIMIDFAR	0.64	32	9		YES	0.64	6	1.80	-3.50	4.50	1.90	4.50	-3.50	2.80	1.80	-4.50																		
11	YWHGDDLPFDGPGGILAHAF	-0.23	23	23		NO			-1.30	-0.90	-3.20	-0.40	-3.50	-3.50	3.80	-1.60	2.80	-3.50	-0.40	-1.60	-0.40	-0.40	4.50	3.80	1.80	-3.20	1.80	2.80	2.80	-1.60	-3.90				
12	THR	-2.80	4	3		NO			-0.70	-3.20	-4.50																								
13	EGDVHFDYDETWTIGDDQGT	-0.50	17	43		NO			-3.50	-0.40	-3.50	4.20	-3.20	2.80	-3.50	-1.30	-3.50	-3.50	-0.70	-0.90	-0.70	4.50	-0.40	-3.50	-3.50	-3.50	-0.40	-0.70	-3.50	3.80	3.80	-3.50	4.20	1.80	1.80
14	ALMSAFYTFR	0.76	35	10		YES	0.76	7	1.80	3.80	1.90	-0.80	1.80	2.80	-1.30	-0.70	2.80	-4.50																	
15	YPLSLSPDDCR	-0.68	12	11		YES	-0.68	1	-1.30	-1.60	3.80	-0.80	3.80	-0.80	-1.60	-3.50	-3.50	2.50	-4.50																
16	GVQHLYGQPWPTVTSR	-0.68	13	16		YES	-0.68	2	-0.40	4.20	-3.50	-3.20	3.80	-1.30	-0.40	-3.50	-1.60	-0.90	-1.60	-0.70	4.20	-0.70	-0.80	-4.50											
17	TPALGPQAGIDTNEIAPLEPDA	-0.18	26	38		NO			-0.70	-1.60	1.80	3.80	-0.40	-1.60	-3.50	1.80	-0.40	4.50	-3.50	-0.70	-3.50	-3.50	4.50	1.80	-1.60	3.80	-3.50	-1.60	-3.50	1.80	-1.60	-1.60	-3.50	1.80	2.50
18	GELFFFK	0.63	31	7		NO			-0.40	-3.50	3.80	2.80	2.80	2.80	-3.90																				
19	AGFVWR	0.50	30	6		NO			1.80	-0.40	2.80	4.20	-0.90	-4.50																					
20	LR	-0.35	20	2		NO			3.80	-4.50																									
21	GGQLQPGYPALASR	-0.49	18	14		YES	-0.49	4	-0.40	-0.40	-3.50	3.80	-3.50	-1.60	-0.40	-1.30	-1.60	1.80	3.80	1.80	-0.80	-4.50													
22	HWQGLPSPVDAAFEDAQGHI	-0.19	25	50		NO			-3.20	-0.90	-3.50	-0.40	3.80	-1.60	-0.80	-1.60	4.20	-3.50	1.80	1.80	2.80	-3.50	-3.50	1.80	-3.50	-0.40	-3.20	4.50	-0.90	2.80	2.80	-3.50	-0.40	1.80	-3.50
23	FPVHAALVWGPEK	0.27	29	13		YES	0.27	5	2.80	-1.60	4.20	-3.20	1.80	1.80	3.80	4.20	-0.90	-0.40	-1.60	-3.50	-3.90														
24	NK	-3.70	3	2		NO			-3.50	-3.90																									
25	IYFFR	0.86	36	5		NO			4.50	-3.90	2.80	2.80	-4.50																						
26	GR	-2.45	7	2		NO			-0.40	-4.50																									
27	DYWR	-2.55	6	4		NO			-3.50	-1.30	-0.90	-4.50																							
28	FHPSTR	-1.33	10	6		NO			2.80	-3.20	-1.60	-0.80	-0.70	-4.50																					
29	R	-4.50	1	1		NO			-4.50																										
30	VDSPVPR	-0.51	16	7		NO			4.20	-3.50	-0.80	-1.60	4.20	-1.60	-4.50																				
31	R	-4.50	1	1		NO			-4.50																										
32	ATDWR	-1.56	9	5		NO			1.80	-0.70	-3.50	-0.90	-4.50																						
33	GVPSEIDAAFQDADGYAYFLR	-0.12	27	21		NO			-0.40	4.20	-1.60	-0.80	-3.50	4.50	-3.50	1.80	1.80	2.80	-3.50	-3.50	1.80	-3.50	-0.40	-1.30	1.80	-1.30	2.80	3.80	-4.50						
34	GR	-2.45	7	2		NO			-0.40	-4.50																									
35	LYWK	-0.58	14	4		NO			3.80	-1.30	-0.90	-3.90																							
36	FDPVK	-0.40	19	5		NO			2.80	-3.50	-1.60	4.20	-3.90																						
37	VK	0.15	28	2		NO			4.20	-3.90																									
38	ALEGFPR	-0.23	24	7		NO			1.80	3.80	-3.50	-0.40	2.80	-1.60	-4.50																				
39	LVGPDFFGCAEPANTFL	0.65	33	17		NO			3.80	4.20	-0.40	-1.60	-3.50	2.80	2.80	-0.40	2.50	1.80	-3.50	-1.60	1.80	-3.50	-0.70	2.80	3.80										

Prostate specific antigen

A

PROSTATE SPECIFIC ANTIGEN

261 a.a.

UniProtKB ID: **P07288**

MWVPVVFLTL SVTWIGAAPL ILSRIVGGWE
CEKHSQPWQV LVASRGRAVC GGVLVHPQWV
LTAAHCIRNK SVILLGRHSL FHPEDTGQVF
QVSHSFPHPL YDMSLLKNRF LRPGDDSSHD
LMLLRLSEPA ELTDAVKVMD LPTQEPALGT
TCYASGWGSI EPEEFLTPKK LQCVDLHVIS
NDVCAQVHPQ KVTKFMLCAG RWTGGKSTCS
GDSGGPLVCN GVLQGITSWG SEPCALPERP
SLYTKVVHYR KWIKDTIVAN P

Kyte & Doolittle Score: +0.01

B

Mass	Position	Sequence
1020.48	25–33	IVGGWECEK
1407.75	34–45	HSQPWQVLVASR
232.14	46–47	GR
2230.17	48–68	AVCGGVLVHPQWVLTAAHCIR
261.16	69–70	NK
757.49	71–77	SVILLGR
3493.70	78–107	HSLFHPEDTGQVFQVSHSFPHPLYDMSLLK
289.16	108–109	NR
1871.94	110–125	FLRPGDDSSHDLMLLR
1272.67	**126–137**	**LSEPAELTDAVK**
3467.64	138–169	VMDLPTQEPALGTTCYASGWGSIEPEEFLTPK
147.11	170–170	K
2346.17	171–191	LQCVDLHVISNDVCAQVHPQK
347.23	192–194	VTK
797.38	195–201	FMLCAGR
548.28	202–206	WTGGK
3966.87	207–245	STCSGDSGGPLVCNGVLQGITSWGSEPCALPERPSLYTK
673.38	246–250	VVHYR
147.11	251–251	K
446.28	252–254	WIK
729.38	255–261	DTIVANP

D

PEPTIDE ANTIGEN

Tryptic peptide:

LSEPAELTDAVK

Synthetic peptide:

Biotin-CSEPAELTDAVK

Hydrophilicity change:

+0.296

C

	A	B	C	D	E	F	G	H	I	J	K	L	M	N	O	P	Q
	e seq into the cells below	Read the K&D	RANK	SET RANGE	9	16	Read K&D	RANK	Amino acid positions with individual K&D scores shown b								
	p to 1000 rows with gaps	score below	all peptides	PEP LENGTH		Suitable			1	2	3	4	5	6	7	8	
3	IVGGWECEK	-0.16	13	9		YES	-0.16	4	4.50	4.20	-0.40	-0.40	-0.90	-3.50	2.50	-3.50	-3.9
4	HSQPWQVLVASR	-0.40	7	12		YES	-0.40	1	-3.20	-0.80	-3.50	-1.60	-0.90	-3.50	4.20	3.80	4.2
5	GR	-2.45	5	2		NO			-0.40	-4.50							
6	AVCGGVLVHPQWVLTAAHCI	1.00	19	21		NO			1.80	4.20	2.50	-0.40	-0.40	4.20	3.80	4.20	-3.2
7	NK	-3.70	4	2		NO			-3.50	-3.90							
8	SVILLGR	1.51	21	7		NO			-0.80	4.20	4.50	3.80	3.80	-0.40	-4.50		
9	HSLFHPEDTGQVFQVSHSFPI	-0.36	9	30		NO			-3.20	-0.80	3.80	2.80	-3.20	-1.60	-3.50	-3.50	-0.7
10	NR	-4.00	1	2		NO			-3.50	-4.50							
11	FLRPGDDSSHDLMLLR	-0.40	8	16		YES	-0.40	2	2.80	3.80	-4.50	-1.60	-0.40	-3.50	-3.50	-0.80	-0.8
12	LSEPAELTDAVK	-0.18	11	12		YES	-0.18	3	3.80	-0.80	-3.50	-1.60	1.80	-3.50	3.80	-0.70	-3.5
13	VMDLPTQEPALGTTCYASGW	-0.26	10	32		NO			4.20	1.90	-3.50	3.80	-1.60	-0.70	-3.50	-3.50	-1.6
14	K	-3.90	2	1		NO			-3.90								
15	LQCVDLHVISNDVCAQVHPQK	0.10	17	21		NO			3.80	-3.50	2.50	4.20	-3.50	3.80	-3.20	4.20	4.5
16	VTK	-0.13	14	3		NO			4.20	-0.70	-3.90						
17	FMLCAGR	1.13	20	7		NO			2.80	1.90	3.80	2.50	1.80	-0.40	-4.50		
18	WTGGK	-1.26	6	5		NO			-0.90	-0.70	-0.40	-0.40	-3.90				
19	STCSGDSGGPLVCNGVLQGI	-0.16	12	39		NO			-0.80	-0.70	2.50	-0.80	-0.40	-3.50	-0.80	-0.40	-0.4
20	VVHYR	-0.12	15	5		NO			4.20	4.20	-3.20	-1.30	-4.50				
21	K	-3.90	2	1		NO			-3.90								
22	WIK	-0.10	16	3		NO			-0.90	4.50	-3.90						
23	DTIVANP	0.17	18	7		NO			-3.50	-0.70	4.50	4.20	1.80	-3.50	-1.60		

Serum amyloid-A

A

SERUM AMYLOID A
122 a.a.
UniProtKB ID: **P0DJI8**

MKLLTGLVFC SLVLGVSSRS FFSFLGEAFD
GARDMWRAYS DMREANYIGS DKYFHARGNY
DAAKRGPGGV WAAEAISDAR ENIQRFFGHG
AEDSLADQAA NEWGRSGKDP NHFRPAGLPE
KY

Kyte & Doolittle Score: -0.50

B

Mass	Position	Sequence
175.12	19-19	R
1550.73	20-33	SFFSFLGEAFDGAR
607.27	34-37	DMWR
742.32	38-43	AYSDMR
996.46	**44-52**	**EANYIGSDK**
693.35	53-57	YFHAR
738.34	58-64	GNYDAAK
175.12	65-65	R
1456.72	66-80	GPGGVWAAEAISDAR
659.35	81-85	ENIQR
2177.96	86-105	FFGHGAEDSLADQAANEWGR
291.17	106-108	SGK
1477.75	109-121	DPNHFRPAGLPEK
182.08	122-122	Y

D

PEPTIDE ANTIGEN

Tryptic peptide:
EANYIGSDK

Synthetic peptide:
Biotin-CGEANYIGSDK

Hydrophilicity change:
+0.268

C

	A	B	C	D	E	F	G	H	I
	aste seq into the cells below	Read the K&D	RANK	SET RANGE	9	16	Read K&D	RANK	Am
2	Up to 1000 rows with gaps	score below	all peptides	PEP LENGTH		Suitable			
3	R	-4.50	1	1		NO			-4.5
4	SFFSFLGEAFDGAR	0.34	14	14		YES	0.34	4	-0.8
5	DMWR	-1.75	4	4		NO			-3.5
6	AYSDMR	-1.07	10	6		NO			1.8
7	EANYIGSDK	-1.18	9	9		YES	-1.18	2	-3.5
8	YFHAR	-0.88	11	5		NO			-1.3
9	GNYDAAK	-1.29	8	7		NO			-0.4
10	R	-4.50	1	1		NO			-4.5
11	GPGGVWAAEAISDAR	-0.01	13	15		YES	-0.01	3	-0.4
12	ENIQR	-2.10	3	5		NO			-3.5
13	FFGHGAEDSLADQAANEWGF	-0.75	12	20		NO			2.8
14	SGK	-1.70	5	3		NO			-0.8
15	DPNHFRPAGLPEK	-1.45	6	13		YES	-1.45	1	-3.5
16	Y	-1.30	7	1		NO			-1.3

Sex hormone-binding globulin

A

SEX HORMONE BINDING GLOBULIN
402 a.a.
UniProtKB ID: **P04278**

MESRGPLATS RLLLLLLLLL LRHTRQGWAL
RPVLPTQSAH DPPAVHLSNG PGQEPIAVMT
FDLTKITKTS SSFEVRTWDP EGVIFYGDTN
PKDDWFMLGL RDGRPEIQLH NHWAQLTVGA
GPRLDDGRWH QVEVKMEGDS VLLEVDGEEV
LRLRQVSGPL TSKRHPIMRI ALGGLLFPAS
NLRLPLVPAL DGCLRRDSWL DKQAEISASA
PTSLRSCDVE SNPGIFLPPG TQAEFNLRDI
PQPHAEPWAF SLDLGLKQAA GSGHLLALGT
PENPSWLSLH LQDQKVVLSS GSGPGLDLPL
VLGLPLQLKL SMSRVVLSQG SKMKALALPP
LGLAPLLNLW AKPQGRLFLG ALPGEDSSTS
FCLNGLWAQG QRLDVDQALN RSHEIWTHSC
PQSPGNGTDA SH

Kyte & Doolittle Score: -0.17

B

Mass	Position	Sequence
3834.00	30–65	LRPVLPTQSAHDPPAVHLSNGPGQEPIAVM TFDLTK
361.24	66–68	ITK
912.44	69–76	TSSSFEVR
1838.86	77–92	TWDPEGVIFYGDTNPK
1152.55	93–101	DDWFMLGLR
2452.26	102–123	DGRPEIQLHNHWAQLTVGAGPR
575.28	124–128	LDDGR
925.49	129–135	WHQVEVK
1889.92	136–152	MEGDSVLLEVDGEEVLR
288.20	153–154	LR
916.51	**155–163**	**QVSGPLTSK**
175.12	164–164	R
653.36	165–169	HPIMR
1441.85	170–183	IALGGLLFPASNLR
1266.72	184–195	LPLVPALDGCLR
175.12	196–196	R
763.36	197–202	DSWLDK
1330.70	203–215	QAEISASAPTSLR
2491.19	216–238	SCDVESNPGIFLPPGTQAEFNLR
2134.10	239–257	DIPQPHAEPWAFSLDLGLK
2968.53	258–285	QAAGSGHLLALGTPENPSWLSLHLQDQK
2372.42	286–309	VVLSSGSGPGLDLPLVLGLPLQLK

D

PEPTIDE ANTIGEN

Tryptic peptide:
QVSGPLTSK

Synthetic peptide:
Biotin-CGQVSGPLTSK

Hydrophilicity change:
-0.021

C

	A	B	C	D	E	F	G	H	I	J	K	L	M	N	O	P	Q	R	S	T	U	V	W	X	Y	Z
2	q into the cells below	Read the K&D	RANK	SET RANGE	9	16	Read K&D	RANK	Amino acid positions with individual K&D scores shown below.																	
3	1000 rows with gaps	score below	all peptides	PEP LENGTH		Suitable			1	2	3	4	5	6	7	8	9	10	11	12	13	14	15	16	17	18
4	TQSAHDPPAVHLSNG	-0.21	18	36		NO			3.80	-4.50	-1.60	4.20	3.80	-1.60	-0.70	-3.50	-0.80	1.80	-3.20	-3.50	-1.60	-1.60	1.80	4.20	-3.20	3.80
5	ITK	-0.03	23	3		NO			4.50	-0.70	-3.90															
6	TSSSFEVR	-0.51	12	8		NO			-0.70	-0.80	-0.80	-0.80	2.80	-3.50	4.20	-4.50										
7	TWDPEGVIFYGDTNPK	-0.88	8	16		YES	-0.88	1	-0.70	-0.90	-3.50	-1.60	-3.50	-0.40	4.20	4.50	2.80	-1.30	-0.40	-3.50	-0.70	-3.50	-1.60	-3.90		
8	DDWFMLGLR	-0.06	22	9		YES	-0.06	5	-3.50	-3.50	-0.90	2.80	1.90	3.80	-0.40	3.80	-4.50									
9	DGRPEIQLHNHWAQLTVGAG	-0.86	9	22		NO			-3.50	-0.40	-4.50	-1.60	-3.50	4.50	-3.50	3.80	-3.20	-3.50	-3.20	-0.90	1.80	-3.50	3.80	-0.70	4.20	-0.40
10	LDDGR	-1.62	3	5		NO			3.80	-3.50	-3.50	-0.40	-4.50													
11	WHQVEVK	-0.94	7	7		NO			-0.90	-3.20	-3.50	4.20	-3.50	4.20	-3.90											
12	MEGDSVLLEVDGEEVLR	-0.07	21	17		NO			1.90	-3.50	-0.40	-3.50	-0.80	4.20	3.80	3.80	-3.50	4.20	-3.50	-0.40	-3.50	-3.50	4.20	3.80	-4.50	
13	LR	-0.35	15	2		NO			3.80	-4.50																
14	QVSGPLTSK	-0.41	13	9		YES	-0.41	3	-3.50	4.20	-0.80	-0.40	-1.60	3.80	-0.70	-0.80	-3.90									
15	R	-4.50	1	1		NO			-4.50																	
16	HPIMR	-0.58	10	5		NO			-3.20	-1.60	4.50	1.90	-4.50													
17	IALGGLLFPASNLR	1.06	29	14		YES	1.06	7	4.50	1.80	3.80	-0.40	-0.40	3.80	3.80	2.80	-1.60	1.80	-0.80	-3.50	3.80	-4.50				
18	LPLVPALDGCLR	1.01	28	12		YES	1.01	6	3.80	-1.60	3.80	4.20	-1.60	1.80	3.80	-3.50	-0.40	2.50	3.80	-4.50						
19	R	-4.50	1	1		NO			-4.50																	
20	DSWLDK	-1.47	4	6		NO			-3.50	-0.80	-0.90	3.80	-3.50	-3.90												
21	QAEISASAPTSLR	-0.19	19	13		YES	-0.19	4	-3.50	1.80	-3.50	4.50	-0.80	1.80	-0.80	1.80	-1.60	-0.70	-0.80	3.80	-4.50					
22	SCDVESNPGIFLPPGTQAEFN	-0.31	16	23		NO			-0.80	2.50	-3.50	4.20	-3.50	-0.80	-3.50	-1.60	-0.40	4.50	2.80	3.80	-1.60	-1.60	-0.40	-0.70	-3.50	1.80
23	DIPQPHAEPWAFSLDLGLK	-0.30	17	19		NO			-3.50	4.50	-1.60	-3.50	-1.60	-3.20	1.80	-3.50	-1.60	-0.90	1.80	2.80	-0.80	3.80	-3.50	3.80	-0.40	3.80
24	QAAGSGHLLALGTPENPSWL	-0.41	14	28		NO			-3.50	1.80	1.80	-0.40	-0.80	-0.40	-3.20	3.80	3.80	1.80	3.80	-0.40	-0.70	-1.60	-3.50	-3.50	-1.60	-0.80
25	VVLSSGSGPGLDLPLVLGLPL	0.97	27	24		NO			4.20	4.20	3.80	-0.80	-0.80	-0.40	-0.80	-0.40	-1.60	-0.40	3.80	-3.50	3.80	-1.60	3.80	4.20	3.80	-0.40
26	LSMSR	-0.08	20	5		NO			3.80	-0.80	1.90	-0.80	-4.50													
27	VVLSQGSK	0.35	25	8		NO			4.20	4.20	3.80	-0.80	-3.50	-0.40	-0.80	-3.90										
28	MK	-1.00	6	2		NO			1.90	-3.90																
29	ALALPPLGLAPLLNLWAKPQG	0.47	26	22		NO			1.80	3.80	1.80	3.80	-1.60	-1.60	3.80	-0.40	3.80	1.80	-1.60	3.80	3.80	-3.50	3.80	-0.90	1.80	-3.90
30	LFLGALPGEDSSTSFCLNGLW	0.06	24	26		NO			3.80	2.80	3.80	-0.40	1.80	3.80	-1.60	-0.40	-3.50	-3.50	-0.80	-0.80	-0.70	-0.80	2.80	2.50	3.80	-3.50
31	LDVDQALNR	-0.54	11	9		YES	-0.54	2	3.80	-3.50	4.20	-3.50	-3.50	1.80	3.80	-3.50	-4.50									
32	SHEIWTHSCPQSPGNGTDAS	-1.16	5	21		NO			-0.80	-3.20	-3.50	4.50	-0.90	-0.70	-3.20	-0.80	2.50	-1.60	-3.50	-0.80	-1.60	-0.40	-3.50	-0.40	-0.70	-3.50

Surfactant-associated protein A

A

PULMONARY SURFACTANT ASSOCIATED PROTEIN A

248 a.a.

UniProtKB ID: **Q8IWL2**

MWLCPLALNL ILMAASGAVC EVKDVCVGSP GIPGTPGSHG
LPGRDGRDGL KGDPGPPGPM GPPGEMPCPP GNDGLPGAPG
IPGECGEKGE PGERGPPGLP AHLDEELQAT LHDFRHQILQ
TRGALSLQGS IMTVGEKVFS SNGQSITFDA IQEACARAGG
RIAVPRNPEE NEAIASFVKK YNTYAYVGLT EGPSPGDFRY
SDGTPVNYTN WYRGEPAGRG KEQCVEMYTD GQWNDRNCLY
SRLTICEF

Kyte & Doolittle Score: -0.46

B

Mass	Position	Sequence
375.22	21–23	EVK
1959.97	24–44	DVCVGSPGIPGTPGSHGLPGR
347.17	45–47	DGR
432.25	48–51	DGLK
3435.51	52–88	GDPGPPGPMGPPGEMPCPPGNDGLPGAP GIPGECGEK
644.30	89–94	GEPGER
2313.16	95–115	GPPGLPAHLDEELQATLHDFR
895.51	116–122	HQILQTR
1490.79	123–137	GALSLQGSIMTVGEK
2144.01	138–157	VFSSNGQSITFDAIQEACAR
360.20	158–161	AGGR
555.36	162–166	IAVPR
1447.71	167–179	NPEENEAIASFVK
147.11	180–180	K
2106.98	181–199	YNTYAYVGLTEGPSPGDFR
1735.77	200–213	YSDGTPVNYTNWYR
586.29	214–219	GEPAGR
204.13	220–221	GK
1873.75	222–236	EQCVEMYTDGQWNDR
755.35	237–242	NCLYSR
725.35	243–248	LTICEF

D

PEPTIDE ANTIGEN

Tryptic peptide:
EQCVEMYTDGQWNDR

Synthetic peptide:
Biotin-CVEMYTDGQWNDR

Hydrophilicity change:
+0.823

C

	A	B	C	D	E	F	G	H	I	J	K	L	M	N	O	P	Q
	e seq into the cells below	Read the K&D	RANK	SET RANGE	9	16	Read K&D	RANK	Amino acid positions with individual K&D scores shown b								
	to 1000 rows with gaps	score below	all peptides	PEP LENGTH		Suitable			1	2	3	4	5	6	7	8	
3	EVK	-1.07	8	3		NO			-3.50	4.20	-3.90						
4	DVCVGSPGIPGTPGSHGLPG	-0.15	17	21		NO			-3.50	4.20	2.50	4.20	-0.40	-0.80	-1.60	-0.40	4.5
5	DGR	-2.80	2	3		NO			-3.50	-0.40	-4.50						
6	DGLK	-1.00	10	4		NO			-3.50	-0.40	3.80	-3.90					
7	GDPGPPGPMGPPGEMPCPP	-0.80	12	37		NO			-0.40	-3.50	-1.60	-0.40	-1.60	-1.60	-0.40	-1.60	1.9
8	GEPGER	-2.32	3	6		NO			-0.40	-3.50	-1.60	-0.40	-3.50	-4.50			
9	GPPGLPAHLDEELQATLHDFR	-0.62	16	21		NO			-0.40	-1.60	-1.60	-0.40	3.80	-1.60	1.80	-3.20	3.8
10	HQILQTR	-1.01	9	7		NO			-3.20	-3.50	4.50	3.80	-3.50	-0.70	-4.50		
11	GALSLQGSIMTVGEK	0.37	19	15		YES	0.37	4	-0.40	1.80	3.80	-0.80	3.80	-3.50	-0.40	-0.80	4.5
12	VFSSNGQSITFDAIQEACAR	0.06	18	20		NO			4.20	2.80	-0.80	-0.80	-3.50	-0.40	-3.50	-0.80	4.5
13	AGGR	-0.88	11	4		NO			1.80	-0.40	-0.40	-4.50					
14	IAVPR	0.88	20	5		NO			4.50	1.80	4.20	-1.60	-4.50				
15	NPEENEAIASFVK	-0.67	14	13		YES	-0.67	3	-3.50	-1.60	-3.50	-3.50	-3.50	-3.50	1.80	4.50	1.8
16	K	-3.90	1	1		NO			-3.90								
17	YNTYAYVGLTEGPSPGDFR	-0.68	13	19		NO			-1.30	-3.50	-0.70	-1.30	1.80	-1.30	4.20	-0.40	3.8
18	YSDGTPVNYTNWYR	-1.41	7	14		YES	-1.41	2	-1.30	-0.80	-3.50	-0.40	-0.70	-1.60	4.20	-3.50	-1.3
19	GEPAGR	-1.43	6	6		NO			-0.40	-3.50	-1.60	1.80	-0.40	-4.50			
20	GK	-2.15	4	2		NO			-0.40	-3.90							
21	EQCVEMYTDGQWNDR	-1.58	5	15		YES	-1.58	1	-3.50	-3.50	2.50	4.20	-3.50	1.90	-1.30	-0.70	-3.5
22	NCLYSR	-0.63	15	6		NO			-3.50	2.50	3.80	-1.30	-0.80	-4.50			
23	LTICEF	1.57	21	6		NO			3.80	-0.70	4.50	2.50	-3.50	2.80			